AN EXPERIMENTAL INVESTIGATION OF THE BEHAVIOR OF CARBON DIOXIDE IN RHYOLITIC MELT

Thesis by

Jennifer Glee Blank

In Partial Fulfillment of the Requirements

for the Degree of

Doctor of Philosophy

California Institute of Technology

Pasadena, California

1993

(Submitted March 2, 1993)

Abstract

The nature and behavior of CO_2 in rhyolitic melt at low to moderate pressures was examined using a variety of experimental and analytical techniques. The results are applicable to and critical for understanding the inventory of carbon in the mantle, the growth and evolution of atmospheres, and the processes governing magma degassing. In this study, Fourier transform infrared (FTIR) spectroscopy was calibrated against vacuum extraction/manometry and used to measure solubilities and diffusivities of CO_2 in rhyolitic glasses. The difference in $^{13}C/^{12}C$ ratios between coexisting CO_2 vapor and CO_2 dissolved as CO_2 molecules in rhyolitic melt was also determined experimentally and measured using vacuum extraction and mass spectrometry. Together, these data establish a basis with which to interpret the interaction of carbon dioxide with silicic systems.

The solubility behavior of CO_2 in rhyolitic melt, studied at 750-850°C and pressures up to ≈ 1500 bars, obeys Henry's Law. Only molecular CO_2 was observed in the glasses under these conditions, but both CO_2 molecules and CO_3^{2-} ions have been detected in a single CO_2-bearing rhyolitic glass quenched from much higher pressure (25 kbars) by other workers, suggesting that the reaction $CO_{2\,(melt)} + O^{2-}_{\,(melt)} = CO_3^{2-}_{\,(melt)}$ is favored in rhyolitic melts as pressure increases. Using the CO_2 solubility data, a thermodynamic model was developed to describe CO_2 solubility in rhyolitic melt as a function of temperature and pressure. The solubility of CO_2 in rhyolite is approximately 30% lower than that in basalt, in which all dissolved CO_2 has been detected as CO_3^{2-}. CO_2 and water solubility data can be used to interpret volatile contents of silicic eruption products. Modeled CO_2-H_2O vapor saturation curves permit estimation of minimum entrapment pressures of rhyolitic melt inclusions.

The diffusive behavior of CO_2 in rhyolitic melt was examined through a set of experiments conducted at 450-1050°C and 550-1050 bars in which the silicate glasses were not allowed to fully equilibrate with CO_2 vapor. CO_2 concentration profiles, determined by FTIR spectroscopy, were fit to an analytical solution of the diffusion equation assuming constant D_{CO_2}. D_{CO_2} has a strong, direct correlation with temperature but is only weakly responsive to changes in pressure. The observed Arrhenius relation between diffusivities and temperature over a 600°C interval was used to calculate the activation energy for CO_2 diffusion. The relation between the size of a CO_2 molecule and its activation energy derived from the experimental results mimics the positive correlation reported for noble gases, suggesting that the diffusive behavior of CO_2 in the melt is similar to that of other neutral species. CO_2 diffusivity in rhyolitic melt is lower than bulk water diffusivity (at 0.2 wt% total water) for temperatures below 1050°C but is higher at higher temperatures. CO_2 diffusivity in rhyolitic melt is similar to that in basaltic melt, but the activation energy for CO_2 diffusion in rhyolite is somewhat lower. These diffusion results can be applied to an evaluation of diffusive transport of CO_2 in magmas, diffusional fractionation of CO_2 and H_2O, and growth rates of CO_2-rich bubbles in magmas.

The effect of increasing water content on CO_2 solubility in rhyolite was examined through another set of experiments involving variable proportions of CO_2 and H_2O in the vapor phase. Under the conditions of the experiments, which are relevant to degassing of common silicic magmas near the earth's surface, Henry's law is obeyed for both water and carbon dioxide in rhyolitic melts. Thus, the amount of CO_2 dissolved in a rhyolitic melt saturated with H_2O-CO_2 vapor at a given pressure and temperature will be lower than if the vapor were pure CO_2 by a factor equal to the ratio of the fugacity of CO_2 in the mixed vapor to the fugacity of CO_2 in pure CO_2 vapor at the same conditions. This is essentially a dilution effect. The same is true for the amount of water dissolved in the melt, except that

it is the amount of *molecular* water that is lowered proportionately to the fugacity of water by this dilution effect. There is no evidence of an enhancement of CO_2 solubility in mixed H_2O-CO_2 systems over systems in which only CO_2 is present, as has been reported previously for significantly higher pressures. Further work will be needed to confirm reported non-Henrian behavior at elevated pressures and the implied significance for solubility mechanisms under these conditions, but in the meantime, it appears that efforts to model high level crustal and volcanic phenomena are considerably simplified by the validity of Henry's law for the major volatile species.

The isotopic partitioning of ^{13}C between CO_2 vapor and coexisting dissolved CO_2 was measured through rhyolite-CO_2 experiments at 800-1200°C and 250-1444 bars. The abundance and isotopic composition of CO_2 dissolved in the glass were determined by stepped heating and the yields were checked against IR spectroscopic analysis. The $^{13}C/^{12}C$ of coexisting vapor was determined by direct sampling. No detectable isotopic fractionation between CO_2 vapor and CO_2 molecules dissolved in rhyolitic melt was observed. These results are very different from those for the system basalt-CO_2, in which degassing leaves behind CO_3^{2-} depleted in ^{13}C dissolved in the melt. The $^{13}C/^{12}C$ ratios of natural rhyolitic samples offer potential for a direct measurement of the carbon composition of the source region of this magma type.

Acknowledgments

About ten years ago I met a crazy man named Ivan Barnes. Ivan used to come into my office when I was a technician at the Survey and rant about carbon dioxide. He'd tell me stories of hunting for evidence of magmatic CO_2 in bubbling thermal springs in the Cascades. He'd tell of helicopter flights over recent eruption sites, such as Mt St. Helens, during which he'd lean out of the craft with a tube to sample the wonderful gas. He'd draw pictures in colored chalk on my blackboard, cross-sections of the crust, and talk about how CO_2 made its way from the interior of the planet to the atmosphere. Well, Ivan is no longer with us, but some of his interest and enthusiasm for CO_2 rubbed off. I enrolled in graduate school at the University of Washington to work with John Delaney, another CO_2 aficionado, and measured carbon isotopes in basaltic glasses. There seemed to be numerous questions about CO_2 in silicate melts that would be best answered in the lab, and this, in part, led me to Caltech. I am grateful to John for encouraging me to come here.

Scientific interaction with my thesis advisor, Ed Stolper, has been the most valuable part of my graduate education. He has shared his hermeneutic skills with considerable nous. In addition, I have enjoyed and benefitted from interaction, both in and out of the classroom, with George Rossman, Peter Wyllie, Hugh Taylor, Tom Ahrens, Gerry Wasserburg, Bob Sharp, Dave Stevenson, Charlie Bacon, Mordeckai Magaritz, John Holloway, and other members of the division faculty.

Regarding aspects scientific, Lynn Abelson introduced me to FTIR spectroscopy and the experimental method. Phil Ihinger introduced me to cold seal pressure vessels and shared his design for the rapid-quench apparatus. Youxue Zhang taught me about diffusion. Mike Baker, John Beckett, and Sally Newman were gracious in their willingness to assist in technical matters. Beckett doled out precious metal and advice. Sam Epstein, George Rossman, Hugh Taylor, and Peter Wyllie generously allowed me free access to their laboratories and shared their considerable expertise. Victor Nenow taught me about electronics, machining, and how to make something worthwhile out of a pile of junk. He laughed when I made mistakes and then helped me remedy them. Bart Pelsue, along with his cohorts in the machine shop, politely accepted my somewhat unprofessional drawings and often gave me priority I didn't deserve! Jean Morrison taught me about modern stable isotope mass spectrometry and kindly allowed me use of her lab at the University of Southern California.

Members of the third floor of Arms have helped to create a friendly and stimulating work environment and have enriched my Caltech experience. I have particularly enjoyed the company of and discussions with Lynn Abelson, Paul Asimow, Mike Baker, John Beckett, Dave Bell, Mike Carroll, Laurinda Chamberlin, Jackie Dixon (sometimes), Phil Ihinger, Jim Kubicki, Wohjer Lee, Glen Mattioli, Greg Miller, Sally Newman, Mike Palin, Dave Pyle, Dan Sykes, Chris Tacker, Laurie Watson, and others. Likewise, I have received inspiration from Xia-Hong Feng, Carey Gazis, Charlie Rubin, Joel Schwartz, Tom LaTourette, Art Spivak, Steve Bushnell, and Oded Navon. Members of the late night club have become good friends.

Division Staff have helped to make my life as a student easier. I especially thank Meg Garstang, Fran Barnard, Priscilla Piano, Bernice Simkins, Jenn Packman & Cara Corngold for their friendly attitude and assistance. Jim O'Donnell provided expert library service and was always ready with a smile - and the reference I was looking for. I am

also grateful for the opportunity to participate in NASA's Graduate Student Researchers' Program, which provided my stipend for three years.

Friendship and support of incredible graduate women outside the division has been very important to me. Andrea Ghez, Suzanne Paulsen, Barb Wyslouzil, Rachel Shinn, Cathy Hayes, and especially Christine Nelson have encouraged, helped me to laugh and keep things in perspective.

Cantoris Atri Mortis provided a thread of harmony to the weekly hum. Peter Hofstee has often given me a weekly baroque fix.

Throughout this all, my parents, Dick and Glee Blank, grandparents, Charles and Virginia Perkins, and sis Barbara Bieler have been supportive and encouraging. My friend Ellen Jameson has helped me remember the romance of geoscience through her steady interest in and questions about my work. The beast Pandora somehow knew what to do when marcescence set in.

Most importantly, I acknowledge Patrick Dobson, who introduced me to the stable isotopes and the stable isotope community, and who has been a great source of motivation. Pat has weathered tenebrous times with patience, and he has shared my exuberance when things went well in the lab. This document is testament to his untiring encouragement and support.

hige scael þe heardre
heorte þe cenre
mod scael þe mare
þe ure mægen lytlað

Table of Contents

Introduction

It is well established, through studies of volcanic emissions (e.g., Jagger, 1940; Giggenbach and Matsuo, 1991), melt and fluid inclusions (e.g., Sommer, 1977; Anderson et al., 1989), and volatile contents in quenched volcanic glasses (Moore et al., 1977; Newman et al., 1988), that CO_2 and H_2O are the principal volatiles associated with most magmas. Volatiles have a profound effect on magma genesis and phase relations (Eggler and Holloway, 1977; Mysen, 1977; Wyllie, 1979), and thus knowledge of their abundance and behavior is critical to petrogenetic investigations.

At shallow levels in the crust, exsolving volatiles play an important role in eruption mechanics (Sparks et al., 1977; Eichelberger and Westrich, 1981; Barnes et al., 1988; Tait et al., 1989), and their eventual escape via degassing has created our atmospheres and oceans (Walker, 1977; Tajika and Matsui, 1992). CO_2 is much less soluble than H_2O in most silicate melts; and consequently it is the more sensitive indicator of the early stages of degassing. The first volatile species to partition into a vapor phase in a magma will be CO_2, and the proportion of H_2O/CO_2 will increase as the magma ascends. To understand degassing behavior, we need first to characterize the physical properties of volatiles dissolved in silicate melts. Solubility, diffusivity, and isotopic fractionation between vapor and melt can help constrain degassing systematics.

The majority of volcanic rocks span the compositional range from basalt to rhyolite (Cox et al., 1979). The eruption dynamics of these two end members differ substantially. A large fraction of basalts erupt in a submarine setting where there is sufficient pressure to prevent complete degassing; vesicles from mid-ocean ridge basalts contain typically >90% CO_2 because water is just beginning to exsolve (Delaney et al., 1978; Javoy and Pineau, 1991). In contrast, the majority of rhyolitic magmas erupt subaerially, and therefore almost all of the CO_2 initially present in rhyolitic magma has degassed (Newman et al., 1988). Due to the trace amounts of CO_2 in rhyolitic samples

(and the difficulties inherent in measuring very low abundances), studies of volatiles in rhyolites have generally focused on the role of water.

Because of its low abundance (typically <<200 ppm in submarine basalts, <<30 ppm in rhyolitic glasses) in most erupted lavas, measurement of CO_2 dissolved in natural silicate glasses has been problematic. (Indeed, for many years the concentrations of CO_2 in natural glasses reported in the literature seemed to vary according to laboratory and measurement technique cf., Des Marais, 1986!) Contamination and calibration are two of the major factors responsible for this variation.

Infrared spectroscopy is a valuable tool for measuring CO_2 dissolved in silicate glasses because (a) it detects individual, IR-active species present in the glass (such as CO_2, CO_3^{2-}, OH, H_2O); (b) it detects only species dissolved in the glass (thereby avoiding problems associated with contamination); and (c) it can be used to measure samples tens of microns in diameter with very low abundances (< 10 ppm) of CO_2. In these respects, the IR analytical technique is ideally suited for measurement of CO_2 in both experimental charges and natural samples (glasses or melt inclusions in phenocrysts). However, quantitative use of the IR technique requires that it be calibrated for the species of interest in each composition of interest.

Vacuum extraction and manometry provide a method for independent (i.e., quantitative) calibration of the IR technique. Using vacuum procedures, CO_2 is physically separated from the silicate glass and measured absolutely. The collected CO_2 gas can be subsequently measured for its carbon isotopic composition using mass spectrometry. CO_2 vapor coexisting with silicate melts can be sampled from vesicles (in the case of natural samples) or from an experimental charge and similarly measured for its $^{13}C/^{12}C$ value. Carbon isotopic fractionation between coexisting CO_2 vapor and CO_2 dissolved in a melt can thus be determined. The isotopic composition of CO_2 in silicate

melts can be used to infer the origin of CO_2 in a magma source region and/or the extent and nature of degassing processes.

IR and RAMAN speciation studies of CO_2-bearing natural and synthetic silicate glasses show that CO_2 dissolves in two forms, as molecules of CO_2 and as carbonate ion complexes, and the speciation is a strong function of melt structure and available cations such as Ca^{2+} and Mg^{2+} (e.g., Brey, 1976; Mysen et al., 1976; Kadik et al., 1981; Fine and Stolper, 1985). In the natural spectrum of silicate glasses, CO_2 dissolves in molecular form in rhyolites and as CO_3^{2-} in basalts (Fine and Stolper, 1986; Newman et al., 1988). Intermediate melt compositions contain both dissolved species, increasing in their CO_2/CO_3^{2-} ratio as the activity of silica in the melt increases (Fogel and Rutherford, 1990).

Advances in the carbon geochemistry of basaltic melts in recent years have provided abundant data both for the speciation, solubility, diffusivity, and carbon isotopic composition of CO_2 in experimental and natural systems. However, a similar data set does not exist for rhyolitic melt. This dissertation is a concatenation of experimental studies pertaining to the interaction of CO_2 with rhyolitic melt. I have organized it so that each chapter is self-contained, with separate descriptions of the relevant experimental method and separate references.

In Chapter 1 I present results on the solubility of CO_2 in rhyolitic melt at pressures and temperatures relevant to degassing. An important component of this study involved calibrating the infrared spectroscopic technique for quantitative CO_2 measurement. This was accomplished by measuring several experimental charges both by IR spectroscopy and vacuum extraction/manometry. The calibration makes it possible to now use the IR technique as a quantitative tool for determining CO_2 concentrations in rhyolitic glass compositions. Using the solubility data, I develop a thermodynamic model

to describe the equilibrium concentration of CO_2 in rhyolitic melt as a function of temperature and pressure.

In Chapter 2 I present results from CO_2 diffusion experiments. Using measured CO_2 concentration gradients in rhyolitic glasses, I determine the diffusivity of CO_2 in rhyolitic melts and glasses over a 600°C temperature interval. I also show that the pressure dependence of CO_2 diffusivity is minimal. The relationship between calculated activation energy and radius of diffusing CO_2 molecules in rhyolitic melts is similar to that of other neutral species, particularly the noble gases.

In Chapter 3, I assess the influence of water on the solubility of CO_2 in rhyolitic melt. This is accomplished through a series of experiments in which I equilibrated variable proportions of CO_2 and H_2O with rhyolitic melt at a single T and P. I show that water present in the vapor phase acts as a diluent and that the behavior of both CO_2 and water in rhyolitic melt equilibrated with a mixed-volatile phase is approximately ideal at low pressures.

Chapter 4 focuses on experimental results pertaining to the isotopic partitioning of ^{13}C between coexisting CO_2 vapor and rhyolitic melt over a range of magmatic temperatures. I demonstrate that there is no discernible carbon isotopic fractionation between CO_2 vapor and CO_2 dissolved in rhyolitic melt. This lack of isotopic fractionation for the system CO_2-rhyolite contrasts with the significant fractionation for the system CO_2-basalt, and this difference may be a consequence of CO_2 speciation.

Finally, included as an Appendix is a paper on the concentration and isotopic composition of carbon in submarine basaltic glasses from the Juan de Fuca Ridge (published this month in *Geochim. Cosmochim. Acta*). The work was initiated while I was a graduate student at the University of Washington and was completed during my tenure at Caltech. In this paper I present the first study of a suite of basaltic glasses from a single spreading center analyzed for their carbon contents and $^{13}C/^{12}C$ ratios. Using

experimentally-determined values for the isotopic partitioning of ^{13}C between vesicle and dissolved carbon, I show that the observed variations can be related by open-system degassing.

The results of this thesis are complementary to previous experimental work on water using the same rhyolitic glass starting material (e.g., solubility- Silver et al. (1990); Ihinger (1991); diffusion- Zhang et al. (1991); speciation- Ihinger (1991); hydrogen isotope fractionation- Dobson et al. (1989); Ihinger (1991).) Together, these studies serve as a powerful foundation with which to interpret and predict the behavior and abundances of the major volatiles, CO_2 and H_2O, in silicic systems under the P-T conditions relevant to degassing.

References--

Anderson A. T. Jr., Newman S., Williams S. N., Druitt T. H., Skirius C. and Stolper E. (1989) H_2O, CO_2, Cl and gas in plinian and ash-flow Bishop rhyolite. *Geology* **17**, 221-225.

Barnes I., Evans W. C. and White L. D. (1988) The role of mantle CO_2 in volcanism. *Appl. Geochem.* **3**, 281-285.

Brey G. (1976) CO_2 solubility and solubility mechanisms in silicate melts at high pressures. *Contrib. Mineral. Petrol.* **57**, 215-221.

Cox K.G., J.D. Bell and R.J. Pankhurst (1975) *The Interpetation of Igneous Rocks.*, George Allen & Unwin, Boston, 401 p.

Delaney J. R., Muenow D. W. and Graham D. G. (1978) Abundance and distribution of water, carbon, and sulfur in the glassy rims of submarine pillow lavas. *Geochim. Cosmochim. Acta* **42**, 581-594.

Des Marais D. J. (1986) Carbon abundance measurements in oceanic basalts: the need for a consensus. *Earth Planet. Sci. Lett.* **79**, 21-26.

Dobson P. F., Epstein S. and Stolper E. M. (1989) Hydrogen isotope fractionation between coexisting vapor and silicate glasses and melts at low pressure. *Geochim. Cosmochim. Acta* **53**, 2723-2730.

Eggler D. H. and Holloway J. R. (1977) Partial melting of peridotite in the presence of H_2O and CO_2: Principles and review. *Oregon Dept. Geol. Mineral. Ind. Bull.* **96**, 15-36.

Eichelberger J. C. and Westrich H. R. (1981) Magmatic volatiles in explosive rhyolitic systems. *Geophys. Res. Letters* **8**, 575-560.

Fine G. and Stolper E. (1985) The speciation of carbon dioxide in sodium aluminosilicate glasses. *Contrib. Mineral. Petrol.* **91**, 105-121.

Fine G. and Stolper E. (1986) Dissolved carbon dioxide in basaltic glasses: Concentrations and speciation. *Earth Planet. Sci. Lett.* **76**, 263-278.

Fogel R. A. and Rutherford M. J. (1990) The solubility of carbon dioxide: A quantitative FTIR study. *Amer. Mineral.* **75**, 1311-1326.

Giggenbach W. F. and Matsuo S. (1991) Evaluation of results from Second and Third IAVCEI Field Workshops on Volcanic Gases, Mt Usu, Japan, and White Island, New Zealand. *Appl. Geochem.* **6**, 125-141.

Ihinger P. D. (1991) An experimental study of the interaction of water with granitic melt. Ph.D. dissertation, California Institute of Technology.

Jagger T. A. (1940) Magmatic gases. *Amer. Jour. Sci.* **238**, 313-353.

Javoy M. and Pineau F. (1991) The volatiles record of a "popping" rock from the Mid-Atlantic Ridge at 14°N: Chemical and isotopic composition of gas trapped in the vesicles. *Earth Planet. Sci. Lett.* **107**, 598-611.

Kadik A. A., Shilobreyeva S. N., M.V. Akhmanova, Slutskiy A. B. and Korobkov V. I. (1981) Solubility of CO_2 in melts of acid composition for the case of the albite-silica system (65:35). *Geokhimiya* **1**, 63-70.

Matsui T. and Abe Y. (1986) Impact-induced atmospheres and oceans on Earth and Venus. *Nature* **322**, 526-528.

Moore J. G., Bachelder J. N. and Cunningham C. G. (1977) CO_2-filled vesicles in mid-ocean basalt. *J. Volcanol. Geotherm. Res.* **2**, 309-327.

Mysen B. O. (1977) The solubility of H_2O and CO_2 under predicted magma genesis conditions and some petrological and geophysical implications. *Rev. Geophys. Space Phys.* **15**, 351-361.

Mysen B. O., Eggler D. H., Seitz M. G. and Holloway J. R. (1976) Carbon dioxide solubilities in silicate melts and crystals. Part I. Solubility measurements. *Amer. Jour. Sci.* **276**, 455-479.

Newman S., Epstein S. and Stolper E. (1988) Water, carbon dioxide, and hydrogen isotopes in glasses from the ca. 1340 A.D. eruption of the Mono Craters, California: Constraints on degassing phenomena and initial volatile content. *J. Volcanol. Geotherm. Res.* **35**, 75-96.

Silver L. A., Ihinger P. D. and Stolper E. (1990) The influence of bulk composition on the speciation of water in silicate glasses. *Contrib. Mineral. Petrol.* **104**, 142-162.

Sommer M. A. (1977) Volatiles H_2O, CO_2, and CO in silicate melt inclusions in quartz phenocrysts from the rhyolitic Bandelier air-fall and ash-flow tuff, New Mexico. *Jour. Geol.* **85**, 423-432.

Sparks R. S. J., Sigurdsson H. and Wilson L. (1977) Magma mixing: A mechanism for triggering acid explosive eruptions. *Nature* **267**, 315-318.

Tait S., Jaupart C. and Vergnoille S. (1989) Pressure, gas content and eruption periodicity of shallow, crystallizing magma chamber. *Earth Planet. Sci. Lett.* **92**, 107-123.

Tajika E. and Matsui T. (1992) Evolution of terrestrial proto-CO_2 atmosphere coupled with thermal history of the earth. *Earth Planet. Sci. Lett.* **113**, 251-266.

Walker, J.C.G. (1977) *Evolution of the Atmosphere*, Macmillan, New York, 318 p.

Wyllie P. J. (1979) Magmas and volatile components. *Amer. Mineral.* **64**, 469-500.

Zhang Y., Stolper E. M. and Wasserburg G. J. (1991) Diffusion of water in rhyolitic glasses. *Geochim. Cosmochim. Acta* **55**, 441-456.

Chapter 1

The Solubility of CO_2 in Rhyolitic Melt

1.1 Introduction

Water and carbon dioxide are the principal volatile constituents in a wide variety of igneous settings and their solubilities in silicate melts dominate the nature of volcanic processes (e.g., Blake, 1984; Holloway, 1976; Kadik and Lukanin, 1985; Mathez, 1984; Spera and Bergman, 1980; Tait and Jaupart, 1990). Such fundamental questions as whether or not magma is likely to erupt explosively, whether bubbles and/or crystals are likely to grow or indeed how planetary atmospheres originated and evolved can only be addressed well if the solubility of volatiles is known. Solubility measurements of gas species in silicate liquids provide upper limits on the amounts of volatiles that can dissolve in melts at various temperatures and pressures. CO_2 solubility information is essential in order to understand the eruptive and degassing behavior of magmas, because CO_2 is one of the first volatile species to partition into a separate gas phase due to its low solubility. Knowledge of CO_2 speciation within the silicate melt framework is also important as it leads to physically correct solution models, more accurate solubility predictions, and a necessary standard state for the study of mixed-volatile H_2O-CO_2 systems. Because most subaerially erupted magmas retain very limited, if any, dissolved CO_2 (e.g., Moore et al., 1977; Newman et al., 1988), workers have studies volatile contents of glass inclusions trapped in phenocrysts that formed at depth (e.g., Bacon et al., 1988; Dunbar et al., 1989; Skirius, 1990; Sommer, 1977; Vogel et al., 1989). Solubility data can be used to interpret relative abundances of dissolved volatiles and place constraints on pre-eruptive conditions within a magma chamber (e.g., Anderson et al., 1989; Skirius, 1990).

Fourier Transform infrared (FTIR) spectroscopy provides a rapid and nondestructive method for determining volatile contents of silicate glasses. With FTIR analysis, the speciation and relative abundance of dissolved volatiles can be determined on a sub-millimeter scale: the technique is therefore well-suited to the in-situ measurement of volatile concentrations in both experimental charges and in glass inclusions trapped within

phenocrysts from erupted magmas. Quantitative use of the FTIR spectroscopic technique, however, requires an independent calibration of the gas species for each bulk glass composition of interest.

In this study, the solubility of CO_2 in rhyolite glass was determined experimentally using FTIR spectroscopy for equilibrium temperatures of 750-850°C and pressures between 200-1500 bars. These P-T conditions are especially relevant to high-silica magmas residing in shallow reservoirs in the upper crust and their eruptive products. The FTIR measurements were calibrated using vacuum extraction and manometry and these solubility data were used to derive a thermodynamic model for the solubility of CO_2 in rhyolitic melts as a function of P and T. As will be shown in Chapters 2 and 4, the expression for CO_2 solubility is applicable to CO_2 solubilities in rhyolitic melts and glasses over a large temperature range, from ≈ 450-1200°C.

1.2 Previous Work

Fogel and Rutherford (1990) conducted an experimental/IR study on the solubility of CO_2 in rhyolitic melt using glasses from the Valles Caldera in New Mexico similar to the one presented here. My investigation differs from the previous one in two important ways: First, I determined the molar absorptivity coefficient for CO_2 in rhyolitic melt and therefore obtain quantitative FTIR results. Fogel and Rutherford used an absorptivity coefficient for CO_2 dissolved in a synthetic jadeite composition (Fine and Stolper, 1985) which, as I will show, leads to concentrations ≈ 15% too high. Second, experiments in this study were conducted over a lower temperature range (750-850°C vs. 950-1150°C) more relevant to natural rhyolitic eruptions (e.g., Bacon, 1977) and lower pressures (200-1500 bars vs. 500-6700 bars) where CO_2 solubility behavior more closely resembles ideality.

1.3 Starting Material

The Glass Buttes rhyolite used as the starting material for my experiments was collected from West Butte, Lake County, Oregon in 1987 by P. Ihinger and M. Carroll. Its major element composition (Table 1-1) indicates that the glass is a high-silica rhyolite. The glass is translucent gray and free of vesicles and phenocrysts, but microlitic Fe-Ti oxides, typically < 10 μm in diameter, are ubiquitous.

To determine the volatile content of the starting material, 3 glass chips several mm in diameter were polished and examined spectroscopically. No dissolved CO_2 was detected. On the basis of 15 infrared spectroscopic measurements of 3 polished chips, the water content of the glass ranged from 0.09-0.28 wt% with an average of 0.17±0.06 (1σ). The measured range was water. As a consequence of the low water content of the starting material, the melting temperature of the glass is relatively high. Chips ≈ 1 mm in diameter, placed in a heated 1-atm furnace, were used to ascertain an approximate melting temperature for the glass of 1225°C.

1.4 Solubility Experiments

1.4.1 Sample Preparation

Glass chips, crushed using a stainless steel mortar and pestle and sieved to 500-1000 μm, were washed ultrasonically and rinsed three times in ethanol. Chips were subsequently dried under a heat lamp and stored in a 100°C furnace for at least 24 hours prior to loading inside precious metal capsules.

Silver palladium ($Ag_{70}Pd_{30}$) capsules, 27.9 mm long and 5.1 mm in diameter, were triple crimped and sealed at their base using an arc welder. During welding, nitrogen gas was passed over the surface of capsule to prevent oxidation. Welded capsules, cleaned and annealed under a Bunsen burner flame, were filled with rhyolitic glass and triple crimped but not welded shut at the top.

A number of the experiments discussed in this chapter were used for purposes supplemental to the CO_2 solubility studies; corresponding samples are noted in Table 1-4. Capsules prepared for CO_2 solubility experiments typically contained ≈ 0.4 g of glass chips. Several of the capsules contained glass cylinders or prisms for measurement of CO_2 diffusion profiles (Chapter 2). In other experiments, CO_2 pressurizing gas was sampled before the capsule was retrieved (Chapter 4).

1.4.2 Experiments

Loaded capsules were placed in nickel-rich René cold seal pressure vessels ("bombs") and held at elevated pressures (200-1500 bars) and temperatures (750-850°C) for periods lasting from 1-3 weeks. René bombs (Tuttle, 1949) were oriented vertically in kanthal-wire resistance furnaces such that the hot spot was at their base. During an experiment, an internal chromel-alumel thermocouple was positioned at the top of the capsule, and a hollow, stainless steal filler rod surrounded the thermocouple inside the bomb to prevent thermal convection of the pressure medium. The temperature gradient at 850°C over the ≈ 30 mm length of a capsule, determined using thermocouples of three different lengths (corresponding to the bottom, middle, and top of where a capsule normally resides), was < 10°C.

Temperatures were monitored and controlled with a Eurotherm FICS10 series controller and read to ±1°C. Pressures were recorded using a high-precision bourdon indicator gauge (Heise). During an experiment, the pressure fluctuated by as much as ±10 bars, in response to changes in room temperature. Samples were pressurized at ambient temperature with high-purity ("bone dry" =<10 ppm H_2O) Matheson CO_2 from a tank using an oil-free gas intensifier pump (Haskel, Inc.). After initial pressurization, samples were raised to their high-temperature setting over a period of 30-40 minutes.

Several isothermal pressure "reversal" experiments were accomplished by holding an experimental charge at high pressure for one week and then lowering the pressure and allowing the sample to reequilibrate.

Samples were quenched by manually removing the bomb from the furnace and blasting it with compressed air until its temperature dropped to ≈ 350°C, after which point the bomb assembly was placed in a cold water bath and cooled to room temperature (30°C). The quenching procedure lasted 3.5-4 minutes. After allowing several hours for equilibration of the bomb to room temperature, the capsule was removed and stored in a glass vial with a Teflon-sealed lid to protect the glasses for extended exposure to the atmosphere.

1.5 Analytical Methods

1.5.1 Manometry

Seven of the rhyolite samples, equilibrated with CO_2 over a range of pressures, were extracted under vacuum using a stepped heating procedure. Prior to extraction, several chips from each sample were set aside for IR spectroscopic analysis. Comparison of the two analytical techniques formed the basis of the calibration of the IR spectroscopic method for CO_2 dissolved in rhyolitic glasses.

The vacuum extraction procedure consisted of the following: Glass chips from an experiment were weighed, placed in a Pt crucible, and loaded inside a quartz extraction vessel which was immediately attached to the vacuum line. After evacuating the vessel for several hours at 150°, the Pt crucible was heated incrementally using an induction furnace. Condensible gases liberated from the rhyolitic chips were collected in a liquid nitrogen (LN) trap. Heating intervals lasted 40 minutes except for the final heating step for each extraction which lasted 90 minutes; temperatures and durations of each heating interval are listed in Table 1-2. After each heating step, noncondensible gases (typically < 1 μmol, and

presumably H_2 released from the Pt crucible) were pumped away, and CO_2 was separated from water using a -115°C slurry of dry ice and M17 ("artificial oil of ants") or a variable temperature trap (Des Marais, 1978), in which case CO_2 was distilled at temperatures $-160°C < T < -130°C$. CO_2 yields for each temperature interval were measured manometrically before being transferred to break seal tubes. Some of the CO_2 samples were also analyzed for their $^{13}C/^{12}C$ isotopic ratios, as discussed in Chapter 4.

The largest contribution of carbon-bearing material in the vacuum line extraneous to the samples came from the heated Pt crucibles. For this reason, only low-C Pt crucibles (special order, Johnson Matthey) were used to minimize the contribution of carbon to the yield. Prior to each sample extraction, the Pt crucible was evacuated and preheated at 1200°C for 30 minutes. A procedural "blank" was collected by adding an LN trap to the line while the crucible was held at 1200°C for an additional 30 minutes. When a satisfactorily low "blank" was obtained (<0.03 μmol CO_2), the Pt crucible was ready for use.

Two vacuum lines were used for CO_2 extraction from the samples. Early extractions were performed on a previously existing line. The second vacuum line was designed and built specifically to extract and measure small quantities of CO_2 in silicate glass. The newer line had a more sensitive manometer (e.g., 0.3 μmol CO_2/cm vs. 7 μmol CO_2/cm Hg displacement), more accurate temperature control at $T \leq 850°$, consistently lower CO_2 blanks (< 0.015 μmol), and was capable of high-precision CO_2 measurements to 0.01 μmoles. The major procedural difference between the two lines is that samples extracted using the newer line were combusted (i.e., heated in the presence of O_2 released from decomposition of CuO at 900°C) whereas samples extracted using the older vacuum line were pyrolyzed (heated under vacuum).

1.5.2 FTIR Spectroscopy

Individual glass chips from the CO_2-saturation experiments were doubly-polished to thicknesses, measured using a digital micrometer, in the range of 80-460 μm and analyzed for intensities of the IR absorption bands corresponding to volatiles dissolved in the silicate network. Fig. 1-1 is a typical spectrum showing the absorption bands for the two volatile species, molecular CO_2 and OH^-, detected in the samples. CO_2 was detected in the samples as an absorption band at 2350 cm^{-1}; this band is attributed to the antisymmetric stretching mode of $^{12}CO_2$ molecules (Fine and Stolper, 1985). Dissolved water was detected as an absorption band at 3550 cm^{-1} corresponding to the fundamental O-H stretching vibration. At the low total water concentrations of the samples, this band is due primarily to OH^- (Newman et al., 1986).

Analyses were conducted on a Nicolet 60 SX FTIR spectrometer. Spectra were collected using the microchamber compartment, a quartz halogen tungsten lamp as the source of exciting radiation, a CaF_2 beamsplitter, and an LN-cooled InSb detector. The spectrometer and sample compartment were purged with dry air or N_2 gas. The IR beam was aimed at the sample using a pinhole aperture (35 μm in diameter). Samples were measured for homogeneous CO_2 contents on this scale to verify that equilibrium CO_2 solubilities were achieved.

Transmission spectra of glasses were obtained in the wavelength region 7500-1250 cm^{-1}. Each spectrum consisted of 1024 or 2048 integrated interferograms with a spectral resolution of 2 cm^{-1}. Sample transmission spectra were ratioed to a background transmission spectrum (sample/background) to remove extraneous IR bands from atmospheric H_2O and CO_2 in the beam path. A background spectrum is typically taken at the start of a work session under conditions identical to those of the sample spectrum, except that the sample is not present.

Transmittance spectra were converted to absorbance (A = -log(T/100), where T is the transmittance in percent and A is the absorbance) and plotted as absorbance versus wave number on chart paper. Absorbance intensities of the two bands measured (2350 cm^{-1} for mol. CO_2 and 3550 cm^{-1} for OH^-) were taken as the peak heights measured directly from a plotted spectrum after drawing a straight background that was tangential to the spectrum on either side of each peak.

Because of the FTIR design and the necessity of opening the sample compartment between analyses, some residual atmospheric CO_2 often remained in the N_2- or dried-air-purged sample chamber and interfered with the absorption due to molecular CO_2 dissolved in the sample. Gaseous CO_2 contributed to the spectra as two absorption bands centered at 2340 and 2360 cm^{-1} and often distorted the dissolved CO_2 peakshape at 3250 cm^{-1} and/or the baseline in the near vicinity. The most efficient and reliable way to remove such extraneous CO_2 from a spectrum was to perform a spectral subtraction of atmospheric CO_2 from each sample spectrum. This subtraction procedure improved measurement reproducibility to within several ppm CO_2.

Data manipulation consisted of two parts: (1) a baseline correction; and (2) spectral subtraction. Baseline corrections were used to allowed different portions of a spectrum to be rolled and ramped. I typically checked to make sure that the trailing ends of the absorption band for total water at 3550 cm^{-1} were horizontal and printed out a spectrum in the range of 4000-2000 cm^{-1}. This involved "rolling" a spectrum typically $\leq$10 degrees to allow the drawing of a horizontal line across the base of the 3550 cm^{-1} absorption band for total water. Following this, I reduced the scale to center about the CO_2 peak at 2350 cm^{-1} and repeated the baseline correction procedure if necessary. Once the baseline of the spectrum was horizontal, I used the Nicolet spectral subtraction subroutine to remove the atmospheric CO_2 from the spectrum. Although this invites a degree of subjectivity to the

data interpretation, I found manual spectral subtraction to be a more reliable and much more efficient procedure than purging alone. Subtracted spectra were reproducible to within 2%.

Corrected peak absorbances are related to concentration by the Beer-Lambert law, written as:

$$c_i = \frac{(abs)(MW)}{(d)(\rho)(\varepsilon_i)} \quad \text{.....(1-1)}$$

where c_i is the concentration of the dissolved species i in weight fraction, abs is the measured IR peak intensity (unitless), MW is the molecular weight of the dissolved species of interest (44 g/mol for CO_2, 18 g/mol for water), d is the thickness of the polished sample (in cm), ρ is the density of rhyolite glass (taken as 2350 g/l; Silver et al., 1990), and ε_i is the molar absorptivity coefficient (here, in units of l/(cm-mol)) corresponding to the IR absorption band of the dissolved species in the composition of interest. In order for the Beer-Lambert law to be valid, we must assume that ε is a constant - and that the analyte is reasonably dilute in the matrix. The value of ε_{3550} for hydroxyl in rhyolitic glass of 88 l/(cm-mol) (Dobson et al., 1989) was used to calculate the abundance of water in the samples. The molar absorptivity coefficient for CO_2 (ε_{3250}) was first determined by comparison with an absolute method (manometry) and then applied to absorbance measurements of the glass samples.

The validity of Lambert's law (i.e., that absorbance is proportional to sample thickness, e.g., Atkins, 1986) for samples from which more than one chip was analyzed was confirmed by measuring band intensities on several pieces of the sample ground to different thicknesses. These measurements also confirmed that the dissolved volatile CO_2 concentrations were homogeneous within a sample.

Uncertainties in the absorbance measurements are due to errors in sample thickness, determination of background placement and subtraction, and to graphical absorbance measurement. The largest errors assigned to water and CO_2 concentrations are based on

the uncertainty in the thickness measurements. For example, samples were typically 100-300 μm thick. Measurements of sample thickness varied from 1-3 μm, leading to an error in concentration of up to 3%.

1.6 Results and Discussion

1.6.1 Manometric results and calibration of the IR technique

FTIR spectroscopy can be used to measure the abundance of a dissolved species in silicate glass, provided that the dissolved species is IR active and that the absorption band(s) corresponding to the species of interest is(are) calibrated against some absolute method. To calibrate the absorbance band corresponding to molecular CO_2, I used vacuum extraction and manometry.

Carbon-bearing species may be present in three locations on a silicate glass (Mathez and Delaney, 1981) (1) dissolved in the glassy matrix; (2) adsorbed on surfaces or cracks; and (3) in vesicles. While the IR technique measures only dissolved species present in a sample, vacuum extraction/manometry has the potential to measure all types of carbon-bearing species associated with the glasses, and thus special care must be taken to ensure that the dissolved component is effectively isolated for accurate measurement.

The temperature conditions of the solubility experiments were such that none of the samples melted; consequently there were no vesicles in any of the experimental run products as there were none in the starting materials. I therefore assumed that the experimental glasses contained only two basic forms of CO_2 - a dissolved form and a surficial component (the latter not necessarily molecular CO_2 but rather an unknown C-bearing species). The procedure used during vacuum extraction of the glasses was carefully designed to separate these two forms of CO_2 by incremental heating.

While the temperature release characteristics of different C-bearing components have not been examined previously in rhyolitic samples, they have been studied in some

detail for basaltic glasses (e.g., Mattey et al., 1984; Mattey et al., 1989; Zimmermann et al., 1988); Craig, 1987 #133; Des Marais, 1984 #115; Des Marais, 1984 #134; Exley, 1987 #117; Wright, 1989 #129. Des Marais and Moore (1984) and Mattey et al. (1984) first noted that post-eruption carbonaceous material associated with the surface of basaltic glasses was released at low temperatures typically < 650°C and CO_2 dissolved in the glass was liberated at temperatures above 750°C. The terms "low-temperature" and "high-temperature" carbon now commonly refer to "contaminant" (or secondary) and "dissolved" carbon components, respectively. Barker and Torkelson (1975) determined experimentally that the quantities of gas adsorption on to the surfaces of tholeiitic and silica glass were similar at room temperature. On the basis of their results, I assumed that the temperature release characteristics for material adsorbed onto my rhyolitic charges would be similar to those for basalt (Des Marais and Moore, 1984) and therefore used a similar extraction procedure.

The results of the stepped-heating CO_2 extractions are given in Table 1-2. CO_2 yields are given in terms of μmoles of gas collected and in ppm CO_2 based on the amount of glass extracted. In all cases, the bulk of the CO_2 was released from the highest temperature step. Samples GB1-26 and GB1-27 were extracted using a greater number of heating steps than the other samples used for the IR calibration; this enabled me to examine the temperature-release characteristics of CO_2 from these glasses in more detail. The temperature release profile for sample GB1-27 is shown in Fig. 1-2. The majority of the "low-temperature" CO_2 is released during the 450°C combustion step; similar observations are common for low-temperature CO_2 extracted from basaltic glasses (e.g., Wright and Pillinger, 1989).

The high-temperature component of CO_2 extracted from the rhyolitic glasses is listed , along with the intensities of the molecular CO_2 absorption band at 2350 cm^{-1} determined by IR analyses, in Table 1-3. CO_2 concentrations within a sample, based on IR

measurements, agree within 4%. The high-temperature CO_2 released from the rhyolitic glasses correlates directly with the normalized IR absorbances for dissolved molecular CO_2 (Fig. 1-3; closed circles). In contrast, bulk CO_2 recovered by manometry has a weaker correlation with the IR results (Fig. 1-3; open circles), suggestive of a y-intercept of a100 ppm additional (i.e., secondary, or not dissolved) CO_2 in the manometric yield. This value is similar to the average sum of the low-temperature CO_2 liberated by the glasses. Another observation to support a surficial correlation for the low-temperature CO_2 is the fact that samples washed in ethanol prior to extraction (GB1-12, 73, 14) had the smallest low-temperature CO_2 yields.

One of the glasses extracted appeared to have an abnormally large high-temperature CO_2 yield. This can be seen in Fig. 1-3 as the sample that deviates most from the line. The CO_2 mass balance for this experiment (GB1-26) suggests that there is an erroneous concentration of CO_2 associated with the manometric measurement of this sample (perhaps due to analyst error). For this reason, data for GB1-26 was omitted from the calculation of the molar absorptivity coefficient.

The relationship between the manometric and IR measurements was evaluated by a linear, least-squares regression of the data (Fig. 1-3). The molar absorptivity coefficient for CO_2 in rhyolite, ε_{2350}, was determined from the slope of the line using the following expression:

$$\varepsilon_{2350} = \left(\frac{\text{abs}}{\text{cm}}\right) \frac{(44\ \text{g/mol})}{(2350\ \text{g/l})\ (\text{ppm}\ CO_2)} \times 10^6 \qquad \text{.....(1-2)}$$

The value of ε_{2350} is 1066±20 g/(cm-mol). This value is 15% higher than the value of 945±45 determined by Fine and Stolper (1985) for jadeite and applied by Fogel and Rutherford (1990) to rhyolitic glasses. CO_2 concentrations reported by the latter authors should all be decreased by 15%.

1.6.2 Dissolved carbon dioxide in rhyolitic glasses

A summary of the IR analyses and corresponding CO_2 (and water) concentrations is given in Table 1-4. Concentrations of dissolved CO_2 ranged from 140-977 ppm for rhyolite equilibrated experimentally at 750-850°C and 200-1444 bars. At constant temperature, the concentration of CO_2 in rhyolitic melt increases ≈linearly as a function of pressure over the low pressure conditions of the experiments. For temperatures of 850°C, the concentration of molecular CO_2 in rhyolite is approximately 340 ppm at 500 bars. The range in values for analyses of 3 to 7 glass chips from the same experiment is usually less than 15 ppm CO_2. Sample heterogeneity, based on replicate analyses, ranged from 0-33 ppm CO_2, or 0-7% variability.

1.6.3 Water concentrations in the experimental glasses

Concentrations of dissolved water in the run products ranged from 0.07-0.38 wt% (Table 1-4). This variation is approximately 30% greater than I observed in the starting material and suggests that some of the glasses may have acquired water over the course of an experiment. There is no correlation between water content and CO_2 abundance, run duration, or pressure, however, so the manner in which the glasses gained or lost water is unclear. If the CO_2 pressurizing medium was pure and if the water originally present in the glasses had sufficient time to diffuse out, the concentration of the run products would be zero. That this is not observed probably reflects a nonzero f_{H2O} in the vapor phase. On the basis of mixed CO_2-H_2O solubility experiments in rhyolitic melt, presented in Chapter 3, the maximum f_{H2O} for the nominally pure CO_2 solubility experiments was ≤ 7 bars and the effect of such low water fugacity on the CO_2 solubility in the rhyolitic glasses is negligible.

1.6.4 Henry's law behavior of CO_2 in equilibrium with rhyolitic melt

From IR spectroscopy, we know that carbon dioxide is dissolved in rhyolitic melt as molecules of CO_2. The interaction between gaseous and dissolved CO_2 can therefore be described by the reaction:

$$CO_2 \text{ (vapor)} = CO_2 \text{ (melt)} \quad \text{.....(1-3)}$$

The equilibrium constant for this reaction is:

$$K = \frac{a^m_{CO_2}}{a^v_{CO_2}} \approx \frac{X^m_{CO_2}}{f_{CO_2}/f^o_{CO_2}} \quad \text{.....(1-4)}$$

where $a^m_{CO_2}$ and $a^v_{CO_2}$ are the activities of carbon dioxide in the melt and vapor, f_{CO_2} is the fugacity of CO_2 in the vapor, and $f^o_{CO_2}$ is the fugacity of pure CO_2 at a reference P and T. If Henry's law is valid for CO_2 in rhyolitic melt, the activity of CO_2 in the melt should equal its mole fraction (X_{CO_2}).

Fig. 1-4 shows that at 850°C the solubility of CO_2 in rhyolitic melt obeys Henry's law for f_{CO_2} up to ≈ 1300 bars. The Henry's law constant at 850°C, determined by a linear regression through the data for experiments held at pressures up to P_{CO_2} = 1035 bars, is $2.36 \pm 0.31 \times 10^6$.

1.6.5 Thermodynamic treatment

The simplest way to link the experimental measurements to the thermodynamic properties of silicate liquids is to assume that Henry's law is valid over the range of CO_2 concentrations, that is, to assume that the activity of CO_2 in the melt is proportional to its mole fraction. As shown in the previous section, however, the linear form of Henry's law is no longer applicable above ≈ 1300 bars and must be modified to account for the effect of pressure. This can be accomplished incorporating the expression:

$$\left(\frac{\partial \ln f_{CO_2}}{\partial P}\right)_T = \frac{v^{o,m}_{CO_2}}{RT} \quad \text{.....(1-5)}$$

(Prausnitz et al., 1986), into the equation for Henry's law, where $v^{o,m}_{CO_2}$ is the partial molar volume of CO_2 in the melt. Similarly, incorporation of the following expression modifies Henry's law to account for changes in temperature:

$$\left(\frac{\partial \ln f_{CO_2}}{\partial T}\right)_P = \frac{\Delta H^o_{CO_2}}{RT^2} \quad \text{.....(1-6)}$$

where $\Delta H^o_{CO_2}$ is the enthalpy of the reaction (1-3). Henry's law, incorporating changes due to pressure and temperature, can thus be written as:

$$\ln\left(\frac{f^o_{CO_2}(P,T)}{X^m_{CO_2}(P,T)}\right) = \ln\left(\frac{f^o_{CO_2}(P_o,T_o)}{X^m_{CO_2}(P_o,T_o)}\right) + \frac{v^{o,m}_{CO_2}}{RT} - \frac{\Delta H^o_{CO_2}}{RT^2}\left(\frac{1}{T} - \frac{1}{T_o}\right) \quad \text{.....(1-7)}$$

where P_o and T_o refer to a reference pressure and temperature. Note that I assumed $v^{o,m}_{CO_2}$ to be independent of temperature and pressure, and $\Delta H^o_{CO_2}$ to be independent of temperature.

The activity of CO_2 in CO_2-saturated melts can now be readily calculated as a function of temperature and pressure provided it is known at some reference P and T:

$$X^m_{CO_2}(P,T) = X^m_{CO_2}(P_o,T_o)\frac{f^o_{CO_2}(P,T)}{f^o_{CO_2}(P_o,T_o)} * \exp\left\{-\frac{v^{o,m}_{CO_2}}{RT}(P - P_o) + \frac{\Delta H^o_{CO_2}}{R}\left(\frac{1}{T} - \frac{1}{T_o}\right)\right\} \quad (1\text{-}8)$$

To calculate values for $v^{o,m}_{CO_2}$ and $\Delta H^o_{CO_2}$, I used the CO_2 solubility data from this study along with the data of Fogel and Rutherford (1990) corrected using the molar absorptivity coefficient for CO_2 in rhyolite obtained in this study and performed a least squares regression to equation (1-7) above. The reference temperature and pressure used were 850°C and 0 bars. Fugacities were calculated using a modified Redlich-Kwong equation of state (Holloway, 1977) . Calculated parameters are:

ln (1/K) (P_o,T_o)	$v^{o,m}_{CO_2}$(cc/mol)	$\Delta H^o_{CO_2}$ (Kjoules/mol)
-14.44±0.02	28.1±1.6	-27.1±2.0

The value for the Henry's law constant at the reference T and P (K (P_o,T_o)), calculated using all of the data is very similar but slightly lower (1.88±0.05 vs. 2.36±0.31 x 10^6) than the value I obtained using only the low pressure, 850°C data (Fig. 1-4). The value for the molar volume of CO_2 dissolved in rhyolitic melt is similar to the value of the b-parameter in the Redlich-Kwong equation of state (29.7 cc/mol), and also very similar to the value obtained by Stolper et al. (1987) for the molar volume of molecular CO_2 dissolved in albite (28.6±0.5 cc/mol).

1.6.6 Temperature dependence of CO_2 solubility

Isotherms of CO_2 solubility in rhyolitic melt calculated using the thermodynamic parameters listed above are plotted in Fig. 1-5 and illustrate the inverse correlation between solubility and temperature. Data from this study and corrected data from Fogel and Rutherford (1990) are included for comparison. The temperature dependence of CO_2 solubility in rhyolitic melt is pronounced. For example, sample GB1-8 equilibrated at 500 bars and 750°C contains 25% more dissolved CO_2 than sample GB1-26 equilibrated at 500 bars and 850°C. The effect of temperature on solubility diminishes as temperature increases, as can be seen by comparing the differences in CO_2 solubilities between isotherms at a constant pressure.

1.6.7 Comparison of CO_2 solubility in rhyolite and basalt

The most distinctive difference between the solubility behavior of CO_2 in rhyolitic and basaltic melts at relatively low pressures is the mode of speciation, and this is readily observed through FTIR analysis. CO_2 dissolves in rhyolitic melt in molecular form, with a

single IR absorbance band at 2350 cm^{-1} whereas CO_2 reacts with basaltic melt to form carbonate ions (CO_3^{2-}). Carbonate in basaltic glass is identified by two absorption bands (attributed to a v_3 antisymmetric stretch) at 1515 and 1430 cm^{-1} (Fine and Stolper, 1986). These two dissolved species of CO_2 are labeled in Fig. 1-6, which illustrates spectra of a rhyolitic and a basaltic glass with roughly equal quantities of dissolved CO_2 (i.e., 115 ppm CO_2 in the rhyolitic sample; 100 ppm CO_2 as CO_3^{2-} in the basaltic glass). The difference in CO_2 speciation is consistent with a trend of a decreasing ratio of CO_3^{2-}/CO_2 with increasing silica activity observed by Fine and Stolper (1985) for glasses along the $NaAlO_2$-SiO_2 join. Fogel and Rutherford (1990) concluded that a similar relation between CO_3^{2-}/CO_2 ratios and silica activity exists for natural melts based on unpublished data on CO_2 dissolved in basalt, andesite, and rhyodacite.

Previous workers (e.g., Eggler and Rosenhauer, 1978; Mysen et al., 1976) have suggested differences in speciation should influence the degree of CO_2 solubility in these melts, favoring higher solubility in basaltic melt. The data presented here can be compared directly with those of Pan et al. (1991), who quantitatively measured CO_2 solubility in basaltic melt at 1170-1600°C and 1-15 kbar[1]. As shown in Fig. 1-7, CO_2 has a higher solubility in basaltic melt at 1200° than in its silicic counterpart (580 vs. 360 ppm at 1000 bars).

However, because the temperatures of rhyolitic melts in their natural setting are considerably lower (700-750°C; e.g., Bacon, 1977) than for basalts, rhyolites would actually favor a higher CO_2 solubility for any given depth. For example, at P_{CO_2} = 1000 bars, a basaltic melt at 1200° will contain 580 ppm CO_2 whereas a rhyolitic melt at the same pressure and 750°C will contain about 890 ppm CO_2.

---

[1] There have in fact been several recent studies of CO_2 solubility in basaltic melt. Initially, I compared my data with those of Stolper and Holloway (1988) on CO_2 solubility in basalt at 1200°C and pressures to 1500 bars. However, Dixon (1992) has recently shown that, on the basis of improved background-fitting techniques, the concentrations determined by Stolper and Holloway (1988) by IR anlaysis should be ≈ 30% higher than reported. Pan et al. (1991) and, more recently, Pawley et al. (1992) report similar CO_2 solubilities that are roughly 30% higher than the published results of Stolper and Holloway.

CO_2 solubility in rhyolitic melts exhibits a much greater temperature dependence than in basaltic melts. For example, Pan et al. (1991) observed no temperature dependence at 1170-1600°C for CO_2 solubility in basaltic melts, whereas I have found a substantial temperature dependence in rhyolitic melt. Also included in Fig. 1-7 are data for CO_2 solubility in rhyolitic melt (Chapter 4) not used in the thermodynamic treatment in this chapter. The close agreement between calculated and measured solubilities of rhyolite at 1200°C and 1000 bars is encouraging.

1.6.8 Application to natural rhyolitic systems

Initial studies of degassing of silicic magmas focused on the role of water (e.g., Taylor et al., 1983). This was due in part to the much (an order of magnitude) higher water concentrations in erupted silicic lavas and the inherent difficulty in measuring small (ppm) quantities of dissolved CO_2.

Armed with solubility data and a method for quantitative IR evaluation of volatile species, concentrations of both CO_2 (Blank et al., 1989; this study) and water (Newman et al., 1986; Silver et al., 1990) can now be evaluated in natural rhyolites. Recent FTIR spectroscopic investigations by Newman et al. (1988) provided the first examination of both dissolved CO_2 and H_2O in rhyolitic glasses. These authors observed a positive correlation between water and CO_2 contents and, using models relying on knowledge of CO_2 and H_2O solubilities in rhyolitic melts, demonstrated that the measured volatile concentrations could be explained by variable degrees of degassing.

The low solubility of CO_2 in silicic magmas at crustal pressures (Holloway, 1976), and a potential source of CO_2 from associated underlying basaltic magmas (Hildreth, 1981) suggests that a CO_2-rich vapor could coexist with the melt throughout its ascent and emplacement in the crust. Interpretation of CO_2 and H_2O analyses of melt inclusions within individual phenocrysts suggests that a variety of processes operated in the

preeruptive magma during crystallization of the host phenocryts. Anderson et al. (1989) and Skirius (1990) have outlined the significance of variation of CO_2 and H_2O in melt inclusions and have identified 5 principal factors that may control observed CO_2/H_2O in melt inclusions: (1) gas saturation, (2) gas retention (or loss), (3) mass fraction of gas, (4) crystallization, and (5) decompression. As a consequence of the strong partitioning of CO_2 relative to H_2O into a coexisting equilibrium gas phase, initially exsolved gas from a CO_2-poor (100s of ppm) melt will be CO_2-rich with tens of wt% CO_2. It is expected therefore that the CO_2/H_2O ratio of residual melt will decrease during the evolution of a gas resulting from decompression or gas-saturated crystallization. The extent of decrease in the CO_2/H_2O ratio of the melt will depend on whether the system is open or closed, the amount of gas (if closed), and the degree of decompression and crystallization.

CO_2 solubility data can be used to estimate the CO_2 content of magmas at a given temperature and pressure. These solubility relations permit the use of measured volatile contents of natural rhyolites to infer depths of equilibration prior to their eruption. As an example, volatile contents of rhyolitic melt inclusions in quartz grains from the youngest Toba tuff eruption (74,000 years b.p.; Chesner et al., 1991) are compared with isobaric curves (Fig. 1-8) calculated for the inferred melt temperature of these natural glasses (750°C, cf. Newman and Chesner, 1989). Solubility information is used to determine minimum trapping pressures of the melt inclusions (*minimum* because melt inclusions could have been vapor-undersaturated when trapped in crystals). CO_2 is much less soluble than H_2O in silicate melts at high pressures and therefore a more sensitive indicator of the conditions during early stages of degassing. Equilibrium vapor-saturation curves in Fig. 1-8 delineate the composition of vapor in equilibrium with rhyolitic melt at specified temperatures and pressures and can be used to predict the depth at which the inclusion was enclosed in its host phenocryst. These calculations assume Henrian behavior of the two gas species and use CO_2 and H_2O fugacities determined by a modified Redlich-Kwong

equation of state (Holloway, 1977). In Fig. 1-8, the highest entrapment pressure for the Toba tuff melt inclusions (≈ 2300 bars) corresponds to the sample with the highest CO_2 content. The concentrations of all of the inclusions appear to be related by variable degrees of open-stage degassing, as indicated by the dashed line in the figure.

Although water is the dominant volatile component in rhyolite (note that CO_2 concentrations are in ppm in Fig. 1-8, H_2O in wt%), the CO_2 content is an important consideration in estimating pressures. If water contents alone were considered, inferred equilibration pressures would be up to 700 bars lower for the Toba samples. As indicated by the isobaric curves in Fig. 1-8, melt inclusions with similar H_2O contents but variable CO_2 concentrations were probably trapped at significantly different depths. At these low pressures (<3 kbars), the use of vapor solubilities is a more sensitive indicator than mineralogic geobarometers.

1.7 Conclusions

1. The IR absorption band for molecular CO_2 in rhyolitic melt was calibrated against manometry; its molar absorptivity coefficient, ε_{2350}, has a value of 1066±20 g/cm^{-1}, which is ≈ 15% greater than the value for CO_2 dissolved in molecular form in jadeite glass (Fine and Stolper, 1985). This calibration allows for the first time accurate determinations of CO_2 concentrations in rhyolitic glasses using IR spectroscopy.
2. The equilibrium CO_2 solubility of in rhyolitic melt was determined experimentally at 750-850°C and 200-1444 bars. The behavior of CO_2 in rhyolitic melt is approximately ideal over the low pressures of this study. At pressures up to ≈ 1300 bars, the Henrian behavior is linear.

3. Thermodynamic treatment of the experimental data yield values for $v^{o,m}_{CO_2}$ of 28.1±1.6 cc/mol and for $\Delta H^{o}_{CO_2}$ of -27.1±2.0 Kjoules/mol. These results were used to develop an equation for the solubility of CO_2 as a function of T and P.
4. The solubility of CO_2 in rhyolite is ≈ 30% lower than in basalt at 1200°C at pressures up to 1500 bars.
5. Its low solubility in rhyolitic melt makes CO_2 a sensitive indicator of degassing processes. Knowledge of CO_2 and H_2O solubilities coupled with IR measurements of both CO_2 and water in melt inclusions of natural samples provide important constraints on degassing styles (e.g., open- vs. closed-system) and can be used to study magmatic differentiation and zonation with in high-level silicic magma chambers.

1.8 References

Anderson A. T. Jr., Newman S., Williams S. N., Druitt T. H., Skirius C. and Stolper E. (1989) H_2O, CO_2, Cl and gas in plinian and ash-flow Bishop rhyolite. *Geology* **17**, 221-225.

Atkins P. T. (1986) *Physical Chemistry*. W.H. Freeman & Co.

Bacon C. R. (1977) High temperature heat content and heat capacity of silicate glasses: Experimental determination and a model for calculation. *Amer. Jour. Sci.* **277**, 109-135.

Bacon C. R., Newman S. and Stolper E. (1988) Preeruptive volatile content, climatic eruption of Mount Mazama, Crater Lake, Oregon. *(abstr.). Geol. Soc. Amer. Abstr. with Prog.* **20**, A248.

Barker C. and Torkelson B. E. (1975) Gas adsorption on crushed quartz and basalt. *Geochim. Cosmochim. Acta* **39**, 212-218.

Blake S. (1984) Volatile oversaturation during the evolution of silicic magma chambers as an eruption trigger. *J. Geophys. Res.* **89**, 8237-8244.

Blank J. G., Stolper E. M., Sheng J. and Epstein S. (1989) The solubility of CO_2 in rhyolitic melt at pressures less than 1500 bars. *(abstr.). Geol. Soc. Amer. Abstr. with Prog.* **21**, A157.

Carroll M. R. (1991) Diffusion of Ar in rhyolite, orthoclase and albite composition glasses. *Earth Planet. Sci. Lett.* **103**, 156-168.

Chesner C. A., Rose W. I., Deino A. and Drake R. (1991) New $^{40}Ar/^{39}$ Ar dates of the Toba Tuff and caldera complex, Sumatra, Indonesia. *Geology*

Des Marais D. J. (1978) Variable temperature cryogenic trap for the separation of gas mixtures. *Anal. Chem.* **50**, 1405-1406.

Des Marais D. J. and Moore J. G. (1984) Carbon and its isotopes in mid-oceanic ridge basaltic glasses. *Earth Planet. Sci. Lett.* **69**, 43-57.

Dixon J. E. (1992) Water and Carbon Dioxide in Basaltic Magmas. Ph.D. dissertation, California Institute of Technology.

Dobson P. F., Epstein S. and Stolper E. M. (1989) Hydrogen isotope fractionation between coexisting vapor and silicate glasses and melts at low pressure. *Geochim. Cosmochim. Acta* **53**, 2723-2730.

Dunbar N. W., Hervig R. L. and Kyle P. R. (1989) Determination of pre-eruptive H_2O, F, and Cl contents of silicic magmas using melt inclusions: Examples from the Taupo volcanic center, New Zealand. *Bull. Volcanol.* **51**, 177-184.

Eggler D. and Rosenhauer M. (1978) Carbon dioxide in silicate melts: II. Solubilities of CO_2 and H_2O in $CaMgSi_2O_6$ (Diopside) liquids and vapors at pressures to 40 kb. *Amer. Jour. Sci.* **278**, 64-94.

Fine G. and Stolper E. (1985) The speciation of carbon dioxide in sodium aluminosilicate glasses. *Contrib. Mineral. Petrol.* **91**, 105-121.

Fine G. and Stolper E. (1986) Dissolved carbon dioxide in basaltic glasses: Concentrations and speciation. *Earth Planet. Sci. Lett.* **76**, 263-278.

Fogel R. A. and Rutherford M. J. (1990) The solubility of carbon dioxide: A quantitative FTIR study. *Amer. Mineral.* **75**, 1311-1326.

Hildreth W. (1981) Gradients in silicic magma chambers: implications for lithospheric magmatism. *J. Geophys. Res.* **86**, 10,153-10,192.

Holloway J. R. (1976) Fluids in the evolution of granitic magmas: Consequences of finite CO_2 solubility. *Geol. Soc. Amer. Bull.* **87**, 1513-1518.

Holloway J. R. (1977) Fugacity and activity of molecular species in supercritical fluids. In *Thermodynamics in Geology* (ed. D. Fraser). pp. 161-181. D. Reidel.

Kadik A. A. and Lukanin O. A. (1985) Paths of mantle outgassing during melting: The role of partial melting of upper mantle rocks in the evolution of fluid composition and redox regime. *Int. Geol. Rev.* **27**, 563-572.

Mathez E. A. (1984) Influence of degassing on oxidation states of basaltic magmas. *Nature* **310**, 371-375.

Mathez E. A. and Delaney J. R. (1981) The nature and distribution of carbon in submarine basalts and peridotite nodules. *Earth Planet. Sci. Lett.* **56**, 217-232.

Mattey D. P., Carr R. H., Wright I. P. and Pillinger C. T. (1984) Carbon isotopes in submarine basalts. *Earth Planet. Sci. Lett.* **70**, 196-206.

Mattey D. P., Exley R. A. and Pillinger C. T. (1989) Isotopic composition of CO_2 and dissolved carbon species in basalt glass. *Geochim. Cosmochim. Acta* **53**, 2377-2386.

Moore J. G., Bachelder J. N. and Cunningham C. G. (1977) CO_2-filled vesicles in mid-ocean basalt. *J. Volcanol. Geotherm. Res.* **2**, 309-327.

Mysen B. O., Eggler D. H., Seitz M. G. and Holloway J. R. (1976) Carbon dioxide solubilities in silicate melts and crystals. Part I. Solubility measurements. *Amer. Jour. Sci.* **276**, 455-479.

Newman S. and Chesner C. (1989) Volatile compositions of glass inclusions from the 75 Ka Toba Tuff, Sumatra. *Geological Society of America Abstracts with Programs* **21**, A271.

Newman S., Epstein S. and Stolper E. (1988) Water, carbon dioxide, and hydrogen isotopes in glasses from the ca. 1340 A.D. eruption of the Mono Craters, California: Constraints on degassing phenomena and initial volatile content. *J. Volcanol. Geotherm. Res.* **35**, 75-96.

Newman S., Stolper E. M. and Epstein S. (1986) Measurement of water in rhyolitic glasses: Calibration of an infrared spectroscopic technique. *Amer. Mineral.* **71**, 1527-1541.

Pan V., Holloway J. R. and Hervig R. L. (1991) The pressure and temperature dependence of carbon dioxide solubility in tholeiitic basalt melts. *Geochim. Cosmochim. Acta* **55**, 1587-1595.

Pawley A. R., Holloway J. R. and McMillan P. (1992) The effect of oxygen fugacity on the solubility of carbon-oxygen fluids in basaltic melt. *Earth Planet. Sci. Lett.* **110**, 213-225.

Prausnitz J. M., Lichtenthaler R. N. and Gomes de Azevedo G. (1986) *Molecular Thermodynamics of fluid-phase equilibria.* Prentice-Hall.

Silver L. A., Ihinger P. D. and Stolper E. (1990) The influence of bulk composition on the speciation of water in silicate glasses. *Contrib. Mineral. Petrol.* **104**, 142-162.

Skirius C. M. (1990) Pre-eruptive H_2O and CO_2 content of plinian and ash-flow Bishop Tuff magma. Ph.D. dissertation, University of Chicago.

Sommer M. A. (1977) Volatiles H_2O, CO_2, and CO in silicate melt inclusions in quartz phenocrysts from the rhyolitic Bandelier air-fall and ash-flow tuff, New Mexico. *Jour. Geol.* **85**, 423-432.

Spera F. J. and Bergman S. C. (1980) Carbon dioxide in igneous petrogenesis: I. Aspects of the dissolution of CO_2 in silicate liquids. *Contrib. Mineral. Petrol.* **74**, 55-66.

Stolper E., Fine G., Johnson T. and Newman S. (1987) Solubility of carbon dioxide in albitic melt. *Amer. Mineral.* **72**, 1071-1085.

Stolper E. M. and Holloway J. R. (1988) Experimental determination of the solubility of carbon dioxide in molten basalt at low pressure. *Earth Planet. Sci. Lett.* **87**, 397-408.

Tait S. and Jaupart C. (1990) Dynamics of eruptive phenomena. *Rev. Mineral.* **24**, 125-152.

Taylor B. E., J.C. Eichelberger and Westrich H. R. (1983) Hydrogen isotope evidence of rhyolitic magmas degassing during shallow intrusion and eruption. *Nature* **306**, 541-545.

Tuttle O. F. (1949) Two pressure vessels for silicate-water studies. *Geol. Soc. Amer. Bull.* **60**, 1727-1729.

Vogel T. A., Mills J. G. Jr., Aines R. D. and Merzbacher C. I. (1989) Pre-eruptive volatiles in a chemically zoned magma body based on melt inclusions. *(abstr.). Geol. Soc. Amer. Abstr. with Prog.* **21**, A271.

Wright I. P. and Pillinger C. T. (1989) Carbon isotopic analysis of small samples by use of stepped-heating extraction and static mass spectrometry. *U.S.G.S. Bulletin* **1890**, 9-34.

Zimmermann J.-L., Jambon A. and Guyetand G. (1988) Manometric and mass spectrometric analysis of fluids in geological materials. *Geochemical Journal* **22**, 9-21.

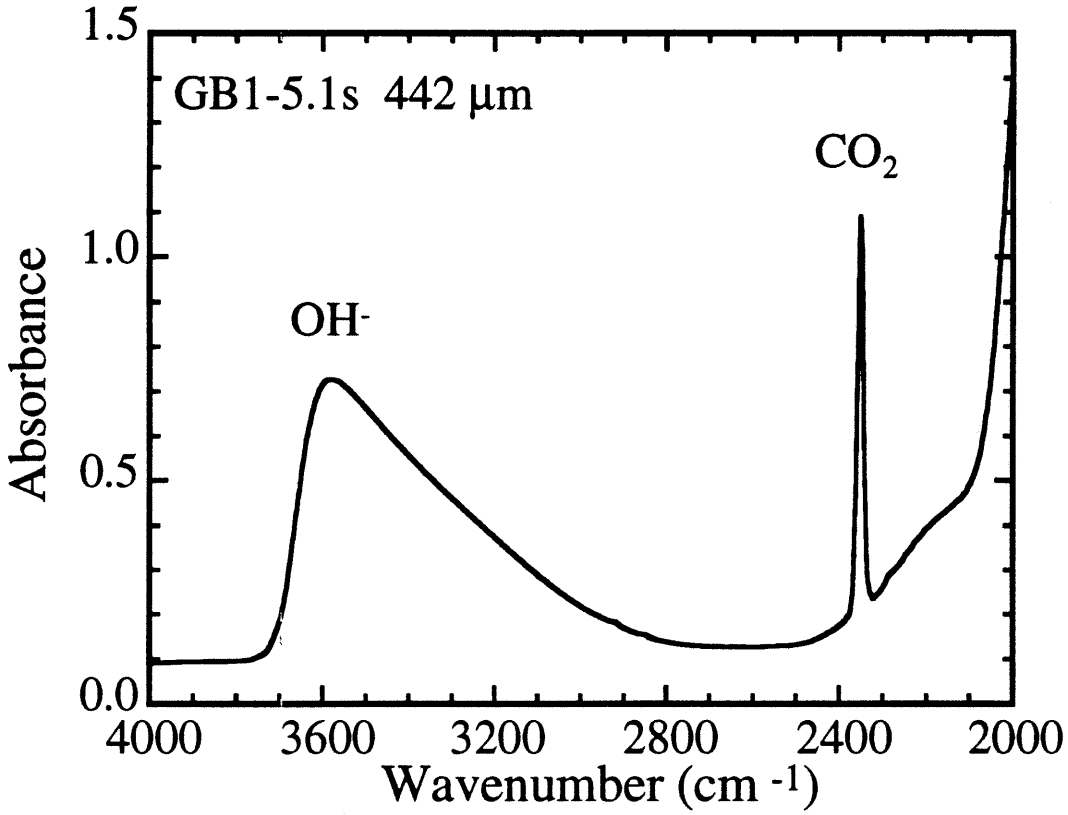

Fig. 1-1 IR spectrum of dissolved volatile species present in the experimental, CO_2-saturated rhyolitic glasses. The absorption peak at 2350 cm^{-1} corresponds to molecular CO_2 and is interpreted to be due to an antisymmetric stretch of $^{12}CO_2$ molecules. The absorption peak at 3550 cm^{-1} corresponds to hydroxyls and is due to a symmetric O-H stretch. Sample GB1-5.1 was a doubly-polished glass plate 422 μm thick containing 440 ppm CO_2 and 0.12 wt% water.

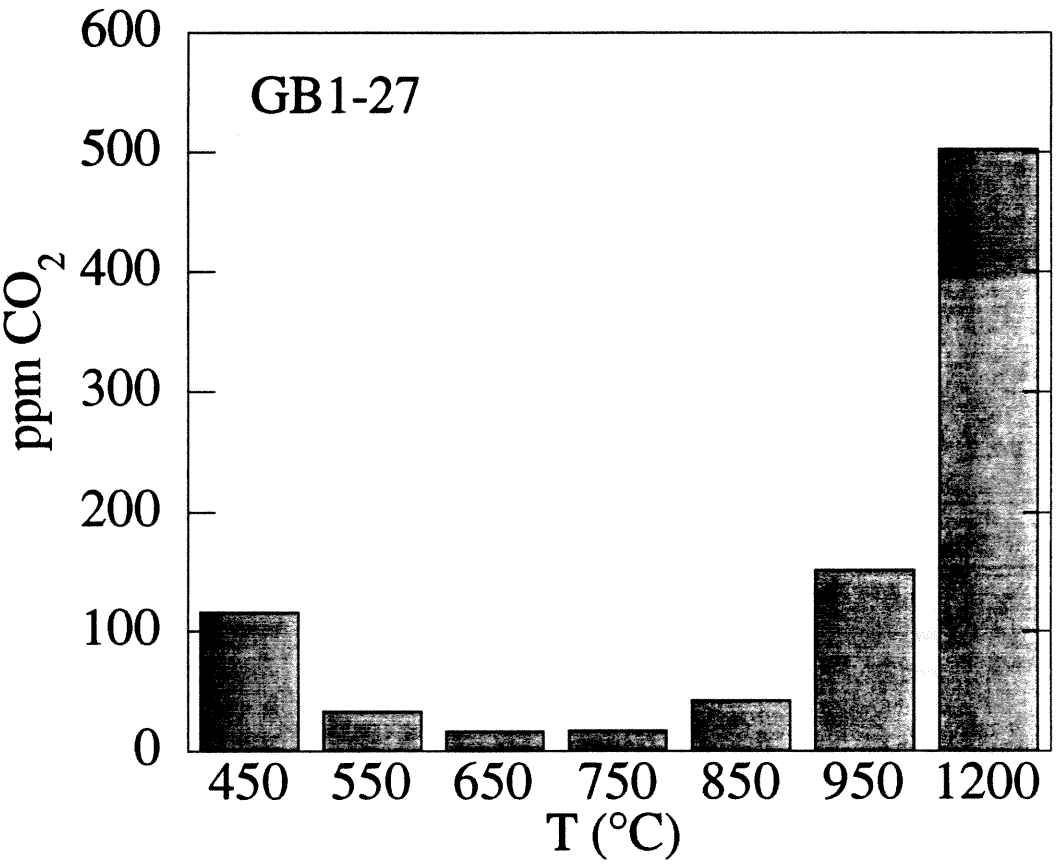

Fig. 1-2 A characteristic temperature-release profile of CO_2 extracted from rhyolitic glass determined by vacuum extraction and manometry. As was the case for all of the extracted samples, the majority of the CO_2 was liberated during the final, high-temperature heating step. The bulk of the CO_2 released below 650°C was recovered during the 450°C heating step. CO_2 released at T≤650°C (referred to as "low temperature" CO_2) is interpreted to be material adsorbed on the surface of the glass and CO_2 released at T>650°C ("high-temperature" CO_2) is interpreted to be the dissolved component (see text).

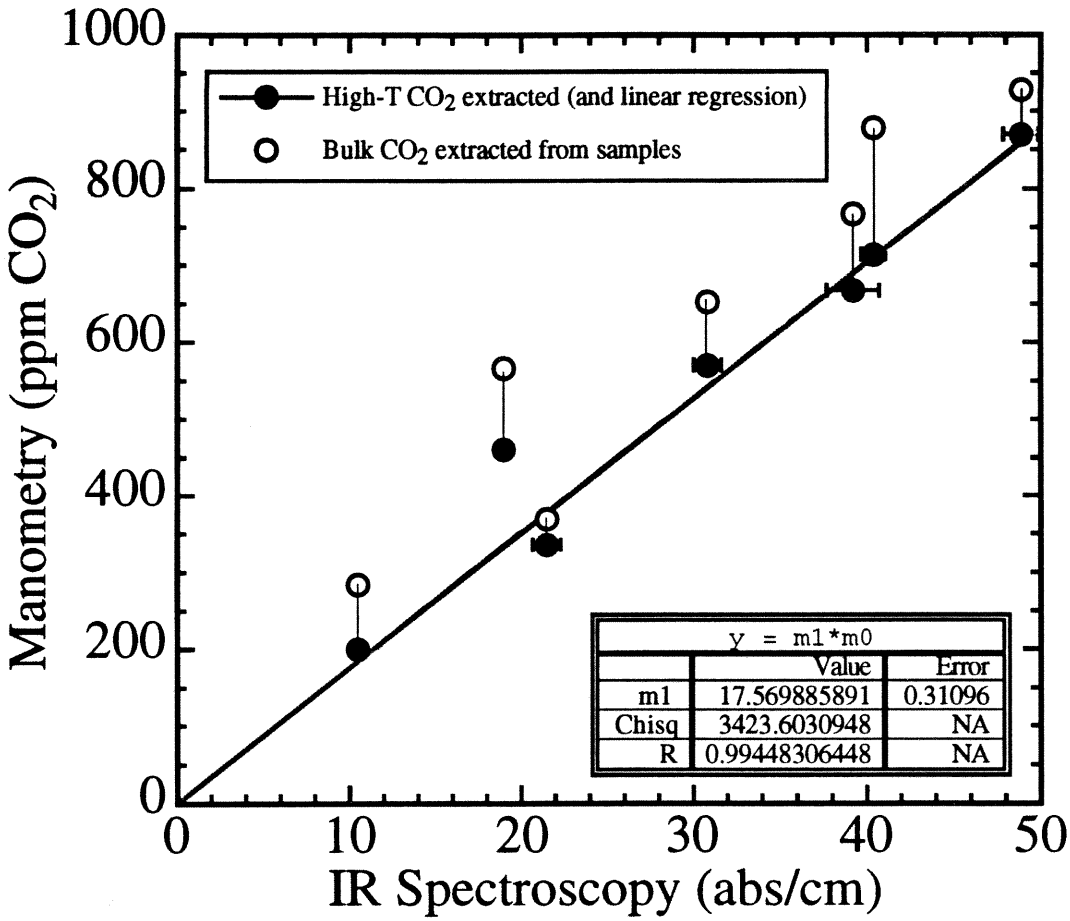

Fig. 1-3 Comparison of the height of the CO_2 absorption band at 3250 cm^{-1} normalized to sample thickness determined by FTIR spectroscopy with the manometric measurement of CO_2 released during vacuum pyrolysis or combustion of CO_2-saturated rhyolitic glasses (ppm). Solid circles indicate the high-temperature CO_2 fraction, open circles indicate bulk CO_2 extracted. The molar absorptivity coefficient for CO_2 dissolved in rhyolitic glass, ε_{2350}, is derived from the slope of the linear regression through the high-temperature data (straight line). Its value is 1066±20 l/(cm-mol). GB1-26 had an erroneously high manometric CO_2 yield; data for this sample was not included in the regression.

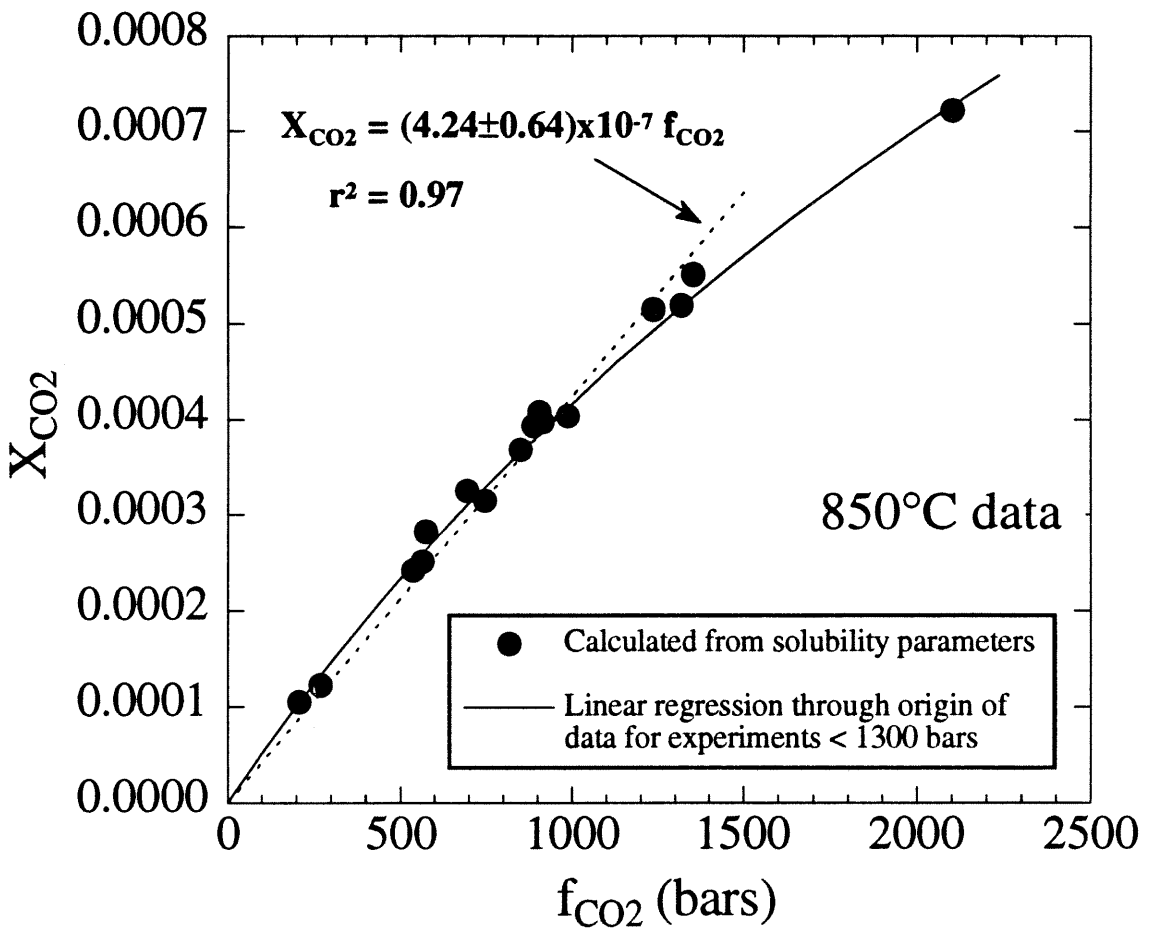

Fig. 1-4 Demonstration of Henry's law behavior for the 850°C CO_2 solubility data. Dashed line is a linear regression ($r^2 = 0.97$) through the origin of data with f_{CO2} < 1500 bars and illustrates the ideal behavior of CO_2 dissolved in rhyolitic melt at these low pressures. At higher f_{CO2}, pressure begins to have an effect on the CO_2 solubility behavior; this is shown by curvature of the predicted CO_2 solubility (solid curve) derived from thermodynamic treatment of the data.

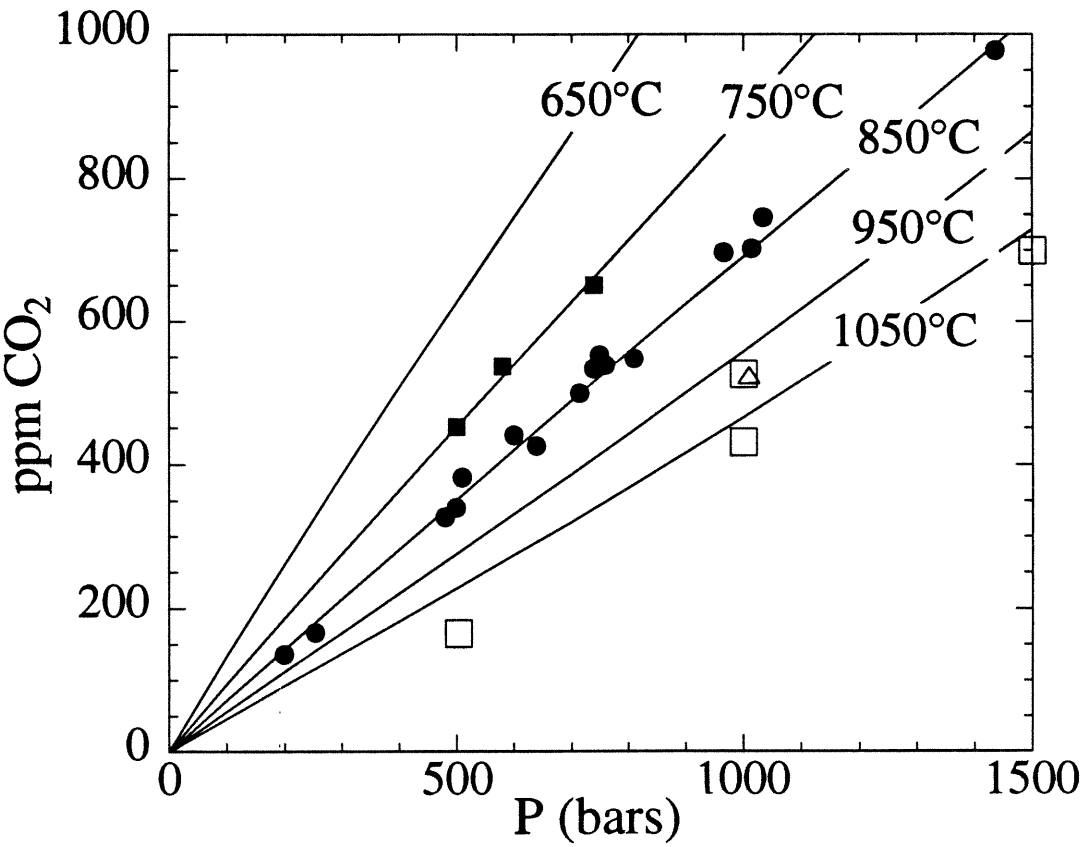

Fig. 1-5 Temperature dependence of CO_2 solubility in rhyolitic melt. Isothermal solubility curves were calculated using thermodynamic parameters derived from the CO_2 solubility data. Filled symbols indicate: 850°C data (circles), 750°C data (squares); open symbols represent 950°C datum (open triangle), and 1050°C data (open squares) from Fogel and Rutherford (1990). Higher-pressure data of Fogel and Rutherford are not shown.

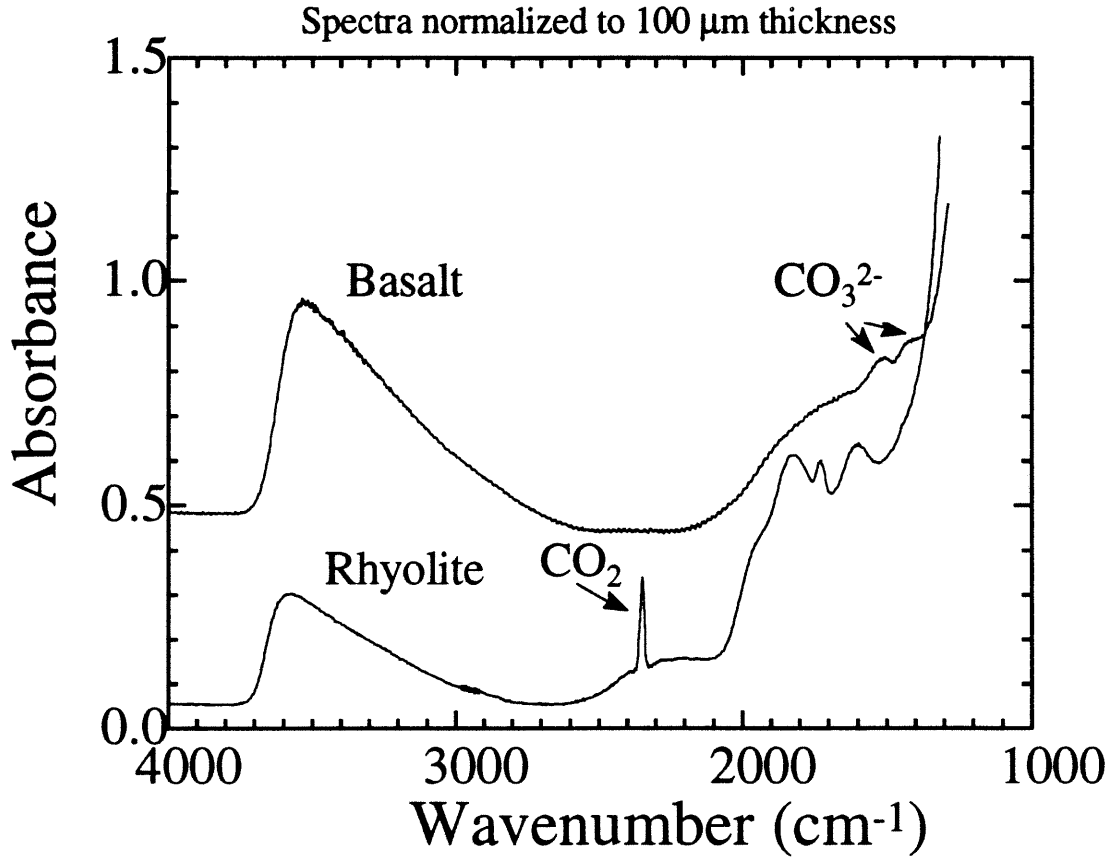

Fig. 1-6 Comparison of speciation of CO_2 dissolved in rhyolitic vs. basaltic melt. Spectra are normalized to 100 μm sample thickness. Basaltic glass (WOK28-3; Newman, unpublished) is from the Lau Basin and contains 100 ppm dissolved CO_2 (as CO_3^{2-}) determined by the magnitude of the carbonate absorption bands at 1515 cm^{-1} and 1430 cm^{-1} (Fine and Stolper, 1986). Rhyolitic glass (GB1-6P; Chapter 2) is a spectrum from a diffusion profile of rhyolitic melt with approximately the same amount (115 ppm) of dissolved CO_2 (as CO_2 molecules). Spectra are normalized to 100 μm sample thickness.

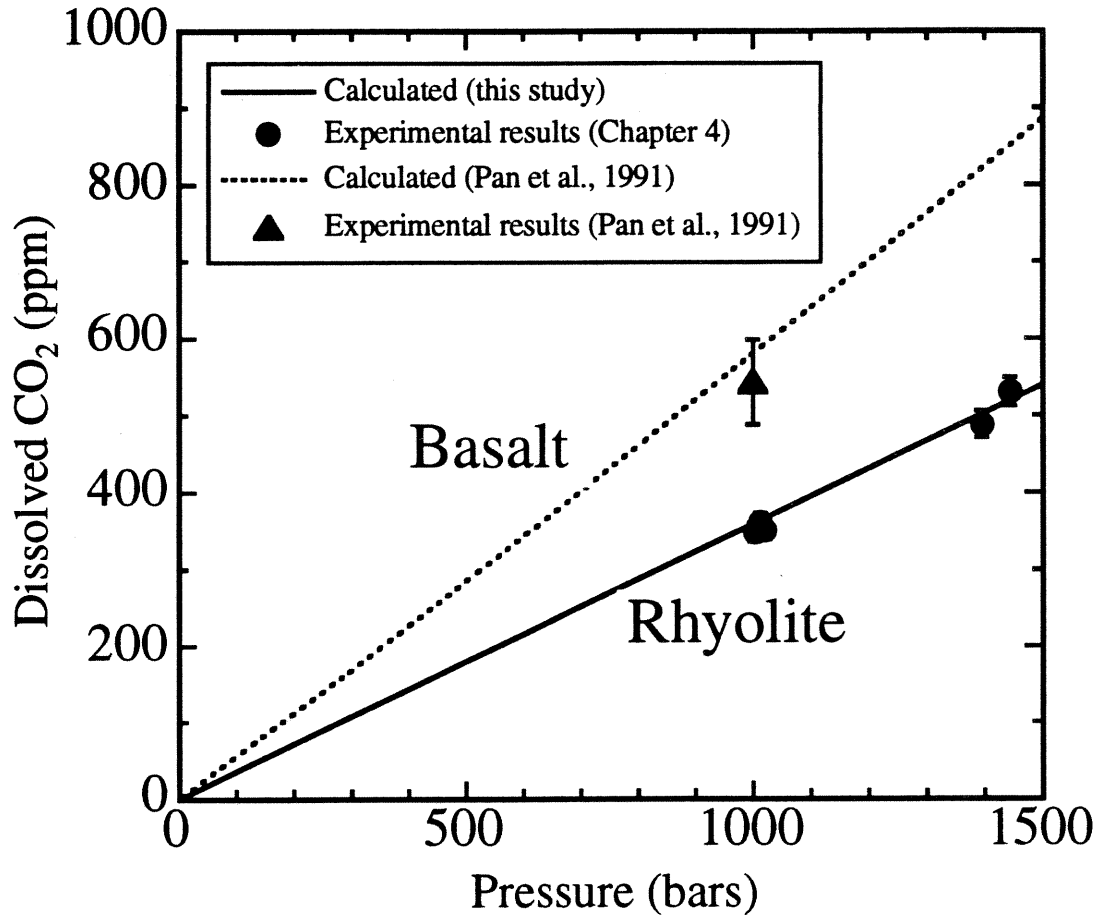

Fig. 1-7 Comparison of CO_2 solubility in rhyolitic and basaltic melts at 1200°C. Solubility curve for basalt (dashed line) was calculated using the thermodynamic parameters of Pan et al. (1991); filled triangle is a datum for their 1200°C solubility experiment. Solubility curve for CO_2 in rhyolitic melt was extrapolated to 1200°C using the thermodynamic parameters determined in this study. Closed circles represent samples used in CO_2-rhyolite isotope fractionation experiments at 1200°C (Chapter 4); these data were not used to derive the thermodynamic description of CO_2 solubility in rhyolitic melt as a function of P and T, and the good agreement gives confidence in the solubility model.

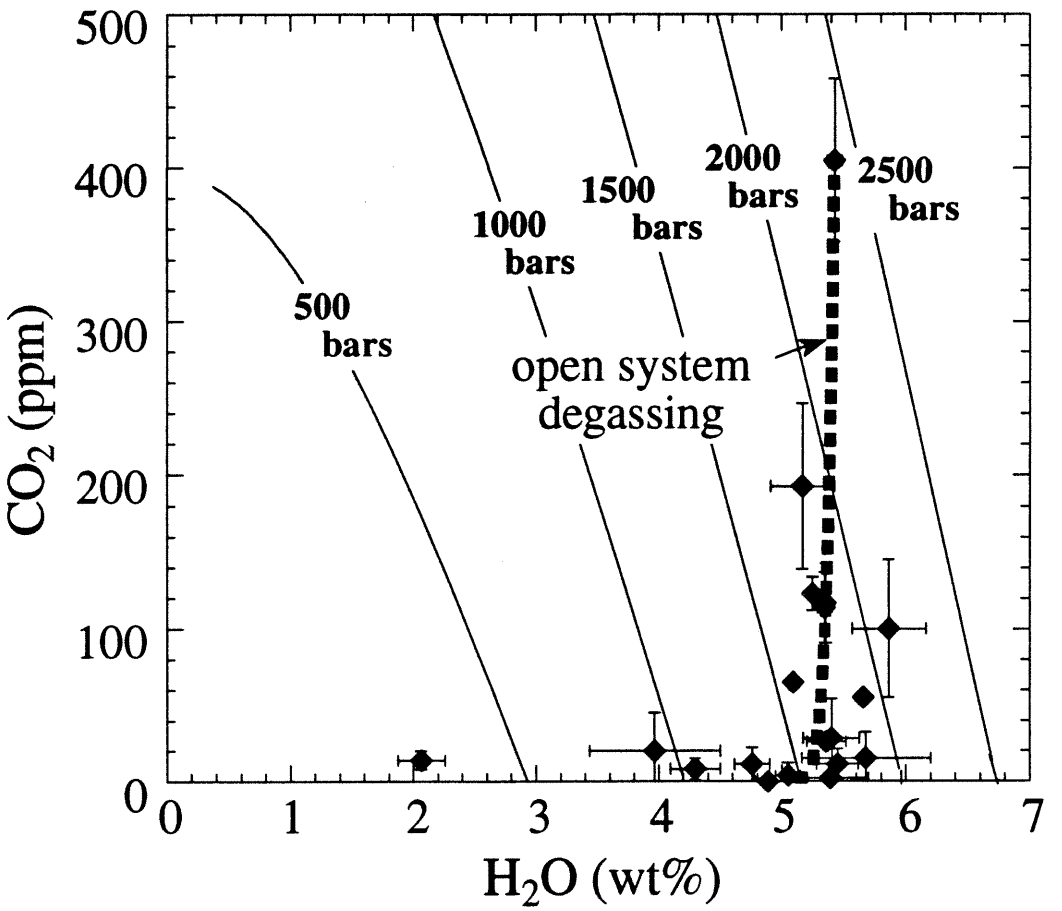

Fig. 1-8 Volatile concentrations in melt inclusions in quartz phenocrysts from the Youngest Toba Tuff (Unpublished data courtesy of S. Newman). Isobars are calculated vapor-saturation curves for CO_2 and H_2O in rhyolitic melt assuming ideal mixing. Dashed line indicates trend for open-system degassing.

Table 1-1 Major element composition of Glass Buttes starting material

Oxide	wt% [1]	wt% [2]
SiO_2	77.7	77.3
TiO_2	0.07	0.06
Al_2O_3	13	13
FeO*	0.38	0.75
MnO	0.04	0.03
MgO	0.05	0.05
CaO	0.52	0.52
Na_2O	4.08	4.12
K_2O	4.19	4.16
Σ	100.03	99.99

FeO* = total Fe as FeO.

[1] Microprobe analysis performed at Caltech (Dobson et al., 1989).

[2] Microprobe analysis performed at Universität Bayreuth (Carroll, 1991).

Table 1-2 Manometric measurement of CO_2 extracted from rhyolitic glasses by stepped-heating procedure

Sample	comments †	amount	T	time	yield	concentration
		g	°C	min	µmol CO_2 ¥	ppm CO_2
GB1-12a	a,c	0.4026	200	40	≈0	0
b			400	40	0.8	83
c			1125	90	5.2	570
GB1-13a	a,c	0.4258	250	40	0.2	22
b			400	40	0.4	36
c			1125	90	8.4	870
GB1-14a	a,c	0.4063	350	40	0.1	10
b			400	40	0.2	24
c			1125	90	3.1	336
GB1-17a	a,c	0.3791	250	40	0.2	22
b			450	40	0.4	42
c			520	40	0.2	27
d			600	40	0.1	9
e			1125	90	5.8	667
GB1-19a	b,d	0.4212	450	40	0.37	37
b			650	40	0.39	41
c			650	40	0.06	6
d			1200	90	1.91	200
GB1-26a	b,d	0.3992	450	40	0.86	95
b			550	40	0.02	2
"			650	40	0.08	9
c			750	40	0.18	20
d			850	40	0.31	34
e			950	40	0.30	33
f			1050	40	1.04	115
g			1200	90	2.35	259
GB1-27a	b,d	0.4231	450	40	1.12	116
b			550	40	0.32	33
c			650	40	0.15	16
d			750	40	0.16	17
e			850	40	0.40	42
f			950	40	1.46	152
g			1200	90	4.84	503

† a = sample analyzed by pyrolysis on low-sensitivity vacuum line; b = sample analyzed by combustion on new, high-sensitivy vacuum line; c = sample cleaned in ethanol prior to extraction; d = sample not cleaned.

¥ Sensitivity of manometers: Low-sensitivity manometer = 7 µmol/cm Hg displacement, reading error is 0.4 µmol.; High-sensitivity manometer = 3.5 cm Hg/µmol CO_2 , with a reading error of ±0.01 µmol.

Table 1-3 Manometric and FTIR spectroscopic analyses of CO_2 in rhyolitic glasses used for calibration

Sample	High-T Manometry [a] ppm CO_2	2350 cm^{-1} [b] abs/cm	1σ [c] abs/cm	chip thickness cm
GB1-12	570	30.8	0.8	0.0208
GB1-13	870	48.9	1.0	0.0189
GB1-14	336	21.5	0.8	.0219/0.0131
GB1-17	667	39.2	1.5	0.0344/.0120
GB1-19	200	10.5	0.0	0.0214
GB1-26	461	19.3	0.3	.0348/.0320
GB1-27	714	40.4	0.7	0.0205/.0159/.0133

[a] Based on CO_2 extracted from rhyolitic glasses at T>650°C.
[b] Mean abs/cm based on the number of spots analysed (See Table 1-4)
[c] 1σ from mean abs/cm

Table 1-4 Summary of Experimental Run Conditions and IR results

Sample	Experimental Conditions					FTIR RESULTS: Dissolved Volatile Contents				
	P	fCO_2¢	T	t	wt rhyolite	molecular CO_2		OH-		
GB1-	bars	*bars*	°C	hours	g	abs/cm 2350cm^{-1}	1σ	abs/cm 3550cm^{-1}	1σ	#chip, spots †
1	200	*209*	850	360	0.0828	8.053	0.210	8.042	3.053	1,6
3	715	*852*	850	158.1	0.1262	28.703	1.840	17.101	4.877	3,7
4	740	*888*	750	168.2	0.2340	37.447	0.000	15.82	1.214	1,3
5	600	*694*	850	166.4	0.1665	25.310	0.299	12.07	2.133	1,3
6	510	*576*	850	326.7	0.2635	21.973	0.690	25.53	2.127	1,3
7	580	*667*	750	503.9	0.2986	30.889	1.240	27.182	0.150	2,6
8	500	*563*	750	552.7	0.2113	26.000	0.010	26.17	1.096	1,4
9	740	*887*	850	573.5	0.2516	30.659	0.286	27.936	2.286	1,3
10	480	*538*	850	384.6	0.2516	18.810	0.290	13.206	2.028	1,3
11	760	*916*	850	336	0.2118	30.947	0.460	22.135	1.036	1,3
12	810	*989*	850	312.8	0.4167	31.464	0.800	26.424	4.596	1,3
13	1436	*2102*	850	214.6	0.4468	56.199	1.000	21.829	3.447	1,3
14	640	*747*	850	291.7	0.4228	24.504	0.800	12.638	6.893	3,8
17	966	*1238*	850	552	0.4167	40.093	1.500	18.328	3.444	3,7
18	1035	*1354*	850	744	0.4163	42.911	0.863	16.524	2.058	2,6
19	255	*271*	850	960	0.4589	9.549	0.115	43.658	6.893	1,3
26	500	*566*	850	527.17	0.4562	19.557	0.288	32.169	2.298	1,3
27	1015	*1319*	850	527.5	0.4564	40.380	0.345	14.693	2.298	2,6
28	750	*907*	850	527.25	0.5126	31.752	0.345	32.169	2.298	2,6

¢ Fugacities calculated using a modified Redlich-Kwong equation of state (Holloway, 1977).

† Indicates number of individual glass chips analyzed by IR spectroscopy, and the number of spectra collected.

Table 1-4 (Continued)

Sample	VOLATILE CONTENTS				comments
	CO_2 ¥		Water £		
GB1-	ppm	1σ, ppm	wt%	1σ, wt%	§
1	140	4	0.07	0.03	-
3	499	33	0.15	0.04	d
4	651	0	0.14	0.01	d
5	440	3	0.11	0.02	d
6	382	12	0.22	0.02	d
7	537	22	0.24	0.00	d
8	452	2	0.23	0.01	d
9	533	5	0.24	0.02	d
10	327	5	0.12	0.02	d
11	538	8	0.19	0.01	d
12	547	5	0.23	0.04	e,f
13	977	6	0.19	0.03	e,f
14	426	12	0.11	0.06	e,f
17	697	26	0.16	0.03	r 1250/966
18	746	15	0.14	0.02	r 1450/1035
19	166	2	0.38	0.06	e,f
26	340	5	0.28	0.02	e,f,r 1003/500
27	702	6	0.13	0.02	-
28	552	6	0.28	0.02	-

¥ CO_2 concentrations calculated using the molar absorptivity coefficient for CO_2 of 1066 l/c m-mol determined in this study, and assuming a constant glass density of 2350 g/l.

£ Water concentrations were determined using a molar absorptivity coefficient of 88 l/mol-cm (Dobson et al., 1988), assuming a constant glass density of 2350 g/l.

§ Many experiments were used for additional studies, as indicated by: d=diffusion, e=used for calibration, f=fractionation, r=isothermal reversal (sample was held at a higher pressure for 1 week, then lowered to the final pressure for the remainder of the experiment).

Chapter 2

The Diffusion of CO_2 in Rhyolitic Melts and Glasses

2.1 Introduction

There has recently been considerable interest in the diffusion of volatile components in silicate melts. This stems in part from the possibility that accurate values for diffusion coefficients of volatiles in melts can be used to quantify the degassing of magmas and to improve our understanding of fractionations that can occur between volatile components during degassing. Thus, for example, it is known that submarine basaltic liquids can erupt on the sea floor supersaturated with respect to CO_2-rich vapor under some circumstances (Moore, 1969) and that gradients in dissolved CO_2 can be present in glass adjacent to vesicles in submarine glasses (Metrich and Mosbah, 1988). These observations could be used to quantify timescales of depressurization and bubble-growth in magmas that erupt on the sea floor given knowledge of the diffusivity of CO_2 in basaltic melt. The conditions necessary for diffusive fractionations between volatile components during bubble growth were discussed by Watson et al. (1982). They determined the diffusivity of carbon dioxide in simple analogs of basaltic melts and showed that if water diffuses more slowly than carbon dioxide, as they thought likely, then exsolving vapor could be more carbon dioxide-rich than expected at equilibrium. Zhang and Stolper (1991) later showed that water actually diffuses faster than carbon dioxide in basaltic liquids but verified that diffusive fractionations (although opposite in sign from earlier predictions) could occur during degassing. Carroll (1991) applied measurements of the diffusivities of noble gases in silicate melts to evaluating the possibility that such diffusive fractionations could also influence ratios of rare gases in natural bubbles and glasses. Taylor (1986) and Anderson and Fink (1989) proposed that diffusive fractionations of this sort can occur in nature and that observed negative correlations between total water contents and D-H ratios in volcanic glasses from Hawaii and Mt. St. Helens result from such fractionations of H- relative to D-bearing species in degassing magmas.

There is also interest in understanding at a fundamental level the factors that influence the diffusivities of volatile components in geological materials. Such an understanding can contribute to a general framework for analyzing and quantifying diffusive phenomena in geological materials. For example, recent studies on glasses and melts have noted simple relationships between diffusion coefficients of neutral atomic and molecular species and their "radii" (e.g., Carroll, 1991; Jambon and Shelby, 1980; Zhang and Xu, 1993). These observations may relate to the hypothesis of Farver and Gilleti (1989) that "ionic porosity" exerts a significant control on diffusivities of neutral and ionic species in crystalline silicates. In another example, Zhang et al. (1991; 1993) emphasized the role of speciation in understanding the diffusion of volatile components in silicates and particularly the complexities that can be introduced if several species contribute to the flux of a single component. They showed that many experiments designed to measure oxygen "self diffusion" in silicates may have been dominated by oxygen carried by rapid diffusion of volatile components such as water and carbon dioxide molecules.

In this paper, I report on measurements of the diffusion coefficients of carbon dioxide in water-poor rhyolitic glass and melt at 450-1050°C, 500-1050 bars. The results are complementary to the studies of Fogel and Rutherford (1990) and Watson (1991) and are applicable to understanding concentration gradients in CO_2 in rhyolitic glasses and possible diffusive fractionations that could occur among various volatile species during degassing of rhyolitic magmas. In addition, since carbon dioxide is present nearly entirely as CO_2 molecules in rhyolitic glasses at low pressures (e.g., Newman et al., 1988), comparison of diffusivity in rhyolitic melts of this linear molecule with the diffusivity of more nearly spherical neutral atomic and molecular species can contribute to understanding mechanisms of diffusion in silicate melts.

2.2 Experiments

2.2.1 Starting materials

Rhyolitic glass used in the experiments was collected from Glass Butte, an extrusive dome in south central Oregon. The glass contains abundant microlites but lacks phenocrysts and vesicles. Major element concentrations are reported in Dobson et al. (1989). Based on infrared (IR) spectroscopic measurements described below, the starting material contains between 0.09 to 0.28 wt% water and no detectable CO_2.

Samples, prepared from a large hand sample, were cut into cylinders or rectangular prisms. Cylinders were 8 to 16 mm long and 3-5 mm in diameter, and the prisms were of similar size (Table 2-1). Cylinders used in the earliest experiments were not polished and their surfaces paralleling their long axes were smoothed as they were formed by a drill bit. Two parallel faces of each prism were ground and polished prior to an experiment with a final polish using 1 micron paper. The ends of two of the cylindrical samples (TZM5 and TZM6) were also polished. Prepared glasses were stored in a 110°C drying oven for at least 24 hours before being loaded into metal capsules.

Each sample was loaded into one of two types of pre-cleaned capsules 27 mm in length. Silver palladium (Ag_{25}-Pd_{75}) tubing (5.1 mm o.d./4.7 mm i.d.) was used for all experiments conducted at temperatures below 950°C. Each capsule, welded at one end, was soaked in 0.3 N nitric acid for 2 to 4 hours, heated in air at 850°C for 6 hours, then stored at 110°C prior to use. Platinum tubing (3.8 mm o.d./3.5 mm i.d.), used for the 950° and 1050°C experiments, was annealed in air at 1100°C for 3 hours, then stored at 110°C.

2.2.2 Experiments

All experiments were conducted in vertical cold-seal bombs made of René-41 (Ni-rich) steel (Tuttle, 1949) or a titanium-molybdenum-zirconium alloy (TZM; Williams, 1968) heated by an external furnace. Pressures were monitored with Heise bourdon tube gauges.

(1) The experiments in the René bombs followed the procedure initially described by Tuttle (1949) with hotspot down, an internal thermocouple, and a filler rod. Temperatures were monitored and controlled using a Type K thermocouple inside the bomb with its hotspot just above the sample. The temperature varied 5 to 8 °C over the length of the sample-bearing capsule. Capsules used in the René experiments were welded shut only at one end and pressurized using "bone dry" CO_2 gas. Samples were quenched by removing the bomb from the furnace and blasting it with compressed air followed by immersion in a water bath. The total time needed to cool the capsule to room temperature was approximately 4 minutes. (2) Higher-temperature (950-1050°C) experiments at pressures of 730 and 734 bars were conducted in a rapid-quench, TZM bomb assembly modeled after Ihinger (1991), in which the sample is magnetically levitated. Glass samples were sealed in Pt capsules with silver oxalate ($Ag_2C_2O_4$) as a source of CO_2, and the bomb assembly was pressurized with argon gas. Quenching was initiated by releasing a magnet, causing the sample to drop to a water-chilled region of the bomb where it cooled to room temperature in a few seconds. Temperature, monitored and controlled with a Type S thermocouple at the same level as the sample but outside the inconel sheath, varied less than 2°C along the length of the capsule. The temperature difference between the interior of the bomb where the capsule rested and the thermocouple monitoring point, was less than 10°C. After quenching, capsules produced an audible hiss when punctured, verifying that the seal had remained intact throughout the experiment.

The duration of experiments ranged from less than one day to approximately six weeks (Table 2-2). After each experiment, wafers were cut perpendicular to the long axis of the glass cylinder or prism near its center (Fig. 2-1) and ground and polished on both sides with a final polish using 1 μm grit polishing paper. The polished wafers ranged in thickness from 120 to 600 μm (Table 2-1).

2.3 Analytical methods

CO_2 concentration profiles perpendicular to the edge of a sample were measured from spectra taken with a Nicolet 60SX Fourier Transform Infrared (FTIR) spectrometer using a visible light source and an InSb detector. Spectra were obtained in the main sample compartment or in the microchamber compartment with a highly focused beam; no apparent differences were detected between spectra of the same sample made in the two compartments. Typically, 1024 scans were collected for each data point. All dissolved CO_2 was detected as CO_2 molecules, and relative abundances were determined from the height of the absorption band at 2350 cm^{-1} (Fine and Stolper, 1985).

The IR beam was aimed at portions of a sample using a circular aperture 37 μm in diameter for the cross sections of most of the cylindrical samples and some of the rectangular cross-sectional wafers. Slit apertures (10 x 500 μm and 20 x 1000 μm,) were used for the majority of the rectangular prisms (Table 2-1). Analyses at selected distances from the sample edge were obtained by repositioning the aperture after an analysis either manually or with a micrometer-driven stage (Zhang et al., 1991). The location of the circular aperture relative to the edge of a sample was determined with a micrometer eyepiece under the microscope and from photomicrographs taken before an analysis. The position of the slit relative to the sample was determined from the reading of the micrometer that drives the stage. In the latter case, it was difficult to see the edge of a sample under the microscope and accurately locate the edge of a sample. I compared the measurements made using the micrometer stage against those made without it by measuring CO_2 concentrations in 6 positions near the edge of samples GB1-22 and GB1-23 with a 10 x 1000 μm aperture slit positioned manually about a sample. I also compared, for GB1-4, the CO_2 concentrations determined using a slit versus a circular aperture by measuring 3 locations near the edge with a 10 x 1000 μm slit and the rest with a round aperture. The good agreement each time provided a check on the measurements of CO_2 concentrations near the

edge of samples where it is more difficult to position the aperture. Variations in thickness across a single sample was less than 10 μm. I estimate the uncertainty in the relative position of an aperture relative to a sample edge to be less than 10 μm based upon comparison between measurements made with the micrometer versus those made using a microscope.

Although diffusion coefficients can be determined from measured absorbance profiles without knowledge of the actual concentration of CO_2, absolute concentrations were calculated from the measured peak heights assuming a glass density of 2.35 g/cm^3 and a molar absorptivity of 1066 l/mol-cm (Chapter 1). Total water abundances were also determined at each point analyzed for CO_2. Absorbance (peak height) measurements were made for the fundamental -OH stretching vibration at 3550 cm^{62} and converted to water concentrations using an absorption coefficient of 88 l/mol-cm (Dobson et al., 1989).

Because the configuration of the FTIR requires that the sample compartment be exposed to the air each time the aperture is repositioned relative to the sample, atmospheric CO_2 in the sample chamber may interfere with the absorption due to CO_2 dissolved in the sample, even though the system was purged with N_2- or CO_2-H_2O-filtered air. This "background CO_2" contributes to the spectrum as two absorption bands centered at 2340 and 2360 cm^{-1} and, while its presence does not significantly affect the CO_2 measurements of samples with high CO_2 contents, it may contribute noticeably to spectra of samples with low CO_2 concentrations (< 30 ppm). I corrected for this interference by subtracting from each glass spectrum a reference spectrum of the empty sample chamber (which includes these two bands due to CO_2) scaled such that the two bands due to background CO_2 are minimized. The correction is typically on the order of 5 to 10 ppm CO_2. I was able to reproduce an absorption band height to within about 3 ppm CO_2 using this technique. CO_2 concentrations determined using this method agree with those obtained by lengthy purging of the chamber with dry N_2 to generally within 10% (the agreement is much better for

samples with higher CO_2 contents as this background correction is roughly the same for all samples of a given thickness). I estimate a CO_2 detection limit of approximately 3 ppm for a sample 100 μm thick.

Error in the reported CO_2 concentrations is a function of uncertainties contributed from measurements in sample thickness, height of the CO_2 absorbance peak, accuracy in measurement of the absorbance peak and, as noted above particularly for samples with low CO_2 contents, my ability to subtract the contribution of any residual atmospheric CO_2 from a spectrum. Zhang et al. (1991) showed that convolution effects due to the shape and dimensions of the aperture and to beam spreading are not detectable in these measurements. It follows that, for a given sample thickness, samples with lower CO_2 concentrations are subject to a larger percentage error than samples with higher CO_2 contents. Based on replicate analyses, the low-CO_2 (less than ≈ 10 ppm) measurements are reproducible to within 5 ppm.

2.4 Results

Details of individual experiments (pressures, temperatures, run duration) are given in Table 2-2, in order of increasing temperature. Lengths of the diffusion profiles varied from ≈80 to 2100 μm (Table 2-1), depending upon the duration and temperature of the run. The concentration of CO_2 in the center of all samples was below the detection limit, and I therefore assumed that CO_2 never penetrated the entire sample.

Although the highest run-temperatures were well above the glass transition for rhyolitic compositions (≈700°C, Bacon, 1977), none of the samples deformed during the experiments. Microlites present in the glass before heating were present in the same proportions after an experiment, and no color changes in the glasses were observed. I checked the melting temperature of low-water rhyolite by heating 0.5 g of glass (sieved to

500-1000 μm) in air in a 1-atmosphere furnace for 2 days. Under these conditions, the melting temperature of the Glass Butte rhyolite was found to be ≈ 1225°C.

2.4.1 Determination of diffusion coefficients

The CO_2 concentration profile for each experiment was used to determine values of D_{CO2}, the diffusion coefficient of CO_2 in rhyolitic glass. The depth of penetration of CO_2 into the samples relative to the half-width or diameter of a wafer was small, and I modeled my data using solutions for concentration-independent diffusion through a cylinder of infinite length or through a semi-infinite medium depending on the sample geometry (Crank, 1975). These solutions assume an infinite external reservoir and a constant surface concentration of CO_2, C_o, for all time, $t > 0$. The initial CO_2 content of the glass was taken to be zero.

For the cylindrical wafers, the following approximate solution was used:

$$C = C_o \sqrt{\frac{a}{r}}\ \mathrm{erfc}\left(\frac{a-r}{2\sqrt{D_{CO_2}t}}\right) \qquad \text{.....(2-1)}$$

where D_{CO2} is the diffusion coefficient, a the radius of the cylinder, r the radial distance from the surface, and C is the concentration of CO_2 in the glass at a given t and distance (a-r) from the reservoir of CO_2 vapor. Equation (1) is valid provided the value of r/a is not too small (Crank, 1975, p. 73). For all samples, the CO_2 concentration dropped to $^1/_e$ of the surface concentration by $^r/_a \geq 0.10$.

For the prismatic wafers, an exact solution to the diffusion equation was used :

$$C = C_o\ \mathrm{erfc}\left(\frac{x}{2\sqrt{D_{CO_2}t}}\right) \qquad \text{.....(2-2)}$$

where x is the distance from the edge of a sample.

Error function solutions were fit to the data using the method of least squares (Kreyszig, 1988). I did this in two ways. In one case, both C_o and D_{CO_2} were treated as unknowns. A value of C_o was chosen and then a best-fit value of D_{CO2} was obtained from a least-squares fit of $\text{erfc}^{-1}\ [(C/C_o)*(\sqrt{r}/a)]$ (for circular cross-sections) or $\text{erfc}^{-1}(C/C_o)$ (for rectangular cross-sections) against distance. I then evaluated the sum of the square of the residuals between values of C calculated from equations (1) or (2) using these values of C_o and D_{CO_2} and the data from a measured CO_2 concentration profile. This procedure was repeated until a minimum in the sum of the square of the residuals was obtained.

In the second case, C_o was fixed to the equilibrium CO_2 concentration at the P and T of an experiment as determined by Blank et al. (1989), who measured the solubility of CO_2 in Glass Butte rhyolite at 650-850°C. I used their solubility equation to constrain values of C_o at the temperatures of my experiments. With C_o fixed, values of D_{CO2} were obtained in a manner similar to that described above.

The calculated values of D_{CO2} and C_o appear in Table 2-2. Typical 1σ errors associated with profile fits are 1%. Calculated diffusion profiles are compared with those determined by IR spectroscopy in Fig. 2-2. The profiles calculated with fixed values of C_o are indicated by the dashed curves, and solid curves indicate the diffusion profiles calculated for the value of C_o determined by the data. Those with measured CO_2 concentrations of relatively constant spacing (μm) were determined using a micrometer stage; others were analyzed by positioning the sample about the aperture manually. With one exception described below, the two calculated values of D_{CO2} for each experiment are within 15%. Likewise, the values of C_o agree well, varying less than 12%. The best-fit value of C_o is generally lower than the calculated equilibrium CO_2 solubility value for samples run at temperatures <850°C.

For the sample run at 450°C (GB1-31), the value of C_o calculated from a best-fit to the data is 33% lower than the predicted equilibrium CO_2 solubility. For this sample, CO_2

diffusivities determined using the two values of C_0 differ by 37%. This difference in C_0 may reflect difficulties in measuring concentrations very close to the interface and the increased importance of such points in the fit to C_0 in shorter diffusion profiles. The discrepancy may also indicate that the temperature dependence of the solubility data is not as large as predicted.

2.4.2 Dependence of D_{CO_2} on temperature, pressure, and water content

The CO_2 diffusivities determined in my study increase dramatically with temperature and are well described by an Arrhenius relationship. D_{CO2} at 750°C, in the vicinity of the glass transition (~700°C; Bacon, 1977) does fall below the general trend in Fig. 2-3, and the linear relationship in Fig. 2-3 could arguably be described by two curves, above and below 750°C. However, the absence of a large break in slope in Fig. 2-3 suggests that the glass transition does not significantly influence D_{CO2}. Jambon (1982) and Mazer et al. (1991) came to similar conclusions regarding the diffusion of cations and water in rhyolite.

From the diffusion data for experiments in the range 715-734 bar and 550-1050°C, the temperature-dependence of D_{CO2} in rhyolitic melt is given as follows:

$$\ln D_{CO_2}\ (cm^2/s) = (-5.09 \pm 0.53) - (144{,}600 \pm 4100) / RT(K), \quad \text{.....(2-3)}$$

where R is the gas constant in Joules per mole, T the temperature in degrees Kelvin, and the activation energy for diffusion of CO_2 in rhyolitic melt is ≈ -145 kJ/mole. At 750°C (≈ 725 bars), $D_{CO2} = 2.55 \times 10^{-10}$ cm^2/s, and a characteristic diffusion length (~$\sqrt{Dt}$) for a 24 hour interval is approximately 50 μm. D_{CO2} values obtained using both a fixed value of C_0 and a value fit to the data were used to determine this expression for D_{CO2} as a function of temperature. I did not include the results obtained for the 450°C experiment (GB1-31) in the regression because of the uncertainties concerning the correct value of C_0. Including the

450°C data in the expression for ln D_{CO_2} lowers the activation energy slightly to -140 kJ/mol.

The effect of pressure on D_{CO2} is small. I observed a slight decrease in D_{CO2} with increasing pressure (Fig. 2-4), but this small pressure-dependence is poorly constrained by my data. Based on my limited data for D_{CO2} at different pressures, I predict that the activation volume, v_{CO2} is greater than 25 cm^3/mole for CO_2 dissolved in rhyolitic melt. Previous determinations derived from the pressure dependence of diffusion of dissolved CO_2 (as CO_3^{2-}) in synthetic basaltic melts suggest an activation volume of ≈11 cm^3/mole (Watson et al., 1982); for values on this order, changes in D_{CO_2} of only 5%, half the observed variation, would be expected over the 550 bar interval over which my data were collected.

The dissolved water content of glasses at the end of an experiment varied from 0.06-0.28 wt%. Concentrations of water (detected spectroscopically as -OH) decreased by 15-25% towards the edge of samples run in the René bombs and increased by approximately 5% from the center to the edge of samples from the two TZM experiments. If the confining vapor reservoir was pure CO_2, I would expect the water concentrations at the sample edge to be zero, but this was clearly not the case In the René experiments, rhyolite in an open capsule was exposed to the pressure medium. P_{H_2O} was fixed at the surface by the effective P_{CO_2} in the bone dry CO_2 and tubing. Water vapor would reduce the fugacity of CO_2 in the vapor, and the solubility of CO_2 in the melt might decrease as a consequence. For the TZM experiments, the sealed capsule is permeable to H_2 (not H_2O); P_{H_2} is fixed on both sides (diffusion of H_2 through Pt is fast relative to the time scale of the experiment); the presence of more than one volatile in the vapor phase ($H_2 \pm H_2O$) would also dilute the fugacity of CO_2.

Some effort was made to make the experimental assemblies water-free. Metal tubing connecting the bombs to the pressurizing gas were heated and then evacuated for

several hours prior to an experiment to remove adsorbed water from its inner walls. Bone dry gas (containing < 10 ppm H_2O; Bob Gable, Matheson Gas Products, personal communication, 1991) was used to pressurize my experiments. To check for the presence of water in the silver oxalate used in the TZM experiments, I decomposed a measured quantity of the material and measured the CO_2 by manometry and obtained a 99% yield. Despite these precautions, I was unable to avoid the presence of water in my samples. From the solubility of water in rhyolitic melt (Ihinger, 1991), I estimate that the mole fraction of CO_2 in the vapor was > 0.96 for every experiment. The water contents in my samples and those used by Blank et al. (1989) to determine CO_2 solubilities were similar, and presumably the small amounts of water in the experiments would affect the results of the two studies (conducted using the same apparatus) to a similar extent. I found no systematic covariation between D_{CO_2} and water content, and I have assumed that the presence of small amounts of H_2O in the vapor phase or dissolved in the melt does not have a significant effect on D_{CO2}.

2.4.3 Comparison with previous studies of CO_2 diffusion in rhyolite

I noted above that CO_2 diffusivities in rhyolitic melt exhibit a strongly positive temperature dependence over the 600°C interval of my study but the pressure dependence of D_{CO2} appears to be very slight. Diffusivities of CO_2 in rhyolitic melt at high-temperatures have been reported in two previous studies. Fogel and Rutherford (1990) conducted three TZM experiments at 1100° and 1 to 3 kilobars and used FTIR spectroscopy to measure acquired CO_2 concentrations in initially CO_2-free cylindrical rhyolitic glass samples. Fogel and Rutherford's values of D_{CO2}, estimated from the ratio $[CO_2]_{center}/[CO_2]_{edge}$ in their samples, (Crank, 1975, p. 74.), agree well with those reported here (Fig. 2-5).

Watson (1991) reported the results of a series of CO_2 diffusion experiments in rhyolitic melt at 10 kilobars containing variable water contents ranging from ≈0.2 to 11 wt.%. Using ß-active ^{14}C as a thin-source tracer deposited as aqueous Na_2CO_3 at one end of a rod-shaped glass sample, Watson determined diffusion profiles based on densitometer scans of ß-track maps made by exposing nuclear emulsion plates to quenched and sectioned diffusion capsules. His values of D_{CO2} for his nominally "dry runs" (those initially bearing < 0.2 wt% water), conducted at 1100 and 1000°C, also agree well with my results.

2.5 Discussion

2.5.1 Comparison with diffusivities of other, neutral molecular species

Previous workers have observed an increase in diffusion activation energies with increasing radius among species of similar charge (e.g., Anderson and Stuart, 1954; Carroll, 1991; Jambon, 1982; 1983; Lux, 1987; Zhang and Xu, 1993). This correlation is generally explained in terms of the elastic theory of diffusion, in which for neutral species the activation energy is a function of the shear modulus, the radius of the diffusing species, and a "gate radius" (a constant), the size of the space through which a diffusing species must pass in order to reach its next site in the matrix (Frenkel, 1955). In Fig. 2-6, I compare my calculated activation energy for CO_2 with data for He (Jambon and Shelby, 1980), Ne (Matsuda et al., 1989), Ar (Carroll, 1991), and H_2O (Zhang et al., 1991). Radii of the noble gases are from Dean (1985), based on nearest-neighbor distances in face-centered cubic crystals. The radius for molecular water is taken from Zhang et al. (1991) based on the O-O separation in hexagonal ice. These neutral species can be approximated by spheres, but the same is not necessarily true for CO_2 molecules because there are two large atoms in the molecule. CO_2 is linear so I estimated an "effective radius" for a CO_2 molecule by equating an expression for the translational diffusivity of two connected rigid spheres (representing the two oxygens in a CO_2 molecule) to an expression for diffusion of a single

sphere and solved for the radius of the sphere (cf., Fig. 2-6 caption; John Brady, personal communication, 1991). Use of alternative radii for CO_2, H_2O, and the noble gases shifts the points in Fig. 2-6, but the general trend remains the same.

2.5.2 Comparison with water diffusivities in rhyolitic melts

It has been proposed that the noble gases dissolve in holes in the glass structure (Doremus, 1973) and are only weakly interactive with their surroundings in a silicate framework. The diffusion coefficients of such species should be essentially independent of concentration. The good agreement between the behavior of CO_2 and the noble gases as shown in Fig. 2-6 and the fact that the measured CO_2 diffusion profiles can be described with simple error function solutions to the diffusion equation suggests that CO_2 dissolves into highly polymerized glasses almost entirely in its molecular form. This is in sharp contrast to water dissolved in rhyolitic melt, which is present as both hydroxyl and molecular species. The water diffuses almost exclusively as water molecules ($D_{H2O} \approx 10^6 D_{OH}$; Zhang et al., 1991), and this leads to a strong, positive dependence of the diffusion coefficient for bulk water (D_{water}^*) on the concentration of H_2O.

Diffusivities of CO_2 and bulk water (Zhang et al., 1991) for 0.2 wt% total water contents are compared in Fig. 2-7. Because the activation energy for bulk water diffusion (~80 kJ/mol at this total water content) is approximately half that of CO_2, D_{CO2} exhibits a greater dependence on temperature than D_{water}^*. This difference is due to the smaller size of water molecules as well as the influence of enthalpy change required for the reaction of water molecules with oxygens in the rhyolitic melt to produce hydroxyl groups. The two curves in Fig. 2-7 intersect at $\approx$ 1200°C, and at T<1200°C,, $D_{CO2} < D_{water}^*$. For these total water contents of about 0.2 wt%, D_{water}^* is approximately five times greater than D_{CO2} at 850°C, and about nine times greater at 750°C. The differences in diffusivities of molecular

water and CO_2 are even larger; $D_{H2O,molecular}$ is about 60 times greater than D_{CO2} at 850° and 95 times greater at 750°C (Zhang et al., 1991).

As the total water content and hence $[H_2O]/[OH]$ ratios approach zero, D_{CO2}/D_{water}^* becomes very large due to the very low value of D_{OH}. At temperatures of 750-850°C, typical of rhyolitic eruptions (Hildreth, 1981), however, only for total water contents less than about 0.02 wt% is CO_2 diffusion expected to be faster than bulk water diffusion. Such water contents are lower than the driest known obsidians (e.g., Newman et al., 1986) so it is likely that, even under conditions of dome extrusion or during the final stages of degassing of rhyolitic magma, the bulk diffusivity of water will exceed that of carbon dioxide.

Although bulk water diffusion is generally faster than carbon dioxide diffusion in water-poor melts, recent work suggests that most rhyolitic magmas at depth typically contain several wt% water and up to several thousand ppm carbon dioxide (e.g., Anderson et al., 1989; Skirius, 1990). The effects of increasing water contents on CO_2 and H_2O diffusivities can be examined by comparing these results with diffusion studies of samples with higher total water contents (Fig. 2-7). The Arrhenius curve for D_{CO2} at 3 wt% total water is estimated from the 10 kbar experiments of Watson (1991, Fig. 4), and D_{water}^* at 3 wt% total water is from Karsten et al. (1982) for experiments at 700 bars. Pressure effects on diffusivity have been ignored for simplicity. The differences in diffusivities of these two volatile species are greater at higher total water contents; the calculated value for D_{water}^* is 32 times greater than D_{CO2} at 750° and 18 times greater at 850°C. The marked increase in D_{water}^* relative to D_{CO2} at 3 wt% total water is due to the increased molecular water component in the more water-rich rhyolitic melts.

2.5.3 Comparison with diffusivities of dissolved CO_2 in basaltic melts

In Fig. 2-8, I compare the diffusivities of CO_2 and total water as a function of temperature in rhyolitic and basaltic melts with low water contents. The trend for basaltic melt was determined by Watson et al. (1982) for a synthetic, Fe-free basaltic analog. As indicated by the differences in slope of the two curves, the activation energy for CO_2 diffusion in rhyolite (-145 kJ/mol) is approximately 25% lower than that for dissolved CO_2 (as CO_3^{2-}) in the synthetic basalt (-195 kJ/mol; Watson et al., 1982). The absolute values of D_{CO_2} in rhyolite and basalt, however, differ by less than 5-12% over the 600°C temperature range of my study. This observation is surprising for several reasons. The chemical compositions and physical properties of these two melts are very different and this is reflected in the speciation of dissolved CO_2: in rhyolitic melts, CO_2 is present almost exclusively in molecular form, but in basalts it reacts to form carbonate ions (CO_3^{2-}; e.g., Fine and Stolper, 1985). The solubilities of CO_2 in the two melt compositions are also slightly different (Chapter 1), with CO_2 more soluble in the mafic melt.. The reasons for the similar diffusive behavior of CO_2 in rhyolite and basalt are unclear and may be coincidental at the relatively low pressures of these studies.

2.5.4 Influence of fractional diffusion on degassing

Magmas migrating toward the earth's surface release volatile species that are eventually incorporated into the atmosphere. The amount and composition of the escaping vapor depend upon several factors, including the solubility of different gas species in the melt, the rate at which the magma ascends, the nucleation and growth of bubbles and the rate at which these bubbles move through the magma. Growth rates of bubbles are dependent on the rates at which the dissolved volatile constituents migrate toward a bubble from their environment in the melt. Erupted lavas often contain an excess of volatiles relative to their

equilibrium volatile solubilities, suggesting that processes associated with dissolved volatile transport in a melt are slower than the rates of magma ascent and eruption. For example, rhyolitic glasses from the Mono Craters in California contain water and CO_2 in excess of their expected equilibrium solubilities (Newman et al., 1988). CO_2 contents of glassy rinds from submarine basalt pillow lavas and sheet flows are similarly supersaturated (e.g., Dixon et al., 1988; Stolper and Hollaway, 1988). Observed CO_2 gradients with decreasing CO_2 contents away from vesicle rims (Metrich and Mosbah, 1988) suggest that the "excess" CO_2 present in basaltic glasses is primarily a result of incomplete degassing.

Previous workers have used the ratios of CO_2 and H_2O in melt inclusions in trapped in phenocrysts to infer entrapment pressures assuming equilibrium degassing (e.g., Anderson et al., 1989; Newman and Chesner, 1989; 1990; Skirius, 1990), but Watson et al. (1982) and Zhang et al. (1991) have cautioned that fractional diffusion may influence observed CO_2/H_2O ratios and lead to erroneous estimates. Volatile transport is initially rate-limited by diffusion of these species from the melt into a bubble. The diffusivities of both volatile species are greater in basaltic liquids particularly because of the high liquidus temperature of molten basalt (≈1200°C). In water-poor basaltic melts, D_{CO2} and D_{water}^* are nearly equal (to within a factor of two or so; Watson et al., 1982; Zhang et al., 1991) at 1200°C, and therefore the effects of fractional diffusion will be modest. In natural rhyolitic melts on the other hand, typically containing a few wt% dissolved water, differences in diffusivities between CO_2 and total water are more pronounced and thus fractional effects will be more significant.

2.6 Summary and Conclusions

I examined the diffusive behavior of CO_2 in rhyolitic melt over a 600°C temperature interval (450-1050°C) at pressures of 500 to 1050 bars. While the small pressure dependence of CO_2 diffusion is difficult to determine over the small range in pressure (~550 bars)

investigated here, the temperature-dependence of CO_2 diffusivity is quite pronounced. For the experiments conducted at P_{CO2} of 715-744 bars, CO_2 diffusivity varies with temperature such that:

$$\ln D_{CO2}\ (cm^2/s) = (-5.09 \pm 0.53) - (144{,}600 \pm 4100) / RT(K), \quad \text{.....(2-4)}$$

where R is in Joules per mole.

The activation energy of CO_2 dissolved in rhyolitic melt (as molecular CO_2) is approximately 25% higher than that for dissolved CO_2 (as CO_3^{2-}) in basalts. This difference is not surprising in light of the fact that CO_2 is a neutral species and has a smaller partial molar volume than carbonate. The same reasoning can be applied to explain why there are differences in activation energy between CO_2 and molecular H_2O diffusing in rhyolite; the activation energy for H_2O diffusion in rhyolite is approximately 30% lower than for CO_2.

Absolute diffusivities of CO_2 in rhyolite and CO_2 (presumably as carbonate ions) in basalt are similar over the 500°C temperature interval of my study. This is unexpected because of the differences in the diffusing species as well as differences in melt compositions. The similarities may be coincidental.

The calculated activation energy for CO_2 is consistent with the positive correlation established between activation energy and radius for other neutral, more-spherical molecules. Because the diffusive behavior of CO_2 in rhyolitic melt appears to be similar to that of noble gases, dissolved CO_2 molecules may also interact only weakly with the silicate framework.

The results from this study are applicable toward understanding diffusive transport of CO_2 in magmas, diffusive fractionation of CO_2 and H_2O, and growth rates of CO_2-rich bubbles. Relatively slow rates of CO_2 diffusion may be responsible for non-equilibrium

CO_2 concentrations in melt inclusions and degassed magmas, and these new D_{CO2} values can be incorporated into detailed degassing models.

2.7 References

Anderson A. T. Jr., Newman S., Williams S. N., Druitt T. H., Skirius C. and Stolper E. (1989) H_2O, CO_2, Cl and gas in Plinian and ash-flow Bishop rhyolite. *Geology* **17**, 221-225.

Anderson O. L. and Stuart D. A. (1954) Calculation of activation energy of ionic conductivity in silica glasses by classical methods. *Journal of the American Ceramic Society* **37**, 573-580.

Anderson S. W. and Fink J. H. (1989) Hydrogen-isotope evidence for extrusion mechanisms of the Mount St. Helens lava dome. *Nature* **341**, 521-523.

Bacon C. R. (1977) High temperature heat content and heat capacity of silicate glasses: experimental determination and a model for calculation. *Amer. Jour. Sci.* **277**, 109-135.

Blank J. G., Stolper E. M., Sheng J. and Epstein S. (1989) The solubility of CO_2 in rhyolitic melt at pressures less than 1500 bars. *(abstr.). Geol. Soc. Amer. Abstr. with Prog.* **21**, A157.

Carroll M. R. (1991) Diffusion of Ar in rhyolite, orthoclase and albite composition glasses. *Earth Planet. Sci. Lett.* **103**, 156-168.

Crank J. (1975) *The Mathematics of Diffusion.* Clarenden Press.

Dean J. A. (1985) Lange's Handbook of Chemistry. p. 3-121.

Dixon J. E., Stolper E. and Delaney J. R. (1988) Infrared spectroscopic measurements of CO_2 and H_2O in Juan de Fuca ridge basaltic glasses. *Earth Planet. Sci. Lett.* **90**, 87-104.

Dobson P. F., Epstein S. and Stolper E. M. (1989) Hydrogen isotope fractionation between coexisting vapor and silicate glasses and melts at low pressure. *Geochimica Cosmochimica Acta* **53**, 2723-2730.

Doremus R. H. (1973) *Glass Science*. J. Wiley & Sons, Inc.

Farver J. R. and Giletti B. J. (1989) Oxygen and strontium diffusion kinetics in apatite and potential applications to thermal history determinations. *Geochim. Cosmochim. Acta* **53**, 1621-1631.

Fine G. and Stolper E. (1985) The speciation of carbon dioxide in sodium aluminosilicate glasses. *Contrib. Mineral. Petrol.* **91**, 105-121.

Fogel R. A. and Rutherford M. J. (1990) The solubility of carbon dioxide: a quantitative FTIR study. *Amer. Mineral.* **75**, 1311-1326.

Frenkel J. (1955) *Kinetic Theory of Liquids*. Dover.

Hildreth W. (1981) Gradients in silicic magma chambers: implications for lithospheric magmatism. *J. Geophys. Res.* **86**, 10,153-10,192.

Ihinger P. D. (1991) The interaction of water with granitic melt. Ph.D. dissertation, California Institute of Technology.

Jambon A. (1982) Tracer diffusion in granitic melts: experimental results for Na, K, Rb, Cs, Ca, Sr, Ba, Ce, Eu to 1300°C and a model of calculation. *J. Geophys. Res.* **87**, 10,797-10,810.

Jambon A. (1983) Diffusion dans les silicates fondus: un bilan des connaissances actuelles. *Bulletin de Minéralogy* **106**, 229-246.

Jambon A. and Shelby J. E. (1980) Helium diffusion and solubiltiy in obsidians and basaltic glass in the range 200-300°C. *Earth Planet. Sci. Lett.* **51**, 206-214.

Karsten J. L., Holloway J. R. and Delaney J. R. (1982) Ion microprobe studies of water in silicate melts: temperature-dependent water diffusion in obsidian. *Earth Planet. Sci. Lett.* **59**, 420-428.

Kreyszig E. (1988) *Advanced Engineering Mathematics*. John Wiley & Sons.

Lux G. (1987) The behavior of noble gases in silicate liquids: solution, diffusion, bubbles and surface effects, with applications to natural samples. *Geochim. Cosmochim. Acta* **51**, 1549-1560.

Matsuda J.-I., Matsubara K., Yajima H. and Yamamoto K. (1989) Anomalous Ne enrichment in obsidians and Darwin glass: diffusion of noble gases in silica-rich glasses. *Geochim. Cosmochim. Acta* **53**, 3025-3033.

Mazer J. A., Bates J. K. and Bradley C. R. (1991) Molecular water diffusion in obsidian and tektite glasses between 110 and 230°C. *Geological Society of America Abstracts with Programs* p. 321.

Metrich N. and Mosbah M. (1988) Determination des teneurs en carbone de quelques verres basaltiques: analyses par reaction nucleaires. *Bull. Minéral.* **111**, 511-522.

Moore J. G. (1969) Vesicularity and CO_2 in mid-ocean ridge basalt. *Nature* **282**, 250-253.

Newman S. and Chesner C. (1989) Volatile compositions of glass inclusions from the 75 Ka Toba Tuff, Sumatra. *Geological Society of America Abstracts with Programs* **21**, A271.

Newman S., Epstein S. and Stolper E. (1988) Water, carbon dioxide, and hydrogen isotopes in glasses from the ca. 1340 A.D. eruption of the Mono Craters, California: constraints on degassing phenomena and initial volatile content. *J. Volcanol. Geotherm. Res.* **35**, 75-96.

Newman S., Stolper E. M. and Epstein S. (1986) Measurement of water in rhyolitic glasses: Calibration of an infrared spectroscopic technique. *Amer. Mineral.* **71**, 1527-1541.

Pauling L. (1960) *The nature of the chemical bond.* Cornell University Press.

Skirius C. M. (1990) Pre-eruptive H_2O and CO_2 content of plinian and ash-flow Bishop Tuff magma. Ph.D. dissertation, University of Chicago.

Stolper E. and Hollaway J. R. (1988) Experimental determination of the solubility of carbon dioxide in molten basalt at low pressure. *Earth Planet. Sci. Lett.* **87**, 397-408.

Taylor B. E. (1986) Magmatic volatiles: Isotopic variation on C, H, and S. In *Stable Isotopes in High Temperature Geological Processes* (ed. J. W. Valley, H. P. Taylor Jr. and J. R. O'Neil). pp. 185-226. Reviews in Mineralogy 16. Bookcrafters, Inc.

Tuttle O. F. (1949) Two pressure vessels for silicate-water studies. *Geol. Soc. Amer. Bull.* **60**, 1727-1729.

Watson E. B. (1991) Diffusion of dissolved CO_2 and Cl in hydrous silicic to intermediate magmas. *Geochimica et Cosmochima Acta* **55**, 1897-1902.

Watson E. B., Sneeringer M. A. and Ross A. (1982) Diffusion of dissolved carbonate in magmas: experimental results and applications. *Earth Planet. Sci. Lett.* **61**, 346-358.

Williams D. W. (1968) Improved cold seal pressure vessels to operate to 1100°C at 3 kilobars. *Amer. Mineral.* **53**, 1765-1769.

Zhang Y. and Stolper E. M. (1991) Water diffusion in a basaltic melt. *Nature* **351**, 306-309.

Zhang Y., Stolper E. M. and Wasserburg G. J. (1991) Diffusion of a multi-species component and its role in oxygen and water transport in silicates. *Earth Planet. Sci. Lett.* 228-240.

Zhang Y., Stolper E. M. and Wasserburg G. J. (1991) Diffusion of water in rhyolitic glass. *Geochimica Cosmochimica Acta* **55**, 441-456.

Zhang Y. and Xu Z. (1993) Neutral atomic radii of noble gas elements in crystal structures. submitted.

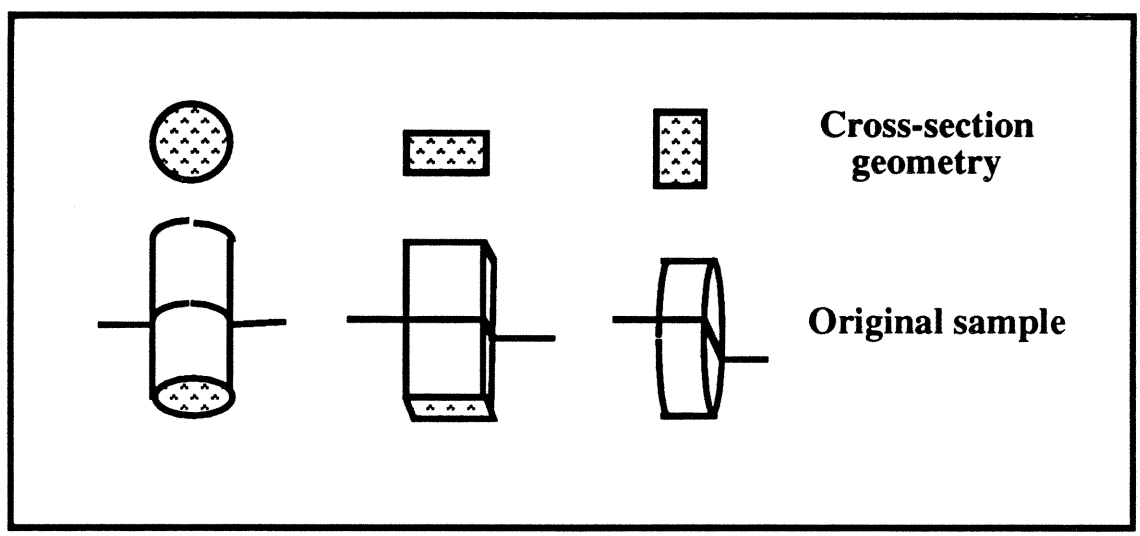

Fig. 2-1 Sample geometries used in the experiments. Lines bisecting representative sample shapes denote the region from which cross-sectional wafers (circles or rectangles) were sectioned.

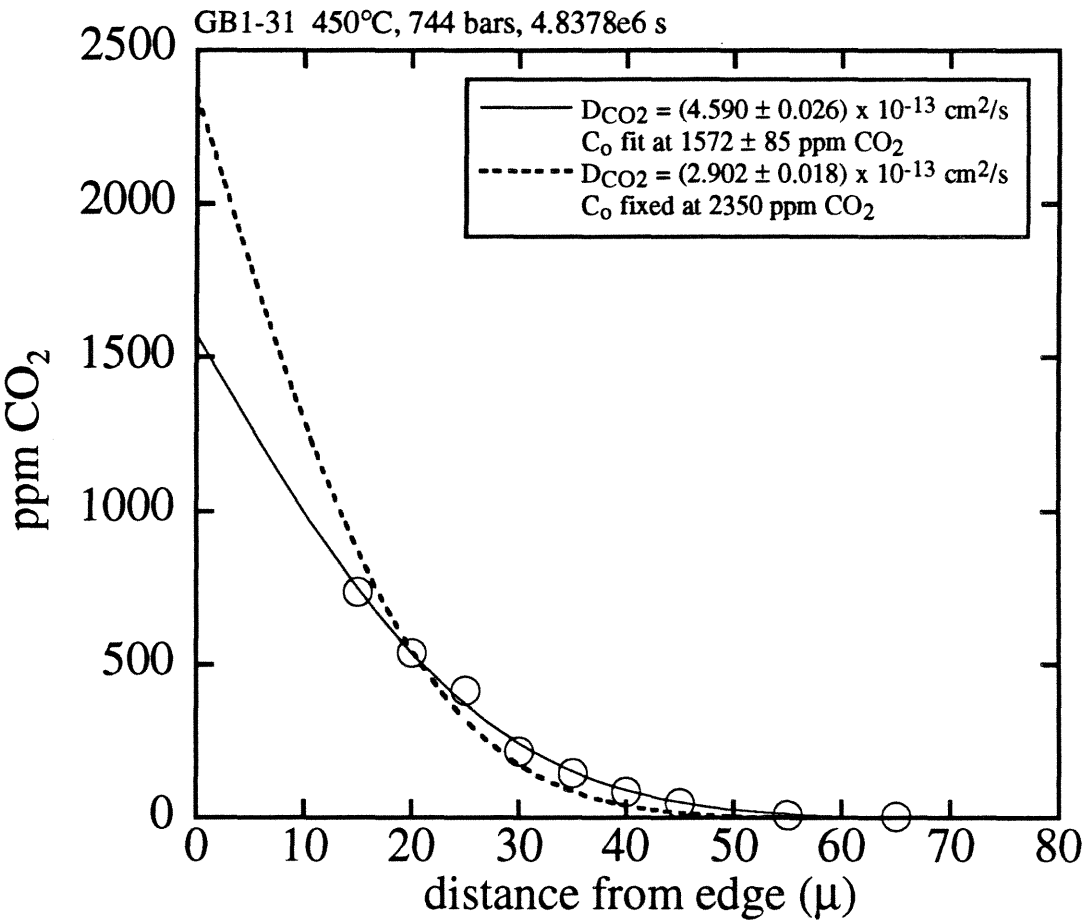

Fig. 2-2 CO_2 concentrations and diffusion profiles of the rhyolitic glasses determined by infrared (IR) spectroscopy. Diffusion curves for each experiment are error function solutions to the diffusion equation assuming constant D_{CO2}, where C_o is fixed (dashed curves) or determined from the data (solid curves). Where present, filled circles indicate IR spectroscopic analyses of a profile made near the edge of a sample using a 10 x 1000 μm slit aperture. Profiles for samples run at 715 to 740 bars (Figs. 2b-g) were used to derive an expression for D_{CO2} as a function of T. **(a)** GB1-31

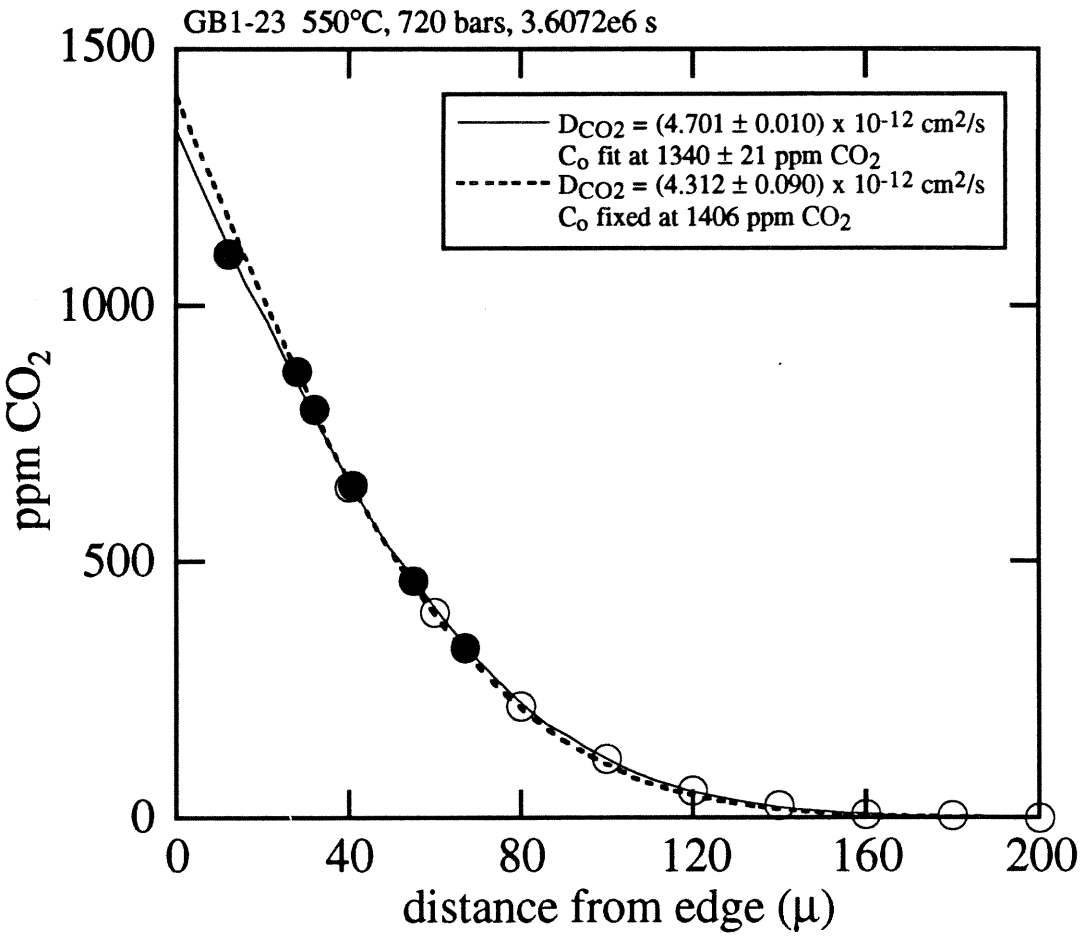

Fig. 2-2(b) GB1-23

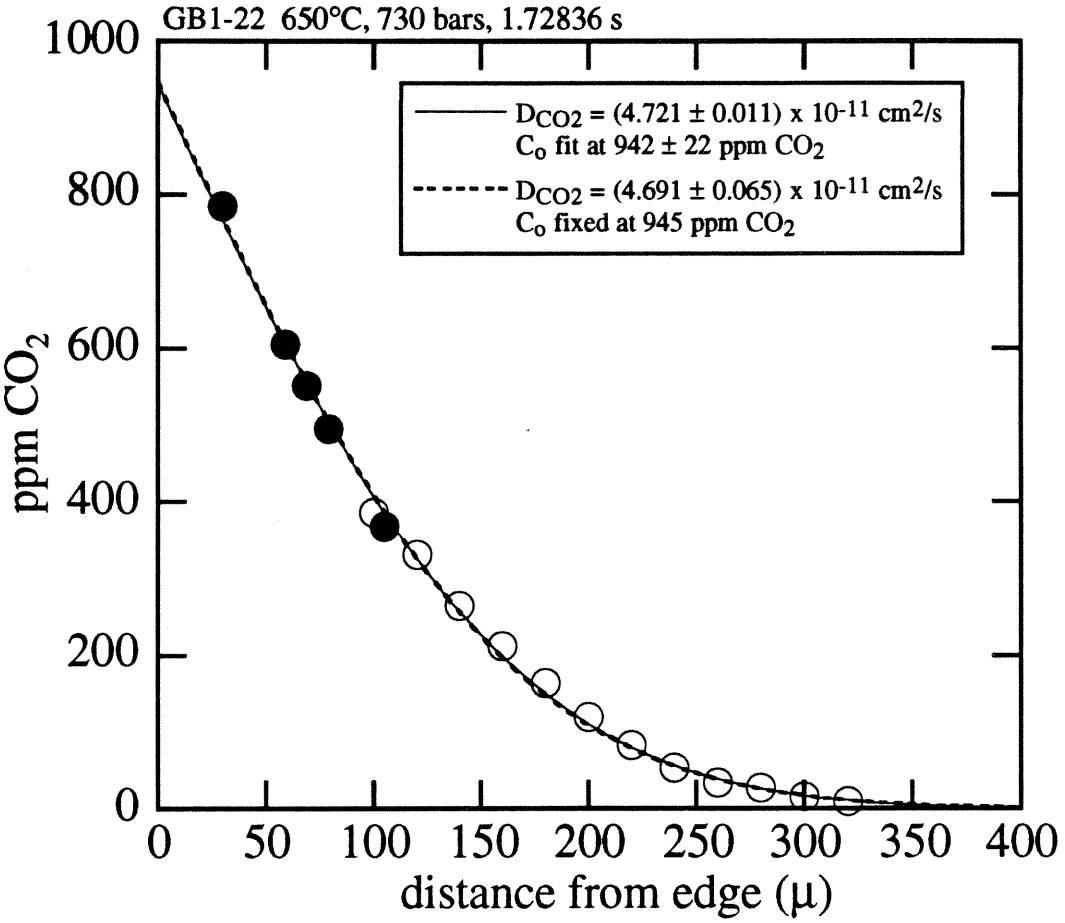

Fig. 2-2(c) GB1-22

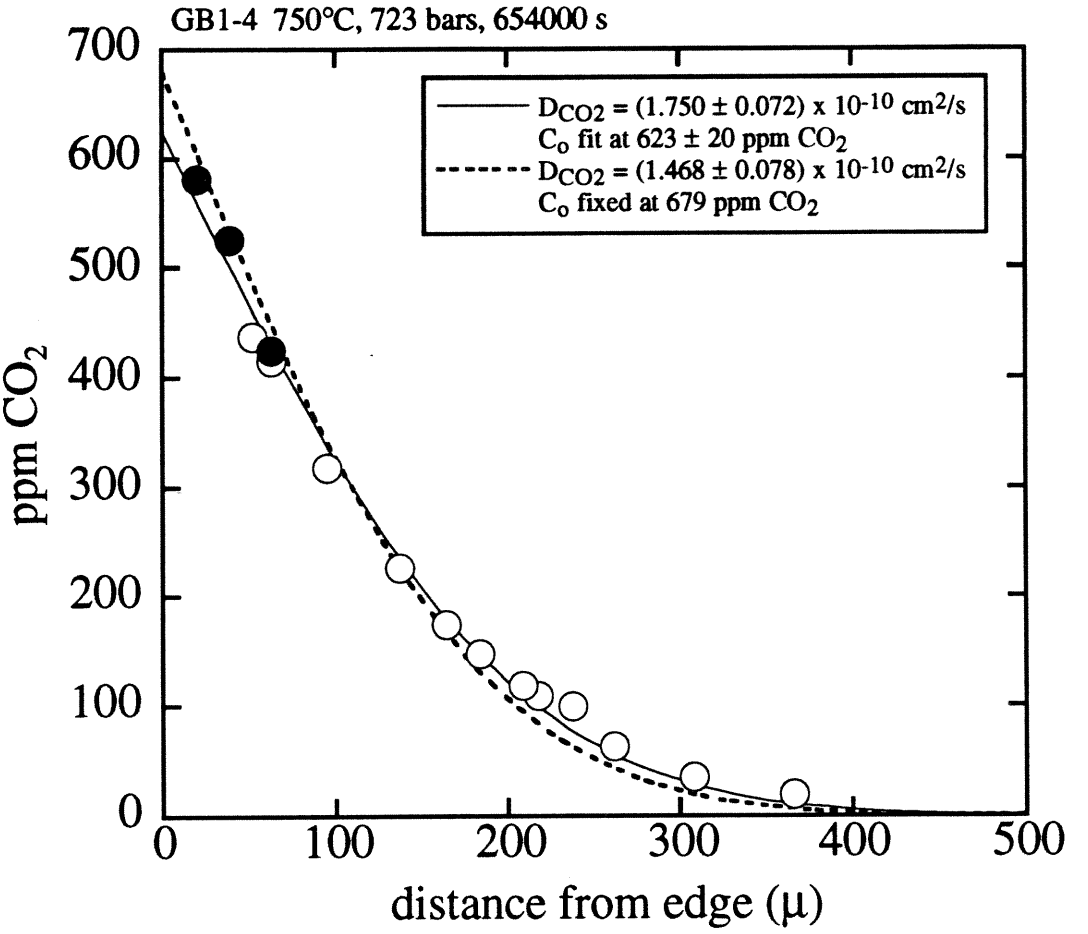
GB1-4 750°C, 723 bars, 654000 s
D_{CO2} = (1.750 ± 0.072) x 10^{-10} cm^2/s
C_o fit at 623 ± 20 ppm CO_2
D_{CO2} = (1.468 ± 0.078) x 10^{-10} cm^2/s
C_o fixed at 679 ppm CO_2
ppm CO_2
0
100
200
300
400
500
600
700
distance from edge (μ)

Fig. 2-2(d) GB1-4

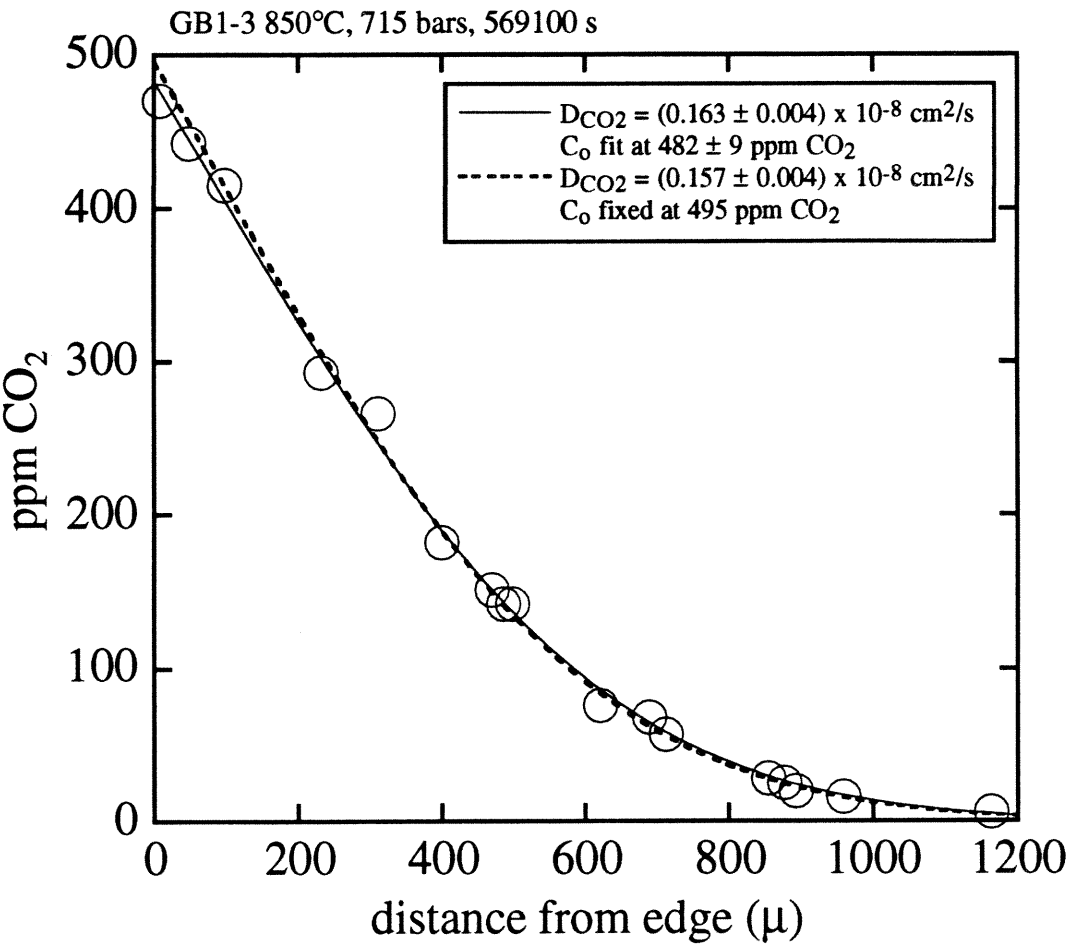
GB1-3 850°C, 715 bars, 569100 s
D_{CO2} = (0.163 ± 0.004) x 10^{-8} cm^2/s
C_o fit at 482 ± 9 ppm CO_2
D_{CO2} = (0.157 ± 0.004) x 10^{-8} cm^2/s
C_o fixed at 495 ppm CO_2
ppm CO_2
0
100
200
300
400
500
0
200
400
600
800
1000
1200
distance from edge (μ)

Fig. 2-2(e) GB1-3

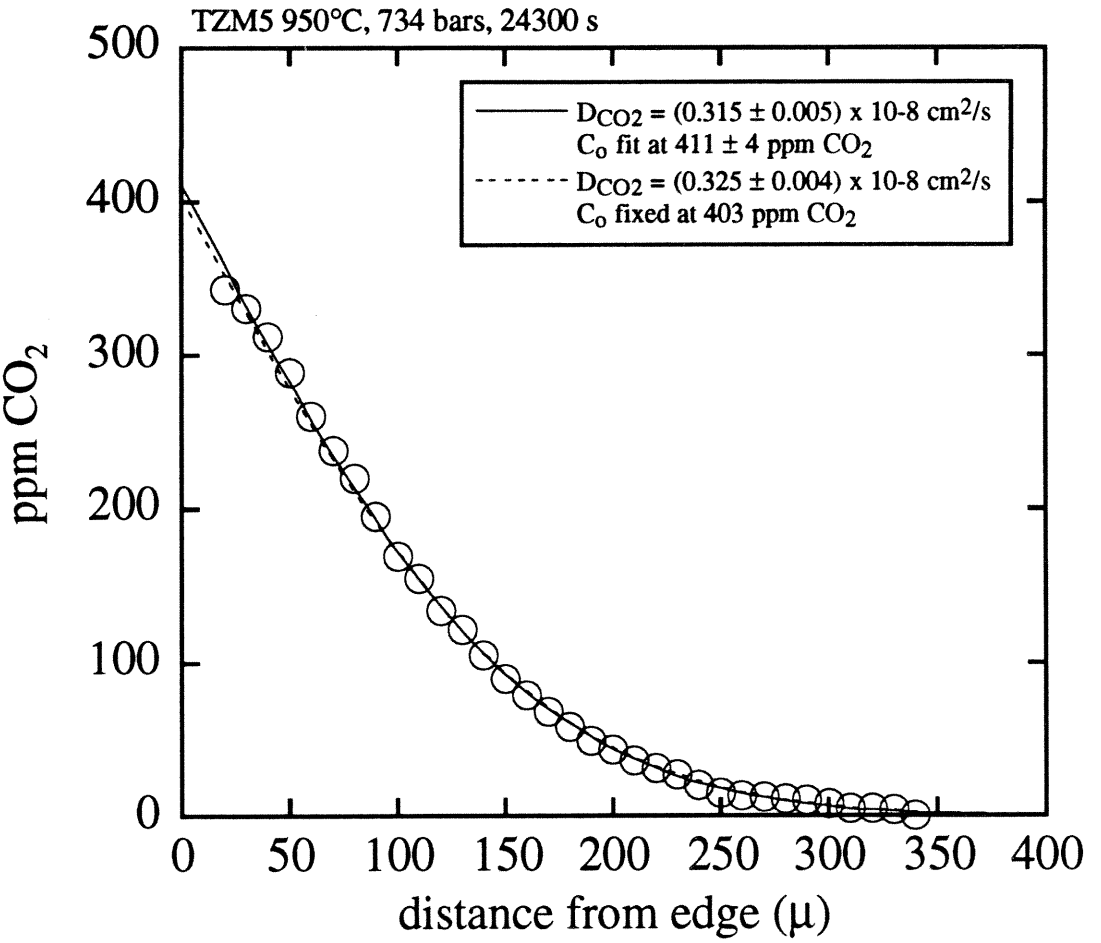
TZM5 950°C, 734 bars, 24300 s
D_{CO2} = (0.315 ± 0.005) x 10-8 cm2/s
C_o fit at 411 ± 4 ppm CO_2
D_{CO2} = (0.325 ± 0.004) x 10-8 cm2/s
C_o fixed at 403 ppm CO_2
ppm CO_2
0
100
200
300
400
500
0
50
100
150
200
250
300
350
400
distance from edge (μ)

Fig. 2-2(f) TZM5

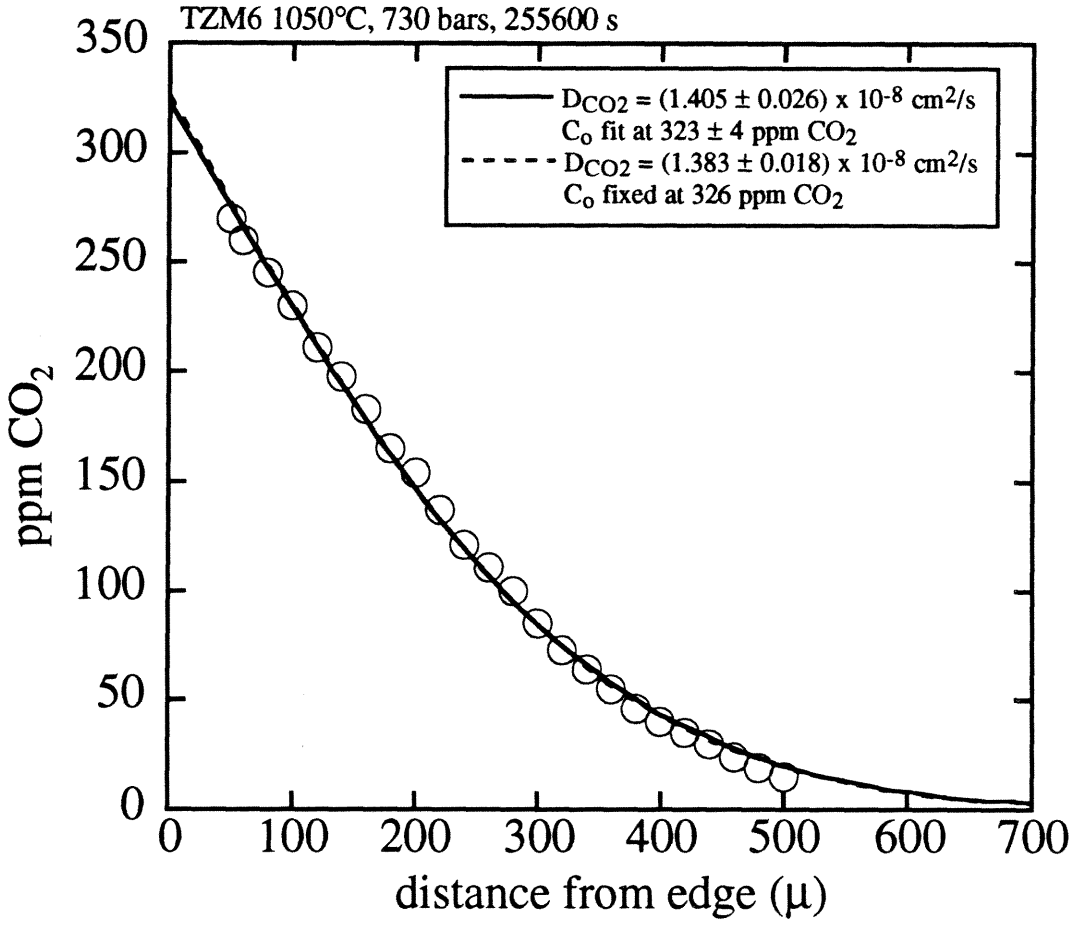
TZM6 1050°C, 730 bars, 255600 s
D_{CO2} = (1.405 ± 0.026) x 10^{-8} cm^2/s
C_o fit at 323 ± 4 ppm CO_2
D_{CO2} = (1.383 ± 0.018) x 10^{-8} cm^2/s
C_o fixed at 326 ppm CO_2
ppm CO_2
0
50
100
150
200
250
300
350
0
100
200
300
400
500
600
700
distance from edge (μ)

Fig. 2-2(g) TZM6

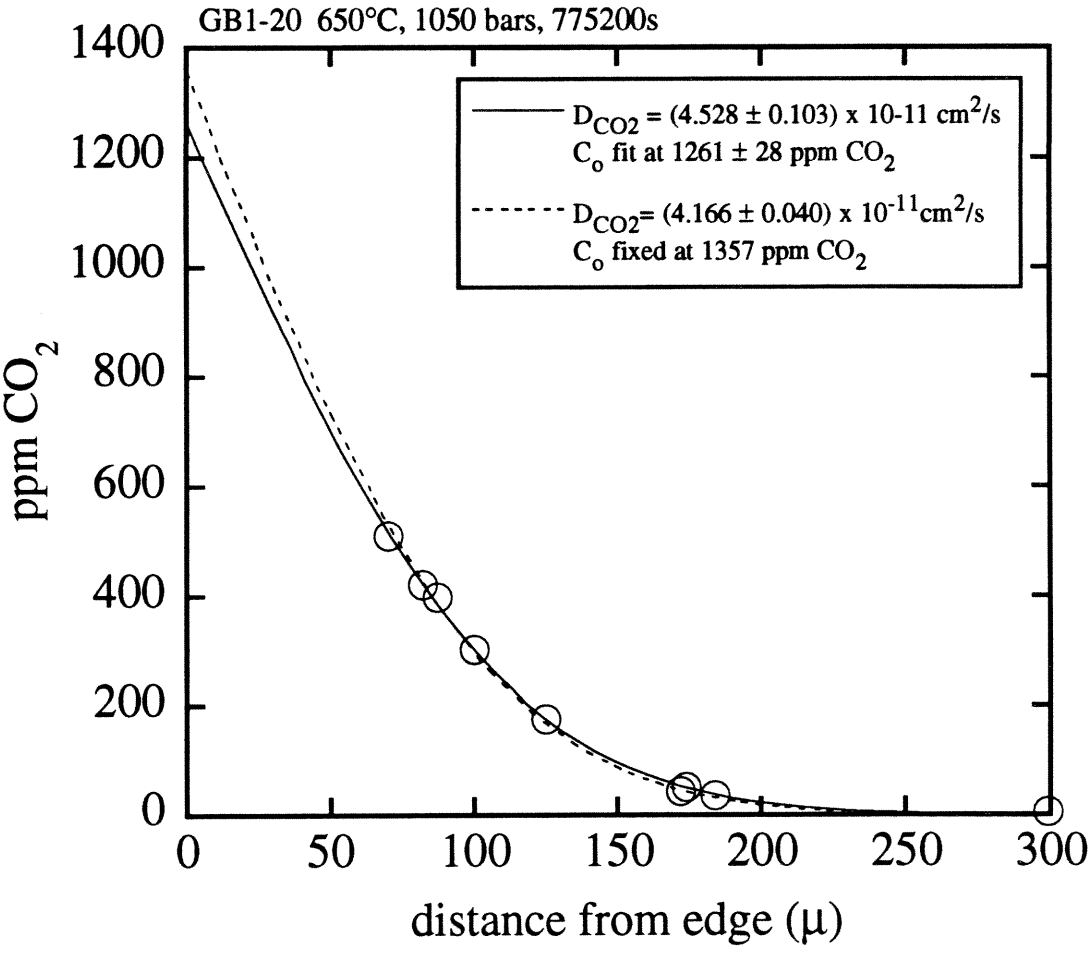

Fig. 2-2(h) GB1-20

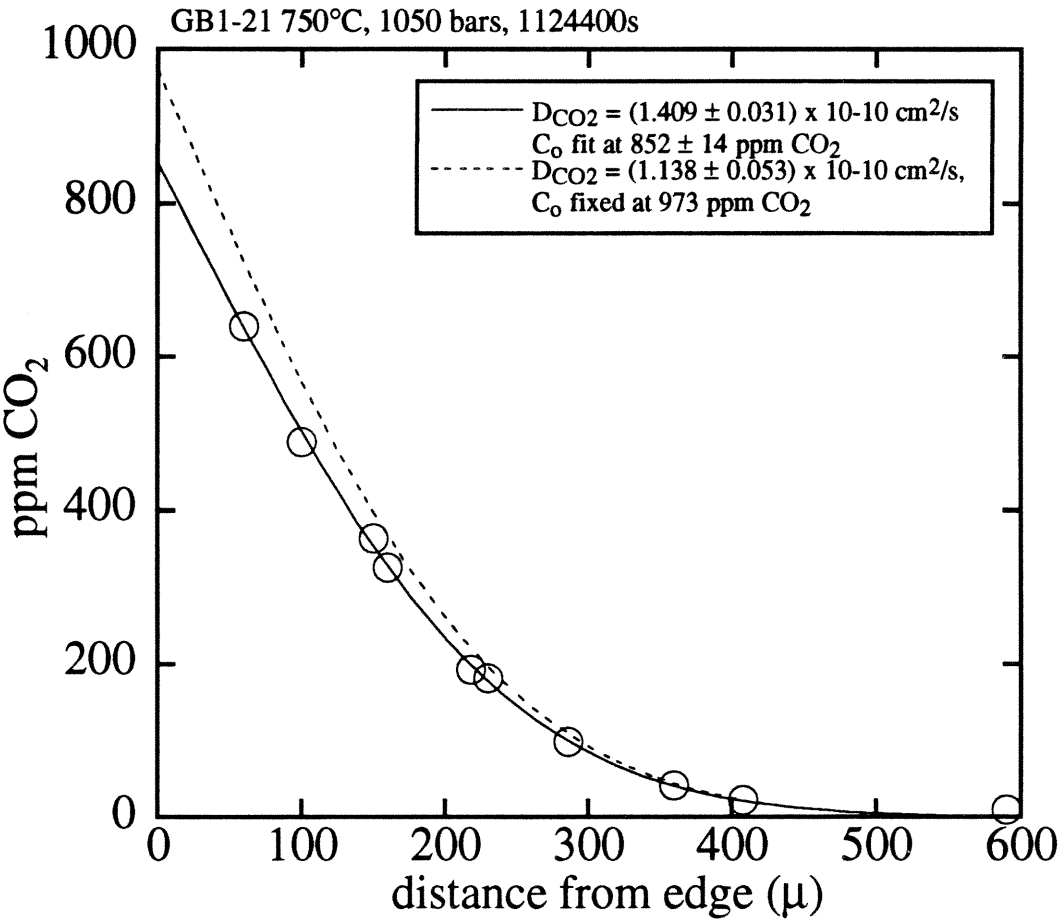

Fig. 2-2(i) GB1-21

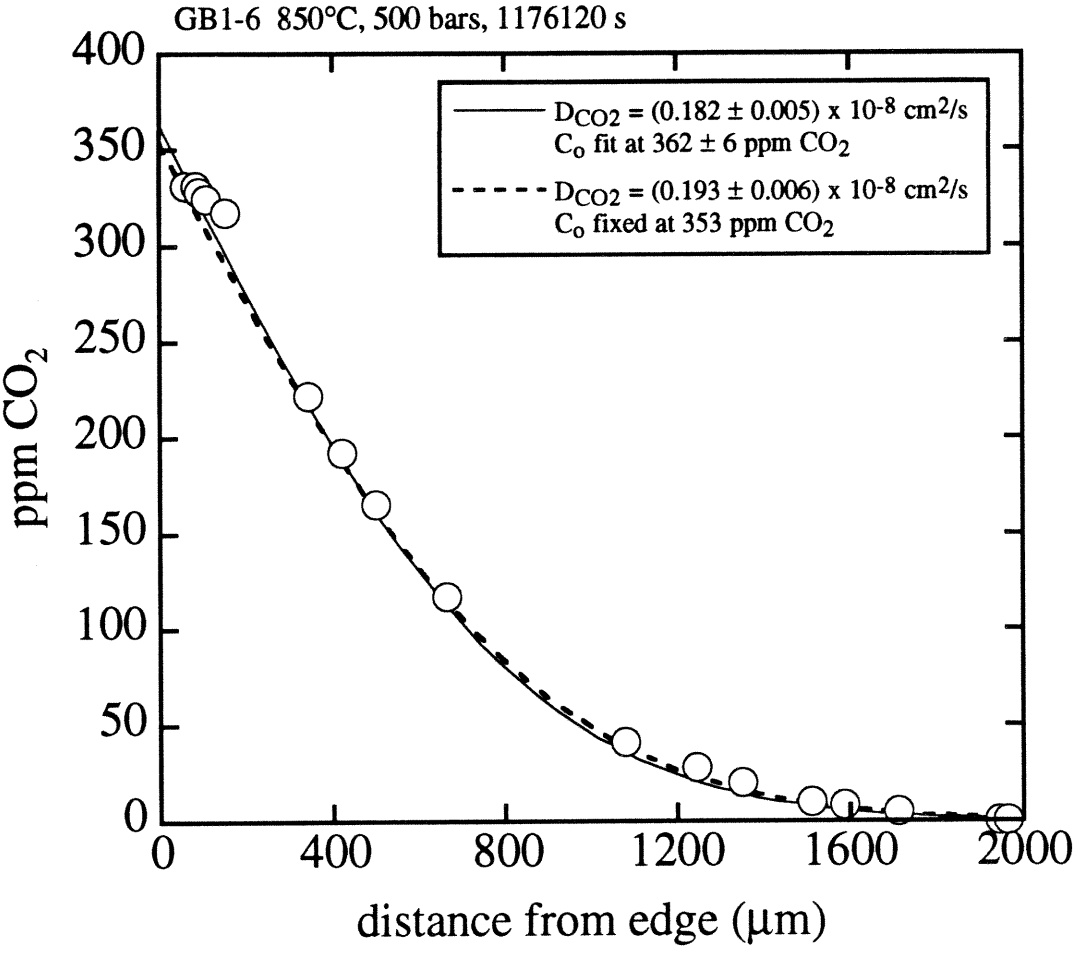
GB1-6 850°C, 500 bars, 1176120 s
D_{CO2} = (0.182 ± 0.005) x 10^{-8} cm^2/s
C_o fit at 362 ± 6 ppm CO_2
D_{CO2} = (0.193 ± 0.006) x 10^{-8} cm^2/s
C_o fixed at 353 ppm CO_2
ppm CO_2
0
50
100
150
200
250
300
350
400
0
400
800
1200
1600
2000
distance from edge (μm)

Fig. 2-2(j) GB1-6

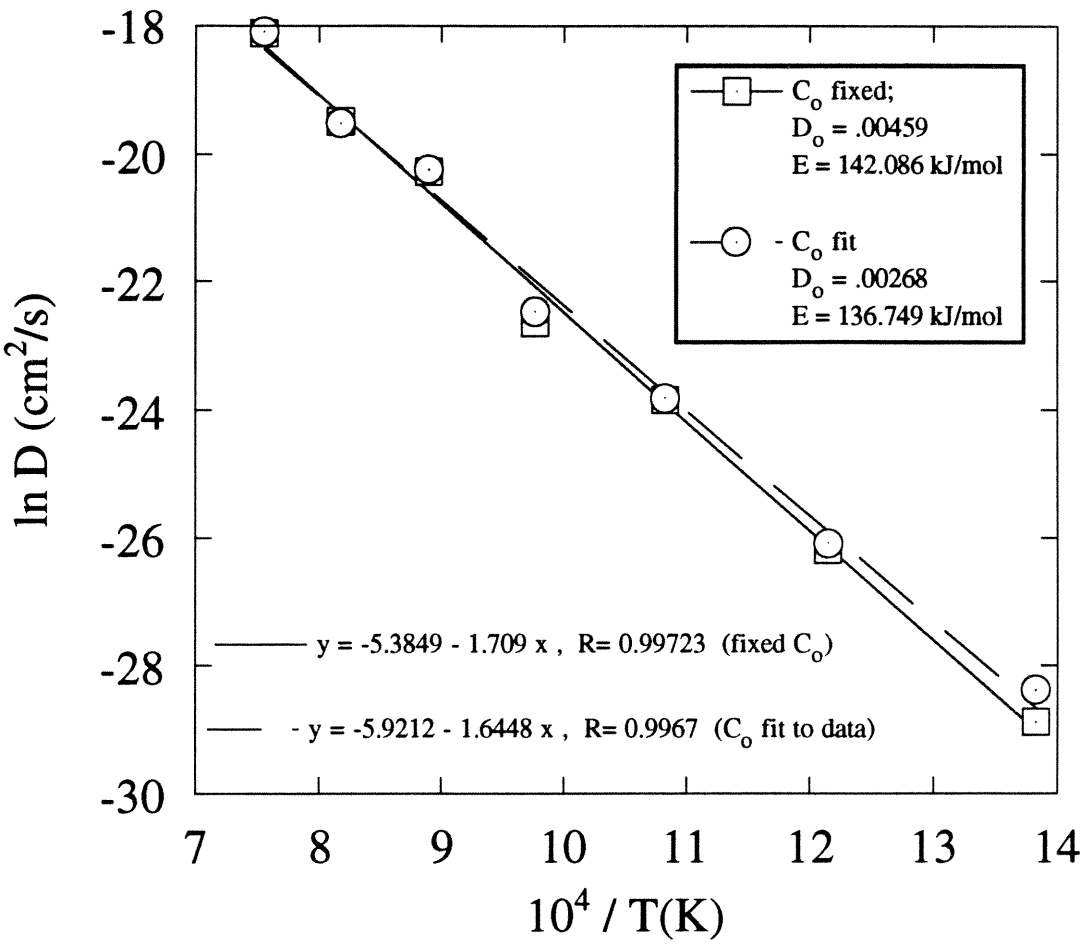

Fig. 2-3 Temperature-dependent Arrhenius graph for the 715-744 bar data. Squares represent D_{CO2} values determined by fixing C_o according to the equilibrium CO_2 solubility value (see text) and circles denote values determined without fixing C_o. The expression for ln D_{CO2} (straight line through points) was determined from a linear regression through the diffusion results (for both fit and fixed values of C_o) obtained for samples run at 1050 to 550 °C; the D_{CO2} values obtained for the 450°C sample were not included in the fit because of the discrepancies between the predicted and measured surface CO_2 concentrations (C_o).

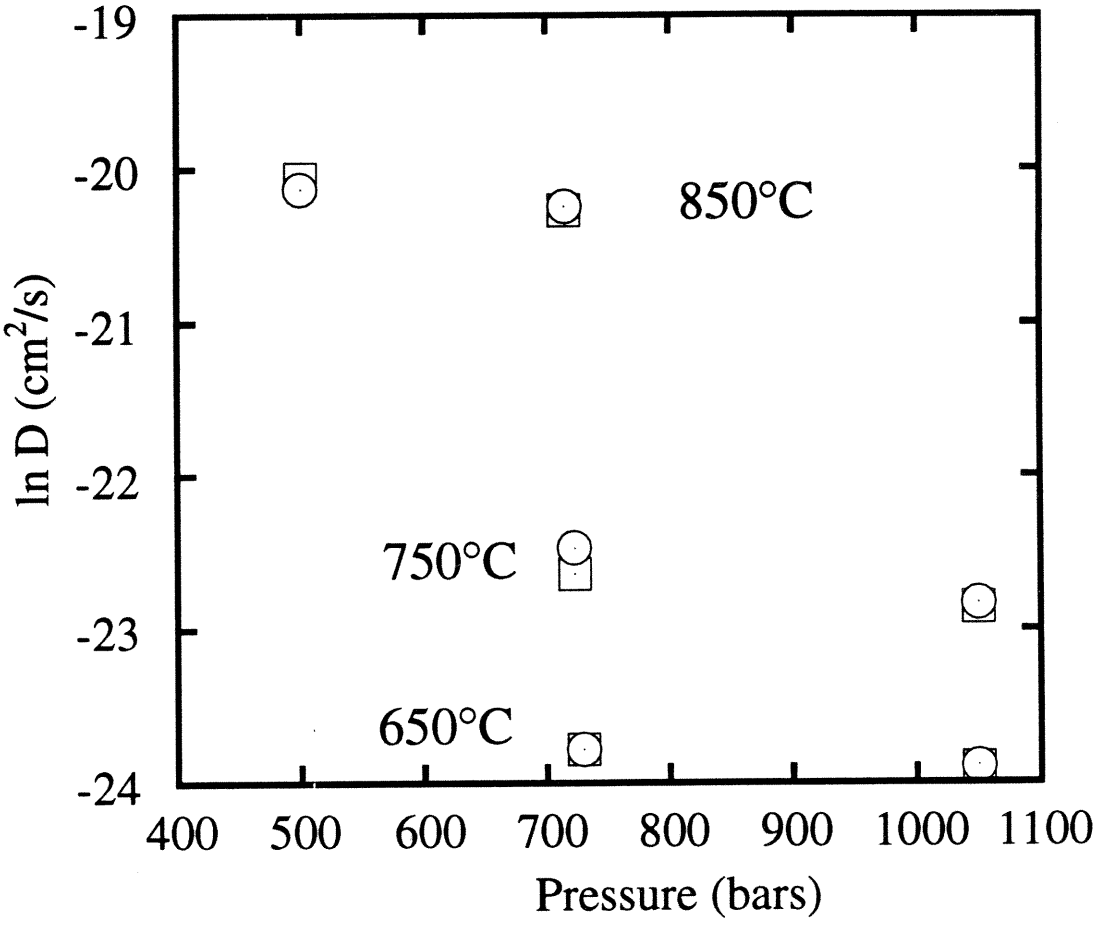

Fig. 2-4 Pressure-dependent Arrhenius plot showing the small influence of pressure on the CO_2 diffusivities I measured.

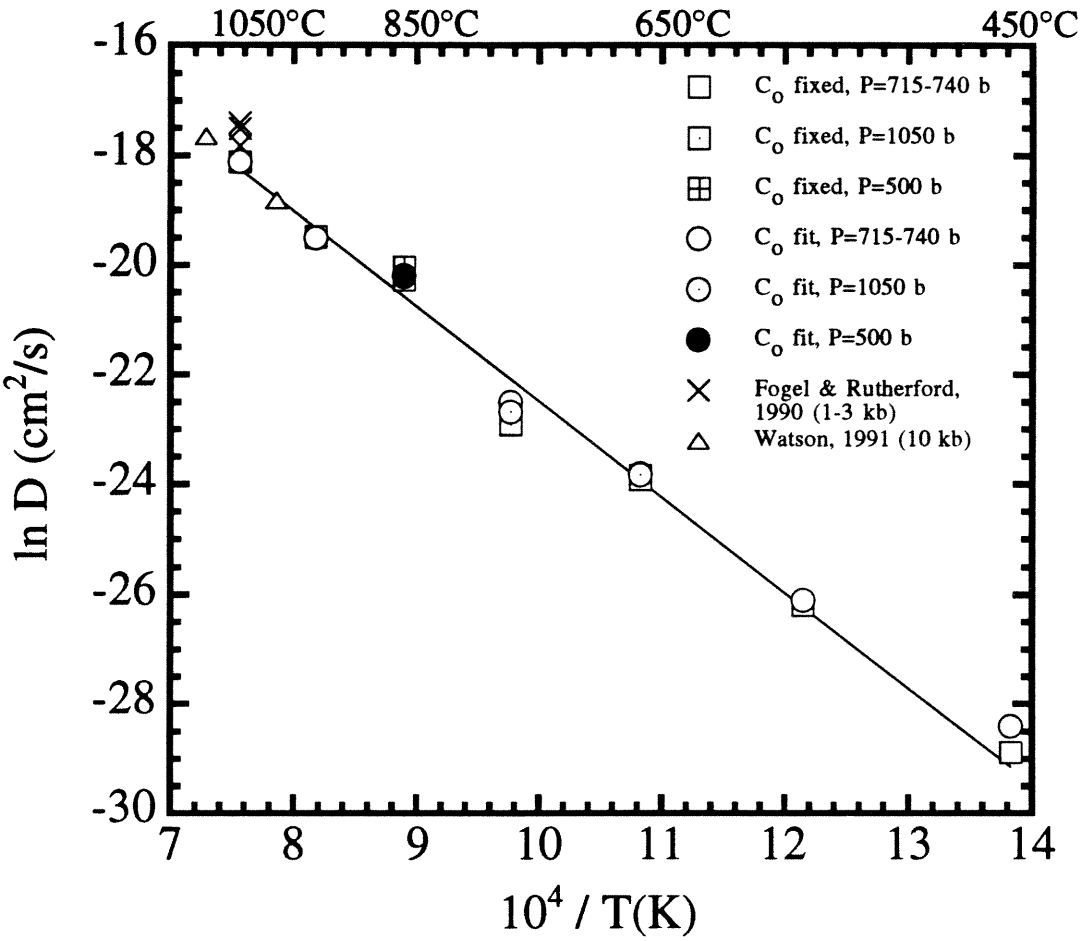

Fig. 2-5 Temperature-dependent Arrhenius plot comparing data from this study and others. Circles and squares, this study; 715-755 bars (see legend). D_{CO2} values from Fogel and Rutherford (1990) (denoted by x) are from experiments run at 1-3 kilobars and 1100°C; D_{CO2} values from Watson (1991) (denoted by Δ) were run at 10 kilobars and 1100°C and 1000°C. All data were obtained on rhyolitic glasses with low water contents (<0.3 wt%).

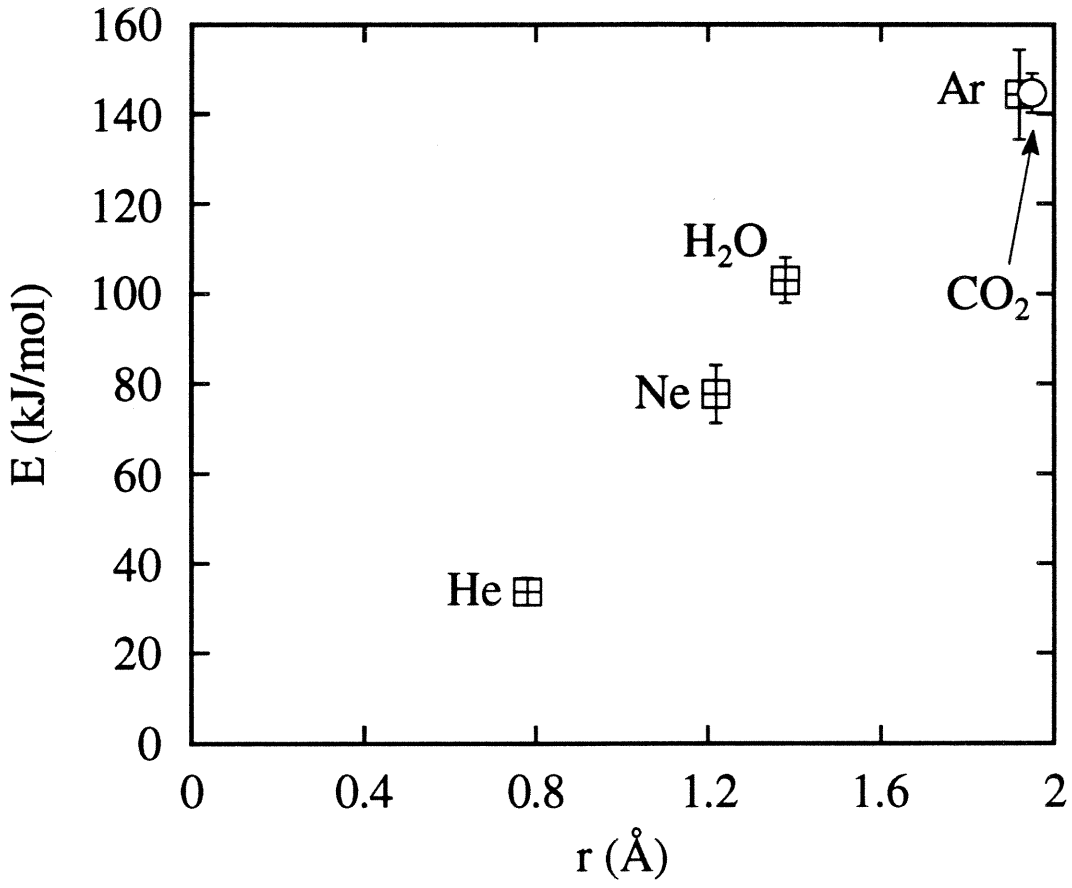

Fig. 2-6 The relation between activation energy (E) and radius of a neutral diffusing species in rhyolitic melt. The size of a "CO_2 radius" was calculated as follows. First, an expression for the translational diffusion of a linear CO_2 molecule (modeled as 2 attached, rigid spheres corresponding to 2 oxygen atoms) was derived (John Brady, personal communication, 1991):

$$D_{trans.} = \frac{kT}{6\pi\eta}\left[\frac{1}{3}\cdot\frac{1}{(1.29)a} + \frac{2}{3}\cdot\frac{1}{(1.45)a}\right],$$

where k is Boltzman's constant, T is the temperature, and η is the viscosity of the matrix, and a is the radius of one of the spheres (in this case, 1.4Å for oxygen). Next, $D_{trans.}$ was equated to the expression for the diffusion of a sphere ($D = {}^{kT}/_{6\pi\eta r}$, where r is the radius of the sphere), and solved for r using the value a = 1.4Å (Pauling, 1960), r = 1.95Å.

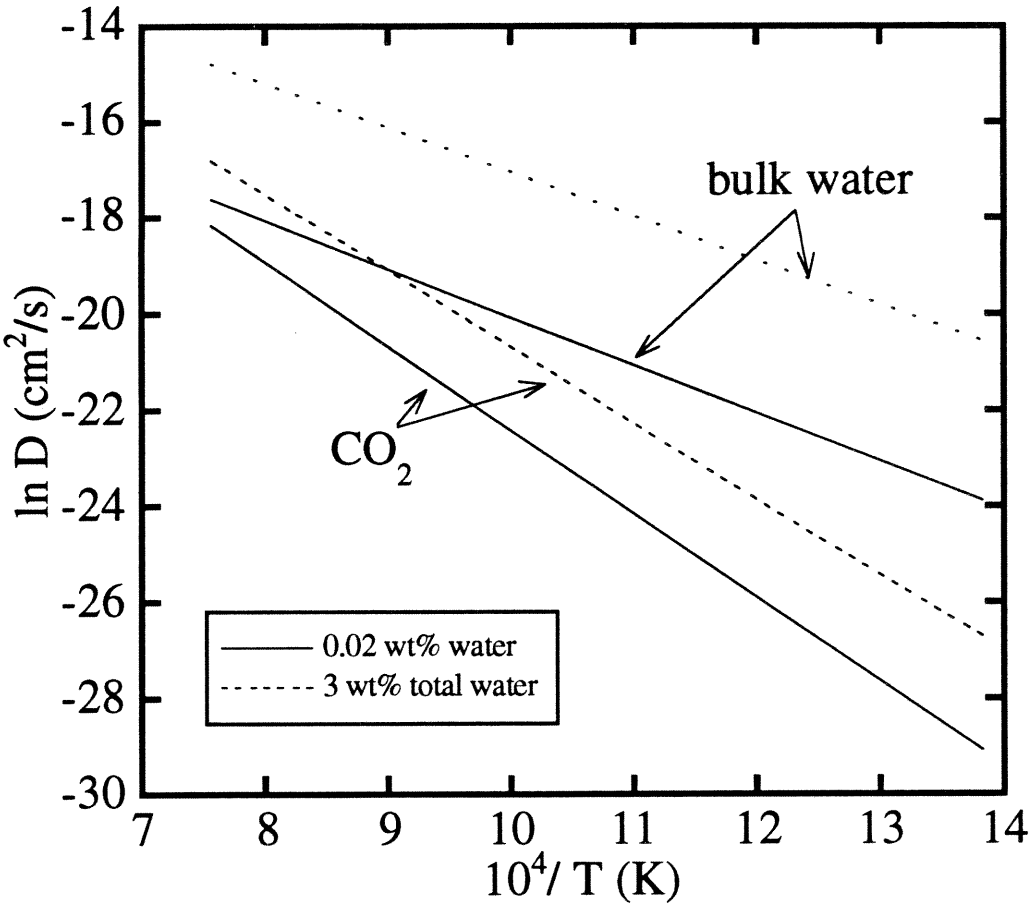

Fig. 2-7 Comparison of D_{CO2} and D_{water}^* in rhyolitic melts and glasses. D_{water}^* at 0.2 wt.% total water are from Zhang et al. (1991b), Data for D_{water}^* at 3 wt.% total water from Karsten et al. (1982), D_{CO2} values for rhyolites with 3 wt% water are estimated from Watson (1991).

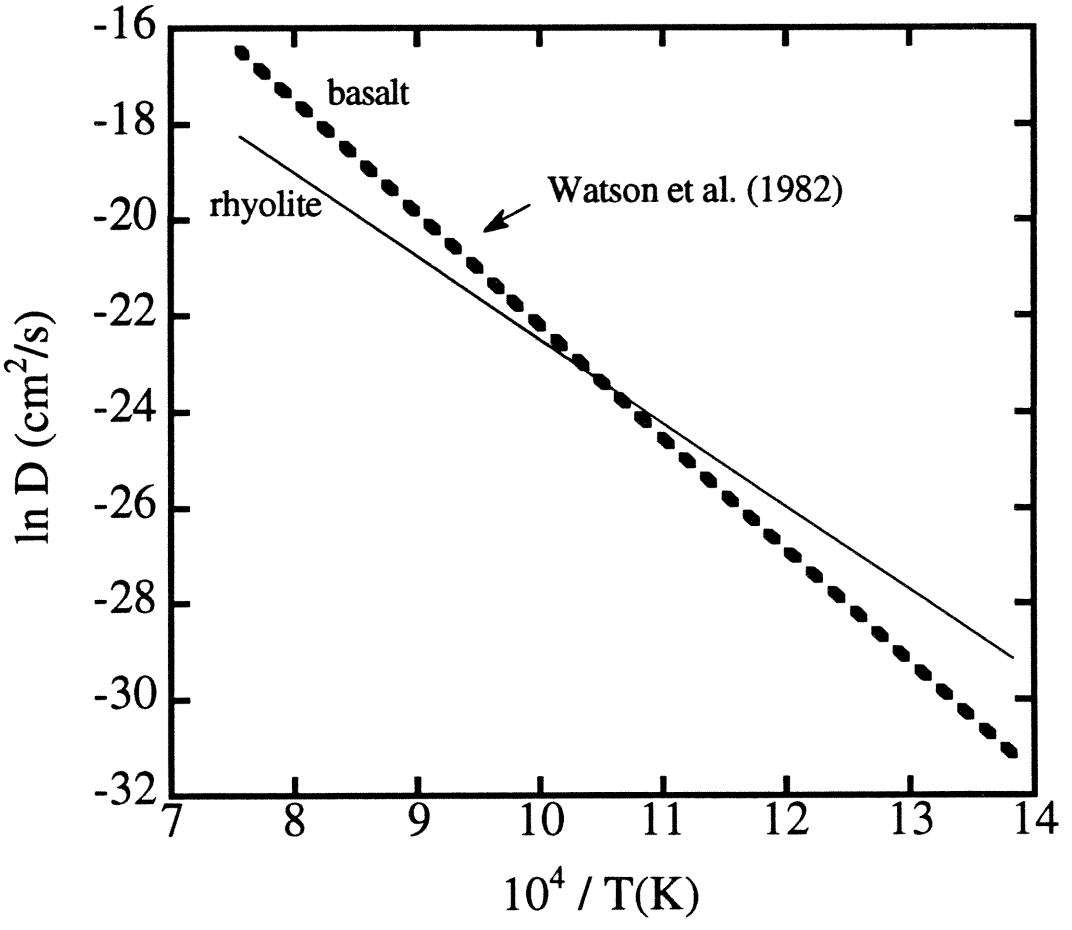

Fig. 2-8 Comparison of D_{CO2} in rhyolite at 715-740 bars (this study) and D_{CO3}^{2-} in basalt at 500 bars. The curve for basalt is taken from Watson et al. (1982) and was determined from 2 measurements of D_{CO3}^{2-} on a basaltic analog (60:30:10 wt.% SiO_2, Na_2O, and Al_2O_3, respectively) at 500 bars and 5 measurements of D_{CO3}^{2-} at 2 and 6 kilobars pressure-corrected to 500 bars.

Table 2-1 Sample Description

Run I.D. No.	*Run Type*[1]	*Aperture (μm) Used for IR*	*Sample Geometry*[3]	*Approx. Dim. (mm)*[4]	*Approx. Profile Length (μm)*	*X-Section Geometry*	*No. Points in Profile*	*Wafer Thickness (μm)*
GB1-31	R	10x1000 slit	s	3.3 x 3.4 x 9.0	80	rectangle	10	135
GB1-23	R	20x1000 slit[2]	s	3.3 x 3.3 x 8.6	200	rectangle	16	444
GB1-20	R	36.9 circle	c	4.1 (d) x 15.5	370	circle	16	119
GB1-22	R	20x1000 slit[2]	s	11.7 x 2.8 x 3.6	380	rectangle	23	238
GB1-21	R	36.9 circle	c	4.1 (d) x 16.0	780	circle	15	600
GB1-4	R	36.9 circle[2]	c	3.0 (d) x 8.6	450	circle	24	324
GB1-3	R	36.9 circle	c	3.0 (d) x 11.4	1730	circle	19	427
GB1-6	R	36.9 circle	c	3.0 (d) x 9.7	1950	circle	24	230
TZM5	TZM	10x1000 slit	c	4.6 (d) x 5.6	340	rectangle	35	403
TZM6	TZM	10x1000 slit	c	4.6 (d) x 5.6	720	rectangle	25	602

Notes:

[1] Experiment conducted in René (R) or TZM bomb assembly.

[2] Six analyses near the edges of samples GB1-23 and GB1-22 and three analyses near the edge of GB1-4 were performed using a 10x1000 μm aperture.

[3] Slab (s) or cylinder (c) geometry.

[4] Dimensions of glass sample used for an experiment. "(d)" is the diameter of a cylinder.

Table 2-2 Summary of Run Conditions and Results

Run No.	*P (bars)*[1]	*T (°C)*	*time (sec)*	*D(cm^2/s)*[1]	*±1σ*[1]	*D(cm^2/s)*[2]	*±1σ*[2]	*C_o(fixed)*[3] *(ppm CO_2)*	*C_o(fit) (ppmCO_2)*	*±1σ, ppm CO_2*[4]
GB1-31	744	450	4.84E+06	2.90E-13	1.80E-15	4.59E-13	2.60E-15	2350	1572	85
GB1-23	720	550	3.61E+06	4.31E-12	9.00E-14	4.70E-12	1.00E-14	1406	1340	21
GB1-20	1050	650	775200	4.17E-11	4.00E-13	4.53E-11	1.03E-12	1357	1261	28
GB1-22	730	650	1.73E+06	4.69E-11	6.50E-13	4.72E-11	1.10E-13	945	942	16
GB1-21	1050	750	1.12E+06	1.14E-10	5.30E-12	1.41E-10	3.10E-12	973	852	14
GB1-4	723	750	654000	1.47E-10	7.80E-12	1.75E-10	7.20E-12	679	623	19
GB1-3	715	850	569100	1.57E-09	4.00E-11	1.63E-09	4.00E-11	495	482	9
GB1-6	500	850	1176120	1.93E-09	6.00E-11	1.82E-09	5.00E-11	353	362	6
TZM5	734	950	24300	3.25E-09	4.00E-11	3.15E-09	5.00E-11	403	411	4
TZM6	730	1050	25560	1.37E-08	1.80E-10	1.41E-08	2.60E-10	326	323	4

Notes:

1 Results of an error function fit assuming D_{CO2} is independent of concentration and fixing C_o, the concentration at the edge of a sample, equal to the equilibrium CO_2 solubility value. 1σ variations are reported in the adjacent columns.

2 Similar error function fit except that C_o is determined based on a best-fit to the data. 1σ variations relative to lnD are also listed.

3 Equilibrium CO_2 solubility concentration, from Blank et al., 1989 (or, see Chapter 1).

4 1σ variation from C_o (fit).

Chapter 3

Solubilities of Carbon Dioxide and Water in Rhyolitic Melt at 850°C and 750 bars

3.1 Introduction

Water and carbon dioxide are the most abundant volatile components in terrestrial magmas (Allard et al., 1991; Anderson, 1975; Fyfe et al., 1970; Gerlach and Nordlie, 1975; Jagger, 1940). They exsolve from molten silicate into bubbles as magmas rise toward the earth's surface and depressurize. The vapor exsolving from magmas can be almost pure CO_2 at high pressure but becomes progressively enriched in H_2O upon decompression because carbon dioxide is much less soluble than water in most silicate liquids (e.g., (Holloway, 1981; Kadik et al., 1972). On eruption at the surface all but a few ppm CO_2 and 0.1-0.2 wt% H_2O have typically partitioned into bubbles or escaped into the atmosphere (Anderson et al., 1989; Gerlach and Thomas, 1986; Newman et al., 1986). Escape of these and other gases from magmas in near-surface environments is a significant factor in powering explosive volcanic eruptions (Druitt et al., 1989; Tait and Jaupart, 1990) and is the ultimate source of the earth's atmosphere and oceans (Holland, 1984).

Key to understanding degassing phenomena of magmas are the solubilities of carbon dioxide and water in silicate liquids similar in composition to magmas, and there has been much work over many decades directed toward this goal (Fogel and Rutherford, 1990; Goranson, 1931; Hamilton et al., 1964; Kadik and Lukanin, 1973; Kadik and Lukanin, 1985; Khitarov et al., 1959; Mysen et al., 1976; Shilobreyeva and Kadik, 1990; Silver et al., 1990; Stolper and Holloway, 1988). It is frequently assumed in efforts to model the volatile contents of magmas that Henry's law is obeyed for gaseous species dissolved in silicate melts (Anderson et al., 1989; Gerlach and Graeber, 1985; Newman et al., 1988; Skirius, 1990; Vogel et al., 1991; Westrich et al., 1988); that is, the fugacity (or partial pressure at sufficiently low total pressure) of a gaseous species is assumed to be proportional to the amount dissolved in the melt. If valid, this assumption considerably simplifies modeling of degassing of systems with both water and carbon dioxide since it means that one need only determine the behavior of the end member systems (i.e., silicate-CO_2 and silicate-H_2O) and

the equation of state of mixed H_2O-CO_2 vapor. A potential complication, however, is that water may influence the solubility of carbon dioxide in silicate melts and vice versa. Thus it is essential that experimentation on the partitioning of water and carbon dioxide between vapor and silicate melt in systems containing *both* volatile components be conducted. Indeed, although most efforts to model degassing phenomena have assumed Henrian behavior, studies conducted to-date on mixed-volatile systems have reported significant deviations from Henry's law (Brey, 1976; Brey and Green, 1975; Eggler and Rosenhauer, 1978; Holloway, 1981; Holloway and Lewis, 1974; Mysen et al., 1975; Mysen et al., 1976). Specifically, the addition of water to carbon dioxide-bearing systems has been reported to *increase* the amount of carbon dioxide that dissolves in vapor-saturated silicate melt, even though this leads to a *decrease* in the fugacity of CO_2 in the coexisting fluid. This result is important both because it has relevance for understanding degassing of magmas and because it has been viewed as providing insights into molecular-scale mechanisms by which water and carbon dioxide are incorporated into silicate liquids.

In this chapter, I report results of an experimental study of the amounts of water and carbon dioxide that dissolve in rhyolitic liquid coexisting with vapor containing known amounts of both of these volatile components at 850°C and a total pressure of 750 bars. The results are used to evaluate the validity of Henry's law in the low pressure range relevant to magma degassing. They are directly applicable to natural volcanic systems since recent work has suggested that vapor rich in both water and carbon dioxide plays a role in the evolution of high level silicic magmatic systems (Anderson et al., 1989; Newman et al., 1988; Skirius, 1990).

3.2 Experimental and Analytical Methods

Rhyolitic obsidian from the Glass Buttes extrusive dome in Oregon was used as starting material; its composition is given in Dobson et al. (1989). Silver oxalate

($Ag_2C_2O_4$) powder, liquid (doubly-distilled, deionized) water, and rhyolitic glass chips (sieved to 500-1000 μm in size) were loaded in known proportions into Pt capsules (28 mm L x 3.8 mm d x 0.2 mm wall thickness) that were then welded shut and pressurized with water in rapid-quench cold seal pressure vessels (René 41 alloy). Experiments were conducted at 850°C and 750 bars for approximately 6 days. Samples were magnetically levitated inside a vertical pressure vessel; at the end of an experiment, the magnet was removed and the sample dropped to a water-cooled portion of the pressure vessel where it cooled nearly isobarically (pressure increased by 25-30 bars during the quench) to room temperature in 2-3 seconds (Ihinger, 1991).

After quenching, sealed capsules were dried, weighed, and then placed on a vacuum line. The capsules were pierced, and their vapor was slowly transferred to a liquid nitrogen trap. Several hours were necessary for complete transfer of the water vapor, during which time the capsule was periodically heated with a hot air gun. Afterwards, <1 μmoles of noncondensable gas were pumped away. Carbon dioxide was distilled from water cryogenically with a -115°C slurry of "M17" (furfural: $C_5H_4O_2$) and dry ice; the water ice that remained was evaporated and then converted to H_2 by being passed over hot uranium at 800°C (Bigeleisen et al., 1952). Hydrogen and carbon dioxide were transferred separately into a manometer with a Toepler pump and their quantities measured. Blanks for H_2 and CO_2 were measured by pumping from the main portion of the line to the manometer with the Toepler pump for 0.5 hour for each gas and were ~0.5 μmoles and ~0.3 μmoles. Yields of H_2 and CO_2 from the experimental charges were corrected for these blanks.

Concentrations of carbon dioxide and water dissolved in the quenched glasses were determined from transmission infrared spectra of doubly-polished glass plates. One fragment from each experimental charge was analyzed. Analytical methods are similar to those described for water in Newman et al. (1986) and for CO_2 in Chapter 1. Samples were placed in the microchamber of a Nicolet 60SX FTIR spectrometer, and spectra were taken

with 1024 scans, a gain of 32, a KBr beamsplitter, a visible light source, and a liquid-N_2-cooled, InSb detector. Round apertures (37 μm diameter) in metal foils were used as masks to aim the infrared beam at selected regions of the polished glass fragment. Spectra were taken at 3-5 spots on each polished piece, including regions near the centers and edges of each glass fragment analyzed.

Water is dissolved in the quenched glasses both as hydroxyl groups (OH^-) and molecules of water (H_2O_{mol}), the concentrations of which were determined by Beer's Law from the intensities of absorptions at 4500 cm^{-1} (OH^-) and 5200 cm^{-1}(H_2O_{mol}) using molar absorptivities from Newman et al. (1986), glass densities calculated iteratively using their dependence on water content in glasses quenched from similar conditions (1990), and the measured sample thicknesses. For most samples, the reported total dissolved water content is the sum of the amounts of water dissolved in these two forms. Glass from Experiment 9 had a low bulk water content (0.51±0.06 wt%) and contained an amount of dissolved molecular water below the detection limit (≈0.05 wt%); the total dissolved water for this sample was determined from the intensity of the absorption at 3550 cm^{-1} using the molar absorptivity from Dobson et al. (1989). Concentrations of dissolved carbon dioxide molecules were determined using the intensity of the absorption at 2350 cm^{-1} (Fine, 1986) and the molar absorptivity from Chapter 1. Each sample spectrum was also checked in the 1300-1800 cm^{-1} region using a Globar light source, a CaF_2 beamsplitter, and a HgCdTe (MCT) detector for absorbances at 1365 cm^{-1} and 1610 cm^{-1} due to carbonate ions. These bands have been observed in a CO_2-rich (≈0.43 wt% total dissolved CO_2) rhyolitic glass quenched from 1550°C and 25 kbar (Fine, 1986), but they were absent in our samples. Baselines for all spectra were fit by smooth curves.

3.3 Results and Discussion

Run conditions and analytical results are reported in Table 3-1.

All samples quenched to glass. Concentrations of dissolved CO_2 molecules in the glasses increased from 23(±6) ppm for a sample equilibrated with the most CO_2-poor vapor to 515(±16) ppm for the one equilibrated with the most CO_2-rich vapor. The amount of total dissolved water in the glass varied from 0.51(±0.06) to 3.34(±0.08) wt% over the range of vapor compositions. The samples were homogeneous (within error) with respect to dissolved volatile contents. Microlites were present in the starting material and in several of the run products but were absent in the quenched run products with the highest dissolved water contents (Table 3-1). Bubbles were enclosed in the glass in several of the samples (Table 3-1); constituting less than ≈ 2 vol% of the enclosing glass, these bubbles ranged in diameter from approximately 5 to 30 μm but were usually smaller than 10 μm in diameter.

The mole fraction of CO_2 in the final vapor, $X^v_{CO_2}$, varied from 0.06 to 0.91. Amounts of water and carbon dioxide in the vapor as measured manometrically and calculated assuming mass balance (i.e., H_2O and CO_2 contents of the vapor calculated as the difference between the total H_2O and CO_2 loaded into the capsule, including the small amount initially present in the glass, and the amounts in the glass at the close of the experiment based on the infrared measurements) are in excellent agreement as shown by the close correspondence of the results shown in Fig. 3-1 to the 1:1 line. The CO_2 mass balance is effectively independent of the CO_2 content of the quenched glass because <1 μmole is dissolved in the glass compared to tens to hundreds of μmoles in the vapor. This is not the case for water which has much higher solubility in the melt. There is a small deficiency in the manometric measurements of the water contents of the vapor compared to the mass balance estimates. The reason for this is uncertain, but it may reflect incomplete removal of H_2O vapor from the platinum sample capsule (e.g., either because CO_2 is more readily removed during vacuum extraction or because of the unaccounted for contribution of bubbles trapped in the quenched glasses). The important point is that the values for $X^v_{CO_2}$

determined using the two different methods agree very well, in no case differing by more than 0.02 (Table 3-1).

In the data analysis below I used $X^{v}_{CO_2}$ determined from the manometric measurements of vapor composition as a basis for calculating CO_2 and H_2O fugacities (except for Experiment 3, for which the mass-balance-calculated value had to be used because the CO_2 vapor collected from the capsule was lost). Doing so allowed us to avoid uncertainties due to propagation of errors in the amounts of liquid water and silver oxalate powder loaded into an experimental charge and in the measured concentrations of volatiles dissolved in the quenched glasses.

My treatment assumes that the vapor in the capsule consisted entirely of CO_2 and H_2O, but other C-O-H gases must also be present. If, as is usually supposed to be the case (Holloway and Reese, 1974), the f_{H_2} inside the capsule is identical to that in the water outside the capsule in equilibrium with the Ni-rich René bomb (at an f_{O_2} approximately one order of magnitude above Ni-NiO (Geschwind and Rutherford, 1992), then I would expect up to 2% of the gas to be CO plus H_2 (CH_4 would be negligible) in the most CO_2-rich runs (and less in the more H_2O-rich runs) (Holloway and Reese, 1974). The measured abundances of noncondensable gases such as CO and H_2 are even lower than these low abundances expected based on f_{H_2} equilibration (Holloway and Reese, 1974). Although the reason for this is not clear, the observation of low amounts of noncondensable gases combined with the close agreement between the manometric and calculated CO_2 and H_2O yields indicate that the proportions of other C-O-H gases in our experiments are very small.

3.3.1 CO_2

Concentrations of CO_2 molecules in the quenched glasses (expressed as mole fraction of dissolved CO_2 in the melt, $X^{m}_{CO_2}$) are plotted in Fig. 3-2a versus the fugacity of CO_2 (f_{CO_2}) in the vapor (based on a modified Redlich-Kwong equation of state for the

vapor (Holloway, 1977)). The fugacity of CO_2 in the mixed H_2O-CO_2 experiments is directly proportional to the mole fraction of dissolved molecular CO_2, demonstrating clearly that Henry's law is satisfied for molecular CO_2 in rhyolitic melts coexisting with H_2O-CO_2 vapor under these conditions. In particular, there is no suggestion of an increase in the amount of CO_2 dissolved in vapor-saturated melt as $X^v_{CO_2}$ decreases from 1. This result is very different from that obtained for albite liquid at 20 kbars and 1450°C, where the dissolved CO_2 content was observed to increase by ≈ 50% as $X^v_{CO_2}$ decreased from 1.0 to 0.8 (Mysen, 1976). Mysen (1976) observed that the enhancement of CO_2 solubility in aluminosilicate melts by the addition of water at 10-30 kbars and 1450-1625°C diminishes with increasing temperature and with decreasing pressure. Other studies of melts equilibrated with H_2O-CO_2 fluids at 5-40 kbars (Brey, 1976; Brey and Green, 1975; Eggler and Rosenhauer, 1978; Holloway and Lewis, 1974; Mysen et al., 1975) report smaller but still significant enhancements of CO_2 solubility by addition of water for similar or lower values of $X^v_{CO_2}$. If these earlier results are correct and applicable to rhyolitic melts, the much smaller *amount* of water dissolved at $X^v_{CO_2}$ = 0.8 at 750 bars compared to 20 kbar might explain the difference between our result and those obtained at higher pressures. In other words, since only 1-2 wt% water is dissolved in melt coexisting with vapor with $X^v_{CO_2}$ = 0.8 at 750 bars but ~ 5-10 wt% water is dissolved in melt coexisting with this vapor at 20 kbars, the amount of dissolved water at lower pressures may simply not be sufficient to have a measurable effect on CO_2 dissolution. If this is the correct explanation of the difference between the low and high pressure results, it could imply that solution of water as H_2O molecules rather than as hydroxyl groups plays the major role in stabilizing excess dissolved CO_2 since there are already substantial amounts of water dissolved as hydroxyl groups at 1-2 wt% dissolved water, and most additional dissolved water beyond this level is added as H_2O molecules (Silver et al., 1990).

The Henrian behavior of CO_2 in the melt is clearly indicated in Fig. 3-2b by the 1:1 correspondence between the activity of CO_2 in the vapor and the ratio of the concentration of CO_2 in the rhyolitic melt saturated with H_2O-CO_2 vapor to its concentration in melt saturated with pure CO_2 vapor at this pressure and temperature. The latter is equivalent to the activity of CO_2 in the melt given a Henry's law standard state taken as CO_2 in the melt saturated with pure CO_2 vapor at P and T. The activity of CO_2 in the vapor is the ratio of the CO_2 fugacity in a mixed CO_2-H_2O experiment to that of pure CO_2 vapor at the pressure and temperature of the the mixed-volatile experiments, namely 750 bars and 850°C; for a vapor that obeys the Lewis-Randall rule, which H_2O-CO_2 approximately does under these conditions, this is equivalent to $X^v_{CO_2}$.

The open symbols in Fig. 3-2a show the variation in solubility of CO_2 in rhyolitic melt saturated with pure CO_2 vapor at 850°C versus f_{CO_2} where the variation in f_{CO_2} is achieved by varying total pressure (as opposed to the constant pressure experiments reported here, in which the variation in f_{CO_2} is due to dilution of the vapor with H_2O); the dashed curve shows the fit to these data using the formulation given by (Stolper et al., 1987). The concave downward curvature of this fit to the open symbols in Fig. 3-2a, which becomes more pronounced at higher pressures, reflects the finite partial molar volume of CO_2 in rhyolitic melt (28±2 cc/mole; Chapter 1). Although this curve is in excellent agreement with the results of our mixed-volatile solubility experiments (the closed symbols in Fig. 3-2a), the correspondence cannot be exact even if Henry's law is strictly obeyed. This is because in experiments such as those reported here in which the variation in f_{CO_2} is due to dilution at constant pressure rather than to variable total pressure, a Henrian relationship between solubility and fugacity will be strictly proportional, with no curvature. There is a suggestion of this difference in Fig. 3-2a, in which the mixed-volatile experiments are better fit by a straight line passing through the origin (solid curve) than by the slightly curved relationship that best fits the pure CO_2 vapor experiments. Although not actually

resolvable given the uncertainties in our data, such a difference should become more pronounced as the total pressure increases.

3.3.2 H_2O

The interaction between water and rhyolitic melt at these pressures is more complex than for CO_2 in that water molecules dissolve directly in the melt and also react with it to generate hydroxyl groups (Stolper, 1982). Consequently, the relationship between total dissolved water content (expressed as X_B^m, the mole fraction of water calculated on a single oxygen basis (Silver et al., 1990; Silver and Stolper, 1989)) and the fugacity of water (f_{H_2O}) is roughly parabolic (Fig. 3-3). Note in Fig. 3-3 that the results of our mixed-volatile experiments fall on the same trend as that of experiments in which rhyolitic melts were equilibrated with pure water vapor (Silver et al., 1990), demonstrating that the activity coefficient for bulk water in rhyolitic melt is insensitive to the low concentrations of dissolved carbon dioxide in these experiments. Also included in Fig. 3-3 are data from an early study by Kadik and others (1972) on the solubilities of CO_2 and H_2O in rhyolitic melts. These authors measured bulk water and CO_2 dissolved in the glasses using a gravimetric method. Although the measured CO_2 contents of their quenched glasses are an order of magnitude higher than our values, their measured water contents for experiments conducted at 1200°C agree well with ours. This agreement is consistent with the small temperature dependence of water solubility in silicate melts noted by previous workers (e.g., (Burnham and Jahns, 1962; Karsten et al., 1982; Stolper, 1989)).

Henrian behavior for dissolved water can be demonstrated by showing that the concentration of dissolved *molecular* water is proportional to f_{H_2O} or $a^v_{H_2O}$, the activity of water in the vapor (Silver et al., 1990). This is shown in Figs. 4a and 4b for our data set using previously-determined relationships between total water content, molecular water content, and temperature (Silver et al., 1990; Zhang et al., 1991). Note that I have the

corrected the observed H_2O_{mol} concentrations to account for changes in dissolved water speciation during quenching of the rhyolitic glasses (Ihinger, 1991). The validity of Henry's law for molecular water in rhyolitic melts containing both dissolved water and carbon dioxide, as has been previously demonstrated for a range of compositions containing dissolved water only (Silver et al., 1990; Silver and Stolper, 1989), demonstrates a negligible influence of CO_2 on the solution behavior of water; this is not surprising given the very low concentrations of CO_2 in the quenched glasses. Note that over the pressure range I have investigated there is no discernible difference between the solubility curve for molecular water dissolved in rhyolitic melt equilibrated with pure water vapor and a best-fit line defined by the mixed-volatile results (Fig. 3-4a). As discussed for CO_2 solubility above, some deviation between the constant pressure-variable vapor composition results and the pure water vapor-variable total pressure results must exist given the finite partial molar volume of water in rhyolitic melt, but this would only be detectable at much higher pressures than I have studied (Silver et al., 1990).

3.4 Conclusions

My results demonstrate that under the conditions of our experiments, which are relevant to degassing of common silicic magmas near the earth's surface, Henry's law is obeyed for both molecular water and carbon dioxide in rhyolitic melts. Thus, the amount of CO_2 dissolved in a rhyolitic melt saturated with H_2O-CO_2 vapor at a given pressure and temperature will be lower than if the vapor were pure CO_2 by a factor equal to the ratio of the fugacity of CO_2 in the mixed vapor to the fugacity of CO_2 in pure CO_2 vapor at the same conditions. This is essentially a dilution effect. The same is true for the amount of water dissolved in the melt, except that it is the amount of molecular water that is lowered proportionately to the fugacity of water by this dilution effect. There is no evidence of an enhancement of CO_2 solubility in mixed H_2O-CO_2 systems over systems in which only

CO_2 is present, contrary to previous reports for significantly higher pressures (Brey, 1976; Brey and Green, 1975; Eggler and Rosenhauer, 1978; Holloway, 1981; Holloway and Lewis, 1974; Mysen et al., 1976). Henrian behavior has also been reported recently for H_2O-CO_2-basalt (Dixon, 1992; Dixon et al., 1991) and for CO_2-CO-basalt (Pawley et al., 1992) at pressures under 1 kbar. While it is not surprising that the small amounts of CO_2 that dissolve in the melt have little influence on the solubility of water and thus that Henry's law is obeyed for molecular water for the full range of vapor compositions, the situation for CO_2 is different. Water has a significant effect on melt structure and is not a minor component of the melt in our experiments, so it would not be surprising if, as has been observed in other melt compositions at significantly higher total pressures, solution of water influenced the solubility mechanisms and thermodynamics of dissolved CO_2. Further work will be needed to characterize the transition between the observed Henrian behavior at low pressure and reported non-Henrian behavior at elevated pressures and the implied significance for solubility mechanisms under these conditions. However, it appears that efforts to model high level crustal and volcanic phenomena are considerably simplified by the validity of Henry's law for the major volatile species.

3.5 References

Allard P., Carbonnelle J., Dajlevic D., Le Bronec J., Morel P., Robe M. C., Maurenas J. M., Faivre-Pierret R., Martin D., Sabroux J. C. and Zettwoog P. (1991) Eruptive and diffusive emissions of CO_2 from Mount Etna. *Nature* **351**, 387-391.

Anderson A. T. (1975) Some basaltic and andesitic gases. *Rev. Geophys. Space Phys.* **13**, 37-55.

Anderson A. T. Jr., Newman S., Williams S. N., Druitt T. H., Skirius C. and Stolper E. (1989) H_2O, CO_2, Cl and gas in plinian and ash-flow Bishop rhyolite. *Geology* **17**, 221-225.

P.R. Bevington (1969) Data Reduction and Error Analysis for the Earth Sciences, McGraw-Hill Book Co., San Francisco.

Bigeleisen J., Perlman M. L. and Prosser H. C. (1952) Conversion of hydrogenic materials to hydrogen for isotopic analysis. *Anal. Chem.* **24**, 1356-1357.

Brey G. (1976) CO_2 solubility and solubility mechanisms in silicate melts at high pressures. *Contrib. Mineral. Petrol.* **57**, 215-221.

Brey G. and Green D. H. (1975) The role of CO_2 in the genesis of olivine melilitite. *Contrib. Mineral. Petrol.* **49**, 93-103.

Burnham C. W. and Jahns R. H. (1962) A method for determining the solubility of water in silicate melts. *Amer. Jour. Sci.* **260**, 721-745.

Dixon J. E. (1992) Water and Carbon Dioxide in Basaltic Magmas. Ph.D. dissertation, California Institute of Technology.

Dixon J. E., Stolper E. M. and Holloway J. R. (1991) Solubilities of water and carbon dioxide in basaltic magmas. *(abstr.). Geol. Soc. Amer. Abstr. with Prog.* A93.

Dobson P. F., Epstein S. and Stolper E. M. (1989) Hydrogen isotope fractionation between coexisting vapor and silicate glasses and melts at low pressure. *Geochim. Cosmochim. Acta* **53**, 2723-2730.

Druitt T. H., Mellors R. A., Pyle D. M. and Sparks R. S. J. (1989) Explosive volcanism on Santorini, Greece. *J. Geophys. Res.* **93**, 15314-15328.

Eggler D. and Rosenhauer M. (1978) Carbon dioxide in silicate melts: II. Solubilities of CO_2 and H_2O in $CaMgSi_2O_6$ (Diopside) liquids and vapors at pressures to 40 kb. *Amer. Jour. Sci.* **278**, 64-94.

Fine G. (1986) Carbon dioxide in synthetic and natural silicate glasses. Ph.D. dissertation, California Institute of Technology.

Fogel R. A. and Rutherford M. J. (1990) The solubility of carbon dioxide: A quantitative FTIR study. *Amer. Mineral.* **75**, 1311-1326.

Fyfe W. S., Price N. J. and Thompson A. B. (1970) *Fluids in the Earth's Crust*. 1. Springer-Verlag.

Gerlach T. M. and Graeber E. J. (1985) Volatile budget of Kilauea Volcano. *Nature* **313**, 273-277.

Gerlach T. M. and Nordlie B. E. (1975) The C-H-O-S gaseous system. Part I: Composition limits and trends in basaltic gases; Part II: Temperature, atomic composition and molecular equilibria in volcanic gases; Part III: Magmatic gases compatible with oxides and sulfides in basaltic magmas. *Amer. Jour. Sci.* **275**, 353-410.

Gerlach T. M. and Thomas D. M. (1986) Carbon and sulphur isotopic composition of Kilauea parental magma. *Nature* **319**, 480-483.

Geschwind C.-H. and Rutherford M. J. (1992) Cummingtonite and the evolution of the Mount St. Helens (Washington) magma system: An experimental study. *Geology* **20**, 1011-1014.

Goranson R. W. (1931) The solubility of water in granite magmas. *Amer. Jour. Sci.* **22**, 481-502.

Hamilton D. L., Burnham C. W. and Osborn E. F. (1964) The solubility of water and effects of oxygen fugacity and water content on crystallization in mafic magmas. *Jour. Petrol.* **5**, 21-39.

Holland H. D. (1984) *The Chemical Evolution of the Atmosphere*. Princeton University Press.

Holloway J. R. (1977) Fugacity and activity of molecular species in supercritical fluids. In *Thermodynamics in Geology* (ed. D. Fraser). pp. 161-181. D. Reidel.

Holloway J. R. (1981) Volatile interactions in magmas. In *Thermodynamics of Melts and Minerals* (ed. R. C. Newton, A. Navrotsky and B. J. Wood). pp. 273-293. Advances in Physical Geochemistry I. Springer-Verlag.

Holloway J. R. and Lewis C. F. (1974) CO_2 solubility in hydrous albite liquid at 5 kbar. *(abstr.). Eos* **55**, 483.

Holloway J. R. and Reese R. L. (1974) The generation of N_2-CO_2-H_2O fluids for use in hydrothermal experimentation I. Experimental method and equilibrium calculations in the C-O-H-N system. *Amer. Mineral.* **59**, 587-597.

Ihinger P. D. (1991) An experimental study of the interaction of water with granitic melt. Ph.D. dissertation, California Institute of Technology.

Jagger T. A. (1940) Magmatic gases. *Amer. Jour. Sci.* **238**, 313-353.

Kadik A. A. and Lukanin O. A. (1973) The solubility-dependent behavior of water and carbon dioxide in magmatic processes. *Geochem. Int.* **10**, 115-129.

Kadik A. A. and Lukanin O. A. (1985) Paths of mantle outgassing during melting: The role of partial melting of upper mantle rocks in the evolution of fluid composition and redox regime. *Int. Geol. Rev.* **27**, 563-572.

Kadik A. A., Lukanin O. A., Lebedev Y. B. and Kolovushkina E. Y. (1972) Solubility of H_2O and CO_2 in granite and basalt melts at high pressures. *Geochem. Int.* **9**, 1041-1050.

Karsten J. L., Holloway J. R. and Delaney J. R. (1982) Ion microprobe studies of water in silicate melts: Temperature-dependent water diffusion in obsidian. *Earth Planet. Sci. Lett.* **59**, 420-428.

Khitarov N. I., Lebedev E. B., Rengarten E. V. and Arseneiva R. V. (1959) Comparative characteristics of the solubility of water in basaltic and granitic melts. *Geokhimiya* **5**, 479-492.

Mysen B. O. (1976) The role of volatiles in silicate melts: Solubility of carbon dioxide and water in feldspar, pyroxene, and feldspathoid melts to 30 kb and 1625°C. *Amer. Jour. Sci.* **276**, 969-996.

Mysen B. O., Arculus R. J. and Eggler D. H. (1975) Solubility of carbon dioxide in melts of andesite, tholeiite, and olivine nephelinite composition to 30 kbar. *Contrib. Mineral. Petrol.* **53**, 227-239.

Mysen B. O., Eggler D. H., Seitz M. G. and Holloway J. R. (1976) Carbon dioxide solubilities in silicate melts and crystals. Part I. Solubility measurements. *Amer. Jour. Sci.* **276**, 455-479.

Newman S., Epstein S. and Stolper E. (1988) Water, carbon dioxide, and hydrogen isotopes in glasses from the ca. 1340 A.D. eruption of the Mono Craters, California: Constraints on degassing phenomena and initial volatile content. *J. Volcanol. Geotherm. Res.* **35**, 75-96.

Newman S., Stolper E. M. and Epstein S. (1986) Measurement of water in rhyolitic glasses: Calibration of an infrared spectroscopic technique. *Amer. Mineral.* **71**, 1527-1541.

Pawley A. R., Holloway J. R. and McMillan P. (1992) The effect of oxygen fugacity on the solubility of carbon-oxygen fluids in basaltic melt. *Earth Planet. Sci. Lett.* **110**, 213-225.

Shilobreyeva S. N. and Kadik A. A. (1990) Solubility of CO_2 in magmatic melts at high temperatures and pressures. *Geochem. Int.* **27**, 31-41.

Silver L. A., Ihinger P. D. and Stolper E. (1990) The influence of bulk composition on the speciation of water in silicate glasses. *Contrib. Mineral. Petrol.* **104**, 142-162.

Silver L. A. and Stolper E. (1989) Water in albitic glasses. *Jour. Petrol.* **30**, 667-709.

Skirius C. M. (1990) Pre-eruptive H_2O and CO_2 content of plinian and ash-flow Bishop Tuff magma. Ph.D. dissertation, University of Chicago.

Stolper E. (1982) Water in silicate glasses: An infrared spectroscopic study. *Contrib. Mineral. Petrol.* **81**, 1-17.

Stolper E., Fine G., Johnson T. and Newman S. (1987) Solubility of carbon dioxide in albitic melt. *Amer. Mineral.* **72**, 1071-1085.

Stolper E. M. (1989) Temperature dependence of the speciation of water in rhyolitic melts and glasses. *Amer. Mineral.* **74**, 1247-1257.

Stolper E. M. and Holloway J. R. (1988) Experimental determination of the solubility of carbon dioxide in molten basalt at low pressure. *Earth Planet. Sci. Lett.* **87**, 397-408.

Tait S. and Jaupart C. (1990) Dynamics of eruptive phenomena. *Rev. Mineral.* **24**, 125-152.

Vogel T. A., Eichelberger J. C., Younker L. W., Schuraytz B. C. and Horkowitz J. P. (1991) Petrology and emplacement dynamics of intrusive and extrusive rhyolites of Obsidian Dome, Inyo Craters volcanic chain, eastern California. *J. Geophys. Res.* **17**, 17937-17956.

Westrich H. R., Stockman H. W. and Eichelberger J. C. (1988) Degassing of rhyolitic magma during ascent and emplacement. *J. Geophys. Res.* **93**, 6503-6511.

Zhang Y., Stolper E. M. and Wasserburg G. J. (1991) Diffusion of water in rhyolitic glasses. *Geochim. Cosmochim. Acta* **55**, 441-456.

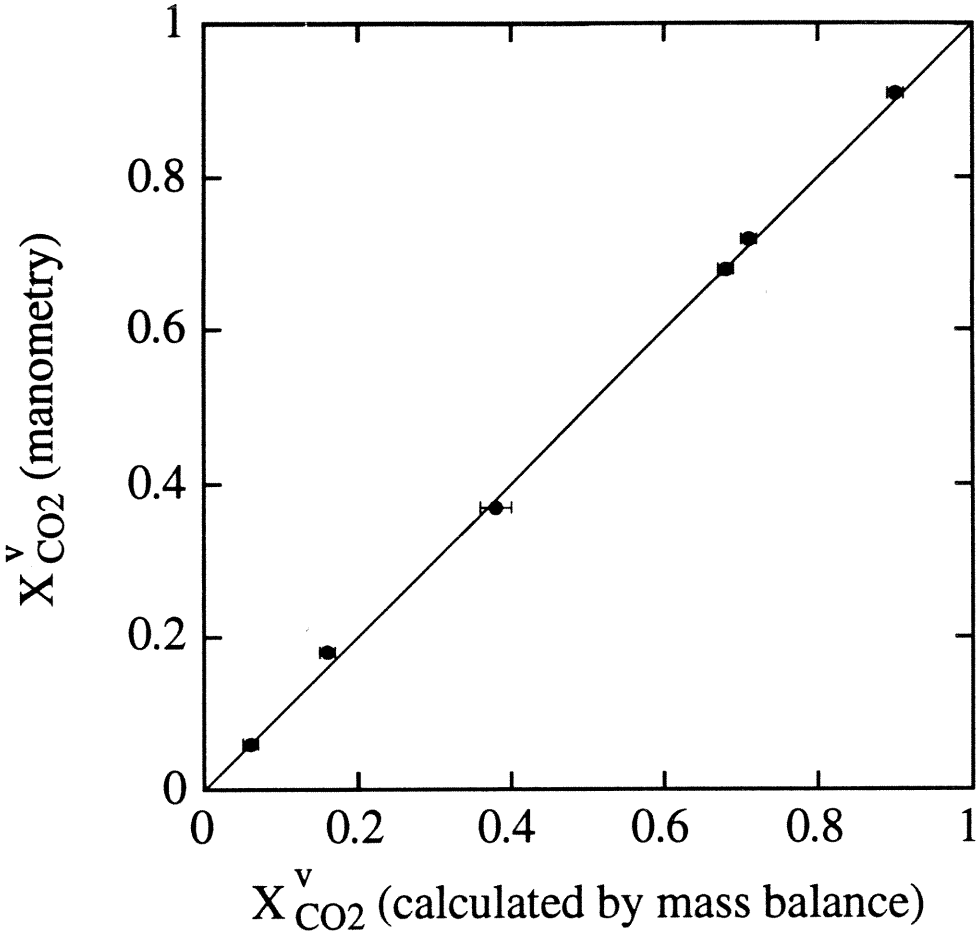

Fig. 3-1 Comparison of $X^{v}_{CO_2}$ based on manometry and mass balance constraints. Errors on manometric measurements are smaller than the symbols. Errors on $X^{v}_{CO_2}$ calculated from mass balance are based on propagation of errors in concentrations of water and carbon dioxide in the starting and quenched glasses (based on 2σ for the distribution of replicate spectroscopic measurements of dissolved CO_2 or H_2O contents) and weighing errors on the amounts of each starting material (water, silver oxalate, glass) loaded into the capsule.

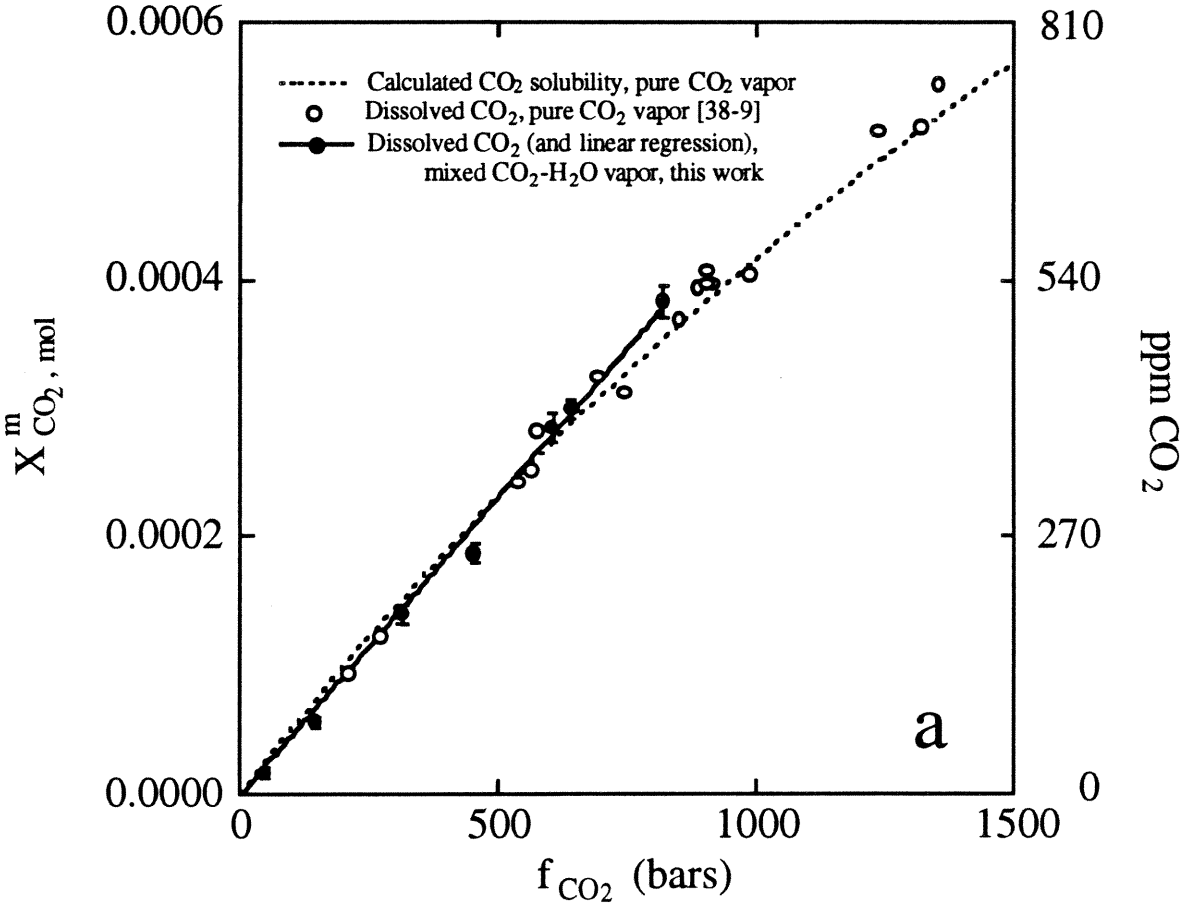

Fig. 3-2a Henrian behavior of CO_2 dissolved in rhyolitic melt equilibrated with pure CO_2 vapor or a mixed CO_2-H_2O vapor at 850°C and 750 bars, as shown by the proportionality of dissolved molecular CO_2 in vapor-saturated rhyolitic melt to f_{CO_2}. Results for melts in equilibrium with mixed H_2O-CO_2 vapor at constant total pressure (closed circles; this work) are compared with results for melts in equilibrium with essentially pure CO_2 vapor over a range of pressures ((1993); open circles). Fugacities were calculated using a modified Redlich-Kwong equation of state (Holloway, 1977). Errors on mixed-volatile data are 2σ. The solid line is a regression through the mixed-volatile data forced through the origin: $X^m_{CO_2} = (4.6\pm0.1)\times10^{-7}\ f_{CO_2}$, or ppm $CO_2 = (6.2\pm0.1)\times10^{-1}\ f_{CO_2}$, where r^2 = 0.99. The dashed curve is the calculated concentration of CO_2 in rhyolitic melt coexisting with pure CO_2 vapor at 850°C, where $P_{CO_2} \approx P_{total}$. This curve was

calculated using equation (4) from Stolper et al. (1987) and my data from Chapter 1 combined with corrected data of Fogel and Rutherford (1990), from which the following parameters were derived: the partial molar volume of molecular CO_2 in the melt, $v^m_{CO_2}$ = 28(±2) cc/mole (assumed independent of P and T); the molar enthalpy change for CO_2 dissolution in the melt, $\Delta H°_{CO_2}$ (P_o) = -27.2(±2.1) kjoules/mole (assumed independent of T), and $\ln[X^{o}_{CO_2}{}^{m}$ (P_o,T_o) / $f^o_{CO_2}$ (P_o,T_o)] = -14.45(±0.02), where the reference P and T (P_o,T_o) are 1 bar, 850°C.

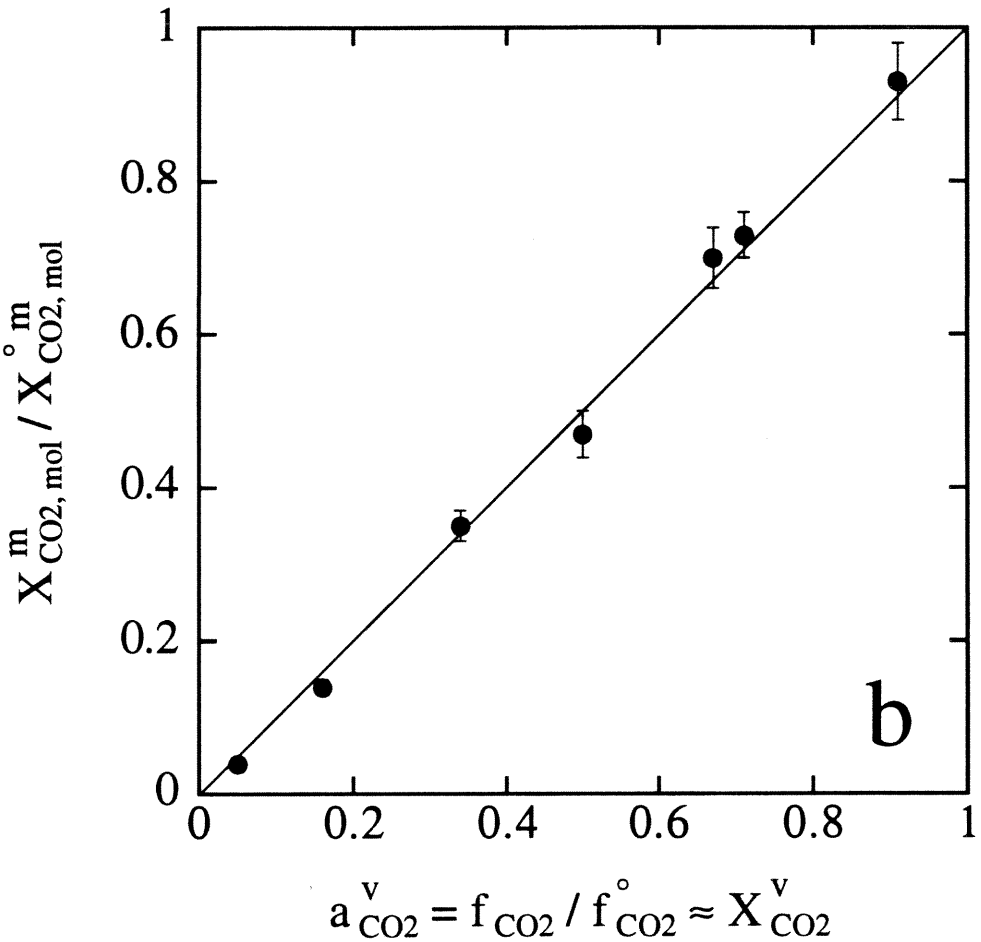

Fig. 3-2b Comparison for each experiment reported in this work between the activity of CO_2 in the H_2O-CO_2 vapor coexisting with the rhyolitic melt (i.e., the ratio of the fugacity of CO_2 in the experiment to 906 bars, the fugacity of pure CO_2 vapor at the pressure and temperature of the experiment) and the ratio of the concentration of CO_2 in the H_2O-CO_2 vapor-saturated rhyolitic melt to its concentration in melt saturated with pure CO_2 vapor at this pressure and temperature (which is equivalent to the activity of CO_2 in the melt given a Henry's law standard state taken as CO_2 in the melt saturated with pure CO_2 vapor at P and T). The 1:1 line corresponds to Henrian behavior. Data for rhyolite-CO_2 at 750 bars, 850°C used to normalize my mixed-volatile results are: f_{CO2} = 906 bars, X^{m}_{CO2} = 3.97(±0.07)x10-4 (Chapter 1). Uncertainties are based on propagation of 2σ errors (Bevington, 1969).

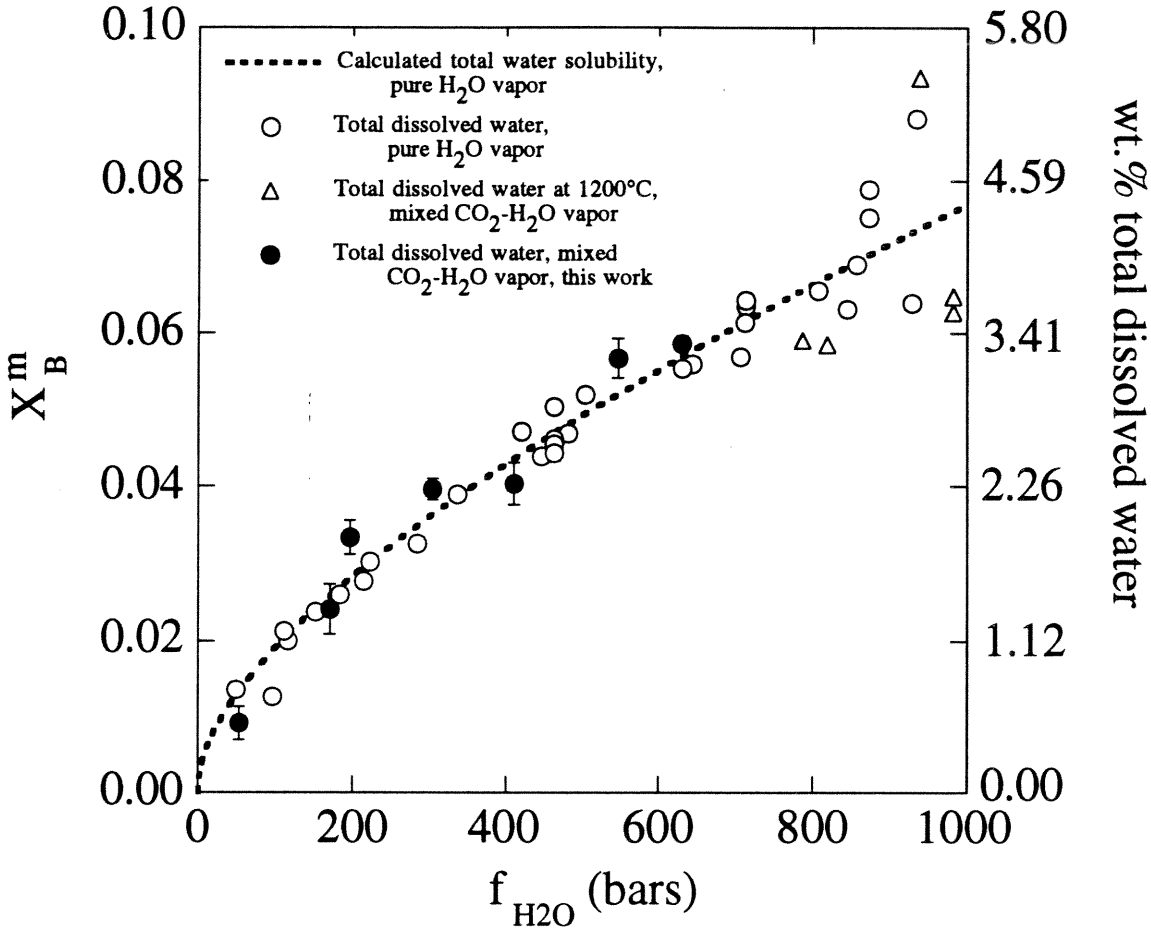

Fig. 3-3. *Total* dissolved water (water dissolved as OH + molecular H_2O) content of vapor-saturated rhyolitic melt (expressed as X_B, calculated on a single oxygen basis (Silver et al., 1990; Silver and Stolper, 1989)) versus the f_{H_2O}. Fugacities were calculated using a modified Redlich-Kwong equation of state (Holloway, 1977). Symbols are: 850°C mixed-volatile results from this work (closed circles); 1200°C mixed-volatile results of Kadik et al. (1972) (open triangles) and 850°C pure water vapor results of Silver et al. (1990) (open circles). Errors on mixed-volatile data are 2σ. The dashed curve is the best-fit concentration of H_2O in rhyolitic melt coexisting with pure H_2O vapor (where f_{H_2O} varies due to changes in total pressure) and was calculated by the method outlined in Silver et al. (1990) (cf., their Fig. 13a) using bulk water data from Silver et al. (1990) and Karsten et al. [1982], and equilibrium molecular water contents calculated from bulk water data using the regular solution model parameters given by Zhang et al. ((1991);

cf., caption to their Fig. 6). Best-fit thermodynamic parameters used in the calculations are: $v^{m}_{H_2O}$ = -2.5(±3.0) cc/mol, $\Delta H^{o}_{H_2O}$ (P_o) = -26.6(±4.4) kjoules/mole, and $\ln[X^{o}_{H2O,mol}(P_o,T_o) / f^{o}_{H_2O}(P_o,T_o)]$ = -10.31(±0.04), where (P_o,T_o) are 1 bar, 850°C.

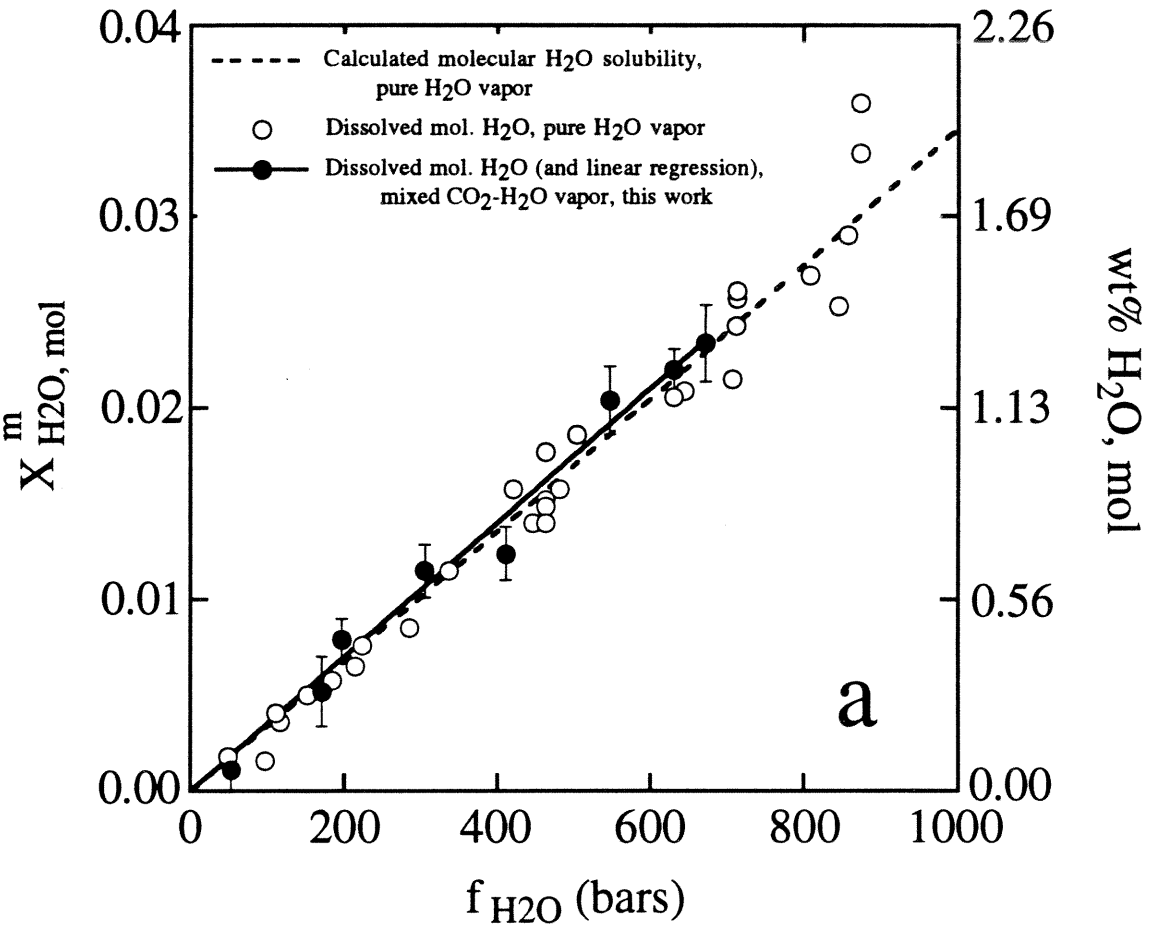

Fig. 3-4a Illustration of Henrian behavior of molecular water dissolved in rhyolitic melt equilibrated with a pure H_2O vapor or a mixed CO_2-H_2O vapor at 850°C and 750 bars, as shown by the proportionality of dissolved molecular water in vapor-saturated rhyolitic melt to f_{H_2O}. Results for melts in equilibrium with mixed H_2O-CO_2 vapor at constant total pressure (closed circles; this work) are compared with results for melts in equilibrium with essentially pure H_2O vapor over a range of pressures (Silver et al., 1990; open circles). Fugacities were calculated using a modified Redlich-Kwong equation of state (Holloway, 1977). Errors on mixed-volatile data are 2σ. Concentrations of dissolved molecular water in rhyolitic glasses have been calculated at 850°C based on the regular solution model parameters of Zhang et al. (1991). The solid line is a linear regression through the mixed-volatile data forced through the origin: $X^m_{H_2O,mol} = (3.5\pm0.1)\times10^{-5}\ f_{H_2O}$,

or wt% $H_2O_{mol} = (19.8\pm0.6)x10^{-4}\ f_{H_2O}$, with $r^2 = 0.98$. The dashed curve is the calculated concentration of molecular H_2O in rhyolitic melt coexisting with pure H_2O vapor at 850°C, where $P_{H2O} \approx P_{total}$, based on the best-fit parameters given in the caption to Fig. 3-3.

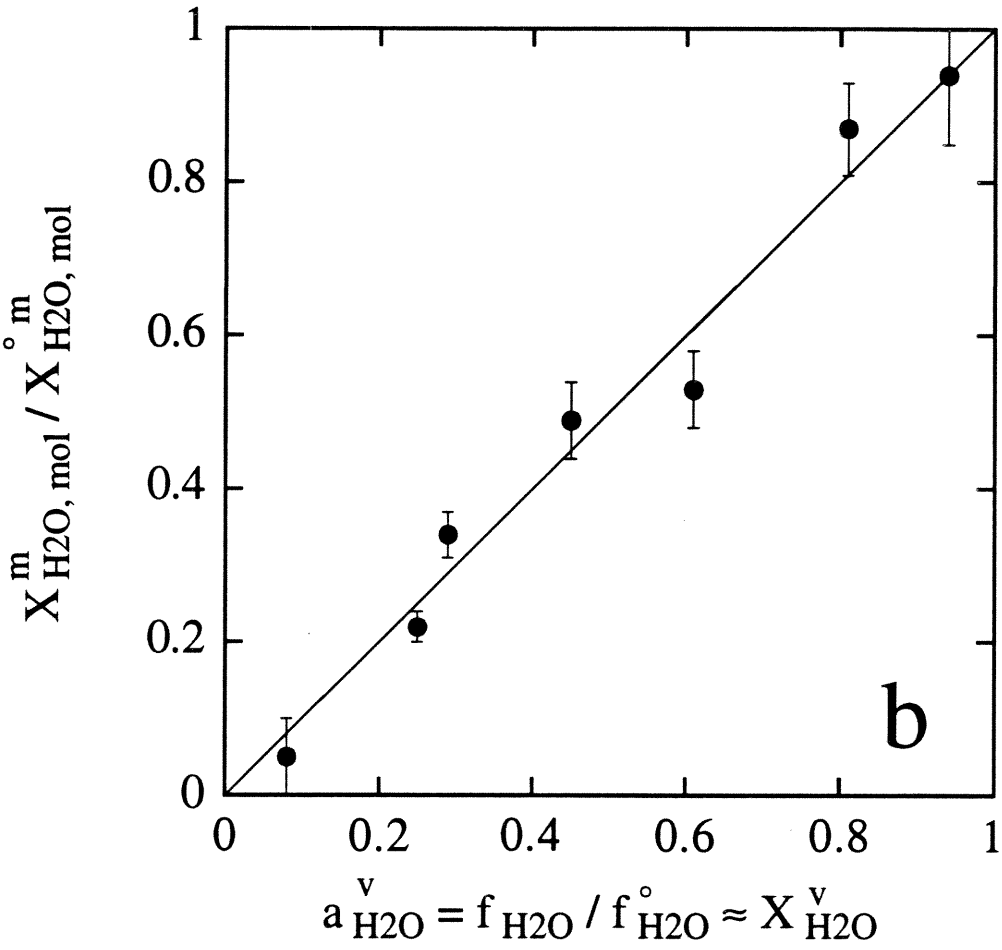

Fig. 3-4b Comparison between the activity of H_2O in the H_2O-CO_2 vapor coexisting with the rhyolitic melt (i.e., the ratio of the fugacity of H_2O in the experiment to the fugacity of pure H_2O vapor at the pressure and temperature of the experiment) and the ratio of the concentration of molecular H_2O in the CO_2-H_2O vapor-saturated rhyolitic melt to its concentration in melt saturated with pure H_2O vapor at this pressure and temperature (which is equivalent to the activity of H_2O in the melt given a Henry's law standard state taken as molecular H_2O in the melt saturated with pure H_2O vapor at P and T). The 1:1 line corresponds line to Henrian behavior. Data for rhyolite-H_2O at 750 bars, 850°C used to normalize

our mixed-volatile results are: $f^{o}_{H_2O}$ = 672 bars (for $P_{tot} = P_{H2O}$) and $X^{om}_{H_2O,mol}$ = 0.0234(±0.0020) (cf., Chapter 1). Errors are based on propagation of 2σ errors Bevington (1969).

Table 3-1 Summary of results of experiments conducted at 850°C, 750 bars, for ≈ 6 days

Experiment No.	2	3	4	5	7	9	10
vapor							
H_2O (liq.) loaded into capsule (μmol)	389	389	596	389	200	120	176
CO_2 (as $Ag_2C_2O_4$) loaded (μmol)	604	395	28	42	52	438	228
H_2O vapor (μmol) (mass balance)[a]	284(19)	273(20)	403(19)	218(21)	84(20)	49(17)	92(20)
H_2O vapor (μmol) (manometry)[b]	280	258	395	193	86	43	86
CO_2 vapor (μmol) (mass balance)[a]	604	395	28	42	51	437	228
CO_2 vapor (μmol) (manometry)[b]	601	*	26	43	50	427	224
dissolved volatiles							
Weight of rhyolitic glass chips (g)	0.10026	0.10013	0.0999	0.10029	0.10019	0.09967	0.0999
Amt. of water in initial glass (μmol)[c]	8.9 (2.8)	8.9 (2.8)	8.9 (2.8)	8.9 (2.8)	8.9 (2.8)	8.9 (2.8)	8.9 (2.8)
Dissolved total water (wt%)[d]	1.88 (.06)	2.24 (.08)	3.34 (.08)	3.23 (.10)	2.28 (.08)	0.51(.06)	1.35 (.10)
" " " (μmol)	105(5)	125(6)	185(6)	180(7)	127(6)	28(3)	75(6)
Dissolved OH (wt%)[e]	1.2(.04)	1.31(.06)	1.43(.06)	1.38(.06)	1.53(.06)	0.47(.04)	0.97(.04)
Dissolved mol H_2O (wt%)[e]	0.68(.02)	0.93(.03)	1.91(.06)	1.85(.04)	0.75(.04)	0.04(.10)	0.38(.08)
Calc. molecular H_2O (wt%)[f]	0.48	0.66	1.26	1.14	0.68	0.05	0.28
Dissolved CO_2 (ppm)[g]	385 (17)	258 (10)	23 (6)	79 (6)	194 (10)	510 (16)	402 (10)
" " (μmol)	0.9(.04)	0.6(.02)	<0.1(.01)	0.2(.02)	0.4(.02)	1.2(.04)	0.9(.02)
Remarks[h]	m	c,b	c	c	c,b	m,c	m,b
No. of IR analyses	4	4	5	4	3	3	3

mole fractions and fugacities [i,j]

$X^{v}_{CO_2}$ (mass balance)	0.68(.01)	0.52(.01)	0.06(.01)	0.16(.01)	0.38(.02)	0.9(.01)	0.71(.01)
$X^{v}_{CO_2}$ (manometry)	0.68		0.06	0.18	0.37	0.91	0.72
f_{H2O} (bars)	197	305	631	547	411	53	171
f_{CO2} (bars)	604	452	45	143	312	820	642
$10^4 X^{m}_{CO_2}$	2.80	1.87	0.17	0.57	1.41	3.72	2.92
$100\ X_B$	3.04	3.77	5.87	5.48	4.04	0.92	2.41
$100\ X_{H2O,mol}$	0.79	1.15	2.20	2.04	1.24	0.11	0.52

Notes:

* Vapor lost.

[a] Amount of H_2O in the final vapor is calculated as {amount of initial water vapor + amount of initial dissolved water - amount of final dissolved water}. Amount of CO_2 in the final vapor is calculated as {amount of initial CO_2 vapor - amount of dissolved CO_2}. Nos. in () are uncertainties in the water content of the vapor based on propagation of errors in initial and final water contents of the glass (2σ deviations based on replicate IR measurements), in the amounts of water loaded into the capsule via microsyringe (± 11 μmole), and in weighing error (±0.0001g) on the amount of glass starting material. Because the molecular weight of $Ag_2C_2O_4$ is large (and therefore weighing error will not significantly affect the amount of CO_2 loaded into a capsule) and little CO_2 is dissolved in the glass at the end of an experiment, mass balance errors for CO_2 are estimated to be very small ($\approx <$ 1μmol).

[b] Precision for the manometric measurements is ±0.3 μmoles.

[c] Based on analyses of 15 glass chips from the same rhyolite starting material. Mean bulk water content was 0.16 ± 0.06 (2σ) wt% total water (Chapter 1). Nos. in () are propagated 2σ uncertainties.

[d] Total water determined from the sum of H_2O_{mol} and water dissolved as OH^-, except for Experiment 9, in which the amount of (H_2O,mol) was below detection. For Experiment 9, total water was determined by the peak height of the absorption at 3550 cm^{-1} (Dobson et al., 1989). Nos. in () indicate 2σ deviations determined from the distribution of IR measurements.

[e] From IR spectroscopic measurement of H_2O_{mol} absorbance at 5200 cm^{-1} and OH^- absorbance at 4500 cm^{-1} (Newman et al., 1986). Molecular water in glass from Experiment 9 was determined by subtracting the amount of (OH^-) determined by the 4500 cm^{-1} band from the amount of total water determined from the 3550 cm^{-1} band.

[f] Equilibrium concentration of molecular water at 850°C calculated using the regular solution model parameters of Zhang et al. (1991). See caption to Fig. 3-3.

[g] Determined using the peak height of molecular CO_2 absorption at 2350 cm^{-1} (Chapter 1). Nos. in () indicate 2σ determined from the distribution of IR measurements.

[h] m=microlites; c=clear glass; b=bubbles present.

[i] Mole fraction calculations: $X^v_{CO_2}$ is defined by (μmoles CO_2 vapor)/(μmoles CO_2 vapor + H_2O vapor); 2σ propagated error for mass balance estimate of $X^v_{CO_2}$ are given in (). $X^m_{CO_2}$ calculated by (wt% CO_2 / 44) / ((100 - wt% H_2O_{tot} - wt% CO_2) / 32.5 + (wt% H_2O_{tot} /18) + (wt% CO_2 / 44)), where 32.5 is the molecular wt. of anhydrous rhyolite on a one-oxygen basis. X_B (bulk water) = (wt% H_2O_{tot} / 18) / ((100-wt% H_2O_{tot} - wt% CO_2) / 32.5 + (wt% H_2O_{tot}) / 18 + (wt% CO_2) / 44); $X_{H2O,mol}$ = (wt% H_2O_{mol} / 18) / ((100 - wt% H_2O_{tot}) / 32.5 + (wt% H_2O_{tot}) / 18 + (wt% CO_2) / 44).

[j] Fugacities calculated using a modified Redlich-Kwong equation of state (Holloway, 1977) based on $X^v_{CO_2}$ determined from manometric measurements.

Chapter 4

The Partitioning of ^{13}C Between Coexisting CO_2 Vapor and Rhyolitic Melt

4.1 INTRODUCTION

Stable isotope studies of C-H-O fluids are an important means of understanding fluid-melt-rock interactions, but all models incorporating isotopic variation ultimately depend on how well equilibrium isotopic fractionation between species is known. The magnitude of this fractionation is dependent on such factors as temperature, speciation, chemical environment, and kinetic effects. The two stable isotopes of carbon, ^{12}C and ^{13}C, are differentially partitioned in many physical processes, and thus variations in the $^{13}C/^{12}C$ ratios of carbon, a principal component of igneous volatiles, offer a potentially important geochemical indicator of magmatic processes.

Studies of partitioning behavior of ^{13}C in igneous systems has been limited to the system CO_2-basalt. Several investigators (e.g., Javoy et al., 1978; Mattey, 1991; Trull et al., 1991) have determined experimentally that CO_2 vapor is enriched in ^{13}C by $\approx$ 2-4 ‰ relative to carbon dioxide dissolved in coexisting basaltic melt. Such fractionation information has been used to interpret the observed variations in $^{13}C/^{12}C$ ratios in submarine basaltic glasses (Blank et al., 1993; Bottinga and Javoy, 1989; Javoy and Pineau, 1991) and fumarole gases (e.g., Gerlach and Taylor, 1990), and also to estimate the initial carbon content of undegassed basaltic magma and calculate the flux of CO_2 from mid-ocean ridge volcanism to the atmosphere (e.g., DesMarais, 1985; Javoy et al., 1982)

At the P-T conditions relevant to magma degassing, dissolved CO_2 in basaltic magmas occurs as carbonate ions, whereas it is present as molecules of CO_2 in rhyolitic melts and glasses, at least to pressures of 7 kbars (Fogel and Rutherford, 1990; Newman et al., 1988). Based on these differences in carbon speciation between basaltic and rhyolitic melts, isotopic fractionation is predicted to be smaller for the CO_2-rhyolite system.

Building on the knowledge of the speciation, solubility, and diffusive behavior of CO_2 dissolved in rhyolitic melts discussed in previous chapters, I conducted experiments to determine the partitioning of ^{13}C between coexisting CO_2 vapor and rhyolitic glasses. To do this, I equilibrated natural, CO_2-free rhyolitic glasses with CO_2 gases having different $^{13}C/^{12}C$ ratios. Experiments were conducted at 800°-1200°C and at pressures ranging from 250-1444 bars. At the end of an experiment, vapor coexisting with rhyolitic melt was collected and analyzed for its $^{13}C/^{12}C$ ratio. The rhyolitic glasses were combusted on a vacuum line using a stepped-heating procedure, and CO_2 was extracted and $^{13}C/^{12}C$ ratios were determined for direct comparison with the vapor. Individual glass chips were also analyzed for dissolved CO_2 using FTIR spectroscopy. The experimental approach used here is different from previous isotopic studies in that the application of both FTIR spectroscopy and manometry allows for a more thorough evaluation of the experimental results. The results serve as a basis for interpreting the $^{13}C/^{12}C$ ratios of natural silicic magmas.

4.2 SAMPLE PREPARATION

Aphyric natural rhyolitic glass from Glass Butte, Oregon, served as the starting material for the experiments (cf., Chapter 1, for description and composition). On the basis of spectroscopic analysis, the glass initially contains 0.09-0.28 wt% dissolved water and no dissolved CO_2. Microlites are ubiquitous.

Starting material was prepared in the following manner. Glass fragments were separated from a hand-sample sized piece of rhyolitic glass with a hammer. Fragments were crushed and sieved using a stainless steel mortar and pestle, and the 0.5-1.0 mm diameter fraction was collected. These sized chips were ultrasonicated in ethanol for 10 minutes and then rinsed in ethanol three times to remove any glass powder or other contaminants that may have adhered to the chips during the crushing procedure. Glass

chips, dried under a heat lamp, were stored in a 100°C oven prior to being loaded into capsules.

Capsules were made from precious metal tubing, 5.1 or 3.8 mm o.d., triple-crimped and sealed at one end using an arc welder. Capsules were annealed until they glowed (>1000°C) in a Bunsen burner gas (mixed CH_4-O_2) flame. This process served to combust organics and other carbon-bearing residue that may have been attached to the metal surfaces.

Prepared capsules were 27.9 mm in length and contained ≈ 0.24-0.45 g rhyolitic glass. "Open-capsules" were triple-crimped at their tops but not sealed. "Closed-capsules," containing glass chips and a source of CO_2, were crimped and welded shut. Silver palladium (Ag:Pd = 70:30) capsules were used in open-capsule experiments. Because they are more malleable and thus less likely to be punctured by the rhyolitic glass chips than AgPd capsules, Pt capsules were used in the closed-capsule experiments.

4.3 EXPERIMENTAL METHODS

Capsules, pressurized at room temperature using Matheson "bone dry" (i.e., containing < 10 ppm H_2O) CO_2 or Ar gas to 250-1444 bars, were held at temperatures of 800°, 850°, or 1200°C for periods lasting from 32 hours to almost 700 hours (≈29 days). On the basis of solubility and diffusion studies (Chapters 1 & 2), all run durations were longer than required to achieve equilibrium CO_2 concentrations in the rhyolitic glass chips. The 800° and 850°C experiments were conducted in conventional cold seal bombs (Tuttle, 1949) with the hot spot at bottom. Methods were similar to those described in Chapter 1, with quenching times of approximately 4 minutes. Experiments at 1200°C were conducted using a rapid-quench TZM vessel; quenching times for these experiments were 3-4 seconds.

Aside from variations in pressure, temperature, and run duration, the principal difference between experiments was the source of the CO_2 in contact with the rhyolitic glasses. This CO_2 gas encompassed a range of $^{13}C/^{12}C$ ratios (Table 4-1) and was supplied to the samples in one of three ways:

(a) CO_2 pressurizing medium entering unwelded ("open") capsules;

(b) Decomposition of silver oxalate in sealed capsules to produce CO_2; or

(c) CO_2 gas loaded directly into capsules that were then welded closed.

In order to determine the carbon isotopic composition of the vapor loaded into capsules, several "control" experiments were conducted in which only $Ag_2C_2O_4$ or CO_2 gas were loaded into Pt capsules and exposed to elevated temperatures and pressures. The "control" experiments were similar in design to those involving rhyolitic glass chips except that they were of shorter duration. The different experimental approaches are described below. At the end of an experiment, CO_2 vapor coexisting with the rhyolitic glass was sampled and collected for analysis.

4.3.1 Open-capsule experiments

In the first series of fractionation experiments, AgPd capsules were crimped but not welded at their tops, leaving the rhyolitic chips inside exposed directly to the CO_2 pressuring medium. Several hours after a run was quenched, time enough for the bomb to thermally equilibrate to room temperature, an aliquot of the pressurized CO_2 from the bomb was sampled. Two sampling methods were employed (Fig. 4-1).

In the first sampling method (Fig. 4-1a), a length of polyurethane tubing connected the bleed valve of the pressure vessel to an F-shaped Pyrex chamber, to which an evacuated 25 ml Pyrex sample tube was attached. The bleed valve was opened slowly, allowing the bomb pressure to decrease by ≈100 bars/min, and CO_2 gas flowed from the bomb through the Pyrex chamber. During this time, the sample tube was opened slowly

so as to minimize the amount of air that entered and allow for collection of a sample of CO_2 flowing out from the bomb.

A second technique for sampling the bomb CO_2 employed a high pressure, 300 ml capacity Monel sampling cylinder (Matheson gas products, model 4HDM300; Fig. 4-1b). This device was attached directly to the bomb bleed valve. After evacuating the sampling cylinder with a vacuum pump, the bleed valve was opened and bomb CO_2 expanded into the sampling cylinder. After waiting for 2 minutes, the bleed valve was closed and the sampling cylinder was reevacuated. This procedure was repeated several times until the pressure of CO_2 present in the cylinder was <2 bars. The sampling cylinder was then removed and attached to a vacuum line, and CO_2 gas was transferred to a conventional sample tube for subsequent mass spectrometric analysis.

4.3.2 Silver oxalate experiments

In a second set of experiments, silver oxalate, which decomposes at ≈140°C according to the reaction:

$$Ag_2C_2O_4 = 2CO_2 + 2Ag$$

served as the source of CO_2 inside sealed capsules. Two types of silver oxalate powder were used, one purchased commercially (K&K Labs, New York)[1] and a second batch prepared in the laboratory from silver nitrate and oxalic acid dihydrate. Both batches of silver oxalate were analyzed for their CO_2 contents prior to use and had CO_2 yields of >98% based on stoichiometry. In these experiments, ≈25-50 μmoles of $Ag_2C_2O_4$ powder (i.e., 50-100 μmoles CO_2) were loaded in to the bottom of a Pt capsule, glass chips were placed on top of the powder, and the top of the capsule was triple-crimped and welded shut. After an experiment, CO_2 vapor was retrieved by piercing the capsule

[1] It is illegal to ship silver oxalate now because of its explosive potential and consequently no chemical laboratories sell it. Our batch from K & K Labs was opened in 1986, purchased in 1985.

under vacuum. Vapor yield was measured and collected for subsequent mass spectrometric analysis.

4.3.3 CO_2 gas experiments

In a final set of experiments, ≈15-25 μmoles of CO_2 gas were loaded directly into Pt capsules and sealed using a vacuum crimping technique (Zachary Sharp, personal communication). This closed-capsule procedure was advantageous in that it avoided the presence of silver (from $Ag_2C_2O_4$) and air in the capsule. Only about half of the amount of glass chips could be loaded in these capsules relative to the previous experiments; the procedure for vacuum crimping a capsule attached to a vacuum line requires a flat crimp rather than a triple-crimp, and thus, limited by the 6.4 mm bore diameter of the pressure apparatus, I used smaller (3.8 mm rather than 5.1 mm) diameter Pt tubing.

To load CO_2 gas directly into a Pt capsule, 40 mm lengths Pt tubing, filled with a known weight of glass chips, were attached to a vacuum line using Cajon ultra-torr adapters. After evacuating the capsule for 5-10 minutes, the base of the Pt tubing was immersed in a liquid nitrogen (LN) bath, and a measured aliquot of CO_2 gas of known isotopic composition was frozen into the capsule. This transfer process took approximately 20 minutes, during which time it was often necessary to warm the Pt tubing to ensure successful freezing of CO_2 toward the base of the tubing rather than the top, where it could be left behind after crimping.

Once the transfer process was complete, a 5 mm region of the Pt tubing was flattened together using pliers, then the Pt was crimped and removed from the vacuum line. Vacuum crimping was accomplished using a cold-weld pinch-off device (CHA Industries, model POD-375), used commonly in cold-welding copper refrigerator tubing. A Pt capsule cold-welded in this manner will hold 4-5 bars of pressure before popping open. Immediately after cold-welding, the capsule was placed in a vice and permanently

sealed using an arc-welder. Successful welds were verified by placing the capsule in a 1-atm furnace at 500°C for 2 minutes; capsules that were leak-tight bulged out near their welded ends.

4.4 ANALYTICAL TECHNIQUES

4.4.1 CO_2 Extraction Procedures

The majority of samples were analyzed using a vacuum line designed especially for extracting and measuring carbon dissolved in glasses. Key features of the vacuum line include an extraction chamber with low temperature (resistance) and high temperature (induction) furnaces, a variable temperature trap (VTT; Des Marais, 1978) for distillation of condensable gases, a source of O_2 from the dissociation of hot CuO, and a bobometer for high-precision measurement of small (~ 1 μmole) gas samples. The bobometer has a maximum sensitivity of 3.5 cm Hg displacement per μmole of gas.

The sample extraction procedure consisted of (1) purifying and measuring CO_2 vapor that equilibrated with rhyolitic melt during an experiment; then (2) conducting a procedural blank prior to (3) heating rhyolitic glasses in timed increments to extract their CO_2. Details of the analytical steps are given below.

CO_2 vapor -- Sample tubes containing aliquots of the CO_2 gas that served as the pressurizing medium in the open-capsule experiments were attached to the vacuum line. Condensable gases were frozen in LN while small amounts of noncondensable gases (air presumably, added during sample collection) were pumped away. CO_2 collected in the Monel sampling cylinder contained very small amounts of noncondensible gases. CO_2 was separated from other condensable gases using a M17-dry ice slurry, and collected in sample tubes for mass spectrometric analysis.

Vapor trapped inside a capsule was retrieved after an experiment by piercing the capsule under vacuum. Sealed capsules were loaded into a NUPRO valve modified for capsule piercing and evacuated for 15-30 minutes. After capsule-piercing,, vapor was transferred slowly (≈10-15 min) to the VTT at LN temperature (-178°C). During gas transfer, capsules were heated (to ≈200°C) using a heat gun. Capsules prepared with silver oxalate contained small amounts of noncondensible gas (< 1μmole), presumably air that was welded inside the capsule. Capsules loaded with CO_2 gas contained no measurable noncondensible phases. CO_2 was distilled from the VTT at -140°C. CO_2 vapor released from capsules was measured manometrically to determine the yield and then sealed into sample tubes for subsequent mass spectrometric analysis.

Pierced capsules were removed from the vacuum line and either (a) opened immediately whereupon the glass inside was extricated and loaded in to the extraction chamber on the vacuum line, or (b) placed in 2.5 ml, Teflon-sealed Pierce sample vials to minimize exposure to air before analysis. "Open-capsules" were transferred at the end of an experiment directly from the pressure vessel into a Pierce vial to minimize sample contamination.

Glasses -- A procedural blank was measured prior to extracting CO_2 from a glass sample. A Pt crucible and a clean quartz cup were loaded into a combustion vessel and then evacuated and heated to 1200°C. After 30 minutes, the combustion chamber was isolated from the main manifold, O_2 from the CuO furnace at 900°C was expanded into the combustion chamber, and an LN trap was positioned to collect condensable phases. The "blank" combustion lasted for 45 minutes, after which point any noncondensible gases (H_2?) were evacuated and CO_2 was separated from other condensable phases using a dry ice-ethanol slurry, and measured. If the blank was larger than ≤0.015 μmoles CO_2, the procedure was repeated. The greatest source of extraneous CO_2 from the line was the

Pt crucibles used to heat the glasses to high temperatures. A procedural blank at 1200°C was conducted for 13.5 hours to have a sufficient amount of gas for isotopic analysis; the $\delta^{13}C$ value of this CO_2 was -28.4‰.

Capsules were opened inside a Lexan glove box immediately prior to loading their contents onto the vacuum line. The glove box minimized exposure of the glass run products to airborne particulates. Plastic gloves were worn while a capsule was opened using pliers, and only metal tweezers or pliers cleaned with dichloromethane (CH_2Cl_2) touched the glasses. A subsample of each glassy run product was removed for FTIR spectroscopic analysis. Glass samples, weighed on filter paper using a Mettler 3000 scale located immediately adjacent to the glove box, were placed into a combusted quartz sample cup and loaded into the extraction vessel. Sample GB1-41 was washed in CH_2Cl_2 for 10 minutes and was still wet when loaded; samples GB1-12,-13, and -14 were rinsed in ethanol prior to loading. The remainder of the samples were transferred from the weighing paper to the extraction vessel. 10-15 minutes elapsed from the opening of a capsule until the glass was placed on the vacuum line. Loaded samples were heated by the low-temperature furnace at 150°C under vacuum for at least 5 hours prior to the start of an extraction.

Glass samples were extracted on a vacuum line using a step-wise heating/combustion procedure. The extraction procedure consisted typically of 3-4 steps at 450°C, 650°C, and 1200°C. CO_2 collected from temperature steps $\leq$ 650°C is defined as "low temperature" gas, and CO_2 liberated above 650°C is "high temperature" gas, indigenous to a sample. A second 650° step was conducted on several samples to verify removal of "low temperature" CO_2. Combustions at T$\geq$1100° were conducted for 90 minutes; combustions at lower temperatures lasted 40 minutes.

Three samples, GB1-12, -13, and -14, were extracted using a different vacuum line. Under vacuum, samples were *pyrolyzed* at 200°, 400°, and 1200°C for intervals similar to those of other glasses.

4.4.2 Mass spectrometric analysis

$^{13}C/^{12}C$ ratios of CO_2 gas samples were determined using a VG Prism Isotope Ratio Mass Spectrometer (IRMS) in the Stable Isotope Laboratory of Professor Jean Morrison at the University of Southern California. Isotopic ratios are given in the delta (δ) notation[2] in parts per thousand, or permil (‰), relative to the PDB standard. All results are reported incorporating Craig (1957) corrections.[3]

It is difficult to transfer small quantities of CO_2 gas in vacuum systems without small amounts of isotopic fractionation of the gas, especially if freezing and thawing procedures are required. The sample inlet volume of the VG Prism is sufficiently large as to necessitate that samples smaller than ≈ 7 μmoles be frozen into a "finger" (a micro-LN trap) and then isolated from the sample inlet port in a smaller volume to produce a sufficiently high pressure of gas flowing in to the mass spectrometer. Most of the CO_2 samples collected from glass extractions were frozen into the sample finger prior to analysis, and it was important therefore to verify that isotopic fractionation resulting from the freezing process was minimal. I found that it was critical to equilibrate fully the temperature of the finger after freezing with that of the rest of the sample inlet portion of the instrument. For example, a zero-enrichment test (i.e., one in which reference gas was

---

2 Where $\delta^{13}C = 1000 \times [(^{13}C/^{12}C)_{sample} / (^{13}C/^{12}C)_{standard} - 1]$.

3 For a triple collector instrument such as the VG Prism, the correction formulae are:

$$\text{delta } ^{13}C = 1.07676 \text{ delta } (45/44) - 0.0338 \text{ delta } ^{18}O$$

and

$$\text{delta } ^{18}O = 1.001 \text{ delta } (46/44) - 0.0021 \text{ delta } ^{13}C$$

While I was not concerned with the absolute value of the $^{13}C/^{12}C$ ratio involved, the oxygen isotope composition of the vapor and the glasses may differ significantly and thus the Craig corrections were important to ensure that the contribution to the measured $^{13}C/^{12}C$ values from oxygen isotopes was minimized. For example, the PDB standard has a contribution of ≈ 6% at mass 45 due to the ^{17}O isotope. (Similarly, 0.2% of mass 46 is derived from isotopic species containing ^{13}C and ^{17}O but not ^{18}O.)

run against itself on the sample side) conducted using the cold finger gave the following results:

Sample Description	$\Delta\ ^{13}C$ reference - sample (‰)
reference gas	0.0
cold finger test, CO_2 at 40°C	0.1
cold finger test, CO_2 at 32°C	0.0

where Δ is the difference in $\delta^{13}C$ values between the reference and sample gases; here, obviously, it should be zero. The ambient temperature of the inlet system is 32°C. When thawing a sample, the temperature of the finger initially overshoots the ambient temperature, and if a measurement is made before the temperature has dropped back down, small amounts of isotopic fractionation may result. Similarly, insufficient transfer time from the sample tube to the finger or after a valve is opened may result in larger fractionations of up to several tenths of a permil. Repeated analyses of splits of larger (>10 μmole) samples to test for fractionation during freezing and transfer of CO_2 revealed that a reproducible isotopic ratio (< ±0.05‰) could be obtained for samples as small as ≈ 0.2 μmoles when very slow freezing/thawing periods were allowed. Analysis of a frozen sample took ≈ 50 minutes.

Reported 2σ precision for a single Prism ISRM measurement of gases analyzed in this study, based on 10 ratios of the sample and standard gases, is <0.05 ‰. Precision (2σ) on multiple analyses of two standard gases is 0.06 permil. However, the overall 2σ standard deviation for extraction and collection of CO_2 and mass spectrometric analysis is probably nearer to 0.1-0.2 ‰ for samples on the order of one μmole and may be larger for smaller samples.

4.4.3 FTIR Spectroscopy

Concentrations of carbon dioxide and water dissolved in the quenched glasses were determined from transmission spectra of glass chips doubly-polished to have two parallel sides. Many of the samples were also examined by IR spectroscopy after they were combusted on the vacuum line. Details of the FTIR spectroscopic method are discussed in Chapter 1. Samples were placed in the microchamber of a Nicolet 60SX FTIR spectrometer, and spectra were taken with 1024 scans, a gain of 32, a KBr beamsplitter, a visible light source, and a liquid-N_2-cooled, InSb detector. Round apertures (100 μm diameter) in metal foils were used to aim the infrared beam at selected regions of the polished glass. Spectra were taken at 2-8 spots, including regions near the centers and edges, on a single polished fragment selected from each experimental charge. Individual polished grains varied in thickness from 90-450 μm. Concentrations of dissolved CO_2 were calculated according to the Beer-Lambert law using the peak height of molecular CO_2 absorption at 2350 cm^{-1}, a molar absorptivity coefficient of 1066 l/(cm-mol), the measured sample thickness, and a glass density of 2350 g/l (Chapter 1). Bulk dissolved water was determined from the absorption at 3550 cm^{-1} using a molar absorptivity coefficient of 88 l/(cm-mol) (Dobson et al., 1989).

4.4.4 CO_2 vapor "control" experiments

Results of the vapor "control" experiments, in which CO_2 gas or $Ag_2C_2O_4$ were sealed inside Pt capsules without glass chips, appear in Table 4-2. The purpose of the these tests was two-fold. First, I wanted to determine the carbon isotopic composition of the initial CO_2 vapor in an experiment. Data in Table 4-2 include results of carbon isotopic analyses of CO_2 gas from $Ag_2C_2O_4$ loaded in Pt capsules and placed in a 1-atm. furnace for decomposition at relatively low temperatures as well as aliquots of CO_2 from the 3 large reservoirs tapped for the gas-loading experiments. These two types of

samples are assumed to have $\delta^{13}C$ compositions that are representative or "expected values." I also wanted to determine, by exposing a vapor-bearing capsule to elevated P and T, whether the $\delta^{13}C$ composition of the vapor would be the same at the end of an experiment. Table 4-2 also includes results of analyses of CO_2 (from $Ag_2C_2O_4$ or direct vacuum transfer) extracted from Pt capsules exposed to P-T conditions similar to those of the CO_2-rhyolite experiments.

In both types of "control" experiments, the carbon isotopic composition of the vapor retrieved from the capsules differed from "expected values" (Table 4-2). For example, CO_2 from experiments $Ag_2C_2O_4$.1-7, consisting 35-100 μmoles of CO_2 from the same batch of silver oxalate, exhibited a variation in $\delta^{13}C$ values of nearly 1.3‰ (or ≈ 1.0‰, ignoring $Ag_2C_2O_4$.1, which due to operator error had an exceptionally low yield of 5%). By contrast, the CO_2 from the three capsules held at low-temperatures in the 1-atm (box) furnace had $\delta^{13}C$ values within 0.2‰ of one another. Samples 10 and 8, consisting of CO_2 gases sealed inside evacuated Pt capsules, also exhibited a significant (0.8‰) shift from their initial $\delta^{13}C$ values. There appears to be no correlation between the $\delta^{13}C$ value of the CO_2 gas and percent yield, pressure, temperature, run duration, or capsule weight change during an experiment.

As I will show in the next section, the $\delta^{13}C$ value of the CO_2 vapor collected from an experimental CO_2-rhyolite charge also differed from the assumed value of the initial vapor. That an apparent isotopic shift was observed whether or not glass chips are present suggests surficial C-bearing contaminant from the glasses is not a major factor on the resulting $\delta^{13}C$ value of the vapor. That it occurred for both silver oxalate and CO_2-loaded capsules suggests that it (a) has something to do with the capsules,[4] or (b) coincidentally there is both isotopic heterogeneity in the silver oxalate and fractionation

[4] I do not know the concentration of elemental carbon present in the Pt tubing, but according to Watson (1987) there could be as much as 10 μmoles of C present in a large capsule. If the capsules are responsible for the apparent carbon isotopic shifts, the heterogeneous nature of C distribution in Pt (Watson, 1987)could perhaps explain the variable degree of isotopic deviation.

during the vacuum CO_2 gas-loading procedure. The nature of this apparent isotopic shift will be investigated in future studies, but for the time being I simply assume that the $\delta^{13}C$ value of the vapor retrieved from a capsule is representative of the experiment and that the variable differences between the carbon isotopic composition of the initial vapor loaded into a capsule and the final vapor has no effect on the measured $\Delta_{vapor\text{-}melt}$.

4.5 RESULTS

Experimental run conditions are listed in Table 4-1. Concentrations of dissolved CO_2 and water in the glassy run products determined by FTIR spectroscopy are listed in Table 4-3, and results of the stepwise heating/combustion extractions are given in Table 4-4. Carbon isotopic fractionations between coexisting CO_2 vapor and CO_2 molecules dissolved in rhyolitic melt, given as $\Delta_{vapor\text{-}melt}$, are summarized in Table 4-5.

4.5.1 Experimental Run Products

The appearance of the rhyolitic glass after an experiment is noted in Table 4-1. Open capsules removed from the René bombs showed no change in coloration or shape, and once the tops of the capsules were cut open, individual glass chips fell out freely. Closed capsules deformed around the rhyolitic glass starting material when the runs were pressurized, and it was more difficult to remove chips from these capsules which were compressed at the end of a run. Pt capsules held at 1200°C recrystallized. Glasses held at pressures <1000 bars retained their shape, but glasses held at higher pressures partially fused together. In two cases, glasses held at the pressures >1000 bars appeared to be smaller than their initial size; these glasses may have been crushed during the initial pressurization of the run. Glasses retrieved from all but one experiment retained their abundant microlite population, presumably an indication that these samples did not melt. Glass from experiment GB1-34 lacked visible microlites and was fused together; this

sample had the highest water content (Table 4-3). Yellow powder (probably silver) was present in the bottom of the capsules prepared with silver oxalate. Glass adjacent to the powder was not discolored.

4.5.2 FTIR spectroscopic analysis of run products

All CO_2 dissolved in the glasses was detected spectroscopically as an absorption at 3250 cm^{-1} corresponding to CO_2 molecules. CO_2 contents of the glasses determined by FTIR spectroscopy ranged from 183-860 ppm (Table 4-3). These results agree well with calculated CO_2 solubilities (Fig. 4-2) based on the thermodynamic parameters for CO_2 solubility in rhyolitic melt determined in Chapter 1.

Water contents of the glasses were determined from the absorption at 3550 cm^{-1} and found to vary from 0.11-0.46 wt% total water. No absorption bands corresponding to individual water species (OH^- at 4500 cm^{-1}; molecular H_2O at 5200 cm^{-1}) were detected. There is no correlation between dissolved water content and temperature, pressure, or run duration among the closed-capsule experiments. The water contents of the three closed-capsule experiments loaded with CO_2 gas have very similar dissolved water contents that are within the range given for the starting material. There is a wider range in water content for the glasses sealed in capsules with $Ag_2C_2O_4$, and this may be due to water in the silver oxalate. There appears to be a direct correlation between run duration and the amount of dissolved water present in glasses from the open-capsules experiments, which may indicate that there was water vapor in the pressurizing medium.

Using the average dissolved water content of glasses from the open-capsule experiments, I calculated maximum water fugacities for the vapor using the results of the mixed CO_2-H_2O solubility study for rhyolitic melts (Chapter 3). Experiment GB1-19 had the highest calculated water fugacity at 14 bars. Other 850°C experiments had f_{H2O} of 1-8 bars. Whether or not this is significant is unclear; any dilution effect that water

vapor may have on CO_2 solubility in the glasses is not detectable for such low f_{H2O} values.

Many of the glasses were analyzed after they had been combusted to verify complete removal of CO_2 during the extraction procedure (Table 4-3). The absence of detectable dissolved CO_2 molecules by IR spectroscopy indicates that the extraction procedure was successful. Removal of dissolved water was incomplete, however; glasses retained 30-50 ppm total water after extraction.

4.5.3 Stepped heating analysis

Vacuum combustion/extraction results for the rhyolitic glasses appear in Table 4-4 Carbon isotopic results are listed along with the CO_2 yields. CO_2 collected at temperatures <650° is interpreted to be derived from adsorbed material on the glass surfaces, and only the CO_2 collected at temperatures >650°C is considered to be CO_2 dissolved in the glasses. Temperature release characteristics of CO_2 associated with the rhyolitic glasses are discussed in detail in Chapter 1. A summary of the high-temperature extraction results appears in Table 4-5.

The most compelling argument to support a surficial origin for the low-temperature CO_2 is the good agreement between high-temperature CO_2 yields and IR spectroscopic measurements of CO_2 dissolved in the glasses; in contrast, bulk (low- + high-temperature) CO_2 yields correlate poorly with IR spectroscopic measurements (Fig. 4-3). Glasses released 1.7-5.6 μmoles of CO_2 during high-temperature combustion or pyrolysis.

The amount of low-temperature CO_2 collected from the samples was highly variable. Glasses washed with solvents prior to extraction yielded the lowest amounts of low-temperature CO_2. Samples GB1-12,-13, and -14, rinsed with ethanol, released 0.31-0.80 μmoles of CO_2 at temperatures ≤ 400°C during pyrolysis. No 650°C heating steps

were performed. The low-temperature CO_2 collected from these samples comprised 9-13 % of the bulk CO_2. In these samples, the amount of CO_2 recovered from pyrolysis at 200°C was less than the amount of gas collected at 400°C. GB1-41, cleaned with CH_2Cl_2 prior to extraction, released only 0.30 μmoles (32 ppm) or 8% of its bulk CO_2 at T ≤650°C. Mattey et al. (1989) routinely clean basaltic glasses with CH_2Cl_2 and are able to strip all but trace amounts (~ several ppm) of carbon released at temperatures <800°C.

The remaining samples liberated a significant portion (0.30-4.95 μmoles or 19-54%) of their bulk CO_2 during the low-temperature combustions. This is probably because the glasses were not cleaned with solvents between removal from the capsules and extraction. Combustion at 450°C usually yielded larger amounts of CO_2 than combustion at 650°C. Two samples, GB1-29 and GB1-39, released > 50% of their total CO_2 at T ≤ 650°C. These two samples appeared to be reduced in grain size after the run (Table 4-1) and may have been crushed during the initial pressurization of the experiments; sample fragmentation would have produced greater surface areas (and higher potential for surficial, low-temperature CO_2).

The carbon isotopic composition of CO_2 extracted from the glasses correlates with the $\delta^{13}C$ value of the initial vapor loaded into a capsule. However, the difference between the carbon isotopic composition of low- and high-temperature CO_2 extracted from an individual sample is variable. Samples whose initial vapor was near 0‰ have low-temperature carbon that is lighter by 3-10‰ than the high-temperature CO_2. Samples whose initial vapor composition was in the range of -20 to -30‰ have low-temperature CO_2 whose $\delta^{13}C$ values are either heavier or lighter than the high-temperature CO_2.

4.5.4 CO_2 vapor and calculation of $\Delta_{vapor\text{-}melt}$

The $\delta^{13}C$ values of CO_2 vapor equilibrated with rhyolite during the fractionation experiments are included in Table 4-4 and Table 4-5 for comparison with the glasses. Detailed mass scans, obtained on the VG Prism IRMS, of the vapor phase released from representative samples confirmed the absence of CO, CH_4 and higher-order hydrocarbons, suggesting that the vapor consisted of almost pure CO_2 gas. Vapor yields are listed in Table 4-6. I retrieved typically ≥ 90% of the vapor present in the capsule at the end of an experiment.

Carbon isotopic fractionations, calculated as $\delta^{13}C_{(CO2\ vapor)} - \delta^{13}C_{(rhyolitic\ melt)} = \Delta_{vapor\text{-}melt}$, are listed in Table 4-5 and depicted in Fig. 4-4. The range in values among all of the experiments is -0.34 to 0.96‰, with a mean value of 0.1(±0.2)‰. Open capsule experiments exhibit the greatest variability in $\Delta_{vapor\text{-}melt}$ (1.3‰), and I interpret this as an indication that the vapor sampling used in these experiments is not as reliable as the method utilizing closed capsules. The -0.16 to 0.15‰ range in calculated $\Delta_{vapor\text{-}melt}$ values among closed capsule experiments is much smaller. The mean $\Delta_{vapor\text{-}melt}$ of the closed capsule experiments is 0 (±0.1‰), and thus my results indicate that there is no fractionation of carbon isotopes between CO_2 vapor and CO_2 dissolved in rhyolitic melts. In following sections I focus on the sealed-capsule experiments only.

The isotopic composition of the bulk CO_2 vapor inside sealed capsules appears to shift slightly (by -0.09 to 1.14 ‰, generally toward a lighter isotopic composition) over the course of experiment (Table 4-6). The cause of this shift is poorly understood, but it does not appear to influence the observed isotopic fractionation between the final vapor and glass samples (Fig. 4-5b).

4.6 DISCUSSION

4.6.1 Attainment of chemical and isotopic equilibrium

While it is difficult to prove absolutely that the rhyolitic glasses achieved chemical and isotopic equilibrium with the coexisting CO_2 vapor, my results suggest in several ways that equilibrium was closely approached. The strongest argument for chemical equilibrium is the uniform concentration determined by IR spectroscopy throughout the glass chips and the closeness to the predicted equilibrium CO_2 solubilities at the P and T of the experiments (Fig. 4-2). I compared the extraction results with the IR spectroscopic measurements, and the agreement is consistent with the high-temperature yield as being representative of the dissolved CO_2. These measured concentrations are also consistent with predicted solubility values at the pressures and temperatures of the experiments.

Calculated fractionations ($\Delta_{vapor\text{-}melt}$) presented in Table 4-5 cannot be distinguished on the basis of the $\delta^{13}C$ of the vapor, yield, temperature, pressure, or run duration (Fig. 4-5). The isotopic fraction between coexisting CO_2 vapor and CO_2 molecules dissolved in rhyolitic melt at magmatic temperatures is therefore ≈ zero.

4.6.2 Mass balance considerations

Differences in capsules weights before and after an experiment were very small, usually within ±0.0003 g (Table 4-6). The fact that the differences were both positive and negative, to similar amounts in either direction, suggests that this weight change is not significant.

On the basis of mass balance constraints, the amount of vapor retrieved from a capsule was 0.3-2.6 micromoles lower than expected (Table 4-6). This amount of CO_2 represents only 1-3% of total vapor loaded in capsules and may well be simply an indication of measurement accuracy. Some, but not all of this discrepancy may be

accounted for by the low-temperature CO_2 component of the glasses; a portion of this "missing" vapor may adsorb onto the surfaces of the hot rhyolitic glass chips during quenching, thus contributing to the low-temperature CO_2 component. The issue of the isotopic and release characteristics of low temperature carbon associated with basaltic glasses has been discussed extensively (e.g., Des Marais, 1984; Exley et al., 1987; Tingle et al., 1990; Wright and Pillinger, 1989). The wide range of reported $\delta^{13}C$ values (-20 to -30‰) for low temperature CO_2 makes it difficult to use mass balance constraints to determine the source of the low-temperature carbon in my experiments.

Using data of Barker and Torkelson (1975) for CO_2 adsorption at STP conditions on to silica glass with surface area similar to that of the glass chips used in this study, a 0.4 g sample could acquire up to 1.4 μmoles of adsorbed CO_2. Des Marais and Moore (1984) demonstrated that basaltic glasses can acquire a low-temperature carbon component quite rapidly. Given this, it is likely that the rhyolitic glass chips loaded into capsules carried with them some surficial CO_2. Likewise, chips removed from capsules probably acquire some "contaminant" carbon during the time between capsule-opening and loading on to the vacuum line.

Bulk CO_2 loaded and recovered from the experimental run products is also examined in the following: (1) CO_2 vapor retrieved from capsule piercing; (2) CO_2 released during high-temperature combustion of the glasses; and (3) CO_2 vapor that adsorbed or reacted with the hot glasses during quenching and came off as part of the low-temperature fraction of CO_2. Most of the closed-capsule runs have good mass balances within 10% of the measured total CO_2 loaded at the beginning of an experiment. Calculated yields based on recovered vapor and the high-temperature CO_2 are typically < 100% whereas yields calculated based on all recovered CO_2 are usually > 100%. The differences between the two estimates of CO_2 yield are similar to the analytical uncertainties, but nevertheless they probably reflect vapor adsorbed on to the glass

surface for yields < 100% and a contribution of low-temperature contaminant CO_2 for yields > 100%. There are 2 exceptions. GB1-34 had a low yield of 64%. This discrepancy is most likely due to analytical difficulties. The capsule was pierced and only a few micromoles of CO_2 were removed. The capsule was removed from the vacuum line, repositioned, and pierced again - and more CO_2 vapor was retrieved. These two bursts of CO_2 were combined for the final measurement of CO_2 vapor. The vapor appeared not be interconnected inside the capsule, and it is possible that the combination of the two piercing events did not release all of the CO_2 trapped inside. The amount of high temperature CO_2 extracted from the sample corresponds to the amount of CO_2 dissolved (IR), however, so there were no pockets of CO_2 in the glass. It is thus likely that if there was additional CO_2 vapor in the capsule, it was lost when the capsule was opened. In contrast, sample GB1-38 had a CO_2 yield 20% higher than expected, and the "surplus" CO_2 appears to be part of the high-temperature CO_2. The origin of this extra CO_2 is unknown, but it may be simply a measurement error. The high yield for sample GB1-38 did not produce an anomalous $\Delta_{vapor\text{-}melt}$, value relative to other experiments. In general the mass balance observed in these experiments are much better than those reported by previous workers (Javoy et al., 1978; Mattey, 1991; Mattey et al., 1990).

4.6.3 Comparison with carbon isotopic fractionation between coexisting CO_2 vapor and other silicate melts

Experimental studies of carbon isotopic fractionation between coexisting CO_2 vapor and silicate melt are limited to natural and synthetic tholeiite and sodamelilite compositions. The reported carbon isotopic fractionations are summarized below:

Table 4.7 Measured carbon isotope fractionation between coexisting CO_2 vapor and silicate melt

System	$\Delta_{vapor\text{-}melt}$	T (°C)	Speciation	Reference
CO_2-basalt	4.3±0.3‰	1120-1280	CO_3^{2-} *	Javoy et al., 1978
CO_2-basalt	4.2±0.4	1200	CO_3^{2-}	Trull et al., 1991
CO_2-sodamelilite	2.4±0.2‰	1200-1400	CO_3^{2-}	Mattey et al., 1990
CO_2-basalt (syn.)	2.0±0.2‰	1200-1400	CO_3^{2-}	Mattey, 1991
CO_2-rhyolite	0.0±0.2‰	800-1200	CO_2	This Study

* Inferred

The representative value for the fractionation between CO_2 vapor and basalt has been the subject of considerable debate, fueled in part by experimental complications or ambiguities in the experimental results. For example, the CO_2 solubilities reported by Javoy et al. (1978) vary by an order of magnitude and are considerably higher than predicted based on solubility studies. Trull et al. (1991) obtained similar fractionation results and report CO_2 solubilities that are consistently ≈ 40% higher than those predicted by IR spectroscopy, but the IR calibration for CO_2 dissolved in basaltic melt may be inaccurate. Mattey and others (1991; 1990), in their studies of a synthetic basalt analog (sodamelilite) and a synthetic basalt, could not adequately account for the mass loss of carbon during their experiments but showed that variable mass loss and shifts in $\Delta^{13}C_{(initial\ vapor\ -\ final\ vapor)}$ did not effect their measured $\Delta_{vapor\text{-}melt}$ fractionations[5].

Irrespective of the "absolute" $\Delta_{CO2\text{-}basalt}$ value, the CO_2 in equilibrium with basaltic melt is enriched in ^{13}C by ≈ 2-4‰, whereas in CO_2 vapor has the same $\delta^{13}C$ value as coexisting rhyolitic melt. The most likely, first-order explanation for this observation is the fact that the speciation of dissolved CO_2 is different in the two silicate melt compositions.

---

[5] It is interesting that Mattey et al. (1990) generally found that the composition of the vapor was heavier at the end of an experiment, although their range in vapor shift was -1.5 to 2.0 ‰, more than two times that of this study. Javoy et al. (1978) did not measure vapor coexisting with the sample after an experiment; this alone could account for the discrepancy in $\Delta_{CO2\text{-}basalt}$ results if the vapor in the Javoy et al. (1978) experiments shifted to heavier compositions. Insufficient detail is given by Trull et al. (1991) to determine their analytical procedure regarding vapor present in a capsule at the end of an experiment.

These two compositions, a tholeiite and a high-silica rhyolite (Chapter 1), represent two end-members in the natural spectrum of igneous rocks with respect to silica content. At the relatively modest pressures (< 2 kbars) of the experimental studies, all dissolved CO_2 has been detected as carbonate in basalt and as molecules of CO_2 in rhyolite (e.g., Fine and Stolper, 1985). To date, there has been no systematic evaluation of the speciation of dissolved carbon dioxide in silicate melts of intermediate composition, but andesitic melt has been observed to contain both molecular CO_2 and CO_3^{2-} (Newman, unpublished). If the relative proportions of CO_2/CO_3^{2-} increase moving from mafic to silicic natural compositions, I would expect that the corresponding $\Delta_{CO2\text{-silicate melt}}$ would decrease.

Only CO_2 dissolved in molecular form has been detected in rhyolitic melts quenched from pressures of up to ≈ 7 kbars (Fogel and Rutherford, 1990). However, a single experiment conducted at 25 kbars (Fine, 1986) revealed the presence of both dissolved CO_2 and CO_3^{2-}; similarly, Fine and Stolper (1987) noted that the proportions of CO_2/CO_3^{2-} decrease with increasing pressure in albitic melt. An obvious study for future work is the comparison of how $\Delta_{vapor\text{-}melt}$ and carbon speciation change in rhyolitic melt as a function of increasing pressure.

Similar studies of $CO_2(g)$-$CO_2(l)$ and $CO_2(g)$-$CO_3^{2-}(aq)$ have found a similar trend in carbon isotope fractionation. Grootes et al. (1969) report that the carbon isotopic fractionation between gaseous and liquid CO_2 [$CO2(g)$-$CO_2(l)$] at low temperatures is nearly zero. Vogel et al. (1970) observed a small fractionation (≈ 1 ‰) between gaseous CO_2 and CO_2 dissolved in water at 0-60°C whereas similar studies of CO_2 vapor and carbonate ion in solution have found 8-12 ‰ fractionation at temperature ≤ 40°C (e.g., Lesniak and Sakai, 1989). Theory alone would predict that CO_2 vapor would be enriched in ^{13}C relative to the liquid state, because the binding energy tends to favor the heavier isotope in symmetric molecules (Grootes et al., 1969).

4.6.4 Comparison with carbon isotopic fractionation studies of CO_2 vapor and silicate melts found for other volatile species.

It is well-known that the lighter isotopes of both hydrogen and oxygen are favored in the vapor phase of water. However, there is very little D/H fractionation between water vapor and water molecules dissolved in rhyolitic melts and glasses molecules show little fractionation between vapor and dissolved molecular form in rhyolitic melt. Dobson et al. (1989) deduced this on the basis of bulk $\Delta_{H2O\ vapor\text{-}bulk\ dissolved\ water}$ of rhyolitic glasses from the Mono Craters, CA, and their experimentally-determined $\Delta_{H2O(v)\text{-}OH(melt)}$ for rhyolitic glasses with very low (≤0.2 wt%) water contents. Ihinger (1991) subsequently determined experimentally a value for $\Delta_{H2O(v)\text{-}OH(melt)}$ of close to zero for rhyolitic melts at magmatic temperatures.

Studies of noble gas partitioning between coexisting vapor and silicate melt have been rare. He isotopes appear to exhibit no isotopic fractionation during the formation of a vapor phase in basaltic magma (Kurz and Jenkins, 1981). Jambon et al. (1985) found a $^{40}Ar/^{36}Ar$ ratio in basaltic glass to be about ten times lower than the ratio in coexisting vesicles based on vacuum crushing experiments . The implied relatively large vapor-melt fraction in $^{40}Ar/^{36}Ar$ ratios of MORB glasses, however, may be attributable to seawater penetration or alteration of the glasses.

The similar lack of isotopic fractionation of carbon in CO_2, H in molecular water, He, and perhaps for other noble gases may for these neutral dissolved volatile species may be in keeping with their similar diffusive behavior in silicate melts (Chapter 2, Fig. 2.8) and may provide insight into the nature of the chemical environment of these neutral species in silicate melts.

4.7 Conclusions

The carbon isotopic partitioning CO_2 dissolved in rhyolitic melts has been determined over the temperature range 800-1200°C and 250-1444 bars pressure using conventional René cold seal and new rapid-quench TZM pressure vessels. The carbon isotopic fractionation between CO_2 vapor and carbon dissolved in rhyolitic melts as CO_2 molecules is approximately zero, within analytical uncertainty (±0.1 ‰). $^{13}C/^{12}C$ ratios measured in natural rhyolitic glasses will therefore not have been affected by degassing of CO_2 from rhyolitic magma.

The lack of any detectable fractionation of ^{13}C between coexisting CO_2 vapor and CO_2 dissolved in rhyolitic melt suggests that variation in $\delta^{13}C$ values among related rhyolitic glasses will reflect other geochemical processes. Examples of such might include: (a) Triggering of silicic eruptions through injections of mafic magmas (e.g., Anderson, 1976; Michael, 1991; Sparks et al., 1977); (b) Mixing of 2 or more magmas of different $\delta^{13}C$ values; or (c) Reaction of magmatic CO_2 with country rock or meteoric waters (e.g., Lyon and Hulston, 1984; Taylor, 1986; White, 1986; White et al., 1990).

However, while a large body of data exist for the isotopic composition of CO_2 derived from basaltic magmas, the available carbon isotopic data for silicic magmas is limited to fumarole gases (Giggenbach and Matsuo, 1991; Giggenbach et al., 1991; White, 1986; White et al., 1990). It is difficult to measure the $\delta^{13}C$ values of silicic magmas directly because most natural samples have lost their CO_2 upon eruption. If no fractionation between melt and vapor occurs, and if no additional processes modify escaping vapors during their ascent to the surface, then the $\delta^{13}C$ values of CO_2 gas in fumaroles associated with silicic volcanism may mirror the C isotopic composition of their host magmas. A useful test to confirm this would be to look at the $\delta^{13}C$ values of melt inclusions trapped in phenocrysts of silicic lavas associated with fumaroles. In most cases, however, such studies are limited for lack of an analytical technique that can

accurately determine the $\delta^{13}C$ composition of very small (picomole-sized) samples. With the recent developments in microanalytical techniques, we will soon be able to measure the $\delta^{13}C$ of melt inclusions, whereupon the fractionation measurements documented in this study will provide a foundation with which to interpret the observed $\delta^{13}C$ values of natural silicic glasses.

4.8 References

Anderson A. T. (1976) Magma mixing: Petrologic process and volcanological tool. *J. Volcanol. Geotherm. Res.* **1**, 3-19.

Barker C. and Torkelson B. E. (1975) Gas adsorption on crushed quartz and basalt. *Geochim. Cosmochim. Acta* **39**, 212-218.

Blank J. G., Delaney J. R. and Des Marsais D. J. (1993) The concentration and isotopic composition of carbon in basaltic glasses from the Juan de Fuca Ridge. *Geochim. Cosmochim. Acta* **57**, 875-887.

Bottinga Y. and Javoy M. (1989) MORB degassing: Evolution of CO_2. *Earth Planet. Sci. Lett.* **95**, 215-225.

Craig H. (1957) Isotopic standards for carbon and oxygen and correction factors for mass-spectrometric analysis of carbon dioxide. *Geochim. Cosmochim. Acta* **12**, 133-149.

Des Marais D. J. (1978) Variable temperature cryogenic trap for the separation of gas mixtures. *Anal. Chem.* **50**, 1405-1406.

Des Marais D. J. (1984) Isotopically light carbon in midocean ridge basalts - fact or artifact? *(abstr.). Geol. Soc. Amer. Abstr. with Prog.* **16**, 486.

Des Marais D. J. and Moore J. G. (1984) Carbon and its isotopes in mid-oceanic ridge basaltic glasses. *Earth Planet. Sci. Lett.* **69**, 43-57.

Des Marais D. J. (1985) Carbon exchange between the mantle and the crust, and its effect upon the atmosphere. In *The Carbon Cycle and Atmospheric CO_2: Natural Variations Archean to Present* (ed. E. T. Sundquist and W. S. Broecker). pp. 602-611. Geophysical Monograph 32. American Geophysical Union.

Dobson P. F., Epstein S. and Stolper E. M. (1989) Hydrogen isotope fractionation between coexisting vapor and silicate glasses and melts at low pressure. *Geochim. Cosmochim. Acta* **53**, 2723-2730.

Exley R. A., Mattey D. P. and Pillinger C. T. (1987) Low temperature carbon components in basaltic glasses--reply to comment by H. Craig. *Earth Planet. Sci. Lett.* **82**, 387-390.

Fogel R. A. and Rutherford M. J. (1990) The solubility of carbon dioxide: A quantitative FTIR study. *Amer. Mineral.* **75**, 1311-1326.

Gerlach T. M. and Taylor B. E. (1990) Carbon isotope constraints on degassing of carbon dioxide from Kilauea Volcano. *Geochim. Cosmochim. Acta* **54**, 2051-2058.

Giggenbach W. F. and Matsuo S. (1991) Evaluations of results from Second and Third IAVCEI Field Workshops on Volcanic Gases, Mt. Usu, Japan, and White Island, New Zealand. *Applied Geochemistry* **6**, 125-141.

Giggenbach W. F., Sano Y. and Schmincke H. U. (1991) CO_2-rich gases from Lakes Nyos and Monoun, Cameroon; Lacher See, Germany; Dieng, Indonesia, and Mr. Gambier, Australia - Variations on a common theme. *J. Volcanol. Geotherm. Res.* **45**, 311-323.

Grootes P. M., Mook W. G. and Vogel J. C. (1969) Isotopic fractionation between gaseous and condensed carbon dioxide. *Zeit Physik* **221**, 257-273.

Ihinger P. D. (1991) An experimental study of the interaction of water with granitic melt. Ph.D. dissertation, California Institute of Technology.

Jambon A., Weber H. W. and Begemann F. (1985) Helium and argon from an Atlantic MORB glass: Concentration, distribution, and isotopic composition. *Earth Planet. Sci. Lett.* **73**, 255-267.

Javoy M. and Pineau F. (1991) The volatiles record of a "popping" rock from the Mid-Atlantic Ridge at 14°N: Chemical and isotopic composition of gas trapped in the vesicles. *Earth Planet. Sci. Lett.* **107**, 598-611.

Javoy M., Pineau F. and Allègre C. J. (1982) Carbon geodynamic cycle. *Nature* **300**,

Javoy M., Pineau F. and Liyama I. (1978) Experimental determination of the isotopic fractionation between gaseous CO_2 and carbon dissolved in tholeiitic magma. *Contrib. Mineral. Petrol.* **67**, 35-39.

Kurz M. D. and Jenkins W. J. (1981) The distribution of helium in oceanic basalt glasses. *Earth Planet. Sci. Lett.* **53**, 41-54.

Lesniak P. M. and Sakai H. (1989) Carbon isotope fractionation between dissolved carbonate (CO_3^{2-}) and CO_2 (g) at 25° and 40°C. *Earth Planet. Sci. Lett.* **95**, 297-301.

Lyon G. L. and Hulston J. R. (1984) Carbon and hydrogen isotopic compositions of New Zealand geothermal gases. *Geochim. Cosmochim. Acta* **48**, 1161-1171.

Mattey D. (1991) Carbon dioxide solubility and carbon isotope fractionation in basaltic melt. *Geochim. Cosmochim. Acta* **55**, 3467-3473.

Mattey D. P., Taylor W. R., Green D. H. and Pillinger C. T. (1990) Carbon isotopic fractionation between CO_2 vapor, silicate and carbonate melts: an experimental study to 30 kbar. *Contrib. Mineral. Petrol.* **104**, 492-505.

Michael P. J. (1991) Intrusion of basaltic magma into a crystallizing granitic magma chamber: The Cordillera del Paine pluton in southern Chile. *Contrib. Mineral. Petrol.* **108**, 396-418.

Newman S., Epstein S. and Stolper E. (1988) Water, carbon dioxide, and hydrogen isotopes in glasses from the ca. 1340 A.D. eruption of the Mono Craters, California: Constraints on degassing phenomena and initial volatile content. *J. Volcanol. Geotherm. Res.* **35**, 75-96.

Sparks R. S. J., Sigurdsson H. and Wilson L. (1977) Magma mixing: A mechanism for triggering acid explosive eruptions. *Nature* **267**, 315-318.

Taylor B. E. (1986) Magmatic volatiles: Isotopic variation on C, H, and S. In *Stable Isotopes in High Temperature Geological Processes* (ed. J. W. Valley, H. P. Taylor Jr. and J. R. O'Neil). pp. 185-226. Reviews in Mineralogy 16. Bookcrafters, Inc.

Tingle T. N., Hochella M. F. Jr., Becker C. H. and Malhotra R. (1990) Organic compounds on crack surfaces in olivine from San Carlos, Arizona, and Hualalai Volcano, Hawaii. *Geochim. Cosmochim. Acta* **54**, 477-485.

Trull T., Pineau F., Bottinga Y. and Javoy M. (1991) Experimental study of CO_2 bubble growth and $^{13}C/^{12}C$ isotopic fractionation in tholeiitic melt. *4th Silicate Melt Workshop: Program and Abstracts, 19-23 March, 1991* 7.

Tuttle O. F. (1949) Two pressure vessels for silicate-water studies. *Geol. Soc. Amer. Bull.* **60**, 1727-1729.

Vogel J. C., Grootes P. M. and Mook W. G. (1970) Isotopic fractionation between gaseous and dissolved carbon dioxide. *Zeit Physik* **230**, 225-238.

Watson (1987) Diffusion and solubility of C in Pt. *Amer. Mineral.* **72**, 487-490.

White A. F. (1986) Chemical and isotopic characteristics of fluids within the Baca Geothermal Reservoir, Valles Caldera, New Mexico. *J. Geophys. Res.* **91**, 1855-1866.

White A. F., Peterson M. L., Wollenberg H. and Flexser S. (1990) Sources and fractionation processes influencing the isotopic distribution of H, O, and C in the Long Valley hydrothermal system, California, U.S.A. *Applied Geochemistry* **5**, 571-585.

Wright I. P. and Pillinger C. T. (1989) Carbon isotopic analysis of small samples by use of stepped-heating extraction and static mass spectrometry. *U.S.G.S. Bulletin* **1890**, 9-34.

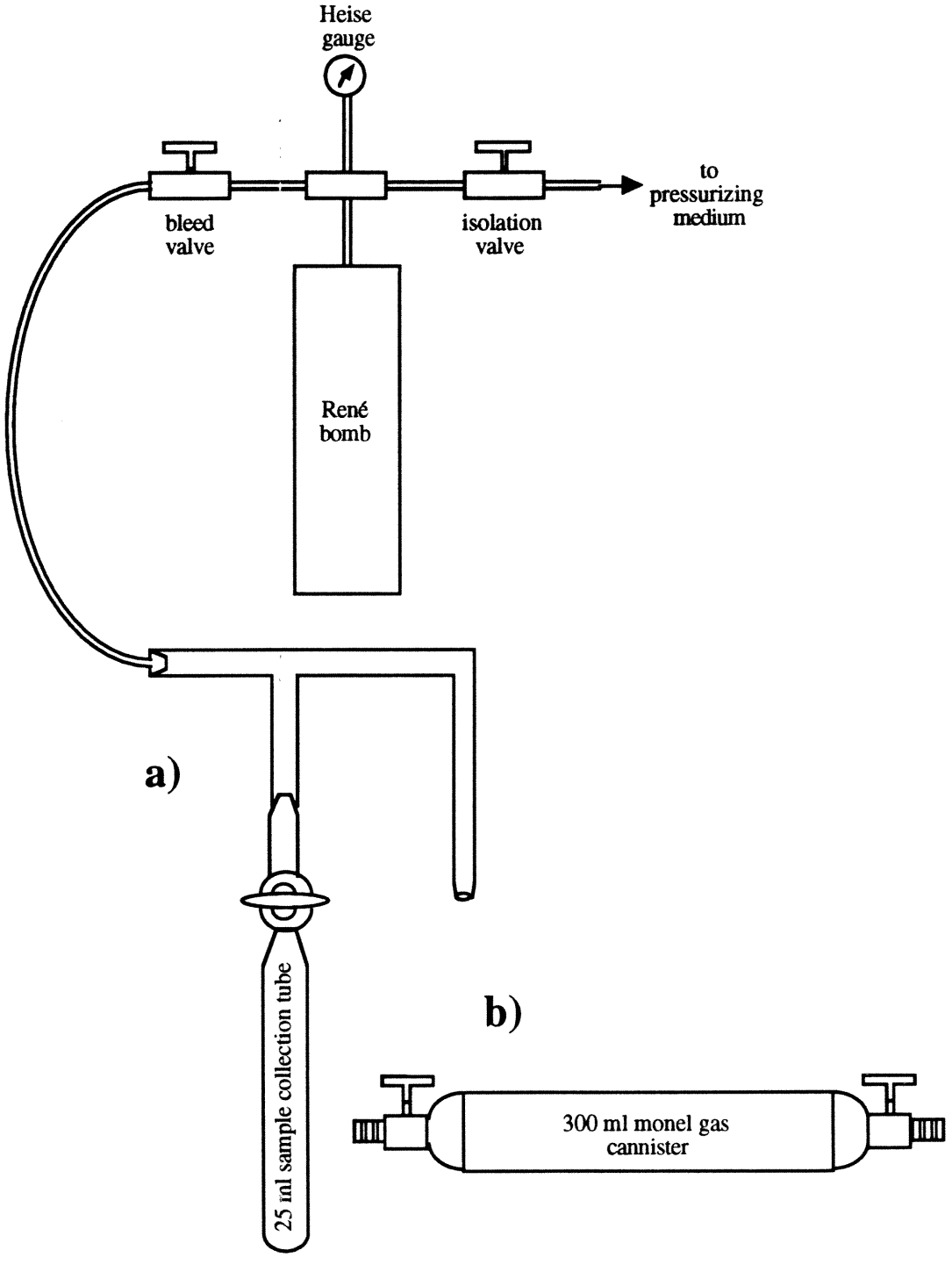

Fig. 4-1 Sampling CO_2 gas pressurizing medium: schematic of cold-seal pressure vessel and gas collectors (not to scale). In **(a)**, an evacuated 25 ml sample collection tube was connected to an F-shaped Pyrex tube that was attached to the bleed valve with polyurethane tubing. The bleed valve was opened and CO_2 was

allowed to escape freely via the F-shaped tube. The sample tube was opened to collect a portion of the CO_2 flowing out of the bomb. In **(b)**, the evacuated monel sampling cannister was attached directly to the bleed valve, with a vacuum pump attached to the other end of the monel cannister. Through a series of repeated steps (opening/closing the bleed valve to fill the cannister, and evacuating the monel cannister), a calculated pressure of ≤ 2 bars was achieved, after which point the cannister was removed for transfer of gas via vacuum line to a standard pyrex tube. See text for additional description.

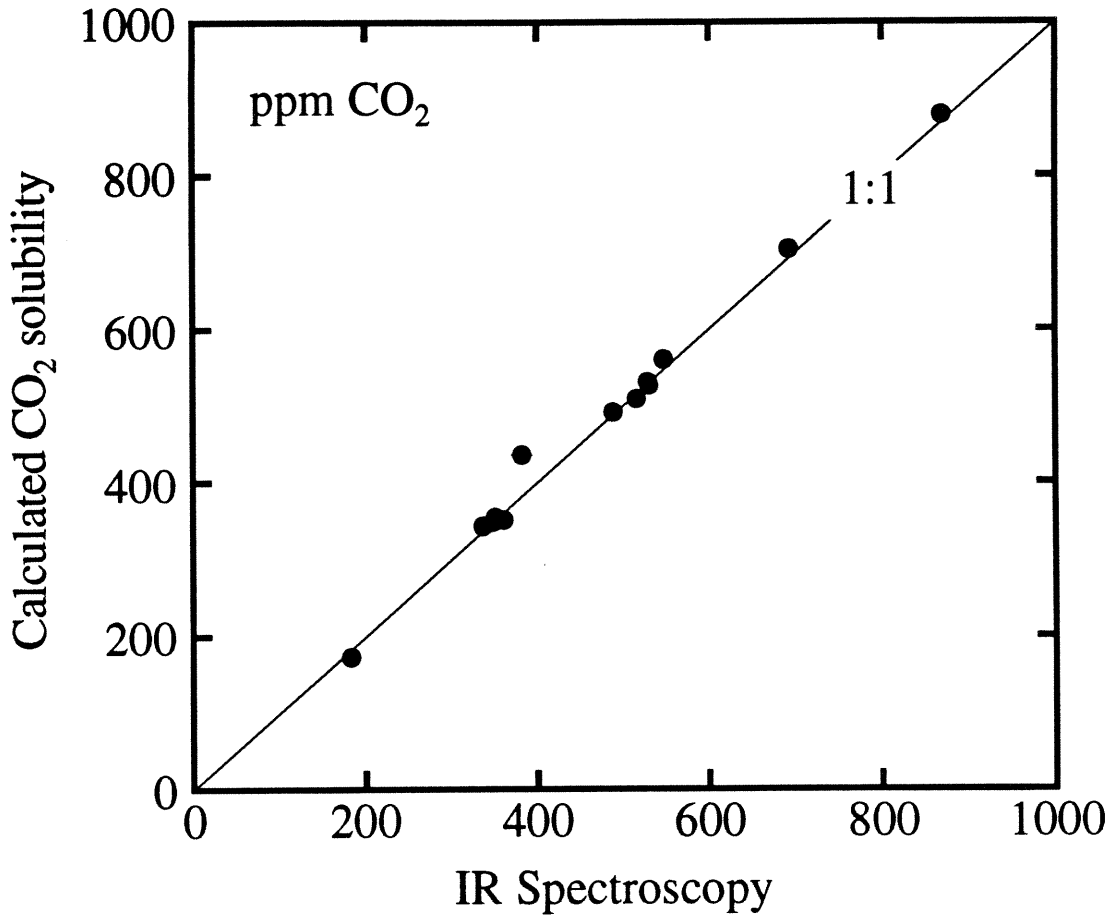

Fig. 4-2 Comparison of calculated CO_2 solubility (Chapter 1) and the dissolved CO_2 contents of the experimental rhyolitic glasses measured using FTIR spectroscopy. Line indicates a 1:1 correspondence.

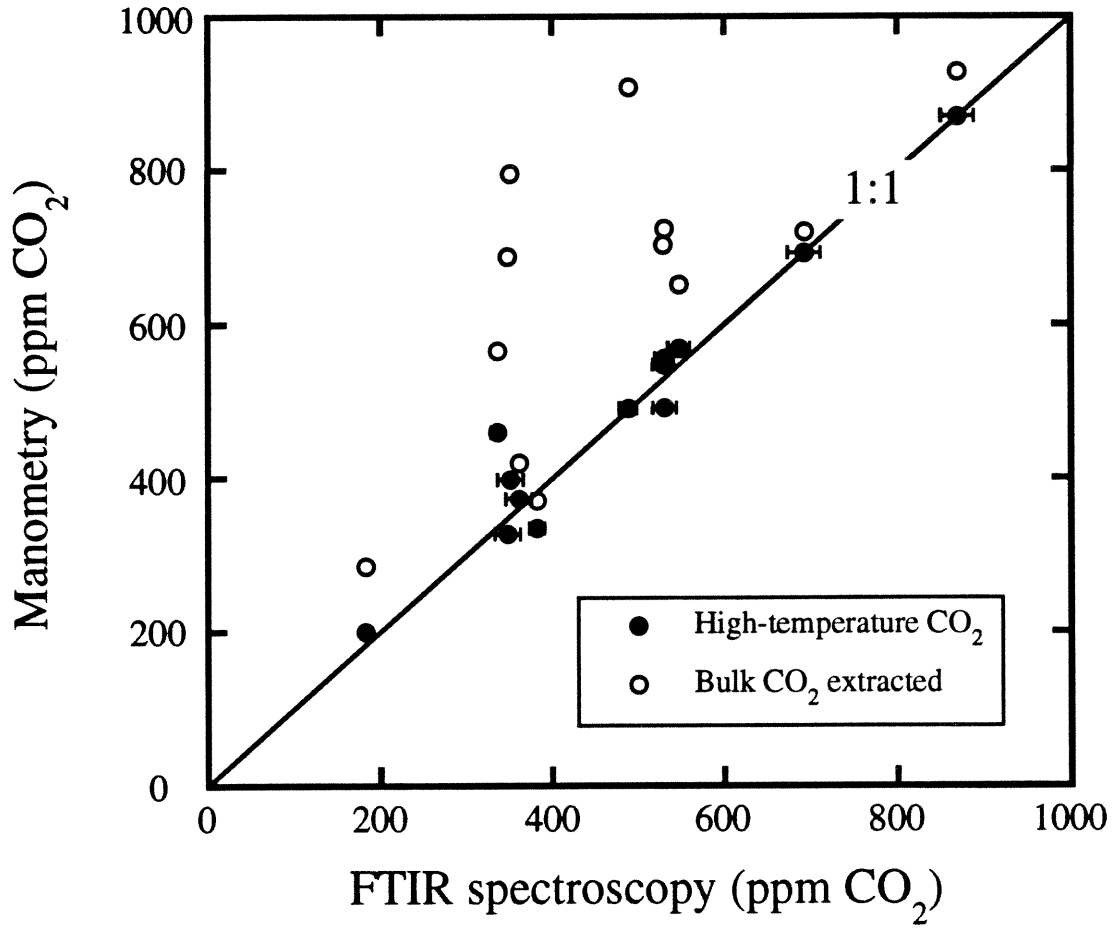

Fig. 4-3 Comparison of IR spectroscopic measurements of CO_2 dissolved in rhyolitic glasses and CO_2 collected from stepped heating/manometry. Symbols indicate: high temperature (>650°C) CO_2 (closed circles); bulk CO_2 extracted from the glasses (open circles). Line indicates a 1:1 correspondence.

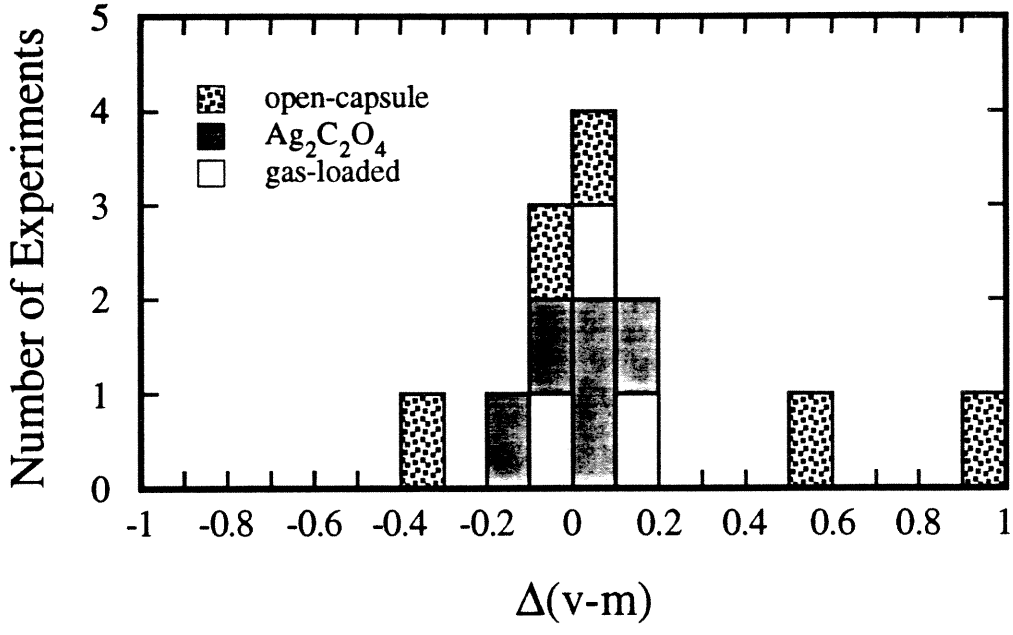

Fig. 4-4 Histogram of fractionation experiment results. Type of experiment is indicated in the legend. The measured $\Delta_{vapor\text{-}melt}$ values of experiments whose CO_2 came from $Ag_2C_2O_4$ or from CO_2 gas welded directly inside a capsule are confined to a narrow range about 0 ‰. In contrast, the measured $\Delta_{vapor\text{-}melt}$ values from the open-capsule experiments show considerable scatter and for this reason are deemed less accurate than the other experiments.

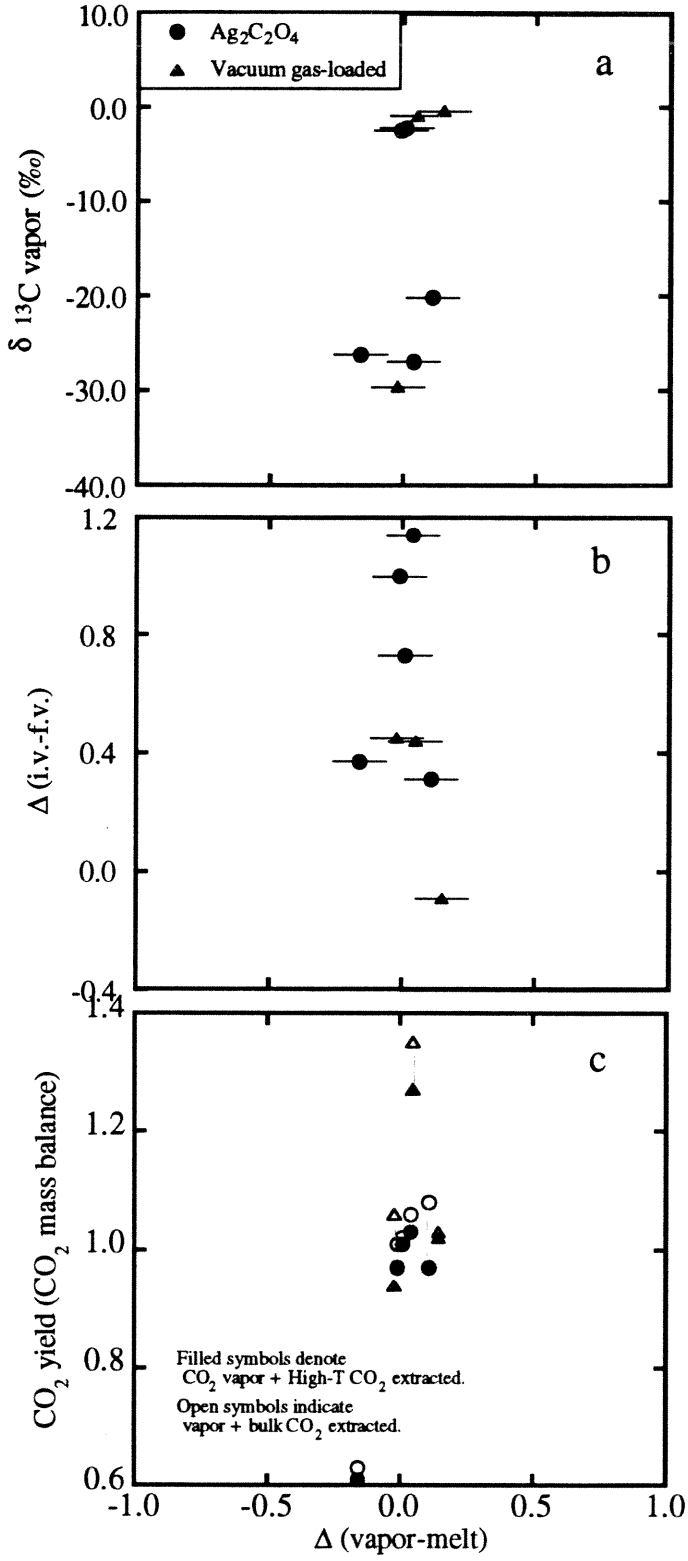
$Ag_2C_2O_4$
Vacuum gas-loaded
a
b
c
δ ^{13}C vapor (‰)
Δ (i.v.-f.v.)
CO_2 yield (CO_2 mass balance)
Filled symbols denote
CO_2 vapor + High-T CO_2 extracted.
Open symbols indicate
vapor + bulk CO_2 extracted.
Δ (vapor-melt)

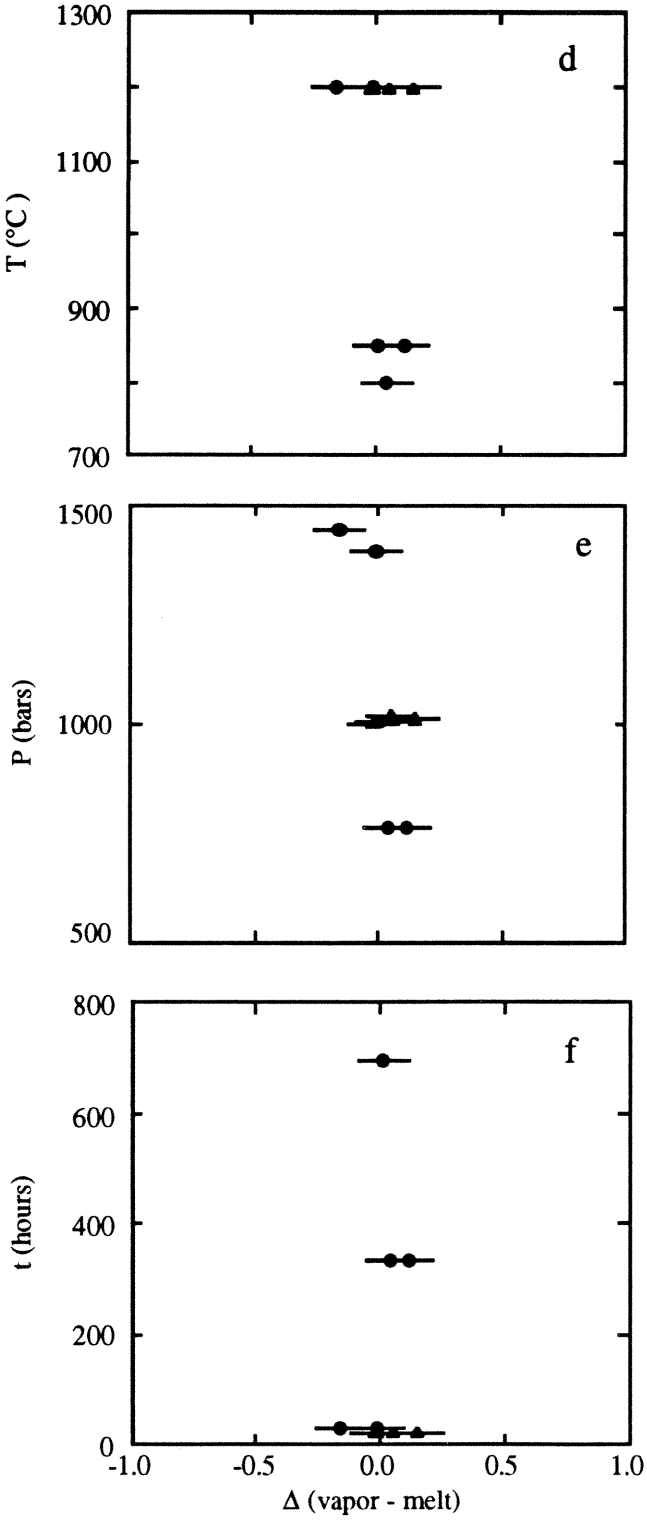
d
e
f
T (°C)
P (bars)
t (hours)
1300
1100
900
700
1500
1000
500
800
600
400
200
0
-1.0
-0.5
0.0
0.5
1.0
Δ (vapor - melt)

Fig. 4-5 Variation of measured $\Delta_{vapor\text{-}melt}$ values with: (a) $\delta^{13}C$ of vapor coexisting with rhyolitic melt; (b) apparent shift in $\delta^{13}C$ of vapor (i.e., Δ (i.v. - f.v.) = $\delta^{13}C_{loaded\ vapor}$ - $\delta^{13}C_{recovered\ vapor}$) from its initial isotopic composition; (c) yield, calculated from a CO_2 mass balance (Table 4-6) of the CO_2 recovered from an experimental charge compared with the CO_2 loaded in a capsule; (d) temperature; (e) pressure; and (f) run duration. Circles indicate silver oxalate experiments; triangles denote experiments with vacuum-loaded CO_2 gas. "Error" bars represent the approximate amount (0.1‰) of uncertainty introduced during the CO_2 extraction procedure.

Table 4-1 Experimental Conditions

Sample	Bomb Type	Pressure Medium	T °C	P bars	Duration hours	Source of CO_2	Capsule Contents Glass chips(g)	#µmolCO_2	initial $\delta^{13}C$(‰)	Comments c
GB1-12	René	CO_2	850	810	311.25	bomb CO_2	0.4167	-	-	nc
GB1-13	René	CO_2	850	1436	214.63	bomb CO_2	0.4468	-	-	nc
GB1-14	René	CO_2	850	695	291.75	bomb CO_2	0.4228	-	-	nc
GB1-19	René	CO_2	850	250	960	bomb CO_2	0.4589	-	-	nc
GB1-26	René	CO_2	850	495	527.17	bomb CO_2	0.4562	-	-	nc
GB1-29	René	CO_2	850	760	336.25	$Ag_2C_2O_4$	0.4407	49.97	-19.82[a]	s
GB1-30	René	CO_2	800	760	336	$Ag_2C_2O_4$	0.4372	49.05	-25.80	nc
GB1-32	René	Ar	850	1007	697.2	$Ag_2C_2O_4$	0.3643	48.95	-1.42	nc
GB1-34	TZM	Ar	1200	1444	31.67	$Ag_2C_2O_4$	0.3892	69.79	-25.80	f
GB1-35	TZM	Ar	1200	1395	32	$Ag_2C_2O_4$	0.4405	98.76	-1.42	s
GB1-38	TZM	Ar	1200	1020	48	loaded CO_2 gas	0.2370	20.58[b]	-0.43	fm
GB1-39	TZM	Ar	1200	1003	48	loaded CO_2 gas	0.2379	16.93[b]	-30.14	fm
GB1-41	TZM	Ar	1200	1012	48	loaded CO_2 gas	0.2402	24.78[b]	-0.43	fm

- = Not determined.

[a] = Prepared from a mixture of two batches of $Ag_2C_2O_4$.

[b] = These initial CO_2 aliquots are "corrected" values - i.e., I recalibrated the manometer in rm008 to my line.

[c] = Description of glass chips after run indicate the following: nc (no change), fm (fused together, visible microlites), f (fused together, no visible microlites), s (crushed chips).

Table 4 -2 Analyses of Vapor from "control" experiments and mass balance constraints

Sample	loaded CO_2	wt diff <> run [a]	wt diff <> pierce [b]	expected CO_2 [c]	CO_2 Yield
	µmol	g	g	µmol	µmol
$Ag_2C_2O_4$.1	97.25	-0.0002	0.0044	100.43	5.03
$Ag_2C_2O_4$.2	33.84	-0.0003	0.0014	32.49	25.19
$Ag_2C_2O_4$.3	37.00	0.0000	0.0015	33.40	34.05
$Ag_2C_2O_4$.4	38.19	-0.0002	0.0013	29.54	33.64
Ag_2C2O_4.5	35.55	-0.0002	0.0016	36.36	35.82
Ag_2C2O_4.6	51.16	0.0001	0.0021	47.26	49.88
Ag_2C2O_4.7	49.38	0.0000	0.0023	52.49	49.01
$Ag_2C_2O_4$.8	48.01	0.0005	0.0019	43.17	46.92
10 ("42-gas")*	27.0	0.0009	0.0012	27.27	27.1
8 ("20-gas")*	21.4	0.0000	0.0009	20.90	21.41
"42-gas"†	≈23	-	-	-	-
"20-gas"	≈45	-	-	-	-
"0-gas"	≈68	-	-	-	-

* loaded CO_2 into capsules 8 and 10 using the vacuum line in rm 008; recalibrated the manometer there afterwards.

† these gases, "42-", "20-", and "0-gas", are aliquots of large CO_2 reservoirs prepared from carbonate standards

\- not applicable

[a] difference in capsule weight (before - after) an experiment

[b] difference in capsule weight (before piercing - after piercing)

[c] µmoles CO_2 expected based on weight difference before and after piercing capsule; these are maxima because there was air in the capsule along with the CO_2 at the end of a run.

Table 4-2 (cont.)

Sample	% yield [d]	err yield [e]	"initial" $\delta^{13}C$	$\delta^{13}C$	Run Conditions	Comments [f]
		%	‰	‰	°C, bars, hours	
$Ag_2C_2O_4$.1	5.2	0.0	-1.4 (?)	-0.94	850,570, 6	René (CO_2)
$Ag_2C_2O_4$.2	74.4	1.4	"	-2.04	850, 720, 2.33	René (CO_2)
$Ag_2C_2O_4$.3	92.0	1.6	"	-1.20	309,1,1	box furnace
$Ag_2C_2O_4$.4	88.1	1.5	"	-2.20	850,670,4.08	René (CO_2)
Ag_2C2O_4.5	100.7	1.8	"	-1.41	850, 450, 4.08	René (Ar)
Ag_2C2O_4.6	97.5	1.2	"	-1.20	250, 1, ?	box furnace
Ag_2C2O_4.7	99.3	1.3	"	-1.42	350, 1, 0.25	box furnace
$Ag_2C_2O_4$.8	97.7	1.3	-25.8 (?)	-25.80	350, 1, 0.25	box furnace
10 ("42-gas")*	100.4	2.4	-0.4	-1.62	1250, 1010, 24	TZM
8 ("20-gas")*	100.0	3.0	-12.9	-13.66	1240, 1007, 24.17	TZM
"42-gas"†	-	-	-	-0.43	-	-
"20-gas"	-	-	-	-12.93	-	-
"0-gas"	-	-	-	-30.14	-	-

[d] % yield expected determined from (CO_2 recovered/CO_2 loaded as $Ag_2C_2O_4$)

[e] error in estimated yield based on 2x weighing error (which is ±0.0001 g, or 2x 0.66 μmol CO_2 loaded as $Ag_2C_2O_4$)

[f] experimental apparatus used (and pressurizing medium where appropriate). Box furnace is open to atmosphere

Table 4-3 Measured dissolved CO_2 and water contents: IR analyses

Sample	ppm CO_2 [a]	wt% water [b]	c	d	(wt%water,post-extraction)
GB1-12	547	0.23	(3, 5,0.04)	o	0.005
GB1-13	869	0.19	(3,6,0.03)	o	0.005
GB1-14	382	0.11	(8,12,0.06)	o	0.003
GB1-19	183	0.38	(3, 2,0.06)	o	0.006
GB1-26	336	0.28	(3,5,0.02)	o	0.005
GB1-29	530	0.12	(2,3,0.01)	o	0.004
GB1-30	528	0.23	(3,7,0.04)	o	0.006
GB1-32	692	0.20	(4,10,0.03)	-	-
GB1-34	530	0.46	(3,2,0.01)	o	0.006
GB1-35	488	0.26	(3,5,0.03)	-	-
GB1-38	351	0.22	(3,4,0.01)	-	-
GB1-39	348	0.23	(2,3,0.02)	-	-
GB1-41	361	0.21	(3,3,0.02)	-	-

[a] Concentration of dissolved molecular CO_2 determined by the measured peak height of the IR absorption at 2350 cm^{-1}, using a glass density of 2350 g/l and a molar absorptivity coefficient of 1066 l/(cm-mol) (Chapter 1).

[b] Concentration of dissolved water determined from the measured peak height of the absorption at 2550 cm^{-1} corresponding to total water, using a glass density of 2350 g/l and a molar absoptivity coefficient of 88 l/(cm-mol) (Dobson et al., 1989).

[c] Numbers in parentheses indicate number of analyses and 2σ error based on replicate analyses, for CO_2 (in ppm) and water (in wt% water), respectively.

[d] "o" indicates that a glass sample was analyzed after vacuum extraction, "-" indicates not analyzed. No dissolved CO_2 was detected in post-extraction glasses and all measured water contents were < 0.01 wt%.

Table 4-4 Results of stepped-heating and combustions of CO_2-saturated rhyolitic glasses

Sample	amount	Comments	T	time	yield	conc.	$\delta^{13}C$
	g	†	°C	min	µmol CO_2¥	ppm CO_2	‰
GB1-12 a	0.4026	e,o,t	200	40	~0	0	-
b			400	40	0.8	83	-31.7
c			1125	90	5.2	570	-31.3
GB1-12bomb							-31.6
GB1-13 a	0.42575	e,o,t	250	40	0.2	22	-9.7
b			400	40	0.4	36	-11.3
c			1125	90	8.4	870	-31.8
GB1-13bomb							-31.8
GB1-14 a	0.40631	e,o,t	250	40	0.1	10	-13.4
b			400	40	0.2	24	-
c			1125	90	3.1	336	-29.5
GB1-14bomb							-28.6
GB1-19 a	0.4212	u,n,t*	450	40	0.37	39	-22.55
b			650	40	0.39	41	-29.11
c			650	40	0.06	6	-
d			1200	90	1.91	200	-33.31
GB1-19bomb*							-33.31
GB1-26 a	0.3992	u,n,t*	450	40	0.86	95	-30.05
b			550	40	0.02	2	-
"			650	40	0.08	9	-
c			750	40	0.18	20	-31.57
d			850	40	0.31	34	-32.83
e			950	40	0.30	33	-39.72
f			1050	40	1.04	115	-38.19
g			1200	90	2.35	259	-34.94
(Σ(>650°C))					4.18	461	-35.78
GB1-26bomb*							-35.19
GB1-29 a	0.3838	u,n,s	450	40	3.14	360	-32.36
b			650	40	1.81	208	-22.06
c			650	40	0.68	78	-22.07
d			1200	90	4.85	556	-20.24
GB1-29v							-20.13
GB1-30 a	0.3997	u,n,s	450	40	0.83	91	-25.08
b			650	40	0.41	45	-
c			650	40	0.17	19	-22.16
d			1200	90	4.98	548	-26.98
GB1-30v							-26.94

Table 4-4 (cont.)

Sample	amount	Comments	T	time	yield	conc.	$\delta^{13}C$
	g	†	°C	min	µmol CO_2¥	ppm CO_2	‰
GB1-32 a	0.3568	u,n,s	450	40	1.02	110	-5.32
b			650	40	0.21	23	-
c			1200	90	5.62	694	-2.16
GB1-32v							-2.15
GB1-34 a	0.3005	u,n,s	450	40	1.43	209	-25.40
b			650	40	0.16	23	-26.60
c			1200	90	3.36	492	-26.01
GB1-34v							-26.17
GB1-35 a	0.3460	u,n,s	450	40	2.56	326	-9.74
b			650	40	0.66	84	-4.17
c			650	40	0.06	8	-
d			1200	90	4.46	491	-2.41
GB1-35v							-2.42
GB1-38 a	0.2001	u,n,g	450	40	0.94	207	-12.37
b			650	40	0.57	62	-11.21
c			1200	90	2.11	399	-0.92
GB1-38v							-0.87
GB1-39 a	0.2337	u,n,g	450	40	1.02	192	-30.19
b			650	40	0.90	169	-29.02
c			1200	90	1.74	329	-30.57
GB1-39v							-30.59
GB1-41 a	0.2382	d,n,g	450	40	0.25	27	-6.26
b			650	40	0.05	5	-
c			1200	90	1.98	373	-0.49
GB1-41v							-0.34

† Details of the extractions. Sample cleaning indicated by: e = cleaned with ethanol; d = cleaned with CH_2Cl_2, u = uncleaned prior to extraction. Method of analysis indicated by: o = analyzed sample using existing vacuum line (low-sensitivity, reading error ±0.4 µmoles based on the manometer) and the old C-O Caltech mass spectrometer; n = analyzed using a high-sensitivity vacuum line (reading error is ±0.01 µmoles) and analyzed for $\delta^{13}C$ values using the Prism ISRM at USC. Source of CO_2 for an experiment indicated by: t = tank CO_2 (* denotes sample collected using monel cannister); s = silver oxalate; and g = gas sealed directly inside capsule.

¥ Samples GB1-12,-13,-14 were measured with low-sensitivity manometer (7 µmol/cm Hg displacement) while other samples were measured using a high-sensitivity manometer (0.3 µmol/cm) and the number of significant figures in the reported yields reflects this.

Table 4-5 Summary of Results

Sample	CO_2 dissolved in Rhyolite (ppm)			Isotope results		
	Measured	Measured	Calculated	glass	CO_2 vapor	$\Delta_{(v-m)}$
	(High-T Manometry)	(IR)	a	$\delta^{13}C$(‰)		‰
GB1-12	570	547	561	-31.29	-31.63	-0.34
GB1-13	870	869	880	-31.80	-31.78	0.02
GB1-14	336	382	437	-29.51	-28.55	0.96
GB1-19	200	183	174	-33.31	-33.31	0.00
GB1-26	461	336	344	-35.78	-35.19	0.59
GB1-29	556	530	527	-20.24	-20.13	0.11
GB1-30	548	528	531	-26.98	-26.94	0.04
GB1-32	694	692	705	-2.16	-2.15	0.01
GB1-34	492	530	510	-26.01	-26.17	-0.16
GB1-35	491	488	492	-2.41	-2.42	-0.01
GB1-38	399	351	355	-0.92	-0.87	0.05
GB1-39	329	348	349	-29.57	-29.59	-0.02
GB1-41	374	361	352	-0.49	-0.34	0.15

Notes:
[a] Calculated using the thermodynamic parameters for CO_2 solubility in rhyolitic melts (Chapter 1).

--->>The mean for all of the results is Δ(vapor-melt)=0.11±0.21‰ (1σ).
--->>The mean for all of the closed-capsule results is 0.02±0.07‰ (1σ).

Table 4-6 Mass balance of CO_2-rhyolite C fractionation experiments

Sample	Capsule wt <> run	Initial V [a]	final CO_2 V	$\Delta_{(v-m)}$	$\Delta_{(i.v.-f.v.)}$	Amt. V init.
	g	‰	‰	‰	‰	µmol
GB1-12	0.0060	-	-31.63	-0.34	-	-
GB1-13	-	-	-31.78	0.02	-	-
GB1-14	-	-	-28.55	0.96	-	-
GB1-19	-	-	-33.31	0.00	-	-
GB1-26	0.0003	-	-35.19	0.59	-	-
GB1-29	0.0003	-19.82	-20.13	0.11	0.31	49.97
GB1-30	-0.0003	-25.8	-26.94	0.04	1.14	49.05
GB1-32	0.0000	-1.42	-2.15	0.01	0.73	48.95
GB1-34	0.0001	-25.8	-26.17	-0.16	0.37	69.79
GB1-35	0.0001	-1.42	-2.42	-0.01	1.00	98.76
GB1-38	0.0000	-0.43	-0.87	0.05	0.44	20.58
GB1-39	0.0004	-30.14	-30.59	-0.02	0.45	16.93
GB1-41	-0.0003	-0.43	-0.34	0.15	-0.09	24.78

- not measured.

[a] Initial vapor was determined from low-tememperature "control" experiments (for $Ag_2C_2O_4$ compositions), or on aliquots of reservoir CO_2 gas (for gas-loaded runs).

Table 4-6 (cont)

Sample	CO_2 V yield	HT CO_2[b]	Bulk XT CO_2[c]	Yield (HT+V)[d,†]	Yield (LT+HT+V)[e,†]
	μmol	μmol	μmol	%	%
GB1-12	-	5.21	5.97	-	-
GB1-13	-	8.42	8.98	-	-
GB1-14	-	3.1	3.41	-	-
GB1-19	-	1.91	2.73	-	-
GB1-26	-	4.18	5.14	-	-
GB1-29	43.63	4.85	10.48	97	108
GB1-30	43.05	4.98	6.39	98	101
GB1-32	42.01	5.62	5.84	97	98
GB1-34	39.00	3.36	4.95	61 ¥	63
GB1-35	92.26	3.86	7.14	97	101
GB1-38	24.10	2.11	3.62	127 §	135
GB1-39	14.23	1.74	3.66	94	106
GB1-41	23.08	1.98	2.28	101	102

[b] CO_2 collected from the high-temperature combustion step.

[c] Total CO_2 extracted from the glass.

[d] Yield determined from the (amount of HT carbon extracted from the glasses + the amount of CO_2 vapor collected)/(the amount of CO_2 loaded initially in the capsule).

[e] Yield based on the (total CO_2 collected from the glasses + collected CO_2 vapor)/(the amount of CO_2 initially loaded in to the capsule).

† The amount of CO_2 dissolved in the glass chips not extracted but removed instead for IR analysis is ≤ 0.5 μmol (usually ≤0.2) and this translates to an error in mass balance estimates of ≈ 1% only.

Error based on propagation of weighing precision (±0.0001 g) and IR analyses changes estimates in yields by less than 2%).

¥ Capsule GB1-34 was pierced under vacuum 2x, and both times batches of CO_2 were recovered. CO_2 in this capsule appeared to be isolated in parcels rather than interconnected.

It is likely that a significant fraction of the CO_2 vapor was not released until the capsule was opened to remove the glass chips; this would explain the low CO_2 vapor yield.

§ There is no obvious explanation for this high yield.

APPENDIX

The concentration and isotopic composition of carbon in basaltic glasses from the Juan de Fuca Ridge

Jennifer G. Blank, John R. Delaney, and David J. Des Marais

(Geochimica et Cosmochimica Acta, Vol. 57, pp. 875-887, 1993)

ABSTRACT

The abundance and $^{13}C/^{12}C$ ratios of carbon were analyzed in basaltic glasses from twenty locations along the Juan de Fuca Ridge using a 3-step combustion/extraction technique. Carbon released during the first two combustion steps at 400-500°C and 600-650°C is interpreted to be secondary, and only the carbon recovered during a final combustion step at ≈1200 °C is thought to be indigenous to the samples. For carbon released at ≈1200 °C, glasses analyzed as 1-2 mm chips contained 23-146 ppm C with $\delta^{13}C$ values of -4.8 to -9.3 ‰, whereas samples crushed to 38-63 μm or 63-90 μm yielded 56-103 ppm C with $\delta^{13}C$ values of -6.1 to -9.2 ‰. The concentrations and isotopic compositions of the primary carbon dissolved in the glasses and present in the vesicles are similar to those previously reported for other ocean-ridge basalts.

The Juan de Fuca basaltic magmas were not in equilibrium with respect to carbon when they erupted and quenched on the seafloor. Evidence of disequilibrium includes: (1) a large range of carbon contents among glasses collected at similar depths, (2) a highly variable calculated C-isotopic fractionation between melt and vapor determined by comparing crushed and uncrushed splits of the same sample, and (3) a lack of correlation between vesicle abundance, C concentration, and depth of eruption. Variations in carbon concentration and $\delta^{13}C$ ratios along the ridge do not correlate with major element chemistry. The observed relationship between carbon concentrations and $\delta^{13}C$ values may be explained by late-stage, variable degrees of open-system (Rayleigh-like) degassing.

INTRODUCTION

Water and carbon dioxide are the dominant volatile species present in magmatic fluids and gases (Anderson, 1975; Fyfe et al., 1970; Roedder, 1965), and because carbon dioxide is much less soluble than water in most silicate liquids (Holloway, 1981), early stages of degassing often generate a nearly pure CO_2 vapor phase (Javoy and Pineau, 1991; Moore et al., 1977). Although basalts erupted subaerially typically have low carbon contents due to substantial amounts of degassing, submarine basalts often retain significant quantities of CO_2 because they are erupted and quenched under pressure. Detailed analysis of dissolved and vesicle carbon in such glassy submarine basalts can be used to constrain degassing histories.

Knowledge of carbon isotopes may provide additional insight into degassing behavior because vapor exsolving from basaltic magmas is preferentially enriched in ^{13}C (Pineau et al., 1976). Early measurements of $^{13}C/^{12}C$ ratios in basalts were puzzling because the bulk carbon content appeared to be isotopically more similar to organic matter than other mantle-derived materials (e.g., Craig, 1953). Pineau et al. (1976), however, first documented in carbon-rich "popping rocks" from the Mid-Atlantic Ridge that CO_2 trapped in vesicles is isotopically heavier than carbon in basaltic glass and is similar to the most commonly-reported $\delta^{13}C$ values for diamonds and other mantle specimens ($\approx$ -4 to -7 ‰; e.g., Mattey, 1987). Pineau and Javoy (1983) examined the temperature-release pattern of CO_2 in basalts and noted that isotopically lighter carbon was released at lower temperatures. Des Marais and Moore (1984) and Mattey et al. (1984) extended this approach and proposed the existence of at least two isotopically distinct populations of carbon in basaltic glasses: a post-magmatic contaminant depleted in ^{13}C that is released below $\approx$650 °C, and an isotopically heavier, high-temperature indigenous C component.

These authors suggested that the indigenous carbon is present as CO_2 trapped in vesicles and as a dissolved species in the basalt glass.

In this study, we measured the concentration and isotopic composition of carbon in a suite of basaltic glasses from the Juan de Fuca Ridge using a three-temperature-step combustion procedure. Key questions we set out to address are: (1) How does the concentration and isotopic composition of carbon vary along the axis of a well-characterized spreading center; and (2) Does this variation correlate with magmatic processes operating along the ridge? Previous workers (e.g., Des Marais and Moore, 1984; Exley et al., 1986; Mattey et al., 1984; 1989; Sakai et al., 1984) have reported that $\delta^{13}C$ values of MORBs are relatively constant, suggesting that the isotopic composition of carbon in MORB source regions is fairly uniform. Furthermore, while in a rough sense carbon concentrations in submarine basalts vary systematically with depth (e.g., Des Marais and Moore, 1984; Harris, 1981; Moore, 1979), recent experimental investigations (Stolper and Holloway, 1988) have shown that, on the scale of a single spreading center, the concentrations of dissolved carbon in basaltic glasses commonly exceed their expected equilibrium values. In the present study, we discuss how eruption depth, magmatic differentiation, and degassing may have led to the observed concentration and isotopic character of carbon in basalts.

SAMPLES

Samples were taken from the 500 km long Juan de Fuca Ridge, situated off the northwest coast of the U.S.A. The Juan de Fuca Ridge, a medium-rate spreading center separating the Pacific and Juan de Fuca plates, is bounded by the Blanco and Sovanco Fracture Zones. Additional details of its structure and tectonics are discussed by Delaney et al. (1981; 1986), Hammond et al. (1984), Hey and Wilson (1982), Karsten (1988), and Karsten et al. (1990), among others. Sample locations are shown in Fig. A-1 and listed in

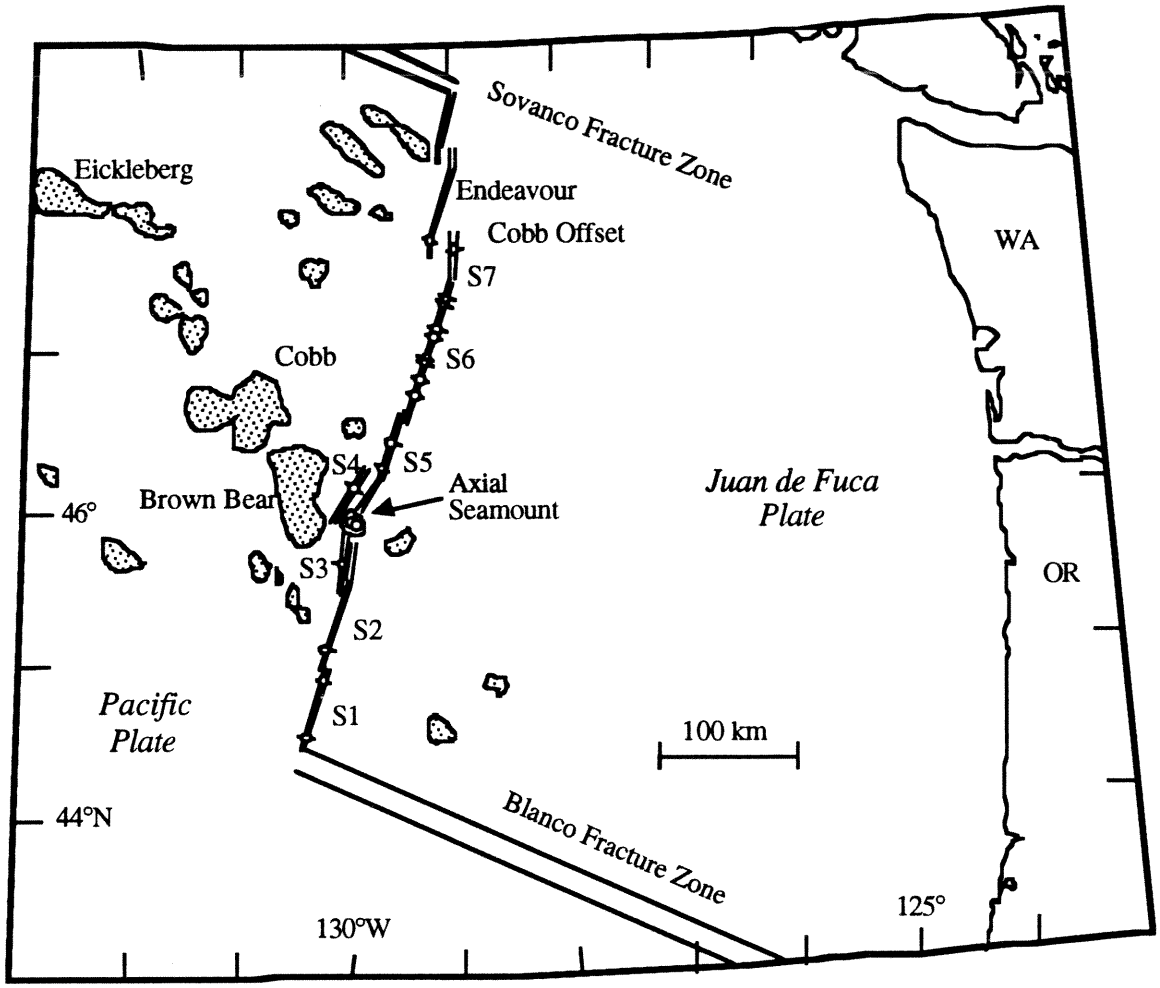

Fig. A-1. Dredging station location map of samples from the Juan de Fuca Ridge used in this study. Detailed locations given in Table A-1. Segments of the ridge (S1 through S7 and Endeavor) after Delaney et al., 1986. Shaded regions indicate major seamounts.

Table A-1. Sample locations and flow types

Sample	Flow Type[a]	Depth (m)[b]	Latitude (°N)[b]	Longitude (°W)[b]	Location[c]
TT152-37	S	2208	44.6170	130.396	S1
TT152-43-19	P	2253	44.9960	130.204	S1
TT152-44	-	2370	45.1340	130.186	S2
TT152-77-6	P	1962	15.6705	130.060	S3
TT152-77-7	P	1962	45.6705	130.060	S3
TT152-55-25	S	1520	45.9385	130.002	AS
TT170-5	-	1460	45.9465	130.027	AS
TT152-61	S	2249	46.0745	129.892	S4
TT152-72	-	2200	46.2845	129.726	S5
TT152-65	-	2278	46.3535	129.684	S5
TT152-29-1	S	2255	46.8625	129.292	S6
TT152-21	S	2430	46.9260	129.264	S6
TT152-13	P	2594	47.2045	129.124	S6
TT152-11-10	S	2634	47.5405	128.954	S6
TT152-11-21	S	2634	47.5405	128.954	S6
HU81-017-11	P	2569	47.6200	129.284	END
HU81-017-2-4	S	2470	47.7275	129.244	END
TT152-16	S	2562	47.0320	129.391	S6
TT152-30-45	S	2355	46.8145	129.324	S6
TT152-17	S	2480	47.0265	129.212	S6
TT152-26A	P	2625	46.9400	129.320	S6
HU81-017-6-11	-	2560	47.2200	129.092	S6

Notes:

[a] Samples are labeled as being from S=sheet flow, or P=pillow flow, when known.

[b] Data for depth of collection, latitude, and longitude are from Delaney et al., in prep.

[c] S = ridge segment; AS = Axial Seamount; END = Endeavor segment (see Fig. A-1).

geographic order from south to north in Table A-1. The 22 basaltic glasses we studied were collected by dredging on cruises 152 (1980; samples denoted TT152-) and 170 (1982; sample TT170-) of the University of Washington's R/V Thomas Thompson and HU81-017 (1981; samples HU81-017-) of the University of British Columbia's R/V Hudson. Glassy fragments from pillow and sheet-flow lavas were obtained along the ridge axis to ensure that only young basalt flows were sampled (e.g., Goldstein et al., 1991). Major and trace element chemistry of these glasses are reported elsewhere (e.g., Delaney et al., 1981; in prep; Karsten, 1988; Liias, 1986).

ANALYTICAL TECHNIQUES

Sample Preparation

Fresh basaltic glass removed from the outer 0.5 cm of the chilled margins of a hand sample from each dredging station (Table A-1) was crushed with a steel mortar and pestle, sieved, washed with distilled water in an ultrasonic cleaner, and dried under a heat lamp. Chips were inspected microscopically and selected in order to minimize the presence of vesicles, phenocrysts, and visible alteration. Each picked size fraction was rinsed once in acetone, then washed twice in distilled water and cleaned ultrasonically. The glass chips, 1-2 mm in diameter and referred to as "uncrushed" samples, were stored in glass vials until analyzed. "Crushed" samples were produced from splits of these chips using a sapphire mortar and pestle. These samples, crushed and sieved to 38-63 or 63-90 μm to release the bulk of CO_2 gas present in vesicles, were prepared immediately prior to analysis to minimize their exposure to air. Samples were handled only with aluminum foil and metal implements that had been cleaned with reagent grade methanol and ethylene chloride. Final sample handling steps were performed in air in a clean glove box.

Analytical Methods

Carbon concentrations were determined using a 3-step combustion procedure (Des Marais, 1978; 1983). Samples weighing 0.3-0.4 g were loaded into a degassed quartz boat (i.e., one heated at 1200°C under vacuum for 30 minutes) in a glove box, placed in the extraction line and evacuated overnight at 100 °C. Gas was extracted at temperatures of 400-450 °C and 600-650 °C for collection of "low-temperature" carbon and at ≈1200 °C for high-temperature carbon. For each combustion step, Matheson UHP grade oxygen at 50 torr pressure was passed slowly through a liquid nitrogen trap before being exposed to sample. During combustion, a circulating pump pushed the gases through an isolated loop. For the first two temperature intervals, samples were combusted for 40 minutes, with a liquid nitrogen trap added to the combustion loop to collect condensible gases during the final 20 minutes. Gases released in the lower temperature ranges were passed through a 1200 °C furnace to ensure their complete oxidation. For the high-temperature combustion, a liquid nitrogen trap was added to the combustion loop for the entire 90 minutes of the heating period. An additional combustion interval was carried out for 30 minutes at 700 °C for samples HU81-017-6-11 and TT152-30-45 to check for additional low-temperature carbon. The sample boat was cooled to below 150 °C after each step, at which point noncondensible gases were evacuated. Condensed gases were then transferred to a variable temperature trap (Des Marais, 1978), and CO_2 and SO_2 were removed through distillation at -155 °C and -100 °C, respectively. Gas concentrations were determined manometrically, and carbon isotopic compositions were determined on a Nuclide-60 RMS mass spectrometer modified for small sample analysis.

Quartz sample holders were combusted at 1200 °C for 30 minutes prior to use and a sample "blank" (quartz boat and holder without sample) was run for the same amount of time at 1200°C in the presence of Matheson UHP grade oxygen at 50 torr pressure. Sample blanks were measured manometrically prior to each extraction and in all cases were

less than 0.01 μmole, an amount too small to measure on the mass spectrometer. To test for possible contamination (loss or gain of CO_2) in the line, a known amount of CO_2 was periodically introduced into the system and circulated within the combustion loop while the main furnace was held at 1200 °C. After 30 minutes, the gas was collected and each time yielded 100±0.01 % recovery. Mass spectrometric analyses of samples larger than 0.1 μmoles have a precision of ±0.1 ‰ on the basis of replicate runs of laboratory CO_2 gas standards. Samples as small as 0.03 μmoles were analyzed with up to 1 ‰ precision. All results are reported in the conventional delta notation relative to the PDB isotopic standard.

Vesicle point counts

Thin sections were cut parallel to the outer surfaces of chilled rims of hand samples obtained from the same dredge hauls as fifteen of the glasses analyzed for carbon. Six thin sections were made from splits of the prepared glass chips. 1,000 counts were made for each section using a 300 x 300 μm grid to determine the average size and abundance of vesicles in the samples. The range in vesicle sizes was determined by visual examination of the thin sections. Because of the low abundance of vesicles in these glasses, the relative errors associated with these measurements may be large.

RESULTS

The carbon concentration and $\delta^{13}C$ value of basaltic chips and crushed glass measured for each temperature step are listed in Tables A-2 and A-3. A typical gas release spectrum for uncrushed and crushed splits of a sample is shown in Fig. A-2. The crushed samples evolved significantly more CO_2 (1-16 times as much, or 4-90 ppm C) at low temperature than uncrushed aliquots of the same samples. Low-temperature carbon for all samples had $\delta^{13}C$ values between -20 and -30 ‰. The bulk of the CO_2 collected from

Table A-2. Analyses of uncrushed basaltic glass chips

Sample No.	Amount (g)	1st Low-Temperature Step			2nd Low-Temperature Step			High-Temperature Step		
		T (°C)	ppm C	$\delta^{13}C$ (‰)	T (°C)	ppm C	$\delta^{13}C$ (‰)	T (°C)	ppm C	$\delta^{13}C$ (‰)
TT152-37	0.4345	452	7	-23.2	601	2	-22.0	1178	146	-6.8
"	0.3023	423	4	-23.7	600	10	-26.0	1221	126	-6.1
"	0.2695	422	<1	-22	623	<1	*	1185	128	-6.3
TT152-43-19	0.3039	-	-	-	593	1	*	1219	69	-7.4
TT152-44	0.3585	416	6	-24.4	630	1	-27.5	1200	84	-7.3
TT152-77-6	0.3163	409	5	-25.1	608	2	-26	1200	88	-5.3
TT152-77-7	0.3011	-	-	-	-	-	-	1205	88	-4.8
TT152-55-25	0.3313	405	4	-21.6	628	<1	*	1201	110	-6.3
TT170-5	0.2988	412	7	-28.7	603	2	-28.6	1198	113	-6.4
TT152-61	0.3067	405	10	-26.0	621	3	-27.5	1200	39	-6.7
"	0.3004	409	7	-28.6	638	10	-27.7	1198	50	-7.5
TT152-72	0.3224	439	10	-25.2	630	1	*	1202	43	-6.4
TT152-65	0.3000	430	6	-24.3	638	<1	*	1199	121	-5.0
TT152-30-45	0.3020	428	7	-23.6	602	1	*	1195	130	-5.0
"	0.3025	414	6	-26.3	601	1	*	1192	130	-5.2
TT152-29-1	0.2983	433	7	-24.0	654	1	*	1201	80	-5.4
TT152-21	0.2915	413	11	-23.0	636	3	-23.6	1195	121	-6.1
TT152-26A	0.3071	401	11	-23.4	606	2	*	1197	41	-5.7
TT152-17	0.3072	431	10	-23.4	618	1	*	1200	63	-6.5
TT152-16	0.3027	416	7	-21.7	625	4	-24.2	1200	56	-6.7
"	0.3315	407	6	-24.6	603	2	*	1202	68	-6.4
TT152-13	0.2065	411	12	-	628	2	*	1197	44	-9.3
HU81-017-6-11	0.3148	422	9	-26.1	604	4	-24.6	1199	116	-6.5
TT152-11-10	0.2948	415	9	-24.8	637	2	-26	1205	58	-7.5
TT152-11-21	0.2211	444	9	-25.0	614	<1	*	1202	23	-8.1
HU81-017-11	0.2921	435	17	-25.4	614	<1	*	1194	73	-7.4
HU81-017-2-4	0.2888	402	15	-25.7	634	6	-24.4	1191	45	-8.6

- Sample not recovered.
* Sample too small for analysis by mass spectrometer.

Table A-3 Analyses of crushed glasses

Sample No.	Amount (g)	Size (μm)	1st Low-Temperature Step			2nd Low-Temperature Step			High-Temperature Step		
			T (°C)	ppm C	$\delta^{13}C$ (‰)	T (°C)	ppm C	$\delta^{13}C$ (‰)	T (°C)	ppm C	$\delta^{13}C$ (‰)
TT152-65	0.3246	38-63	414	87	-26.6	632	9	-23.5	1190	68	-8.3
TT152-30-45*	0.2878	38-63	413	36	-27.2	609	13	-24.5	1201	80	-6.9
"	0.3024	63-90	451	22	-25.5	650	4	-24.1	1199	91	-6.1
TT152-29-1	0.3322	38-63	428	57	-27.3	635	6	-27.3	1199	86	-7.1
TT152-21	0.3342	38-63	426	34	-27.4	633	6	-23.8	1196	103	-7.9
HU81-017-11	0.2997	38-63	421	19	-28.0	627	2	-27.7	1197	56	-9.2
HU81-017-6-11*	0.2875	63-90	443	28	-25.9	649	15	-23.4	1197	57	-9.0

* An additional low-temperature combustion step was performed prior to the high-temperature step for the second crushed aliqot of TT152-30-45 (at 698°C) and for sample HU81-017-6-11 (at 706°C). In both cases, <1 ppm C was recovered.

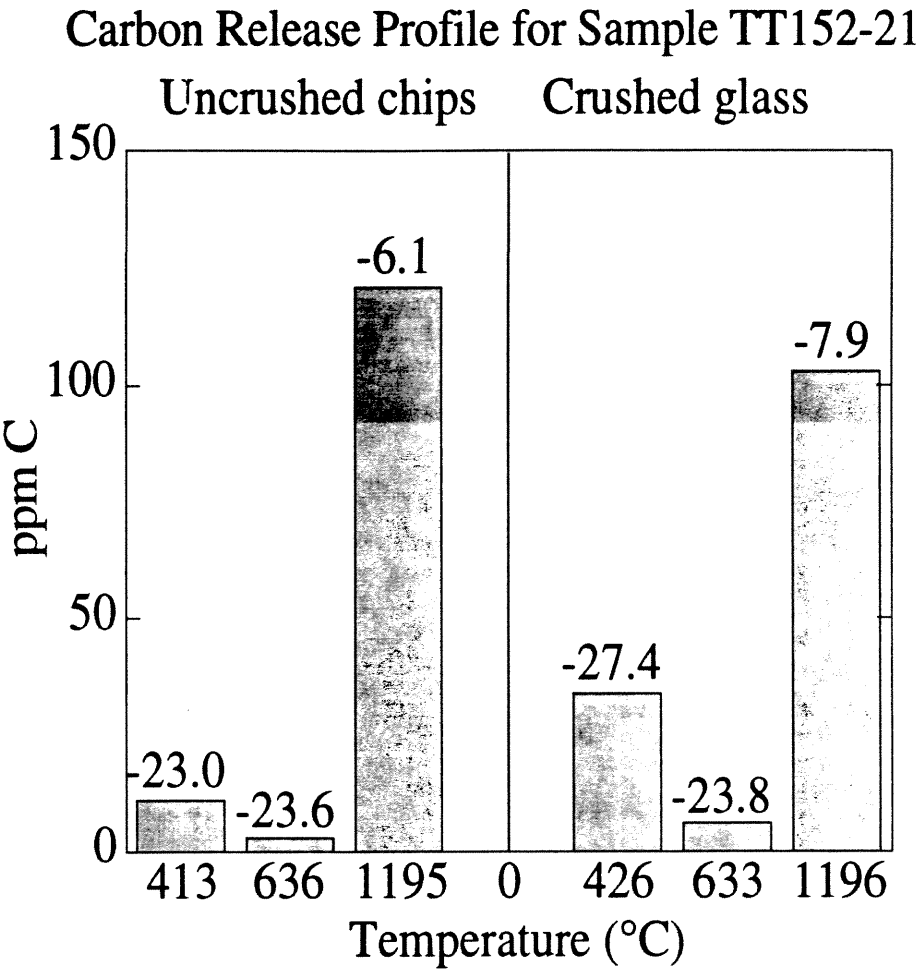

Fig. A-2. Carbon-release profile for uncrushed (1-2 mm chip) and crushed (38-63 μm) samples of TT152-21. Numbers above the columns are the $\delta^{13}C$ values (‰) of CO_2 released during each temperature combustion step. Note the higher abundance of low-temperature C in the crushed sample.

both uncrushed and crushed glass chips was released during the high-temperature combustion stage. The high-temperature carbon in the uncrushed samples is interpreted to be the sum of carbon dissolved in the glass (probably as carbonate groups; Fine and Stolper, 1986) plus gaseous CO_2 in the vesicles. Crushing presumably liberated CO_2 trapped in the vesicles. For all samples, CO_2 collected during the high-temperature interval had $\delta^{13}C$ values greater than -10 ‰.

Low-temperature carbon

The abundance (<1-21 ppm) and isotopic composition (-21.6 to -28.7 ‰) of carbon released from the uncrushed glass chips during the two low-temperature combustion steps were fairly uniform. In contrast, low-temperature carbon reported by other workers (Des Marais and Moore, 1984; Exley et al., 1986; Mattey et al., 1984; Sakai et al., 1984) for basalts from a variety of locations has similar $\delta^{13}C$ values, but extremely variable, usually higher, amounts of C (4-176 ppm). The similar amounts of low-temperature carbon released from our samples may reflect the uniform way in which they were collected, handled, and prepared prior to analysis. The observed abundances of low-temperature carbon for the chip samples were comparable to the amount (10-15 ppm C) of CO_2 predicted, based on adsorption study results of Barker and Torkelson (1975) and Zimmermann (1988), to adsorb on to the surface of similarly-sized basaltic glass in air at room temperature.

The range in abundance of CO_2 released from uncrushed samples during the first temperature interval was <1-17 ppm C (400-500 °C), representing 1-30 % of the total carbon recovered from these samples. The $\delta^{13}C$ values ranged from -21.8 to -28.7 ‰ (Table A-2) and were independent of the amount of CO_2 collected. In the second combustion step (600-650 °C), <1 to 10 ppm (<1-15 % of total) C were collected from the uncrushed samples. There was no correlation between the amount of CO_2 collected during

these two low-temperature combustions and the total carbon yield. In many cases, the amount of gas collected for the second combustion step was too small (<0.03 μmol) to determine its isotopic composition. The $\delta^{13}C$ values (-22.0 to -28.6 ‰) for the second combustion step spanned almost the full range determined for the first temperature combustion and tended to be slightly more negative (by ≈ 1 ‰ on average) than those of the first combustion step (Table A-2). This differs from the findings of Des Marais and Moore (1984) and Mattey et al. (1984), who observed the $\delta^{13}C$ values of the intermediate temperature extraction(s) to be consistently higher than those for the lower temperature extractions by several permil or more.

Crushed samples released 19-87 ppm C (25-53 % of total C) during the first low-temperature combustion step and 2-15 ppm C (3-15 % of total C) for the intermediate temperature combustion (Table A-3). The $\delta^{13}C$ values for these two steps varied from -25.5 to -28.0 ‰ and -23.4 to -27.7 ‰, respectively; the $\delta^{13}C$ values of carbon released during the second combustion step were slightly higher (≈ 2 ‰ on average). While the range of isotopic values of the low-temperature carbon for the crushed glass was similar to that of the uncrushed samples, the amounts of low-temperature carbon are much greater (21-96 ppm vs. <1-21 ppm). The progressive increase in low-temperature carbon with decreasing grain size was demonstrated by analyses of sample TT152-30-45. Uncrushed splits of this sample yielded 6-7 ppm C over the first combustion interval, while an aliquot of this glass crushed to 63-90 μm yielded 22 ppm C. A yet finer size fraction (38-63 μm) released 36 ppm C. Similar relative increases in liberated carbon with decreasing grain size were also observed for the intermediate combustion step (Tables A-2,3).

The purpose of the second temperature step was to ensure that all low-temperature carbon was removed. The temperature interval for this intermediate heating step was in the middle of the range (505-741 °C) of Des Marais and Moore (1984). Two crushed samples (TT152-30-45 and HU017-6-11) subjected to an additional 40-minute combustion at 700 °C released only blank-level amounts of CO_2, suggesting that all low-temperature carbon

was removed by the two low-temperature steps. The consistently light isotopic signature of the second low-temperature combustion carbon fractions implied that release of CO_2 from vesicles, which is ^{13}C-rich, was avoided. Similar behavior was observed by Mattey et al. (1984) for a variety of basalts, although release of vesicle gas can occur at lower temperatures for more vesicle-rich samples such as the rare popping rocks from the Mid-Atlantic Ridge (Pineau et al., 1976).

High-temperature carbon.

High-temperature combustion of uncrushed samples yielded total carbon abundances of 23-146 ppm C with $\delta^{13}C$ values of -4.8 to -9.3 ‰ (Table A-2). Crushed glasses yielded 56-103 ppm with $\delta^{13}C$ values of -6.9 to -9 ‰ (Table A-3). The $\delta^{13}C$ values of replicate samples varied by up to 0.8 ‰. Differences in the amount of high-temperature carbon released from splits of uncrushed pieces from the same hand samples ranged from 0-20 ppm (0-22 % variation). Eight replicate analyses of an Indian Ocean MORB by Mattey et al. (1989) show up to ≈ 70 % variation (101-167 ppm C) in carbon contents; these authors attribute the range of values to variable vesicle and phenocryst abundances within the samples. Replicate analyses of sample TT152-30-45, crushed to two different size fractions, also had differences in C content of 12 %. Des Marais and Moore (1984) found that replicate samples crushed to the same size had the same carbon abundances.

The measured carbon concentrations of our samples are within the range observed for MORB (16-170 ppm) in earlier investigations using similar combustion/extraction techniques (Des Marais and Moore, 1984; Exley et al., 1986; Mattey et al., 1984; 1989; Sakai et al., 1984). The range in $\delta^{13}C$ values determined for the Juan de Fuca Ridge (Fig. A-3) is larger than those for the East Pacific Rise, the Mid-Atlantic Ridge, or Indian Ocean basalts; this may reflect the larger number of samples analyzed from this spreading center.

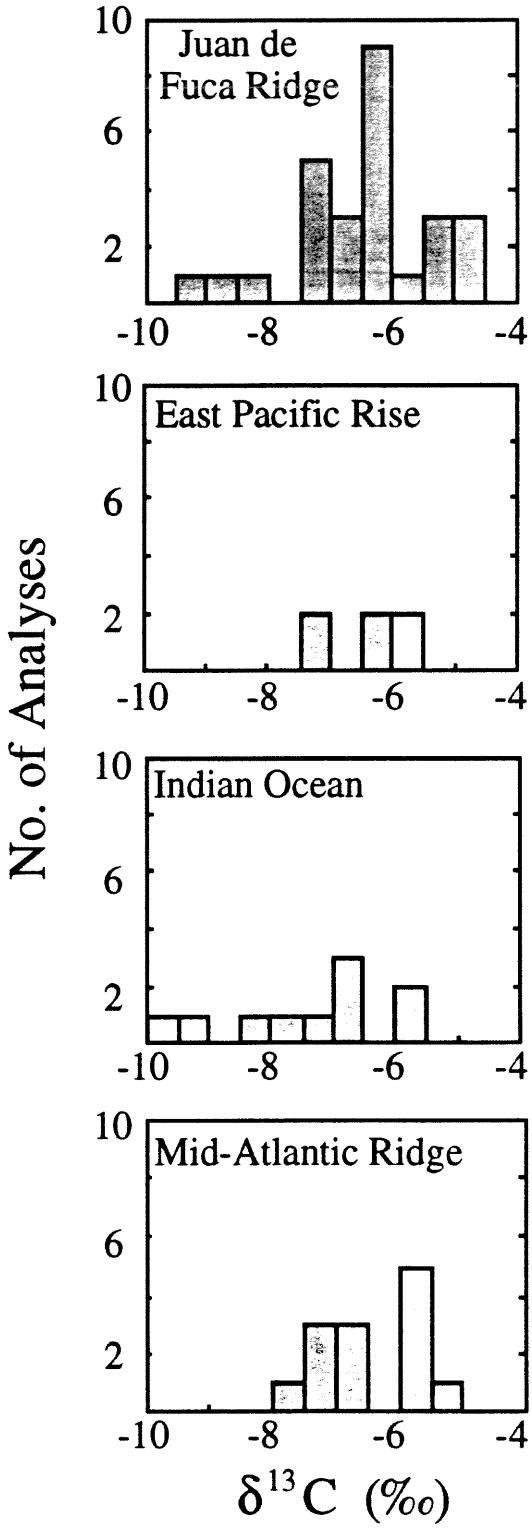

Fig. A-3. Comparison of the reported range in $\delta^{13}C$ compositions of MORB glasses from different regions. Sources of data: Juan de Fuca - this study. Other MORBs - Des Marais and Moore, 1984, Exley et al., 1986; Mattey et al., 1984; 1989; Sakai et al., 1984.

Because the bulk of vesicle carbon is contained in vesicles larger than 100 μm in diameter, crushed samples were prepared as 38-63 μm and 68-90 μm size fractions in order to remove this carbon. If samples are comminuted to even smaller size fractions, fewer vesicles remain intact but more surface area is generated for contamination by adsorbed carbon species (Zimmermann et al., 1988). With one exception, the high-temperature carbon component of crushed samples was smaller than corresponding uncrushed aliquots. All crushed samples released carbon that was isotopically lighter (by 0.9-2.5 ‰) than that found in corresponding uncrushed aliquots (Table A-4).

Vesicle abundances

The results of point counts on thin sections corresponding to twenty-one of the twenty-two samples analyzed for carbon are given in Table A-5. Although most of the samples contained fewer than 1 % by volume vesicles, the range among the samples was relatively large, from <0.1-2.1 volume % based on 1000 counts.

The range in vesicle sizes listed in Table A-4 is 10-1200 μm as determined by thin section study. Average diameters, determined from the mode vesicle size, varied from 60 to >1000 μm. Occasionally, larger (>1000 μm) vesicles were seen in the standard thin sections, but these large vesicles were *a priori* excluded from the vesicle estimates determined from the 1 mm chip thin sections. Aside from this observation, no obvious systematic differences were noted between the point count results for the two types of thin sections. It is possible that vesicles smaller than ≈ 30 μm were preserved during sample crushing; however, these vesicles comprised less than 0.1 % by volume in all of the thin sections examined. Vesicles were predominantly spherical, and in some cases two distinct size populations were observed.

Table A-4 Comparison of C in crushed and uncrushed samples

Sample No.	Uncrushed glasses		Crushed samples		Vesicles (calculated)		Apparent Δ_{v-m}
	C (ppm)	$\delta^{13}C$ (‰)	C (ppm)	$\delta^{13}C$ (‰)	C (ppm)[a]	$\delta^{13}C$ (‰)[b]	(‰)[c]
Juan de Fuca samples (this study):							
TT152-65	121	-5	68	-8.3	53	-0.8	7.5
TT152-30-45	130	-5.1	80	-6.9	50	-2.1	4.7
TT152-29-1	80	-5.4	86	-7.1	-	-	-
TT152-21	121	-6.1	103	-7.9	18	4.1	12.0
HU81-017-6-11	116	-6.5	57	-9	59	-4.1	4.9
HU81-017-11	73	-7.4	56	-9.2	17	-1.5	7.7
Other MORB samples							
TR-14[d]	164	-6.3	115	-7.1	49	-4.4	2.7
KN5444-614[d]	131	-7.1	102	-8	29	-3.9	4.1
FAMOUS-264[d]	136	-6.2	63	-8	73	-4.6	3.4
S714-1-A4[d]	105	-5.6	87	-6.3	18	-2.2	4.1
JC-03-02-01-(a)[e]	167	-7.3	60	-8	107	-6.9	1.1
" (b)	"	"	113	-10.3	54	-1	9.3
" (c)	"	"	124	-10.6	43	2.2	12.8

[a] Vesicle carbon calculated by subtracting the concentrations of carbon in the crushed from the uncrushed samples: $C_{vapor} = C_{bulk} - C_{dissolved}$.

[b] $\delta^{13}C$ of vesicle carbon calculated using the approximation: $C_b(\delta^{13}C)_b = C_v(\delta^{13}C)_v + C_d(\delta^{13}C)_d$.

[c] $\Delta_{v-m} = \delta^{13}C_{vapor} - \delta^{13}C_{melt}$. Values determined for samples with small amounts of calculated vesicle carbon (here, 17 and 18 ppm for samples TT152-21 and HU81-017-11) are somewhat suspect, due to the larger errors associated with the $\delta^{13}C$ values of the calculated vesicle C. Estimates of Δ_{v-m} derived from three of the four remaining Juan de Fuca samples yield a smaller fractionation range of 4.7-7.5 ‰.

[d] From Des Marais and Moore (1984) and Sakai et al. (1984). Crushed samples were reduced to 38-93 μm size and analyzed using methods similar to those described in this study.

[e] From Mattey et al. (1989). These authors report apparent $\Delta_{v\text{-}m}$ of ≈ 0.8-1.4 ‰ based on a number of analyses of a single MORB sample. In their calculations, carbon released at heating steps of 800° and 1000° are not included as high-temperature (indigenous) C. However, corresponding aliquots are included as primary C for the 2-4 mm chip samples. In the table above, we recalculate apparent $\Delta_{v\text{-}m}$ using data for an aliquot crushed to 53-106 μm based on carbon yields for (a) the 1200°C step only (i.e., carbon released at >1000°-1200°C); (b) the 1000°+1200°C steps (carbon released at >800°-1200°C) and (c) the 800°+1000°+1200°C steps (carbon released at >600°-1200°C). Inclusion of the carbon yields from the 800° and 1000°C heating steps results in higher apparent $\Delta_{v\text{-}m}$ values.

Table A-5 Results of point counts of vesicles in samples, and calculation of amount of vesicle carbon

Sample no.	Volume % Vesicles[a]	Size Range (μm)[b]	Av. Size (μm)[c]	Thin Section Type[d]	Calc. Vesicle C (max.)[e]	Estimated Vesicle C (min.)[f]
TT152-37	0.6	50-150	80	p	59	
TT152-43-19	0.9	150-1200	300	p	90	
TT152-44	0.8	200-550	450	c	84	
TT152-77-6	0.7	180-320	220	p	61	
TT152-77-7	0.4	100-300	150	p	35	
TT152-55-25	0.1	40-200	70	c	7	
TT170-5	1.1	50-750	120	p	76	
TT152-61	0.9	200-700	620	c	90	
TT152-72	1.2	150-850	600	p	118	
TT152-65	2.1	150-350	250	c	212	113
TT152-30-45	1.7	10-150	400	c	178	48
TT152-29-1	0.4	500-810	700	p	40	56
TT152-21	0.6	40-150	60	p	64	18
TT152-26A	<0.1	20-40	300	p	<12	
TT152-16	0.4	60-1200	350	p	46	
TT152-13	0.3	130-250	200	p	35	
HU81-017-6-11	1.1	100-2200	500	p	125	59
TT152-11-10	0.6	100-700	180	p	70	
TT152-11-21	<0.1	90-180	130	p	<12	
HU81-017-11	1.2	80-1000	250	c	137	17
HU81-017-2-4	0.3	100-500	200	p	33	

[a] Based on 1000 point counts using 300x300 μm grid spacing.

[b] Range in vesicle size observed in thin section.

[c] Average size of vesicles that registered in the point counts.

[d] Thin section type: p (cut parallel to outer chilled rim of a glassy hand sample) or c (from a sample of chips picked and sorted for extraction).

[e] Vesicle C content calculated using modified MRK-EOS (Holloway, 1977), assuming $P_{CO_2} = P_{total} = 0.01$ x (collection depth), 1% vesicles = 0.0036 cc vesicles, melt density = 2.8 g/cc, and vesicle closure temperature = 900°C (Moore et al., 1977).

[f] Difference in C concentrations between crushed and uncrushed samples.

DISCUSSION

Origin of low-temperature carbon

Low-temperature carbon in submarine basalts appears to be related to their post-eruptive history, but it is unclear how much is generated by processes operating on the seafloor (e.g., condensation of cooling vapors (Mathez and Delaney, 1981); reaction between hot volcanic gases and glass (Mathez, 1987; Tingle et al., 1990; Tingle et al., 1991); reaction with seawater such as low-temperature weathering (Des Marais, 1984)) and how much is contamination acquired during storage, handling, or laboratory processing (Des Marais, 1984; Des Marais and Moore, 1984). The enhanced concentrations of low-temperature components in crushed samples are consistent with the observation of Des Marais and Moore (1984) that a low-temperature component with isotopic characteristics similar to that of the uncrushed samples can be generated by exposure to laboratory air on short time scales. Moreover, the results for two size fractions, 38-63 μm and 63-90 μm, of sample TT152-30-45 also suggest that the abundance of low-temperature carbon is surface correlated: finer-grained glass fractions yield more low-temperature carbon. We cannot rule out a contribution to low-temperature carbon from processes occurring on the sea floor, but our observations indicate that this must be a minor component.

Interlaboratory comparison of C in submarine basalts

Carbon concentrations in Juan de Fuca basalts have been measured using a number of analytical methods. Three samples from locations near TT152-37 at the southern end of the Juan de Fuca Ridge were analyzed by Brett et al. (1987) using vacuum crushing and thermal and laser vacuum extraction techniques, where gases released above 600°C were measured by a quadrapole mass spectrometer or a capacitance manometer. These samples

yielded C concentrations of 35-38 ppm, values at the lower end of the range reported here. Dixon et al. (1988) measured dissolved carbon (as CO_3^{2-}) using infrared spectroscopy on 29 glass chip samples from the Juan de Fuca Ridge and found a range of 14-82 ppm C. Five of our crushed samples can be directly compared with the results of Dixon et al. (1988). The dissolved C contents based on IR measurements are ≈ 30 % lower than the corresponding crushed sample values of our study. More recent work by Dixon (1992) suggests that the IR values of Dixon et al. (1988) are 20 % too low and thus the corrected data are in better agreement with our results. The remaining differences could be due to (1) inaccuracy of the IR calibration, (2) an additional form of carbon not detected with the IR spectroscopic method, (3) heterogeneous distribution of dissolved C in the glasses (Metrich and Mosbah, 1988), (4) incomplete release of vesicle gas during crushing, or (5) heterogeneous phenocryst concentrations.

More significant analytical discrepancies, as summarized by Des Marais (1986), are observed between the results discussed above and those obtained for submarine basalts using a Knudsen cell/mass spectrometer assembly (Byers et al., 1986; Delaney et al., 1978; Garcia et al., 1979; Muenow et al., 1979; Muenow et al., 1991), where reported dissolved carbon concentrations are $10\text{-}10^3$ times greater than the values reported here. It is important to emphasize that our results, those of Brett et al. (1987), and the infrared analyses of Dixon et al. (1988) are all similar. The fairly good correspondence among these three independent analytical techniques strongly suggests that the dissolved carbon contents of Juan de Fuca Ridge glasses (and most MORBs) are ≤ 150 ppm.

Variation in carbon concentration with depth of emplacement

There is no systematic relationship between eruption depth and carbon concentration in the ~1.5 km of bathymetric relief along the Juan de Fuca Ridge (Fig. A-4a). This observation was previously noted for Juan de Fuca samples (Blank et al., 1986; Dixon et

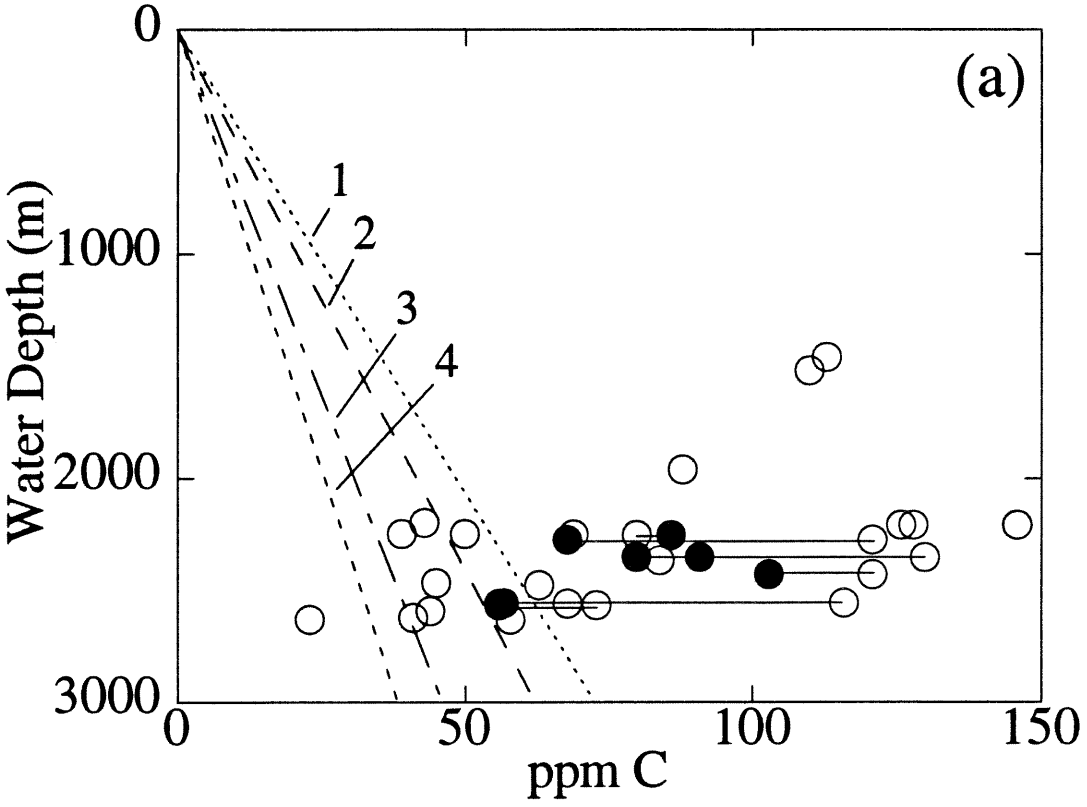

Fig. A-4a. Variation of carbon abundance with depth of sample collection. Open circles - uncrushed glass chips (vesicle + dissolved C); filled circles - crushed chips (dissolved C). Solubility curves are taken from: 1 - Harris (1981; vacuum pyrolysis/quadrupole mass spectrometry of crushed, natural basaltic glasses); 2 - Des Marais and Moore (1984; stepped combustion/manometry of crushed, natural glasses); 3 - Stolper and Holloway (1988; infrared spectroscopy of glasses from experimental charges); 4 - Trull et al. (1991; stepped combustion/manometry of experimental charges). Tie lines connect different crushed and uncrushed aliquots of the same sample.

al., 1986; 1988) and interpreted to reflect incomplete degassing resulting from rapid ascent and eruption of the lavas. Fine and Stolper (1986) and Metrich and Mosbah (1988) proposed a similar interpretation to explain the observed C contents of other MORB glasses. The Juan de Fuca samples with the lowest carbon contents should be the most degassed and thus their C contents may approach near-equilibrium solubility concentrations.

Previously, CO_2 solubility curves for basaltic melts at low pressures were derived empirically from data on crushed MORB glasses from a variety of spreading centers (Harris, 1981; Des Marais and Moore, 1984). However, recent experimental data of Stolper and Holloway (1988) and Trull et al. (1991) imply that carbon solubilities are somewhat lower than the estimates based on natural samples. Almost all of our measured carbon concentrations are in excess of these solubility estimates. The fact that many of the *uncrushed* samples have lower C contents than other *crushed* samples erupted at similar depths (Fig. A-4a) also indicates that most of the Juan de Fuca samples are supersaturated with respect to carbon.

The supersaturated nature of these samples allow us to estimate minimum depths at which the magmas were saturated with respect to carbon (Stolper and Holloway, 1988). Using the carbon concentration of our most C-rich sample (TT152-37; 146 ppm) and the solubility curve of Trull et al. (1991), we predict a minimum magma chamber depth of 2.3 km. This depth corresponds to the proposed top of a magma chamber based on seismic reflection data (2.3 km; Morton et al., 1987) from the southern Juan de Fuca Ridge. A similar estimate of magma chamber depth (2-3 km) beneath the northern Juan de Fuca Ridge has been made by Rohr et al. (1988).

Variation in $\delta^{13}C$ with depth

Degassing of CO_2 preferentially depletes a basaltic melt in ^{13}C (Pineau et al., 1976), and therefore, given similar initial C contents and $\delta^{13}C$ compositions, magmas that have experienced the highest degree of degassing should also have the lowest C concentrations and $\delta^{13}C$ values. Magmas erupted at the shallowest depths should be the most degassed based on solubility constraints, but the lack of correlation between C concentration and depth in Fig. A-4a suggests that this is not the case for the Juan de Fuca samples. There is a slight correlation between $\delta^{13}C$ values and collection depth (Fig. A-4b) but the trend is opposite of that predicted, as samples with the lowest $\delta^{13}C$ signatures were recovered from the greatest depths. With respect to the uncrushed samples, which include both vesicle and dissolved carbon, such a trend may be attributed to the vesicle distribution in the samples, as discussed below.

Vesicle CO_2 content of Juan de Fuca glasses

Vesicle gas in basaltic glasses erupted on the seafloor consists almost entirely of CO_2 (Delaney et al., 1978; Garcia et al., 1979; Moore, 1979), and thus vesicle carbon may comprise a significant portion of the carbon in some of the uncrushed samples. Using our vesicle point count data, we calculated the maximum contribution of carbon from vesicles present in uncrushed samples (Table A-4). These estimates of vesicle gas contents can be compared with differences between measured total (bulk) carbon contents of glass chips and corresponding crushed samples representing dissolved C contents. The calculations of vesicle C concentrations by difference represent minimum estimates since: (1) the glass chips used for C analysis were selected to contain a minimum of vesicles, (2) the glass surrounding the larger vesicles in the bulk (chip) samples may have cracked during sample preparation and released gas prior to analysis, and (3) some very small vesicles may remain intact after the crushing procedure. Small, unbroken vesicles should not contribute significantly to the total carbon because of the very low volume of these vesicles. In all

cases, the maximum vesicle carbon contents calculated from point count data are greater

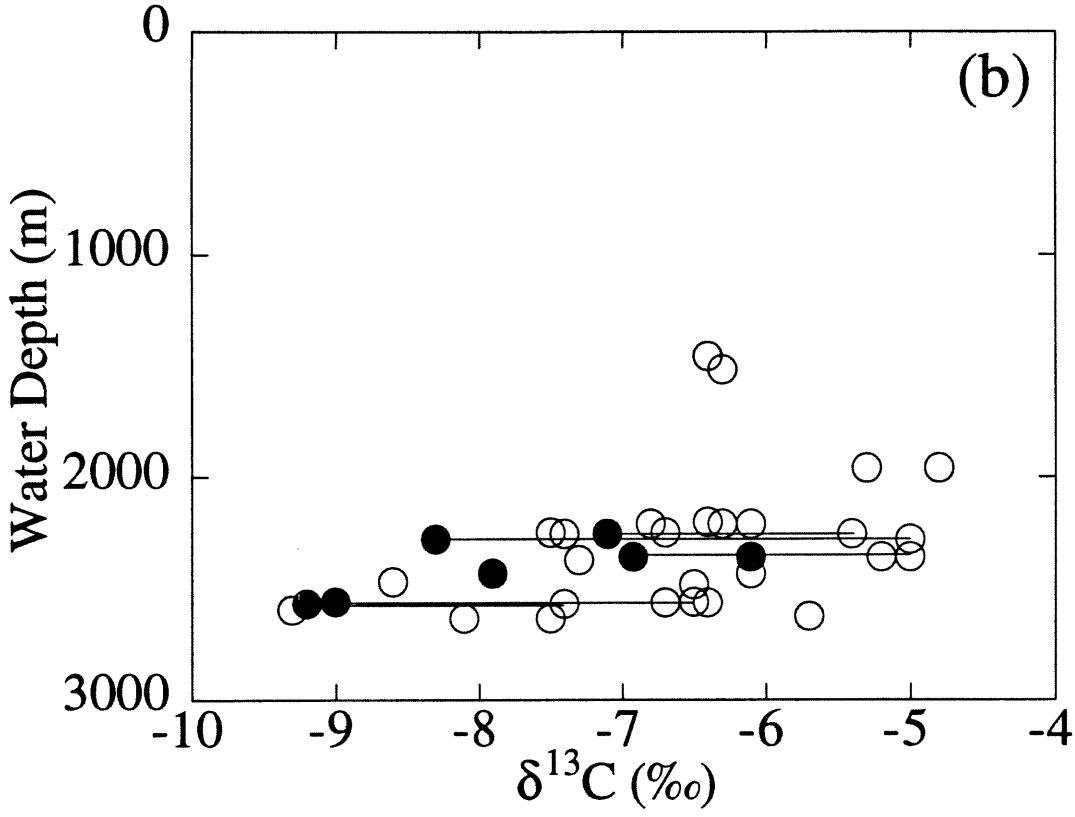

Fig. A-4b. Variation $\delta^{13}C$ value with depth of sample collection. Open circles - uncrushed glass chips (vesicle + dissolved C); filled circles - crushed chips (dissolved C). Tie lines connect different crushed and uncrushed aliquots of the same sample.

than the vesicle C contents estimated by the difference between uncrushed chip and crushed samples.

Neither mean vesicle size nor vesicle abundance (vol. % vesicles) correlates with the depths of sample collection. There is a wide range in $\delta^{13}C$ values and C concentrations for any given vesicle content (Fig. A-5a,b). Only a crude positive correlation between volume percent vesicles and $\delta^{13}C$ value or C content exists. With higher vesicle contents, there is a decrease in the range of observed carbon concentrations and $\delta^{13}C$ values. The poor correlations between depth, degree of vesiculation, C concentration, and $\delta^{13}C$ values all suggest that the glasses were quenched under non-equilibrium conditions.

Effective CO_2 degassing of magmas is controlled by bubble nucleation, diffusion of C from the surrounding melt into bubbles, and buoyant segregation of that volatile phase from the melt (Bottinga and Javoy, 1989; Bottinga and Javoy, 1990; Sparks, 1978). Bubbles in an ascending magma expand due to diffusive influx of exsolving C from the magma, bubble coalescence, and decreasing confining pressure (Bottinga and Javoy, 1990; Tait and Jaupart, 1990). The diffusion of C in basaltic magmas (Watson et al., 1982) is many orders of magnitude slower than estimated eruption rates of $\approx$ 1 m/s (Turcotte and Schubert, 1982), so only the largest vesicles would have sufficient buoyancy to separate from an ascending body of magma over its eruption timescale (cf., Stolper and Holloway, 1988). As a result, equilibrium degassing should be the exception rather than the rule for most MOR basalts. One interesting observation is that the four uncrushed samples with the smallest average vesicle diameters ($\leq$120 μm) have total C concentrations in excess of 120 ppm, among the highest observed for our samples. Small vesicles lack sufficient buoyancy to escape from the melt (Bottinga and Javoy, 1990), and thus these magmas probably did not experience significant degassing during their final ascent to the ocean floor.

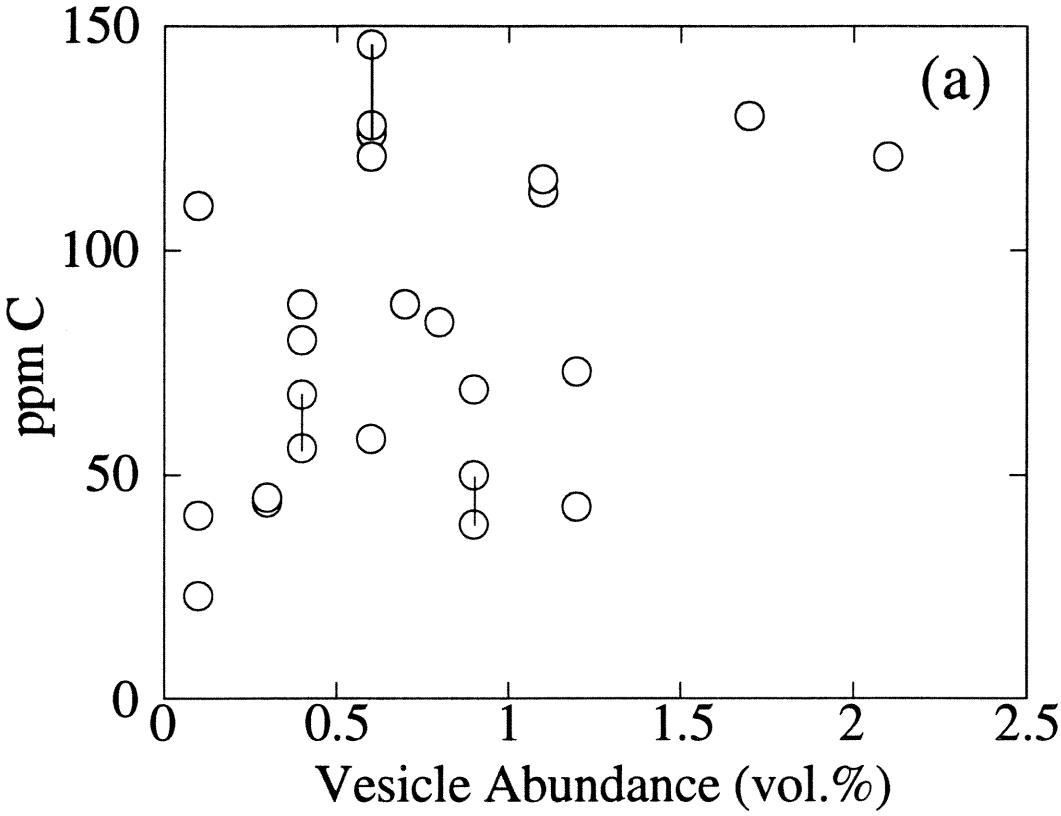

Fig. A-5a. Vesicle content (vol.% based on thin section point count results) versus ppm C for crushed (filled circles) and uncrushed (open circles) samples. Tie lines as in Fig. A-4a.

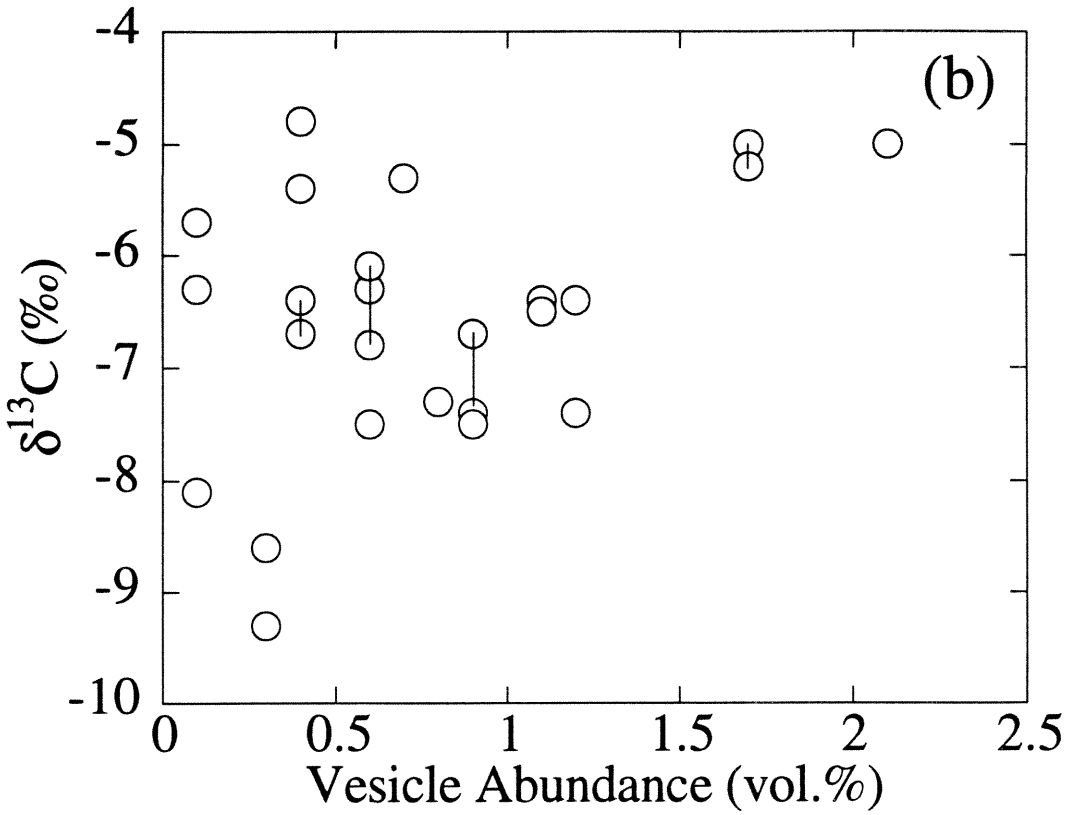

Fig. A-5b. Vesicle content (vol.% based on thin section point count results) versus $\delta^{13}C$ for crushed (filled circles) and uncrushed (open circles) samples. Tie lines as in Fig. A-4b.

Carbon variation along the Juan de Fuca Ridge

Once identified as a hotspot (Morgan, 1973), the Axial Seamount lacks the chemical signatures typical of one (Eaby et al., 1984; Liias, 1986). Nevertheless, the ridgecrest seamount may be the surface expression of a major source of the magma supply along the Juan de Fuca ridge (Karsten and Delaney, 1985). In such a scenario, magma ascending beneath the Axial Seamount could be transported laterally to the various ridge segments. This idea is supported by an observed zonation in the degree of chemical fractionation in the basalts (Delaney et al., in prep; Karsten and Delaney, 1985). There is a general increase in FeO* both to the north and south from ~10 wt. % near the Axial Seamount to 13-15 wt. % near the Blanco Fracture Zone (to the south) and Cobb Offset (to the north). Similarly, Mg# decreases from roughly 60 near the Axial Seamount to approximately 45 near the Blanco Trough and the Cobb Offset. However, there is no systematic correlation between the degree of chemical fractionation and vesicle abundance, carbon concentration, or carbon isotopic composition in the Juan de Fuca basalts studied, suggesting that if lateral migration of magmas along the Juan de Fuca ridge does occur, then it likely takes place at pressures in excess of those required for CO_2 vapor to exsolve.

We have noted earlier that the range in $\delta^{13}C$ values (-4.8 to -9.3 ‰) determined in this study for Juan de Fuca samples is somewhat larger than those previously reported for MORBs. One possible explanation for this variability is the existence of a heterogeneous source with respect to ^{13}C content, but other isotopic and geochemical data indicate that Juan de Fuca parental magma is fairly homogeneous in nature (Delaney et al., in prep; Eaby et al., 1984). Another mechanism that could account for the observed spread of $\delta^{13}C$ values is magmatic degassing; the potential effects of this process on the Juan de Fuca glasses are discussed below.

The observed variations in indigenous C contents and $\delta^{13}C$ values observed in Juan de Fuca basalts is most likely controlled by CO_2 degassing. All samples studied contain vesicles, physical evidence that they were supersaturated with respect to CO_2 and evolved a discrete volatile phase. If the primary C contents of the Juan de Fuca basalts were similar, the variations in the measured bulk C contents may reflect differences in degassing histories during magma ascent and eruption. The degassing behavior of the glasses analyzed in this study can be examined using the two end-member degassing models discussed below by comparing the observed relations between concentration and $\delta^{13}C$ with model-predicted relationships. This requires knowledge of the isotopic fractionation between CO_2 vapor and dissolved carbon ($\Delta_{v\text{-}m} = \delta^{13}C_{vapor} - \delta^{13}C_{melt}$) and estimates of initial C concentrations and $\delta^{13}C$ values of the melt.

As a basaltic melt rises and becomes vapor-saturated, CO_2 is the first major gas species to exsolve, triggering nucleation and bubble growth (e.g., Bottinga and Javoy, 1989). With continued upward rise and eruption of a magma, the concentration of dissolved vapor species in the melt is reduced and the $\delta^{13}C$ value of the remaining dissolved C decreases as CO_2 gas, richer in ^{13}C, is exsolved from the melt (Pineau and Javoy, 1983; Pineau et al., 1976).

Degassing can be described in terms of two end-member scenarios. In closed system degassing, gas does not escape from the magma; the isotopic composition and concentration of C in the melt responds to partitioning of C between melt and vapor during depressurization, but the bulk (total) C content and $\delta^{13}C$ values of the magma remain constant. Vesicle volume %, dissolved C contents, and $\delta^{13}C$ values of dissolved and vesicle C for the closed endmember system change systematically and can be readily calculated using mass balance relationships. Following this model, if the initial melt compositions are all the same, then bulk samples should have similar $\delta^{13}C$ values and C

concentrations and variable vesicle contents, depending on the amount of CO_2 partitioned into a separate gas phase. C contents in the crushed samples should correlate inversely to the vesicle abundance in the corresponding bulk samples. The equilibrium isotopic fractionation between CO_2 vapor and dissolved carbon species represents the maximum possible shift in $\delta^{13}C$ values of the phases during closed system degassing.

In open system degassing, discrete parcels of exsolved CO_2 gas are systematically removed from the melt. The change in isotopic composition can be modeled using a Rayleigh fractionation equation provided that the appropriate isotope fractionation factor (α) and initial $\delta^{13}C$ value and C abundance are known. This model requires that exsolved CO_2 gas is immediately isolated from the system, and a much greater shift in dissolved carbon $\delta^{13}C$ values can be obtained through open system degassing than with the closed system model.

Natural systems differ from these endmember cases in a number of ways (e.g., Gerlach and Taylor, 1990). CO_2-rich bubbles are not immediately removed from a body of magma when they form but remain until they are sufficiently large enough to buoyantly segregate. CO_2 in ascending bubbles may interact with the melt. Kinetic (nonequilibrium) isotope fractionation of carbon partitioning between bubbles and melt may also occur in rapidly ascending and erupting magmas. While the two endmember cases mentioned above are clearly more simplistic than degassing in dynamic, natural systems, they provide a framework in which to consider the evolution of carbon and $^{13}C/^{12}C$ ratios in quenched submarine basalts.

Javoy et al. (1978) have determined experimentally the carbon isotopic fractionation between vapor and basaltic melt at 1120-1280°C and 7-8.4 kbars using two brands of oxalic acid with $\delta^{13}C$ values of -24.1 and -16.6 ‰. They reported $\Delta_{v\text{-}m}$ values of 4.0-4.6 ‰ that closely resemble calculated fractionations for CO_2-CO (Richet et al., 1977) and CO_2-graphite (Bottinga, 1969) at magmatic temperatures. These fractionation values appear to be too large given that the principal dissolved species in basaltic melt is carbonate

(e.g., Fine and Stolper, 1986), and the calculated carbon isotopic fractionation for CO_2-carbonate should be no higher than 1-2 ‰ at magmatic temperatures (Ohmoto and Rye, 1979). Javoy et al. (1978) also report unusually high and variable CO_2 solubilities in their glassy run products, up to an order of magnitude higher than those predicted by Stolper and Holloway (1988) for the same pressure and temperature. Javoy et al. (1978) noted that the presence of an unidentified, reduced species of carbon (graphite?) may have affected their results, and thus the reported C isotope fractionation values are somewhat suspect. A smaller $\Delta_{v\text{-}m}$ value of ≈ 2 ‰ (1.8-2.2 ‰) was determined experimentally by Mattey (1991) for basaltic melt held at 1200-1400°C and 5-20 kbars. These results are comparable to those from similar experiments performed on sodamelilite ($NaCaAlSi_2O_7$), an Fe-poor basaltic melt analog in which dissolved carbon also occurs as carbonate ions (Mattey et al., 1990). We have selected the experimentally-determined fractionation of 2 ‰ as the value most consistent with existing information on the system $CO_{2(vapor)}$-$CO_3^{2-}{}_{(basalt)}$. Using a larger value for $\Delta_{v\text{-}m}$ (e.g., 4-4.6 ‰) will shift the curves in Fig. A-6 but will not significantly alter our interpretation of the observed trends.

The starting point (C_0) chosen for the degassing models is 400 ppm C and $\delta^{13}C$ = -5 ‰, estimated in the following manner. We assumed a global carbon flux of 10^{13} g C/yr; while there is some debate regarding the value for the carbon flux (cf., Gerlach, 1991; Graham and Sarda, 1991), this value is comparable to those reported by Des Marais and Moore (1984), Gerlach (1989), and Sarda and Graham (1990). We used a value of 10 km^3/yr for the volume of new basaltic crust being generated and degassed annually (Javoy et al., 1983), and an average MORB density of 2.8 g/cm^3 to obtain an estimated value of 360 ppm degassed C. An additional amount (≈ 40 ppm) of carbon is retained by MORB lavas after degassing, resulting in an initial C content of ≈ 400 ppm for MOR basaltic melts. This value is somewhat higher than Gerlach's (1989) estimate for MORB parental magmas of 330 ppm based on his study of Erta Alle basalts. The initial $\delta^{13}C$ value of -5‰ is based on previous estimates of 'normal' mantle carbon (Mattey, 1987).

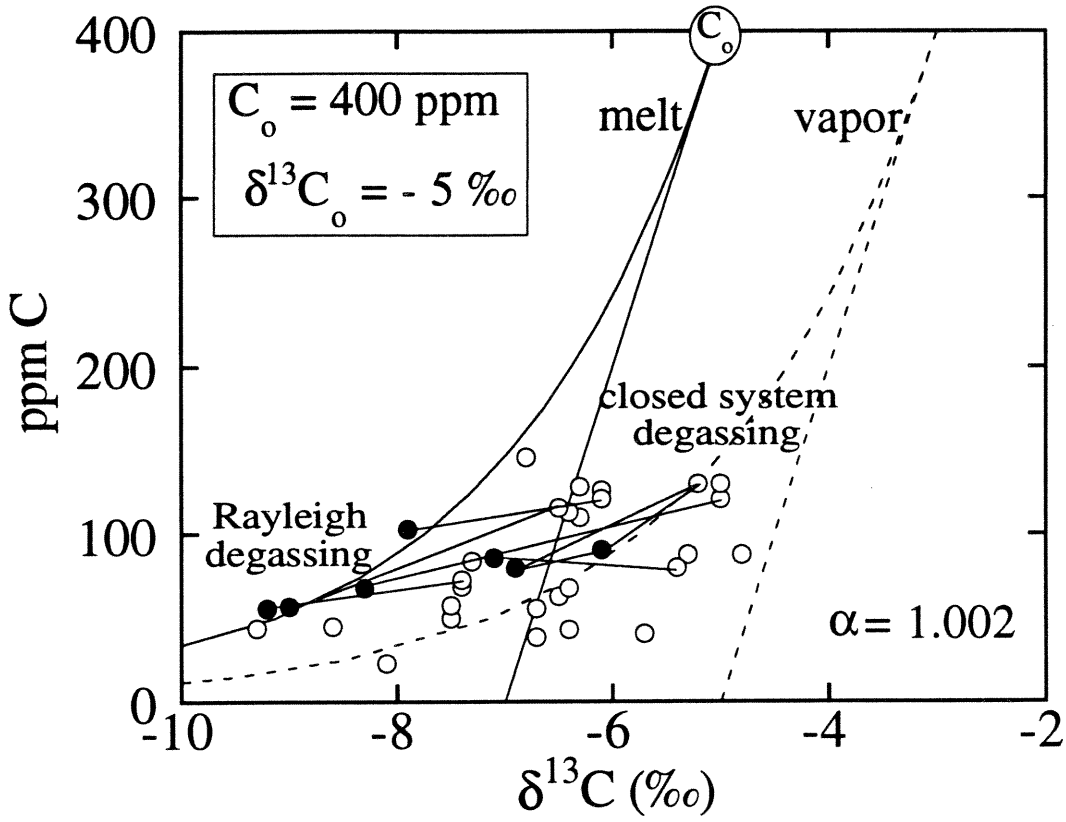

Fig. A-6. Carbon concentrations versus $\delta^{13}C$ values for samples analyzed in this study. Open and filled circles and tie lines as in Figs. A-4,5. Curves are calculated degassing paths for closed and Rayleigh fractionation models assuming a $\Delta_{\text{vapor-melt}}$ of 2 ‰ (Mattey et al., 1991), and initial melt composition (C_0) of 400 ppm C with a $\delta^{13}C_0$ of -5.0 ‰ (see text). Solid lines - concentration and $\delta^{13}C$ values of C dissolved in the melt; dashed lines - $\delta^{13}C$ of CO_2 vapor in equilibrium with a given melt carbon content.

The two end-member degassing models we consider are defined as follows. Closed-system degassing can be described as a mass-balance approximation, where:

$$(x)\delta_d + (1\text{-}x)\delta_v \approx \delta_b$$

and δ_d, δ_v, and δ_b represent isotopic compositions of dissolved, vesicle, and bulk (dissolved+vesicle) C, and (x) and (1-x) are the fractions of carbon in the glass and vesicles, respectively. The other end-member degassing model uses Rayleigh fractionation, described by

$$(\delta_d+1000) / (\delta_o+1000) = f^{(\alpha-1)},$$

where δ_d and δ_o are the isotopic compositions of dissolved C and the initial composition of carbon prior to degassing, f is the fraction of carbon remaining in the melt, and α is the fractionation factor (1.002), related to $\Delta_{v\text{-}m}$ by the approximation $1000(\alpha-1) \approx \Delta_{v\text{-}m}$.

In Fig. A-6, calculated degassing curves are superimposed on a plot of ppm C versus $\delta^{13}C$ values. The solid curves for both Rayleigh and closed system degassing define the calculated $\delta^{13}C$ composition of the melt at a given concentration of dissolved C. The dashed curves indicate the $\delta^{13}C$ composition of vapor in equilibrium with dissolved C of a given $\delta^{13}C$ value. As the fraction of C dissolved in the melt decreases in the Rayleigh model, the residual dissolved carbon becomes progressively depleted in ^{13}C compared to the closed system model. Uncrushed glasses, which contain a combination of dissolved and vesicle carbon, should have higher carbon contents than the crushed samples, and their isotopic composition should lie between the curves for dissolved and vapor carbon species. Samples for which analyses of both crushed and bulk material were obtained are connected by tie lines. While there is much scatter in the diagram, most samples with carbon concentrations below 100 ppm (especially the crushed glasses) follow the trend of the Rayleigh degassing path. The presence of variable carbon concentrations and isotopic compositions for the chip samples violates the initial premise of the closed system model, and suggests that all samples have undergone some open system loss of CO_2.

The correlation between the crushed samples and the Rayleigh degassing curve in Fig. A-6 suggests that the differences in carbon contents and $\delta^{13}C$ values observed among the samples may be explained by variable degrees of degassing. A geologically plausible degassing history for the Juan de Fuca magmas consists of the following: (1) Carbon-bearing melts are generated at depth; (2) Melts saturated in CO_2 reside in shallow magma reservoirs located several km below the Juan de Fuca Ridge and undergo "sedate" degassing; (3) During ascent prior to eruption, additional CO_2-rich bubbles nucleate rapidly and expand; (4) Variable loss of CO_2-rich vapor during eruption and quenching on the sea floor leads to the observed array of carbon concentrations and $\delta^{13}C$ values of the basaltic glasses. In principle, this is not unlike the 2-stage degassing model first proposed by Pineau and Javoy (1983) for lavas from the Mid-Atlantic ridge, although these authors assumed much higher C contents of both their samples and the basalt parental magmas.

The relatively large range in apparent $\Delta_{v\text{-}m}$ values observed for natural basalts (≈1-13 ‰, Table A-6) suggests that dissolved carbon and CO_2 vapor trapped in vesicles in these samples may not be in isotopic equilibrium at the time of sample quenching, as they are certainly not in equilibrium with respect to their predicted solubility concentrations. The generally larger than 2 ‰, empirically-determined $\Delta_{v\text{-}m}$ values could also be due to the presence of varying amounts of an isotopically light carbon film that is released during the high-temperature combustion step (Mathez, 1987; Tingle et al., 1991).

Table A-6 Comparison of C in crushed and uncrushed samples

Sample no.	Uncrushed glasses		Crushed samples		Vesicles (calculated)		Apparent $\Delta_{v\text{-}m}$
	C (ppm)	$\delta^{13}C$ (‰)	C (ppm)	$\delta^{13}C$ (‰)	C (ppm)[a]	$\delta^{13}C$ (‰)[b]	(‰)[c]
Juan de Fuca samples (this study):							
TT152-65	121	-5.0	68	-8.3	53	-0.8	**7.5**
TT152-30-45	130	-5.1	80	-6.9	50	-2.1	**4.7**
TT152-29-1	80	-5.4	86	-7.1	-	-	-
TT152-21	121	-6.1	103	-7.9	18	4.1	**12.0**
HU81-017-6-11	116	-6.5	57	-9.0	59	-4.1	**4.9**
HU81-017-11	73	-7.4	56	-9.2	17	-1.5	**7.7**
Other MORB samples							
TR-14[d]	164	-6.3	115	-7.1	49	-4.4	**2.7**
KN5444-614[d]	131	-7.1	102	-8.0	29	-3.9	**4.1**
FAMOUS-264[d]	136	-6.2	63	-8.0	73	-4.6	**3.4**
S714-1-A4[d]	105	-5.6	87	-6.3	18	-2.2	**4.1**
JC-03-02-01-(a)[e]	167	-7.3	60	-8.0	107	-6.9	**1.1**
" (b)	"	"	113	-10.3	54	-1	**9.3**
" (c)	"	"	124	-10.6	43	2.2	**12.8**

Notes:

[a] Vesicle carbon calculated by subtracting the concentrations of carbon in the crushed from the uncrushed samples: $C_{vapor} = C_{bulk} - C_{dissolved}$.

[b] $\delta^{13}C$ of vesicle carbon calculated using the approximation: $C_b(\delta^{13}C)_b = C_v(\delta^{13}C)_v + C_d(\delta^{13}C)_d$.

[c] $\Delta_{v\text{-}m} = \delta^{13}C_{vapor} - \delta^{13}C_{melt}$. Values determined for samples with small amounts of calculated vesicle carbon (here, 17 and 18 ppm for samples TT152-21 and HU81-017-11) are somewhat suspect, due to the much larger errors associated with the $\delta^{13}C$ values of the calculated vesicle C. Therefore, estimates of $\Delta_{v\text{-}m}$ should only be derived from three of the Juan de Fuca samples (resulting in a smaller fractionation range of 4.7-7.5 ‰).

[d] From Des Marais and Moore (1984) and Sakai et al. (1984). Crushed samples were reduced to 28-93 μm size and analyzed using methods approximately the same as in this study.

[e] From Mattey et al. (1989). These authors report apparent $\Delta_{v\text{-}m}$ of ≈ 0.8-1.4 ‰ based on a number of analyses of a single sample. In their calculations, carbon released at heating steps of 800° and 1000° are not included as high-temperature (indigenous) C. However, corresponding aliquots are included as primary C for the 2-4 mm chip samples. In the table above, we recalculate apparent $\Delta_{v\text{-}m}$ using data for an aliquot crushed to 53-106 μm based on carbon yields for (a) the 1200°C step only (i.e., carbon released at >1000°-1200°C); (b) the 1000°+1200°C steps (carbon released at >800°-1200°C), and (c) the 800°+1000°+1200°C steps (carbon released at >600°-1200°C). Inclusion of the carbon yields from the 800° and 1000°C heating steps results in higher apparent $\Delta_{v\text{-}m}$ values.

CONCLUSIONS

The majority of Juan de Fuca basalts had not reached equilibrium with respect to their carbon contents when they were quenched at the sea floor. Observations supporting disequilibrium include (1) a lack of correlation for $\delta^{13}C$ values and C concentrations with depth; (2) the random nature of the vesicle populations in the samples; and (3) the large range in calculated isotopic fractionations between vesicle and dissolved carbon among different samples. The lack of equilibrium implies that the rate at which a basaltic melt degasses is slower than either transport or eruption rates.

Although we report a wider range of $\delta^{13}C$ values (-4.8 to -9.3 ‰) than noted previously for MORB glasses from a single spreading center, there is no direct evidence that this variation is related to source heterogeneity. While we cannot rule out the possibility of variable ^{13}C enrichment in the source region(s) of the ridge crest magmas, the observed range in carbon concentrations and $\delta^{13}C$ values for the samples can be explained by degassing. At concentrations below ≈100 ppm C, the relation between carbon contents and $\delta^{13}C$ values of crushed samples resembles an open system degassing trend; variable amounts of Rayleigh-like degassing, in which CO_2 vapor exsolves but does not escape from a magma, could produce the measured variation in carbon concentrations and $\delta^{13}C$ values Juan de Fuca Ridge basalts.

Acknowledgements--The authors are grateful to D.S. Kelley for assistance in preparation of the glass chips analyzed in this study, and to S. Rivera and H. Nguyen for assistance with the mass spectrometric work. P.F. Dobson helped initiate this investigation and shared his insight. We thank E.M. Stolper and J.R. Beckett, who commented on an early version of the manuscript, and T.N. Tingle, E.A. Mathez, and an anonymous colleague for careful, official reviews. This study was funded in part by NSF grants OCE 79-25041,

OCE81-11413, OCE83-09812 to JRD, by NASA's Exobiology Program, and by a Penrose Grant to JGB from the Geological Society of America.

References

Anderson A. T. (1975) Some basaltic and andesitic gases. *Rev. Geophys. Space Phys.* **13**, 37-55.

Barker C. and Torkelson B. E. (1975) Gas adsorption on crushed quartz and basalt. *Geochim. Cosmochim. Acta* **39**, 212-218.

Blank J. G., Delaney J. R. and Des Marais D. J. (1986) Carbon in basaltic glass from the Juan de Fuca Ridge (abstr.). *Eos* **67**, 1253.

Bottinga Y. (1969) Calculated fractionation factors for carbon and hydrogen isotope exchange in the system calcite-carbon dioxide-graphite, methane-hydrogen-water vapor. *Geochim. Cosmochim. Acta* **33**, 49-64.

Bottinga Y. and Javoy M. (1989) MORB degassing: Evolution of CO_2. *Earth Planet. Sci. Lett.* **95**, 215-225.

Bottinga Y. and Javoy M. (1990) Mid-ocean ridge basalt degassing: Bubble nucleation. *J. Geophys. Res.* **95**, 5125-5131.

Bottinga Y. and Javoy M. (1990) MORB degassing: Bubble growth and ascent. *Chem. Geol.* **81**, 255-270.

Brett R., H.T. Evans J., E.K. Gibson J., Hedenquist J. W., Wandless M.-V. and Sommer M. A. (1987) Mineralogical studies of sulfide samples and volatile concentrations of basalt glasses from the southern Juan de Fuca Ridge. *J. Geophys. Res.* **92**, 11,373-11,379.

Byers C. D., Garcia M. O. and Muenow D. W. (1986) Volatiles in basaltic glasses from the East Pacific Rise at 21°N: implications for MORB sources and submarine lava flow morphology. *Earth Planet. Sci. Lett.* **79**, 9-20.

Craig H. (1953) The geochemistry of stable carbon isotopes. *Geochim. Cosmochim. Acta* **3**, 53-92.

Delaney J. R., Johnson H. P. and Karsten J. L. (1981) The Juan de Fuca Ridge-hotspot-propagating rift system: new tectonic, geochemical, and magnetic data. *J. Geophys. Res.* **86**, 11747-11750.

Delaney J. R., Karsten J. L. and Hammond S. R. (1986) Petrology and tectonics of the Juan de Fuca Ridge (abstr.). *Eos* **67**, 888.

Delaney J. R., Karsten J. L., Rhodes J. M., Clague D. A. and Schilling J.-G. (in prep) Petrology and tectonics of the Juan de Fuca Ridge Part I: Interaction of the hotspot and the ridge crest.

Delaney J. R., Muenow D. W. and Graham D. G. (1978) Abundance and distribution of water, carbon and sulfur in the glassy rims of submarine pillow basalts. *Geochim. Cosmochim. Acta* **42**, 581-594.

Des Marais D. J. (1978) Carbon, nitrogen, and sulfur in Apollo 15, 16, and 17 rocks. *Proc. 9th Lunar Planet. Sci. Conf.* **9**, 2451-2467.

Des Marais D. J. (1978) Variable temperature cryogenic trap for the separation of gas mixtures. *Anal. Chem.* **50**, 1405-1406.

Des Marais D. J. (1983) Light element geochemistry and spallogenesis in lunar rocks. *Geochim. Cosmochim. Acta* **47**, 1769-1781.

Des Marais D. J. (1984) Isotopically light carbon in midocean ridge basalts - fact or artifact? (abstr.). *Geol. Soc. Amer. Abstr. with Prog.* **16**, 486.

Des Marais D. J. (1986) Carbon abundance measurements in oceanic basalts: the need for a consensus. *Earth Planet. Sci. Lett.* **79**, 21-26.

Des Marais D. J. and Moore J. G. (1984) Carbon and its isotopes in mid-oceanic ridge basaltic glasses. *Earth Planet. Sci. Lett.* **69**, 43-57.

Dixon J. E. (1992) Water and carbon dioxide in basaltic magmas. Ph.D. dissertation, California Institute of Technology.

Dixon J. E., Rosner P. S., Stolper E. and Delaney J. R. (1986) Infrared spectroscopic measurements of H_2O and CO_2 contents in Juan de Fuca Ridge glasses (abstr.). *Eos* **67**, 1253.

Dixon J. E., Stolper E. and Delaney J. R. (1988) Infrared spectroscopic measurements of CO_2 and H_2O in Juan de Fuca Ridge basaltic glasses. *Earth Planet. Sci. Lett.* **90**, 87-104.

Eaby J., Clague D. A. and Delaney J. R. (1984) Sr isotopic variations along the Juan de Fuca Ridge. *J. Geophys. Res.* **89**, 7883-7890.

Exley R. A., Mattey D. P., Clague D. A. and Pillinger C. T. (1986) Carbon isotope systematics of a mantle "hotspot": a comparison of Loihi Seamount and MORB glasses. *Earth Planet. Sci. Lett.* **78**, 189-199.

Fine G. and Stolper E. (1986) Carbon dioxide in basaltic glasses: concentrations and speciation. *Earth Planet. Sci. Lett.* **76**, 263-278.

Fyfe W. S., Price N. J. and Thompson A. B. (1978) *Fluids in the Earth's Crust: Their Significance in Metamorphic, Tectonic, and Chemical Transport Processes.* Springer-Verlag.

Garcia M. O., Liu N. W. K. and Muenow D. W. (1979) Volatiles from the Mariana Island arc and trough. *Geochim. Cosmochim. Acta* **43**, 305-312.

Gerlach T. M. (1989) Degassing of carbon dioxide from basaltic magma at spreading centers: II. Mid-ocean ridge basalts. *J. Volcanol. Geotherm. Res.* **39**, 221-232.

Gerlach T. M. (1991) Comment on "Mid-ocean ridge popping rocks: implications for degassing at ridge crests" by P. Sarda and D. Graham. *Earth Planet. Sci. Lett.* **105**, 566-567.

Gerlach T.M. and B.E. Taylor (1990) Carbon isotope constraints on degassing of carbon dioxide from Kilauea Volcano. *Geochim. Cosmochim. Acta* **54**, 2051-2058.

Goldstein S. J., Murrell M. T., Janecky D. R., Delaney J. R. and Clague D. A. (1991) Geochronology and petrogenesis of MORB from the Juan de Fuca and Gorda ridges by ^{238}U-^{230}Th disequilibrium. *Earth Planet. Sci. Lett.* **107**, 25-41.

Graham D. and Sarda P. (1991) Reply to comment by T.M. Gerlach on "Mid-ocean ridge popping rocks: implications for degassing at ridge crests." *Earth Planet. Sci. Lett.* **105**, 568-573.

Hammond S. R., Malahoff A., Embley R. W., Currie R. G., Davis E. E., Riddihough R. P. and Sawyer B. S. (1984) Juan de Fuca Ridge atlas: preliminary Seabeam bathymetry. Energy Mines and Resources, Canada, Open-File Rep. EMR-84-6.

Harris D. M. (1981) The concentration of CO_2 in submarine tholeiitic basalts. *Jour. Geol.* **89**, 689-701.

Hey R. N. and Wilson D. S. (1982) Propagating rift explanation for the tectonic evolution of the northeast Pacific-the pseudomovie. *Earth Planet. Sci. Lett.* **58**, 167-188.

Holloway J. R. (1977) Fugacity and activity of molecular species in supercritical fluids. In *Thermodynamics in Geology* (ed. D. Fraser). pp. 161-181. D. Reidel.

Holloway J. R. (1981) Volatile Interactions in Magmas. In *Thermodynamics of Minerals and Melts* (ed. R. C. Newton, A. Navrotsky and B. J. Wood). Chapt. 13, pp. 273-293. Springer-Verlag.

Javoy M. and Pineau F. (1991) The volatiles record of a "popping" rock from the Mid-Atlantic Ridge at 14°N: Chemical and isotopic composition of gas trapped in the vesicles. *Earth Planet. Sci. Lett.* **107**, 598-611.

Javoy M., Pineau F. and Allègre C. J. (1983) Carbon geodynamic cycle--reply. *Nature* **303**, 731.

Javoy M., Pineau F. and Liyama I. (1978) Experimental determination of the isotopic fractionation between gaseous CO_2 and carbon dissolved in tholeiitic magma. *Contrib. Mineral. Petrol.* **67**, 35-39.

Karsten J. L. (1988) Spatial and temporal variations in the petrology, morphology and tectonics of a migrating spreading center; the Endeavor Segment, Juan de Fuca Ridge. Ph.D. dissertation, University of Washington.

Karsten J. L. and Delaney J. R. (1985) Comparison of glass geochemistry from seamount and adjacent ridge crest lavas: Juan de Fuca Ridge (abstr.). *Eos* **66**, 1109.

Karsten J. L., Delaney J. R. and Liias R. A. (1990) Spatial and temporal evolution of magmatic systems beneath the Endeavor Segment, Juan de Fuca Ridge - tectonic and petrologic constraints. *J. Geophys. Res.* **95**, 19,235-19,256.

Liias (1986) Geochemistry and petrogenesis of basalts erupted along the Juan de Fuca Ridge. Ph.D. dissertation, University of Massachusetts.

Mathez E. A. (1987) Carbonaceous matter in mantle xenoliths: composition and relevance to the isotopes. *Geochim. Cosmochim. Acta* **51**, 2339-2347.

Mathez E. A. and Delaney J. R. (1981) The nature and distribution of carbon in submarine basalts and peridotite nodules. *Earth Planet. Sci. Lett.* **56**, 217-232.

Mattey D. P. (1987) Carbon isotopes in the mantle. *Terra Cognita* **7**, 31-37.

Mattey D. P. (1991) Carbon dioxide solubility and carbon isotope fractionation in basaltic melt. *Geochim. Cosmochim. Acta* **55**, 3467-3473.

Mattey D. P., Carr R. H., Wright I. P. and Pillinger C. T. (1984) Carbon isotopes in submarine basalts. *Earth Planet. Sci. Lett.* **70**, 196-206.

Mattey D. P., Exley R. A. and Pillinger C. T. (1989) Isotopic composition of CO_2 and dissolved carbon species in basalt glass. *Geochim. Cosmochim. Acta* **53**, 2377-2386.

Mattey D. P., Taylor W. R., Green D. H. and Pillinger C. T. (1990) Carbon isotopic fractionation between CO_2 vapor, silicate and carbonate melts: an experimental study to 30 kbar. *Contrib. Mineral. Petrol.* **104**, 492-505.

Metrich N. and Mosbah M. (1988) Détermination des teneurs en carbone de quelques verres basaltiques; analyses par réactions nucléaires. *Bull. Minéral.* **111**, 511-522.

Moore J. G. (1979) Vesicularity and CO_2 in mid-ocean ridge basalt. *Nature* **282**, 250-253.

Moore J. G., Bachelder J. N. and Cunningham C. G. (1977) CO_2-filled vesicles in mid-ocean basalt. *J. Volcanol. Geotherm. Res.* **2**, 309-327.

Morgan W. J. (1973) *Plate motions and deep mantle convection. Geol. Soc. Amer. Mem.* **132**, 7-22.

Morton J. L., Sleep N. H., Normark W. R. and Tompkins D. H. (1987) Structure of the southern Juan de Fuca ridge from seismic-reflection records. *J. Geophys. Res.* **92**, 11,315-11,326.

Muenow D. W., Graham D. G., Liu N. W. K. and Delaney J. R. (1979) The abundance of volatiles in Hawaiian tholeiitic submarine basalts. *Earth Planet. Sci. Lett.* **42**, 71-76.

Muenow D. W., Perfitt M. R. and Aggrey K. E. (1991) Abundances of volatiles and genetic relationships among submarine basalts from the Woodlark Basin, southwest Pacific. *Geochim. Cosmochim. Acta* **55**, 2231-2239.

Ohmoto H. and Rye R. O. (1979) Carbon and sulfur in ore bodies. In *Hydrothermal Ore Deposits* (ed. H.L. Barnes). Chapt. 10, pp. 509-567. J. Wiley & Sons.

Pineau F. and Javoy M. (1983) Carbon isotopes and concentrations in midocean ridge basalts. *Earth Planet. Sci. Lett.* **62**, 239-257.

Pineau F., Javoy M. and Bottinga Y. (1976) $^{13}C/^{12}C$ ratios of rocks and inclusions in popping rocks of the Mid-Atlantic Ridge and their bearing on the problem of isotopic composition of deep-seated carbon. *Earth Planet. Sci. Lett.* **29**, 413-421.

Richet P., Bottinga Y. and Javoy M. (1977) A review of hydrogen, carbon, nitrogen, oxygen, sulphur, and chlorine stable isotope fractionation among gaseous molecules. *Ann. Rev. Earth Planet. Sci.* **5**, 65-110.

Roedder E. (1965) Liquid CO_2 inclusions in olivine-bearing nodules and phenocrysts from basalts. *Amer. Mineral.* **50**, 1746-1782.

Rohr K. M. M., Milkereit B. and Yorath C. J. (1988) Asymmetric deep crustal structure across the Juan de Fuca Ridge. *Geology* **16**, 533-537.

Sakai H., Des Marais D. J., Ueda A. and Moore J. G. (1984) Concentrations and isotopic ratios of C, N, and S in ocean-floor basalt. *Geochim. Cosmochim. Acta* **48**, 2433-2441.

Sarda P. and Graham D. (1990) Mid-ocean ridge popping rocks: implications for degassing at ridge crests. *Earth Planet. Sci. Lett.* **97**, 268-289.

Sparks R. S. J. (1978) The dynamics of bubble formation and growth in magmas: a review and analysis. *J. Volcanol. Geotherm. Res.* **3**, 1-37.

Stolper E. M. and Holloway J. R. (1988) Experimental determination of the solubility of carbon dioxide in molten basalt at low pressure. *Earth Planet. Sci. Lett.* **87**, 397-408.

Tait S. and Jaupart C. (1990) Dynamics of eruptive phenomena. *Rev. Mineral.* **24**, 125-152.

Tingle T. N., Hochella M. F. Jr., Becker C. H. and Malhotra R. (1990) Organic compounds on crack surfaces in olivine from San Carlos, Arizona, and Hualalai Volcano, Hawaii. *Geochim. Cosmochim. Acta* **54**, 477-485.

Tingle T. N., Mathez E. A. and Hochella M. F. Jr. (1991) Carbonaceous matter in peridotites and basalts studied by XPS, SALI and LEED. *Geochim. Cosmochim. Acta* **55**, 1345-1352.

Trull T., Pineau F., Bottinga Y. and Javoy M. (1991) Experimental study of CO_2 bubble growth and $^{13}C/^{12}C$ isotopic fractionation in tholeiitic melt (abstr.). *4th Silicate Melt Workshop, 19-23 March, 1991: Prog. and Abstr.*, 7.

Turcotte D. L. and Schubert G. (1982) *Geodynamics: Applications of continuum physics to geological problems.* John Wiley and Sons.

Watson E. B., Sneeringer M. A. and Ross A. (1982) Diffusion of dissolved carbonate in magmas: experimental results and applications. *Earth Planet. Sci. Lett.* **61**, 346-358.

Zimmermann J.-L., Jambon A. and Guyetand G. (1988) Manometric and mass spectrometric analysis of fluids in geological materials. *Geochem. J.* **22**, 9-21.